

The Higgs boson and the physics of WW scattering before and after Higgs discovery

Michał Szleper

*National Center for Nuclear Research,
Hoża 69, 00-681 Warszawa, Poland*

Abstract

This work presents a comprehensive overview of the physics of vector boson scattering (VBS) in the dawn of Run 2 of the Large Hadron Collider (LHC).

Recalled here are some of its most basic physics principles, the historical relation between vector boson scattering and the Higgs boson, then discussed is the physics of VBS processes after Higgs discovery, and the prospects for future VBS measurements at the LHC and beyond. This monograph reviews the work of many people, including previously published theoretical work as well as experimental results, but also contains a portion of original simulation-based studies that have not been published before.

Contents

1	Introduction	5
1.1	Preamble - a little philosophical digression	5
1.2	Spontaneous symmetry breaking	5
2	The Higgs boson in the Standard Model	9
2.1	Issues of electroweak unification	9
2.2	The Higgs boson from the principle of gauge invariance	10
2.2.1	The Electroweak Chiral Lagrangian formalism	11
2.2.2	The Standard Model solution	13
2.3	The Higgs boson from the principle of unitarity	16
3	Standard Model experimental status and prospects for BSM	21
3.1	Higgs boson experimental status	21
3.1.1	Higgs mass, width and decay modes	22
3.1.2	Higgs spin and parity	24
3.1.3	Higgs couplings	26
3.1.4	Searches for a non-SM Higgs	29
3.2	Electroweak physics results	31
3.3	Other results of relevance for the study of VV scattering	33
3.4	The VV interaction and why it is still interesting	34
3.4.1	Higgs mass and couplings in VV scattering	35
3.4.2	Gauge boson couplings in VV scattering	37
3.5	Beyond the Standard Model?	49
4	VV scattering at the LHC	55
4.1	Formal signal definition	56
4.2	Computational issues and methods	58
4.2.1	Effective W Approximation and the Equivalence Theorem	59
4.2.2	The “production \times decay” approximation	60
4.3	Emission of a gauge boson off a quark	61
4.4	Interaction of two gauge bosons	63
4.5	Gauge boson decay and possible final states	64
4.6	The uniqueness of $W^\pm W^\pm$	66
4.7	Reducible backgrounds and selected experimental issues	77

5	Simulation-based studies vs. experimental results	85
5.1	Early calculations	86
5.2	Recent works and post-Higgs discovery developments	89
5.3	The quartic coupling perspective	94
5.4	VV scattering in LHC measurements at 8 TeV	95
6	What can the LHC measure	101
6.1	Modeling of the signal and irreducible background	102
6.2	Modeling of the inclusive $t\bar{t}$ production background	104
6.3	Modeling of the W +jets backgrounds	105
6.4	Modeling of the QCD multijet background	106
6.5	WZ and ZZ as backgrounds to WW	107
6.6	WZ and ZZ as signals	107
6.7	Key uncertainties	109
6.8	Higgs couplings in VV scattering	110
6.9	Anomalous triple gauge couplings	121
6.10	Anomalous quartic couplings	125
7	Beyond the LHC	131
7.1	General features of VV scattering at the FCC	131
7.2	Higgs to gauge couplings at the FCC	133
7.3	Anomalous gauge couplings at the FCC	138
8	Summary	147
9	Acknowledgments	149

Chapter 1

Introduction

“In the beginning there was symmetry.” - Werner Heisenberg

1.1 Preamble - a little philosophical digression

In the beginning there was symmetry and it was spontaneously broken. It is time for this ingenious and revolutionary idea to find its way to the recognition and acceptance of the wide public. A recent google search for the phrase “in the beginning there was” produced several suggested endings for the query, including: the word, chaos, light, death, darkness, and even more improbable ideas. Only no symmetry. But unlike all these other ideas, this one has by now a very solid scientific basis.

In his popular book “The Part and the Whole” (1969), Werner Heisenberg wrote: “In the beginning there was symmetry”. He expressed the opinion that basic symmetries of the world define the existing particle spectrum rather than the other way around, and contrasted this view with “in the beginning there was the particle” for which he credited Democritus. While Heisenberg most probably did not mean electroweak gauge symmetry, a concept being back then in its early development and in which he admittedly did not even show much interest, his point of view is even more actual today than it was back in the 1960’s. Today we can tell his assertion was indeed correct. As of 2012, it even seems that we exactly know how this happens. And yes, it was that symmetry breaking act that defined what particles we have today. Not the other way around.

1.2 Spontaneous symmetry breaking

The concept of spontaneous symmetry breaking is a milestone in physics. The realization that certain key features of our physical world are not explicitly determined by any fundamental laws of nature, but rather are the result of a spontaneous choice of a single solution that happened possibly just once, very early on in the history of the Universe, has a profound impact on our understanding of the world. Technically, spontaneous symmetry breaking is a mode of realization of symmetry breaking in a physical system, where the underlying laws are invariant under a symmetry transformation, but the system as a whole changes under such transformations. It thus describes systems where the equations of motion or the Lagrangian obey certain symmetries, but the ground state of the system,

i.e., the lowest energy solutions, do not exhibit that symmetry. Rather than being reflected in the individual solutions, the symmetry of the equations is reflected in the range of possible a priori solutions, even if not observed in the physical world. According to the Goldstone theorem, spontaneous breakdown of a symmetry is necessarily associated with the appearance of new spinless particles, the so called Goldstone bosons, one for each generator of the symmetry that is broken. Unless the underlying symmetry is further broken explicitly, the Goldstone bosons are massless. Conversely, if the symmetry is not exact, the bosons acquire mass, albeit are typically expected to be light. In the latter case we talk of pseudo-Goldstone bosons. A well known example of this kind are the pions, which can be identified with pseudo-Goldstone bosons related to the spontaneous breakdown of the chiral-flavor symmetries of QCD as a result of the strong interaction. The fact that pions are not entirely massless is related to the approximative character of the symmetry, which is due to the different quark masses. Still, it is well known that pions are much lighter than all the rest of the hadron spectrum. Chiral symmetry breaking is an important example of spontaneous symmetry breaking affecting the chiral symmetry of strong interactions. It is responsible for over 99% of the mass of the nucleons, as it allows to comprise heavy baryons out of nearly massless quarks, and thus is in fact responsible for the bulk of the Universe mass. Of course, by saying this we implicitly take for granted the existence of that remaining 1%. Which is in fact far from trivial. The whole clue is that quarks, and leptons for that matter, are only *nearly* massless. Without it, no mass would be there whatever. It is perhaps not so paradoxical as it may seem at first glance that over 99% of the particle physicists' effort in the last few decades, in particular in the field of experiment, has been put to reveal the origin of that remaining 1%. Finally, on July 4, 2012, the tiger broke free. By announcing the discovery of the Higgs boson [1], the ATLAS and CMS collaborations at CERN strongly suggested that in fact this mass too originates from spontaneous symmetry breaking - this time affecting the $SU(2)\times U(1)$ symmetry of electroweak interactions. The effect, as understood from the Standard Model perspective, is intrinsically connected with the so called Higgs mechanism, which was originally proposed to explain how the weak gauge bosons W and Z acquire masses. Nevertheless, both historically and conceptually, the idea of the Higgs mechanism as a theoretical means to explain the weak boson masses, and that of the Higgs particle as its possible experimental consequence are two autonomous entities. And this distinction in a limited sense holds still today, i.e., after the Higgs boson discovery. A technical clarification is in place here. By the term "Higgs mechanism" we will understand a mechanism of providing masses to vector bosons that is based on a particular method developed within the framework of Quantum Field Theory, namely by absorption of scalar fields that thus become the missing longitudinal degrees of freedom of the initially massless vectors. It works regardless of the rest of the model and what triggers electroweak symmetry breaking in particular. As a matter of fact, the idea was initially introduced to particle physics in a somewhat different (and obsolete by now) context. Existence of a physical scalar particle, the Higgs boson, can be regarded as a sufficient proof of correctness of the Higgs mechanism to provide masses to W and Z bosons, and indeed is the only proof of it available at hand and within reach of contemporary particle accelerators. Still, a Higgs boson is far from being a *necessary* condition for the Higgs mechanism be true. Rather, it is a phenomenological consequence of a certain way of realization of this mechanism. Moreover, it does not definitely settle the question of whether this realization

is the one and only, let alone to all its intrinsic details. In particular, we do not know if the Higgs is really an elementary particle or rather a composite object. This alone may have important phenomenological implications to be discovered at some higher energy. The reasons for this will be elucidated further on in the next chapters. Furthermore, a physical Higgs boson per se is a necessary, yet not a sufficient condition to prove that the very same mechanism is responsible for the generation of all the fermion masses. For that one needs to show that it indeed couples to fermions with a strength that is proportional to the fermion mass, such as is assumed in the Standard Model - which is nonetheless another autonomous issue to explore. Cut a long story short, this is the main theme of this work: the success is not yet complete and if we want to understand fully the details of the mechanism of electroweak symmetry breaking, there is still a long way ahead of us. But before we can proceed along these lines, let us first back up to the very origins of the problem: the concept of intermediate vector bosons and the issues they brought up.

This work is organized as follows. In the next chapter, a brief quasi-historical overview of electroweak unification is given, with special emphasis on the Higgs boson as the long-missing ingredient that completes the Standard Model (SM) of elementary particles. The twofold role of the Higgs boson in the Standard Model is discussed. Chapter 3 summarizes the current experimental status of the Higgs boson and discusses the importance of the VV scattering processes, where $V = W, Z$, in the aftermath of Higgs discovery, particularly in relation to existing scenarios of physics beyond the Standard Model (BSM). We also briefly overview other existing LHC results that directly or indirectly relate to the physics of VV scattering. In chapter 4 a detailed study of the VV scattering process at the LHC from a phenomenological point of view is presented. Formal signal and background definitions are given, and computational methods and problems in the evaluation of the signal are discussed. Also discussed are detector-related backgrounds and the relevant detector-specific capabilities and limiting factors that define the size of such backgrounds in a real experiment such as at the LHC. Our present knowledge of these effects, derived from various available detector-specific analyses, is summarized. Finally, it is argued that same-sign WW scattering in particular deserves special attention. Chapter 5 presents a selective review of existing literature on the subject, from the early pre-LHC works which discussed VV scattering mainly in the context of Higgsless models, up to the most recent papers and post-Higgs discovery developments. Ultimately, all this knowledge is gathered to sketch a tentative simulation-based analysis and present the up to date prospects for the observation of physics beyond the Standard Model via VV scattering in the LHC at $\sqrt{s} = 13$ TeV and beyond it.

Any studies of detector-related effects affecting the evaluation of signal and backgrounds contained in this work are based solely on those results which have been officially presented by the relevant collaborations. This work reviews a lot of earlier work published by many people, including the work of theorists as well as results of experiments, but contains also an amount of original studies and results that have not been published before. For the latter, nothing else than publicly available simulation and analysis tools have been used. Conceptually, this work is a continuation of the analysis presented in Ref.[102], with substantial updates and improvements, and with a much extended scope.

Chapter 2

The Higgs boson in the Standard Model

This chapter sketches a vaguely historical derivation of the Standard Model and the Higgs boson as its key component.

2.1 Issues of electroweak unification

Four-fermion contact interactions cannot exist in any complete theory of elementary particles. This is because the corresponding coupling constant is forced to have the dimension of cross section (i.e., inverse energy squared, in units where Planck's constant is set to 1)¹, while the cross section in the lowest order of perturbative expansion must in turn be proportional to the square of the coupling constant. From simple dimensional analysis it immediately follows that asymptotically, at energies much larger than the masses of the particles involved, the total cross section is bound to be quadratically divergent with energy. Unbound amplitude growth inevitably leads to unitarity violation at some energy. Unitarity is an imperative property of quantum systems which ensures the sum of probabilities of all possible final states evolving from a particular initial state is always equal to 1, and so it must hold in any acceptable theory. It is somewhat less straightforward to show that four-fermion interactions also inevitably lead to non-renormalizable perturbation expansion, meaning that calculations of decay rates and cross sections suffer of an increasing number of divergences arising from Feynman diagrams involving loops, and ultimately making the theory lose predictive power. These facts were well known even while the Fermi theory of weak interactions, governed by a coupling constant G_F expressed in GeV^{-2} , was the only existing one and indeed provided a good description of existing data in the low energy region. An improvement of Fermi's model, inescapable from a purely theoretical point of view, required the introduction of a force carrier, which necessarily had to be a vector boson, in analogy to the photon of QED. Note that in this case the lowest order weak interaction process is a second order process in the coupling constant which now governs the coupling of fermions to the intermediate vector bosons. It is easy

¹In the framework of Quantum Field Theory, everything is measured in units of some power of energy. The Lagrangian density has dimension 4, fermionic fields have dimension 3/2, bosonic fields have dimension 1.

to see that due to this the coupling constant itself now becomes dimensionless, pretty much as the fine structure constant of QED, thus eliminating the theoretical shortcomings associated to the Fermi theory. Indeed, the similarity of weak and electromagnetic interactions suggested the possibility of a unified theory, where the photon and the W bosons were part of the same $SU(2)$ multiplet. However, the prerequisite of correspondence of the intermediate vector boson model with the Fermi theory at low energy has an important consequence: the weak force carriers must have a non-zero mass in order to describe a short-range interaction. The success is only partial since non-zero mass is a source of two paramount problems and these provide the two in principle independent ways to derive the full Standard Model as we know it today.

For the sake of completeness one should mention here also another potential problem with electroweak unification, which resided in the parity violating character of the weak interactions. Parity violation effects were first observed experimentally in 1957. The solution consisted in enlarging the gauge group to $SU(2)\times U(1)$ to involve parity violating interactions. This had to be followed by the introduction of another neutral gauge boson, the Z . We know today that *three* weak force carriers, W^+ , W^- and Z , are necessary to describe accurately all the observed phenomenology of weak interactions.

2.2 The Higgs boson from the principle of gauge invariance

One problem with non-zero mass is related to the fact that $SU(2)\times U(1)$ gauge invariance forbids explicit mass terms for gauge bosons. Gauge boson masses must be introduced to the theory in a dodgy way and here is where spontaneous symmetry breaking comes in. The theory must be written so that the Lagrangian exhibits required gauge invariance, but its lowest energy solution cannot. This, however, poses another problem: how to avoid massless spin-zero particles, excluded by experiment, which according to the Goldstone theorem are bound to appear as a result of spontaneous symmetry breaking? In a paper of 1964, Higgs showed [2] that the Goldstone bosons need not physically appear in a relativistic theory when a local symmetry is spontaneously broken. Instead, they may turn a massless vector field into a massive vector field. Regardless of how the relevant concepts actually evolved from the historical point of view, it seems in principle clear that the simplest implementation of this requires adding extra scalar fields to the theory. Namely, at least *three* scalar fields, playing the role of the would-be Goldstone bosons of the broken symmetry, are needed to endow the three gauge bosons, W^+ , W^- and Z , with mass. Expressed the idea in simple words, each apparently massless gauge field and an apparently massless scalar field need to combine to form a massive vector field, while the total number of helicity states remains unchanged. This is the essence of the so called Higgs mechanism, which more adequately is also referred to as the Englert-Brout-Higgs-Guralnik-Hagen-Kibble mechanism [3] [4], to properly honor the many contributors to the idea in its presently known shape. There are no massless scalar fields left, as would be predicted by the Goldstone theorem. In particle physicists' jargon it is often said that those fields are "eaten up". Exactly why longitudinal polarization is intrinsically connected with the emergence of non-zero mass will be explained further below. For the time being let us stick now to the most fundamental question: how does this happen?

2.2.1 The Electroweak Chiral Lagrangian formalism

Inclusion of three scalar fields is the minimum required to provide masses to three gauge bosons. This in itself carries no clues as to the origins of symmetry breaking and moreover, it inherently demands some additional terms in the Lagrangian to couple the three Goldstone bosons to the gauge bosons and known fermions in a gauge invariant way. Once again now, real history put aside, the most general formalism that can be developed at this point, derived from the basic principles of Effective Field Theory, is known as the Electroweak Chiral Lagrangian (EWChL) approach. Without getting here into too much detail of the EWChL (more information on the subject can be found, e.g., in Refs. [5]), let us only recall its main principles and basic features. The main idea is one of having a low-energy effective parameterization of a full theory expressed in a model independent way. The general leading order (LO) Lagrangian in a practically useful form must be $SU(2)_L \times U(1)_Y$ -invariant and contain all the Lorentz-, C- and P-invariant operators up to dimension 4 (in theorists' jargon this means the dimension of the fourth power of energy). In such effective formulation the full Lagrangian can be symbolically written down in the form:

$$\mathcal{L} = \mathcal{L}_{SM} + \mathcal{L}_{EWChL} = \mathcal{L}_{SM} + \sum_i a_i \mathcal{O}_i. \quad (2.1)$$

where \mathcal{L}_{SM} are the familiar pieces that emerge from the Standard Model Lagrangian in the infinite Higgs mass limit and \mathcal{L}_{EWChL} is a collection of additional dimension-4 operators expressed in terms of a 2×2 unitary matrix U

$$U = \exp(i \frac{\vec{\sigma} \vec{\pi}}{v}). \quad (2.2)$$

In the above, $\vec{\pi}$ is a triplet of scalar fields, $\vec{\sigma}$ are Pauli matrices and $v = (\sqrt{2}G_F)^{-1/2} \approx 246 \text{ GeV}$ ². Numerical coefficients a_i play the role of effective new couplings. There is no explicit fundamental Higgs field included and, in the general case, the matrix is *non-linearly* parameterized with the three fields $\vec{\pi}$.

Each specific set of coefficients a_i reproduces the full phenomenology associated to a given physical scenario. It can be shown that only 5 independent operators account for $SU(2)_{L+R}$ -conserving contributions. These coefficients may contribute to gauge boson self-energies (a_1), triboson couplings (a_2, a_3) and effective four-boson couplings (a_4, a_5). If the a_i 's are understood as originating solely from new physics at a TeV scale, then their typical sizes are expected to be of the order $10^{-3} - 10^{-2}$. Precision electroweak data prior to the Higgs discovery defined more stringent experimental limits on their respective values. Once data from LEP became available, it was noticed that there were actually only two dimension-4 operators left in this Lagrangian that could modify the phenomenology related to the mechanism of electroweak symmetry breaking at some higher energy without contradicting any of the existing low energy data from the electroweak sector. The numerical coefficients for these operators are the ones traditionally denoted as a_4 and a_5 . Thus, the relevant part of the Lagrangian was

²Note that this is exactly the quantity known as the Higgs vacuum expectation value, but it does not have such interpretation in this framework

$$\mathcal{L}_{EWChL} = a_4[\text{Tr}(V_\mu V_\nu)]^2 + a_5[\text{Tr}(V_\mu V^\mu)]^2 \quad (2.3)$$

where we have defined $V_\mu = U(D_\mu U)^\dagger$ and D_μ is the electroweak gauge covariant derivative. For reasons that will become completely transparent in the next section, an effective modification of the four-boson couplings could be realized in terms of Higgs exchange (if we do not assume explicitly its existence in the model) or exchange of new, heavy particles. Thus, our ignorance of the electroweak symmetry breaking mechanism could be effectively shown in terms of a two-dimensional (a_4, a_5) plane of which parts had been already excluded on theoretical grounds and other parts remained unexplored. The effective Lagrangians by themselves could only describe accurately the electroweak physics at low energy. They necessarily invoked some new physics to tackle the issues of renormalizability and unitarity. Perturbative EWChL predictions can be extended to higher energies using known techniques of unitarization, the two most commonly known classes of them are called Padé unitarization (a.k.a. Inverse Amplitude Method) and K-matrix unitarization (a.k.a. N/D Protocol). Typically this procedure leads to predictions of new resonances in the particle spectrum. The entire nature: masses, widths, couplings and spins of those resonances are in principle determined by the choice of (a_4, a_5) , but in practice some theoretical uncertainty related to the use of Chiral Perturbation Theory is bound to be present and manifest in that quantitative predictions depend on the unitarization method that had been chosen. Here is where model-independence ends, because unitarization scheme is part of a model. This uncertainty becomes the larger the lighter the predicted resonances, which certifies that the entire approach is for technical reasons mostly suited for Higgsless scenarios (the term Higgsless here should be understood as anything not involving a physical scalar lighter than, say, 700 GeV). The entire formalism makes no a priori assumptions as to the nature or dynamics of the gauge symmetry breaking mechanism. It is interesting to notice that for a specific choice of parameters, the Standard Model phenomenology could also be reproduced *in principle*. Correspondence of the EWChL with the Standard Model has been in fact demonstrated, albeit only in the heavy Higgs limit [6]. This correspondence is given by setting $a_4 = 0$ and a_5 being inversely proportional to the Higgs mass squared. However, the resonance widths obtained by applying e.g. the Inverse Amplitude Method are not exactly the same as the uniquely determined - for a given Higgs mass - Standard Model Higgs widths. Full correspondence between soft and hard electroweak symmetry breaking has not been demonstrated, at least within known unitarization schemes. In any case, existence of a light scalar resonance makes this kind of description of little practical use.

The EWChL approach used to be an important theoretical framework to study the effective phenomenologies in different scenarios of electroweak symmetry breaking. It allowed to confront their predictions with those of the Standard Model with a light Higgs without running into strict model-dependence or into unphysicalness (like in the Higgsless Standard Model). With the Higgs discovery, the minimum list of operators up to dimension 4 has been completed. In principle the SM Higgs can be added to the EWChL by hand and the same formalism can still be applied with this modification. This is the simplest possible upgrade of the EWChL formalism and indeed some studies of physics beyond the Standard Model have been carried in this language. Coefficients a_4 and a_5 can be reinterpreted as modifications to SM couplings which potentially induce simultaneous existence of heavier resonances. However, a somewhat different approach has nowadays

become more popular. The SM is built from operators of up to dimension 4.³ Extensions to the SM can be parameterized in terms of higher dimension operators. On this we will elaborate in a bit more detail in the next chapter. But for now let us still back up to the Standard Model.

2.2.2 The Standard Model solution

All the above being said, history went actually a different way. At this point in history, Higgs and independently Englert and Brout [3], had already come up with a somewhat arbitrary and yet elegant idea of the exact mechanism that triggers the gauge symmetry breakdown, that could solve the problem in a remarkably economical way compared to the technical complicity of the EWChL formulation. The idea was effectively incorporated into the theory of electroweak interactions by Weinberg [7] and ever since then it became the core of the Standard Model of elementary particles. The concept did not call for any new phenomenology, with just one exception: the Higgs boson. And only one parameter suffices here for a complete quantitative description: the Higgs mass. To understand the whole mechanism, let us first consider a toy model. The following explanation is modeled on the one from Ref. [8]. In relativistic field theory the simplest Lagrangian that can realize spontaneous symmetry breaking is given by the addition of a complex scalar field ϕ such that

$$\mathcal{L} = (\partial_\mu \phi)^* \cdot \partial^\mu \phi - V(\phi), \quad (2.4)$$

where

$$V(\phi) = \mu^2 \phi^* \phi + \lambda (\phi^* \phi)^2 \quad (2.5)$$

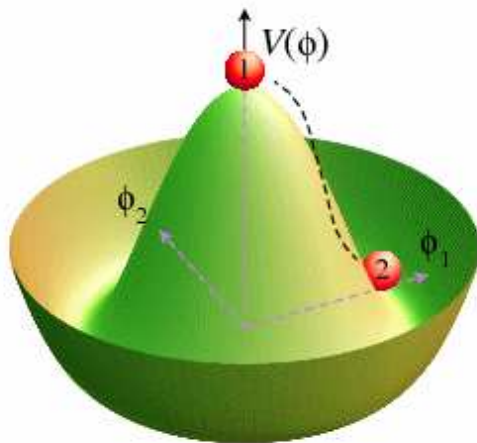


Figure 2.1: The “Mexican hat” potential $V(\phi)$ - the case of $\lambda > 0$, $\mu^2 < 0$.

³Strictly speaking, as long as we do not include Majorana neutrinos. Those can be generated via a dimension 5 operator.

and μ and λ are the mass and self-interaction coupling constant of the physical scalar particles related to the field. The model is invariant under the global transformation $\phi(x) \rightarrow \phi(x)e^{i\alpha}$. If $\mu^2 > 0$, this model describes just a self-interacting scalar field and nothing happens of special interest. If however $\mu^2 < 0$, then $\phi = 0$ is a local maximum of the potential and therefore is bound to be an unstable state. The minimum of potential V has now the form of a circle defined by $|\phi|^2 = -\mu^2/2\lambda$. In other words, in the ground state the value of ϕ is non-zero, its magnitude being actually $v/\sqrt{2}$ with $v = \sqrt{-\mu^2/\lambda}$, but with arbitrary phase. Thus, there will be a degenerate family of vacuum states, accordingly to possible choices of the phase angle α . By choosing a particular minimum, say the one where ϕ is real and positive, one breaks the symmetry with respect to α . We can perform a Taylor series expansion around this location. Defining two real shifted fields $\phi_{1,2}$ such that

$$\phi = \frac{1}{\sqrt{2}}(v + \phi_1 + i\phi_2), \quad (2.6)$$

the Lagrangian rewrites

$$\mathcal{L} = \frac{1}{2}[(\partial_\mu\phi_1)^2 + \partial_\mu\phi_2]^2] - V, \quad (2.7)$$

with

$$V = -\frac{1}{4}\lambda v^4 + \lambda v^2\phi_1^2 + \lambda v\phi_1(\phi_1^2 + \phi_2^2) + \frac{1}{4}\lambda(\phi_1^2 + \phi_2^2)^2. \quad (2.8)$$

Because we have defined ϕ_1 and ϕ_2 so that the vacuum corresponds to a non-zero value of ϕ_1 only, the model describes effectively two kinds of particles: ϕ_1 of mass $\sqrt{2\lambda}v$ and the massless ϕ_2 , along with their respective triple and quartic couplings. Particle ϕ_2 is then the Goldstone boson related to breaking the initial symmetry of the system as a result of the spontaneous choice of a vacuum state, while ϕ_1 is an extra massive scalar particle, prototype of the Higgs boson.

Now comes the Higgs mechanism. By adding a massless gauge field into the picture, e.g., the electromagnetic field with potential A_μ , the Lagrangian of the model can be expressed as

$$\mathcal{L} = (D_\mu\phi)^*D^\mu\phi - \frac{1}{4}F_{\mu\nu}F^{\mu\nu} - V(\phi), \quad (2.9)$$

where we can explicitly define the covariant derivative as $D_\mu\phi = \partial_\mu\phi - ieA_\mu\phi$, and $F_{\mu\nu} = \partial_\mu A_\nu - \partial_\nu A_\mu$ is the electromagnetic field tensor. This Lagrangian is invariant under the local gauge transformations

$$\phi(x) \rightarrow \phi(x)e^{i\alpha(x)}, \quad (2.10)$$

$$A_\mu(x) \rightarrow A_\mu(x) + \frac{1}{e}\partial_\mu\alpha(x). \quad (2.11)$$

Expansion, as before, around the chosen vacuum, yields a term of the form

$$\mathcal{L} = \dots + \frac{1}{2}(\partial_\mu\phi_2 - evA_\mu)^2 + \dots, \quad (2.12)$$

which is nothing but a mass term of an effective vector field B_μ defined as

$$B_\mu = A_\mu - \frac{1}{ev} \partial_\mu \phi_2, \quad (2.13)$$

with a mass equal to ev . There is no Goldstone boson left. Instead, the gauge field acquired mass by interaction with the scalar field ϕ_2 .

So what does it all have to do with providing masses to W and Z bosons while leaving the photon massless in a way that does not violate gauge symmetry of the Standard Model? The key feature behind implementing this idea within the context of the Higgs mechanism resided in postulating a fourth scalar field, in addition to the three would-be Goldstone bosons discussed before, for the formation of an $SU(2)$ isospin doublet of complex scalar fields, usually denoted as

$$\Phi = \frac{1}{\sqrt{2}} \begin{pmatrix} \phi^+ \\ \phi^0 \end{pmatrix} = \frac{1}{\sqrt{2}} \begin{pmatrix} w_1 + iw_2 \\ h + iz \end{pmatrix}. \quad (2.14)$$

Contrary to the general EWChL case, here a *linear* parameterization in the scalar fields is assumed. The vacuum is chosen so that $\langle 0|\Phi|0\rangle = \frac{1}{\sqrt{2}}(0, v)^T$, which means that it carries a non-vanishing value of the neutral h field. Here v is exactly the same quantity we have introduced in the previous section. Note that consequently this vacuum carries a weak charge, but no electromagnetic charge. In this case not the whole $SU(2) \times U(1)$ symmetry is broken. There is an unbroken subgroup related to the fact that Φ does not interact with the photon. Like before, massless fields w_1 , w_2 and z are absorbed to form mass terms for the apparently massless weak bosons. The masses are effectively given by:

$$M_W = \frac{gv}{2} = \sqrt{\frac{\pi\alpha}{\sqrt{2}G_F}} \frac{1}{\sin\theta_W}, \quad (2.15)$$

$$M_Z = \sqrt{\frac{\pi\alpha}{\sqrt{2}G_F}} \frac{1}{\sin\theta_W \cos\theta_W}. \quad (2.16)$$

Here we have introduced the ‘‘electroweak mixing (Weinberg) angle’’ defined via

$$\sin\theta_W = e/g, \quad (2.17)$$

the ratio of the original electromagnetic and the weak coupling constants. The photon remains massless. Since the value of $\sin\theta_W$ may be determined experimentally, e.g., from a measurement of fermion scattering processes, the above formulae represent in fact a *prediction* for the W and Z masses. The fourth field h is needed to trigger spontaneous symmetry breaking by its non-vanishing vacuum expectation value. As a result, the shifted field $H = h - v$ becomes a physical, massive, self-interacting scalar - the Standard Model Higgs boson. The mass of the Higgs boson is given by

$$M_H = \sqrt{2\lambda v^2} \quad (2.18)$$

and hence it is not known a priori without knowledge of λ . However, everything else in the theory is completely determined or at least calculable.

Rewriting the Lagrangian in terms of physical particles, we see that the Higgs couples to the gauge bosons:

$$\mathcal{L} = \dots + M_W^2 \cdot W^{+\mu} W_\mu^- \cdot (1 + H/v)^2 + \frac{1}{2} M_Z^2 \cdot Z^\mu Z_\mu \cdot (1 + H/v)^2 + \dots \quad (2.19)$$

with a coupling proportional to the mass squared. As a byproduct, it also couples to fermions generating their mass terms:

$$\mathcal{L} = \dots + \sum_f m_f f \bar{f} \cdot (1 + H/v)^2 + \dots \quad (2.20)$$

By construction, the coupling to fermions is proportional to the fermion masses.

This completes the Standard Model of elementary particles and fundamental interactions, the most successful theory in modern physics, from the point of view of gauge invariance.

2.3 The Higgs boson from the principle of unitarity

The second reason why non-zero mass is a problem concerns polarization and the issue of unitarity. As already mentioned, the unitarity condition is equivalent to the requirement of the sum of probabilities of all possible final states evolving from a particular initial state be always equal to 1. This sum of probabilities must be in principle calculated to infinite order in perturbative expansion, which is of course impossible to achieve. For the technical issues regarding the concept of unitarity and the connection between unitarity and renormalizability, the reader is referred to more topical literature, e.g., Ref. [9]. In the following we will use the commonly accepted practical criterion of *tree* unitarity which demands for any $2 \rightarrow 2$ process predicted by the theory its tree level amplitude be asymptotically at most flat with energy. Discussion on the validity of this criterion can be found in Ref. [9].

Let us derive the essence of the problem in detail, as this constitutes the theoretical basis of our proper subject. In relativistic Quantum Field Theory, a massive vector boson can be described in terms of a wave function B^μ whose form is a wave-plane solution of the Klein-Gordon equation:

$$B^\mu(x) = C \epsilon^\mu(p) e^{-ipx} \quad (2.21)$$

with the so called Lorenz condition ⁴, $\partial_\mu B^\mu = 0$, imposed. Here p is the four-momentum of the particle, C is a normalization constant whose value is inessential at the present moment and ϵ^μ is the polarization vector corresponding to the plane wave. In the boson rest frame, ϵ^μ can be decomposed into the individual Cartesian coordinates, where

$$\epsilon_x^\mu = (0, 1, 0, 0), \quad (2.22)$$

$$\epsilon_y^\mu = (0, 0, 1, 0), \quad (2.23)$$

$$\epsilon_z^\mu = (0, 0, 0, 1), \quad (2.24)$$

⁴Not Lorenz condition, as is often erroneously called.

and these correspond to the three possible linear polarization states. We have already taken advantage of the fact that the zeroth component is bound to be zero by the Lorenz condition. Alternatively, we may define two linear combinations of ϵ_x^μ and ϵ_y^μ ,

$$\epsilon_+^\mu = \frac{1}{\sqrt{2}}(0, 1, i, 0), \quad (2.25)$$

$$\epsilon_-^\mu = \frac{1}{\sqrt{2}}(0, 1, -i, 0), \quad (2.26)$$

which correspond to two possible circular polarization states. Let us now suppose the boson moves along the z axis. The quantities ϵ_+^μ and ϵ_-^μ will now stand for the two degrees of freedom of polarization transverse to the boson direction, while ϵ_z^μ will become the longitudinal polarization and be further on denoted as ϵ_L^μ . Translated into the language of helicity, i.e., the projection of the boson's spin onto its direction of motion, ϵ_+^μ , ϵ_L^μ and ϵ_-^μ correspond to helicities $+1$, 0 and -1 , respectively.

The general expression for the three components of ϵ^μ for a boson with mass M , energy E and 3-momentum p_z directed along the z axis can be simply found by applying Lorentz transformation. It is however fully sufficient to consider that the transverse polarizations need not change, while ϵ_L^μ , by definition directed along the momentum 3-vector, must be of the form

$$\epsilon_L^\mu = \left(a \frac{|\vec{p}|}{E}, a \frac{\vec{p}}{|\vec{p}|}\right) = \left(a \frac{p_z}{E}, 0, 0, a\right), \quad (2.27)$$

where $a > 0$. The normalization condition readily yields $a = E/M$, hence

$$\epsilon_+^\mu = \frac{1}{\sqrt{2}}(0, 1, i, 0), \quad (2.28)$$

$$\epsilon_-^\mu = \frac{1}{\sqrt{2}}(0, 1, -i, 0), \quad (2.29)$$

$$\epsilon_L^\mu = \frac{1}{M}(p_z, 0, 0, E). \quad (2.30)$$

One can quickly verify that the above indeed satisfies the Lorenz condition expressed as $p_\mu \epsilon^\mu = 0$.

In this moment we have arrived at a very important conclusion. The requirement of $\epsilon_L \neq 0$ makes sense only if $M \neq 0$. For a massless boson there is no solution satisfying the Lorenz condition that would correspond to longitudinal polarization. And this is why, in the language of relativistic Quantum Field Theory, on-shell photons are purely transverse. More generally, for a massless boson of spin J , Lorentz invariance forbids other helicities than $+J$ and $-J$.

The form of ϵ_L defines its key feature which lies in its energy dependence. It is clear that at energies much larger than the boson mass, it grows indefinitely with energy, like $\epsilon_L \sim E$, being a source of potentially fatal misbehavior of the gauge boson sector. To elucidate the problem, let us consider a simple scattering process involving two on-shell, same-sign, longitudinally polarized W bosons:

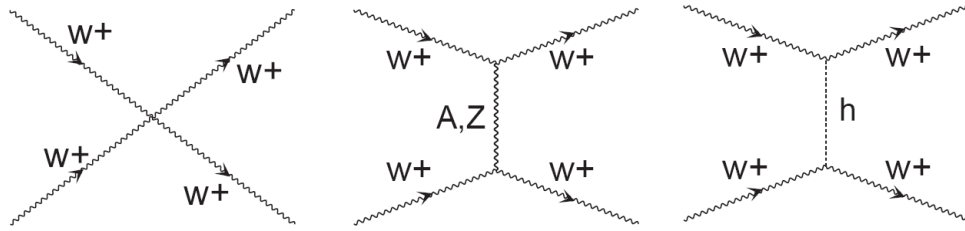


Figure 2.2: Feynman diagrams for the Standard Model process $W^+W^+ \rightarrow W^+W^+$: the four- W contact interaction graph, the γ/Z -exchange graph and the Higgs exchange graph.

$$W_L^+W_L^+ \rightarrow W_L^+W_L^+.$$

In the lowest order, three subprocesses readily contribute to this process: the four- W contact interaction and t -channel (space-like) photon and Z exchange. The amplitude of the contact interaction part must be proportional to

$$\mathcal{M} \sim \epsilon_L \epsilon_L \epsilon_L \epsilon_L \sim s^2, \quad (2.31)$$

where s is the center of mass energy squared of the interacting bosons. Obviously it diverges like the fourth power of energy and so, paradoxically, the electroweak theory leads to similar difficulties as did before the Fermi theory. Even worse at first sight may look the diagram involving t -channel Z exchange, as one may expect in this case the leading divergence to be like $\sim E^6$ from an appropriate combination of all the longitudinal W and Z components. It can be shown, however, that the longitudinal part of the Z propagator vanishes and the full contribution from the t -channel photon and Z exchange in fact also goes like s^2 in the leading term. Moreover, by appropriate choice of the coupling constant for the four- W contact interaction, which in practice is secured by the Standard Model gauge invariance, the two leading terms can be made to cancel each other exactly. It is worth to remember this point, since it will come back to us in further considerations. The triple gauge boson couplings, WWZ and $WW\gamma$, are well constrained by experiment and we need not consider their variation at this point. The same can hardly be told of the quartic couplings which remain largely unconstrained from the experimental point of view. Altogether, there are four quartic boson couplings allowed in the Standard Model: $WWWW$, $WWZZ$, $WWZ\gamma$ and $WW\gamma\gamma$, and their values within the model are completely specified. The $WWWW$ coupling in itself can be probed experimentally at the LHC in an independent way, via measurements of triboson production. Generally, it is expected that new physics may manifest itself in changes of the effective quartic couplings relative to the Standard Model and therefore alter the Standard Model predictions for triboson production, *as well as* the high energy behavior of WW scattering amplitudes. For the sake of this chapter we will assume that quartic couplings correspond exactly to their Standard Model values. Consequently, we are left with

$$\mathcal{M}_{Gauge} = -g^2 \frac{s}{4M_W^2} + \mathcal{O}(s^0). \quad (2.32)$$

Technically, this still implies unitarity violation and non-renormalizability. As usual in particle physics, such problems are fixed by postulating new particles and appropriate interactions to produce counter-terms that will cancel the unwanted divergences. Because of the form of the scalar propagator, the inclusion of a neutral scalar particle H that can be exchanged between the two W lines will result in an additional term

$$\mathcal{M}_H = g_{HWW}^2 \frac{s}{M_W^4} + \mathcal{O}(s^0). \quad (2.33)$$

From dimensional analysis it follows that the coupling constant that governs the interaction of H with the W boson must have the dimension of energy. By looking at the expressions for \mathcal{M}_{Gauge} and \mathcal{M}_H one easily notices that the leading divergences will cancel out *exactly* if and only if the condition $g_{HWW} = gM_W$ is *exactly* fulfilled. Recalling that g in itself is related to the W mass, this in particular means that the scalar H must couple to the W proportionally to M_W^2 . We already have such candidate: it is the Standard Model Higgs boson. Indeed, tedious calculations within the framework of the Standard Model yield the asymptotic result

$$\mathcal{M}_{Gauge} + \mathcal{M}_H = g^2 \frac{M_H^2}{4M_W^2} \quad (2.34)$$

at energies much larger than the Higgs mass.

The same arguments apply to the opposite sign W boson scattering process

$$W_L^+ W_L^- \rightarrow W_L^+ W_L^-.$$

In this case we have to take into account additional diagrams corresponding to s -channel (time-like) photon and Z exchange, as well as an s -channel Higgs exchange diagram. Without repeating the main points nor getting into detailed calculations we can immediately write down the final results for the corresponding amplitudes:

$$\mathcal{M}_{Gauge} = -g^2 \frac{u}{4M_W^2} + \mathcal{O}(s^0), \quad (2.35)$$

$$\mathcal{M}_H = g_{HWW}^2 \frac{u}{M_W^4} + \mathcal{O}(s^0). \quad (2.36)$$

where u is the familiar Mandelstam variable and we have used the high energy approximation $s + t + u = 0$.

Similarly, to the process of $W^\pm Z$ scattering

$$W_L^\pm Z_L \rightarrow W_L^\pm Z_L,$$

the lowest order diagrams that contribute are the $WWZZ$ contact interaction, s - and t -channel W^\pm exchange and t -channel Higgs exchange. And likewise, the divergence resulting from the sum of the former three is exactly canceled by the Higgs exchange diagram in the SM.

With the ZZ scattering process the question is seemingly different, since in the SM it can only occur via Higgs exchange (both s - and t -channel). However, in any real hadron-hadron experiment this process cannot be separated from the dominant $W^+W^- \rightarrow ZZ$ process, where three additional graphs contribute in the lowest order, including the $WWZZ$ contact interaction, t -channel W^\pm exchange and s -channel Higgs exchange. Once again here, Higgs exchange provides cancelation of unwanted divergences.

By introducing a Higgs boson with appropriate couplings to other particles, unitarity in the theory is established. This in turn completes the Standard Model from the point of view of the unitarity principle. But there is more here. A Higgs boson is necessary before the energy scale of unitarity violation. A Higgs that is too heavy is useless in the SM. From these considerations an upper bound on the Higgs mass [10] was derived way before its actual observation.

Chapter 3

Standard Model experimental status and prospects for BSM

The LHC has finished Run 1. Both ATLAS and CMS have produced their preliminary (now every day closer to being final) results based on combinations of the entire datasets from 7 TeV and 8 TeV. Even if some of the results that have been published until now are not yet to be considered final, the most important findings are unlikely to change significantly until the LHC is restarted again with a higher energy (13 TeV) and collects enough new data. To discuss physics of Run 2 of the LHC, it is important to realize what exactly has become known from Run 1 and within what uncertainty margins, then how these uncertainty margins translate into the potential of new discoveries in the forthcoming years. This is of course true not only for VV scattering, but for the entire LHC physics. But the relation between the Higgs boson and VV scattering is special and so this dependence is here even more strict. This chapter will review our current, most up to date, knowledge about the Higgs boson and summarize other measurements with direct or indirect impact on the physics of VV scattering in the next years.

3.1 Higgs boson experimental status

Four well known mechanisms of Higgs production at the LHC are: gluon-gluon fusion via heavy quark loops, Vector Boson Fusion (VBF), Higgsstrahlung off a gauge boson and heavy quark fusion (also called $t\bar{t}$ - or $b\bar{b}$ -associated production). Their relative importance varies with the Higgs mass and the kind of physics we want to study, to a lesser degree with the actual proton beam energies. For a Higgs mass in the vicinity of 125 GeV, gluon-gluon fusion is by far the dominant production mode, with VBF contributing roughly an order of magnitude less and the other modes less still. For Higgs-like resonance masses above the $t\bar{t}$ threshold, the relative amounts of gluon-gluon fusion and VBF become gradually closer to unity, up to the point of the latter becoming over 1/3 of the total cross section at around 1 TeV.

On the other end of the Higgs boson, the relative importance of different decay modes is driven by the respective mass thresholds for the decays into heavy particles. For $M_H < 2M_W$, as is indeed the case for the Standard Model Higgs, decays to fermions like the b or c quarks or to the τ leptons are strongly preferred as far as raw branching fractions

are concerned. Background and event reconstruction efficiency issues define however ZZ and WW as being among the leading light Higgs decay modes to study, the only other fully competitive channel being in fact $\gamma\gamma$ which occurs solely via loop corrections. In the Higgs-like resonance mass region above 150 GeV, decays into WW and ZZ become just about the only relevant ones, and this assertion changes only marginally on the opening of the $t\bar{t}$ channel for masses larger than 350 GeV.

Our process of interest is intrinsically connected with Vector Boson Fusion followed by decay into a pair of vector bosons. In the resonance region it is quite identical with it and so the W^+W^- and ZZ scattering modes are naturally the most widely studied to date. Of course, in an experiment we only know the bosons in the final state. The process $ZZ \rightarrow ZZ$ is in principle the most direct probe of the Higgs boson, as it only proceeds via Higgs exchange in the Standard Model, but it cannot be separated from $W^+W^- \rightarrow ZZ$. Specific VBF analyses have been performed in the low Higgs mass range and will be the basis for future heavy resonance searches at 13 TeV. These studies have come up with a typical experimental VBF signature to search for. It consists of two energetic forward jets and all the final Higgs decay products usually well isolated in the barrel region of the detector, the two direct decay products being typically reconstructed in opposite hemispheres. The purely electroweak character of the process means no QCD color flow occurring in the event and reflects in a large rapidity gap between the two leading jets. The typical VBF signature used in Higgs searches does not explicitly discriminate between the gauge boson polarizations. Indeed such discrimination is impractical in a kinematic regime where at least one of the gauge bosons must be off-shell. The spin and parity of the resonance can be nonetheless determined afterwards from the angular distributions of the decay products, where naturally the ZZ channel keeps the most complete information available in the detector.

3.1.1 Higgs mass, width and decay modes

Higgs signal has been independently observed with more than 5σ significance, in both ATLAS [14] and CMS [13], in two decay modes: $H \rightarrow ZZ^* \rightarrow l^+l^-l^+l^-$ (CMS: 6.5σ , ATLAS: 6.6σ) and $H \rightarrow \gamma\gamma$ (CMS: 5.6σ , ATLAS: 7.4σ). A third bosonic decay mode, $H \rightarrow W^+W^-$, comes close (CMS: 4.7σ , ATLAS: 4.1σ). Observed significances agree with SM expectations.

The Higgs boson mass has now been precisely determined from a combination of data from the two most sensitive decay modes which not unexpectedly also provide the best mass resolution: $H \rightarrow 4l$ and $H \rightarrow \gamma\gamma$. Its final values have been reported to be:

$$M_H = 125.36 \pm 0.37(stat) \pm 0.18(syst) \text{ GeV (ATLAS) and}$$

$$M_H = 125.03 \pm_{-0.27}^{+0.26}(stat) \pm_{-0.15}^{+0.13}(syst) \text{ GeV (CMS).}$$

Higgs masses determined from the two channels separately are in satisfactory agreement at CMS, with the final mass difference being quoted as $M_H^{\gamma\gamma} - M_H^{4l} = -0.87 \pm_{-0.59}^{+0.54}$ GeV. ATLAS observed a marginally larger difference whose statistical significance is likewise weak, $M_H^{4l} = 124.51 \pm 0.52$ GeV vs. $M_H^{\gamma\gamma} = 125.98 \pm 0.50$ GeV. It should be noted that, as far as the central values are concerned, $M_H^{4l} > M_H^{\gamma\gamma}$ for CMS, but $M_H^{\gamma\gamma} > M_H^{4l}$ for ATLAS, which clearly favors statistical and systematic uncertainties rather than physics

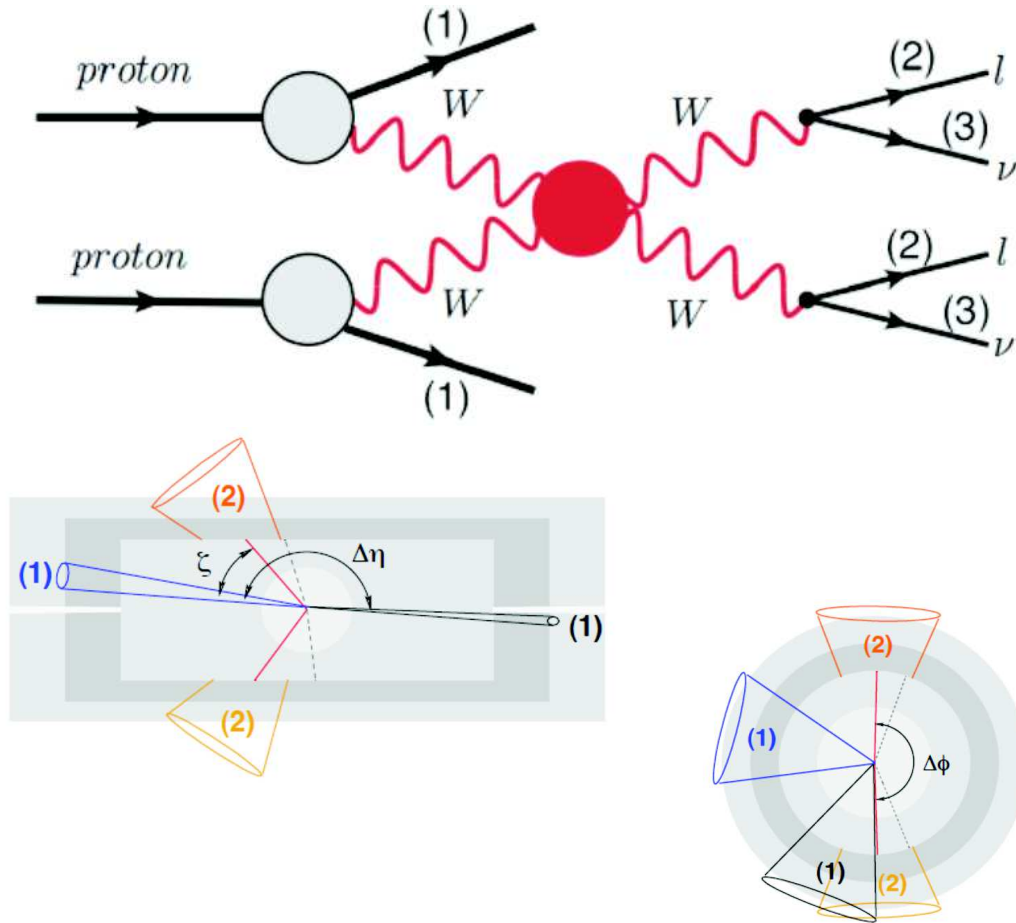


Figure 3.1: The Vector Boson Scattering process at the LHC: a schematic drawing (top) and two views of its basic signature in an LHC detector (bottom). A purely leptonic WW decay channel is assumed. A typical signature consists of two forward high energy jets (labeled (1)) with a large pseudorapidity gap, and two central leptons (labeled (2)) with a large gap in the azimuthal angle. Quantities like $\Delta\eta$ and $\Delta\phi$ are instrumental in isolating the process from the bulk of the background.

as the most plausible interpretation of any possible mass shifts. There is no experimental support to the idea of there actually being two nearly degenerate resonances, at least within the present resolutions.

A study of Higgs decays into $\tau^+\tau^-$ revealed independent evidence of a Higgs signal at the 4.5σ level in ATLAS [15] and at the 3.2σ level in CMS [16], both being compatible with the expectations for a ~ 125 GeV Standard Model Higgs boson and hence strongly suggesting that the Higgs indeed does couple to fermions. On the other hand, no other fermionic decay has been firmly and directly established on its own. The ones that have been directly searched for are the decays to $b\bar{b}$, $\mu^+\mu^-$ [17] and more recently e^+e^- . Analysis of the former does indeed reveal hints at a roughly 2σ level, in consistency with SM expectations. A CMS combination of data from the two most important fermionic Higgs decays: $\tau^+\tau^-$ and $b\bar{b}$, does not yet reach the 5σ significance level [18]. With the amount of data collected so far, lack of signal observation in decays to lighter fermions is fully consistent with the SM. Of course, decays $H \rightarrow \gamma\gamma$ occurring at a rate roughly consistent with the Standard Model indirectly suggest that Higgs couples to the top quark, too. Moreover, theory predicts the main Higgs production mechanism be gluon-gluon fusion via top quark loops and so the total Higgs production rate is driven predominantly by the Higgs coupling to the top. In other words, the simple observation of total Higgs production occurring at a rate roughly consistent with the SM is another (and actually, the strongest), albeit indirect, confirmation that the Higgs couples to fermions.

Certain rare Higgs decays predicted by the Standard Model have been searched for as well. Measurement of the rate of Higgs decaying into, e.g., $Z\gamma$ would be a very interesting test of the Standard Model, but so far data are of not enough statistical precision to do so [19].

The width of the Higgs boson in the SM is fully determined by its mass. For a 125 GeV Higgs, the expected width is close to 5 MeV, which is unfortunately far beyond present experimental resolution. From an analysis of data in the resonance region of the 4-lepton decay channel, CMS found the observed resonance width in agreement with the detector resolution width and placed a 95% CL upper bound on the intrinsic Higgs width at 3.4 GeV. A novel method has been proposed to constrain the Higgs width by examination of the 4-lepton mass spectrum away from the Higgs peak [20]. In the dominant gluon fusion process, Higgs off-shell production and decay into 4 leptons gets enhanced due to the proximity of the Z pair production threshold. The ratio of cross sections for off-shell and on-shell Higgs production, $\sigma(gg \rightarrow H^* \rightarrow ZZ)/\sigma(gg \rightarrow H \rightarrow ZZ^*)$ is directly proportional to the Higgs width. Using this technique, CMS placed a much better upper bound on it at 22 MeV (95% CL) [21].

3.1.2 Higgs spin and parity

Crucial to the identification of the 125 GeV resonance with the SM Higgs is determination of its spin and parity. The SM Higgs boson has spin-parity $J^P = 0^+$. Different spin-parity hypotheses of the observed Higgs-like resonance have been severely constrained by the data. The spin and parity of the Higgs resonance can be independently analyzed in each decay mode, based on angular distributions of the respective decay products. In CMS, this has been achieved so far using the three leading decay modes [23]: $H \rightarrow ZZ^* \rightarrow l^+l^-l^+l^-$,

$H \rightarrow W^+W^- \rightarrow l^+l^-\nu\nu$ and $H \rightarrow \gamma\gamma$ ¹. By far the most sensitive of them is the 4-lepton channel. Strictly speaking, J^P is not *measured*, only the likelihood of different hypotheses can be determined relative to each other (one can of course argue that such procedure qualifies as being a measurement). Each J^P hypothesis translates into specific predictions of the angular distributions that are computed directly from the corresponding matrix elements. For every pair of hypotheses their relative likelihood of consistency with the data can then be quantified. The procedure is more likely to end up in a conclusive result only as long as one of the two selected hypotheses is the correct one (and the other incorrect). Thus, in practice, each non-standard J^P hypothesis is tested against the $J^P = 0^+$ hypothesis. A q value is then determined from data that is equal to the relative likelihood of the tested hypothesis against the reference $J^P = 0^+$ case. Statistical significance of each result is determined by comparing the single q value obtained from data with its predicted probability distributions that are calculated under the assumptions that one or the other J^P hypothesis is correct. The respective probability distributions are obtained from a number of simulated “fake” experiments. The hypotheses that have been tested include $J^P = 0_h^+$ (scalar with higher order couplings), 0^- (pseudoscalar), 1^\pm (vector and pseudovector), 2_m^\pm (tensor and pseudotensor with minimal couplings to SM particles - a graviton analogue) and 2_h^\pm (tensor and pseudotensor with higher order couplings). In addition, a maximum likelihood function can be defined in which a mixed J^P state is allowed, e.g., 0^+ with 0^- .

Analysis of the 4-lepton channel is based on a technique described in detail in literature [22]. It exploits information on five angles that characterize the decay: two angles describe the orientation of the decay plane of one Z boson in the lab, a third angle the relative azimuthal orientation of both Z decay planes and the last two angles describe the two Z decays in the respective Z rest frames. The 4-lepton channel alone allows to reject all of the tested hypotheses at a confidence level (CL) greater than 95%. In the $H \rightarrow \gamma\gamma$ channel, Higgs spin correlates to the polar angle of the $\gamma\gamma$ pair in the Higgs rest frame. According to the Landau-Yang theorem, decays of a massive vector into a couple of massless vectors are forbidden, so $J = 1$ is here excluded. All spin-zero scenarios produce an identical isotropic $\gamma\gamma$ distribution and therefore the $J^P = 0^-$ hypothesis cannot be studied using this channel. Results for the tensor hypotheses depend on the production mechanism, but currently none can be fully excluded at 95% CL. Finally, in the leptonic $H \rightarrow WW$ channel, analysis in a two-dimensional plane spanned by the event transverse mass and the lepton-lepton mass was done. The exclusion of the pseudoscalar hypothesis from this channel is marginal, but $J^P = 2_m^+$ can be excluded at 95% CL or more in the cases where the preferred production mechanism is quark-antiquark fusion. From a combination of $H \rightarrow ZZ$, WW and $\gamma\gamma$ results, the $J^P = 2_m^+$ model is excluded at a 99.9% CL regardless of the combination of the gluon-gluon and quark-antiquark production modes and other spin-2 hypotheses are excluded at 99% CL or higher. Likewise spin-1 hypotheses are excluded at more than 99.99% CL from the combination of decays $H \rightarrow ZZ$ and WW . The pseudoscalar hypothesis is excluded at 99.5% CL. This of course refers to pure J^P hypotheses. The 95% CL limit on the fractional pseudoscalar cross section in the Higgs resonance is 0.43 and so a significantly mixed parity state is by all means allowed.

A combined spin-parity analysis from the three main decay modes was also published

¹The possibility of providing additional evidence based on the $\tau^+\tau^-$ decay mode is being studied

by ATLAS [24]. This analysis excluded the graviton-inspired 2^+ hypothesis at a more than 99.9% CL, spin-1 hypotheses at 99.7% CL and the pure 0^- hypothesis at 97.8% CL. They do not quote numbers for the maximum allowed pseudoscalar admixture. Exclusion limits have been also set on the hypothesis that the observed signal is shared between two nearly degenerate mass states.

3.1.3 Higgs couplings

Finally and most importantly for the sake of this work, Higgs couplings have been probed via measurements of branching fractions for the main decay modes: W^+W^- , ZZ , $\gamma\gamma$ and $\tau^+\tau^-$ (and $b\bar{b}$, in principle), and the respective production mechanisms. All Higgs couplings can in principle be inferred from fits to the observed rates in different combinations of Higgs production mechanisms and decay modes, where each full production \times decay path can be parameterized as a function of the relevant couplings. However, data are not precise enough to determine independently all the couplings with a reasonable accuracy. For this reason, results are usually presented in one of two forms. In the first approach, events are categorized by final state, including the contributions from all production mechanisms and a single parameter μ for each final state is fit to the observed signal yield. The quantity μ is the measured signal strength (cross section \times branching fraction) relative to the predicted SM signal strength. The most recent results of the overall signal strength relative to the SM that is obtained from a simultaneous fit to all Higgs decay channels are [13] [14]:

$$\mu = 1.00 \pm 0.09(stat) \pm 0.07(syst) \pm_{0.15}^{0.13}(theo) \text{ (CMS), and}$$

$$\mu = 1.30 \pm 0.13(stat) \pm_{0.11}^{0.14}(syst) \text{ (ATLAS).}$$

In the channels of most interest for us here, CMS results were:

$$\mu_{WW} = 0.83 \pm_{0.20}^{0.22} \text{ (from } W^+W^-) \text{ and}$$

$$\mu_{ZZ} = 1.00 \pm_{0.26}^{0.32} \text{ (from } 4l).$$

ATLAS most recently published values are:

$$\mu_{WW} = 1.08 \pm_{0.15}^{0.16}(stat) \pm_{0.13}^{0.16}(syst) \text{ and}$$

$$\mu_{ZZ} = 1.44 \pm_{0.33}^{0.40}.$$

While consistent with the SM, these numbers still keep room for sizeable deviations.

Fits of μ were also done in separate categories where events were tagged by production mode, exploiting the distinct kinematic and topological signatures of VBF, Higgsstrahlung and $t\bar{t}$ -associated production (the largest “untagged” sample corresponds mostly to gluon fusion). They revealed consistency with the SM within rather large errors.

The above are pure experimental results, with no model-dependence involved. However, their relations to the genuine Higgs couplings are entangled. In the other approach, events were categorized according to their full production \times decay chains and a simultaneous theoretical fit of the corresponding cross sections \times branching fractions was done to the data in which only two parameters were allowed to vary freely: one to globally modify the Higgs couplings to bosons, another to globally modify the Higgs couplings to fermions.

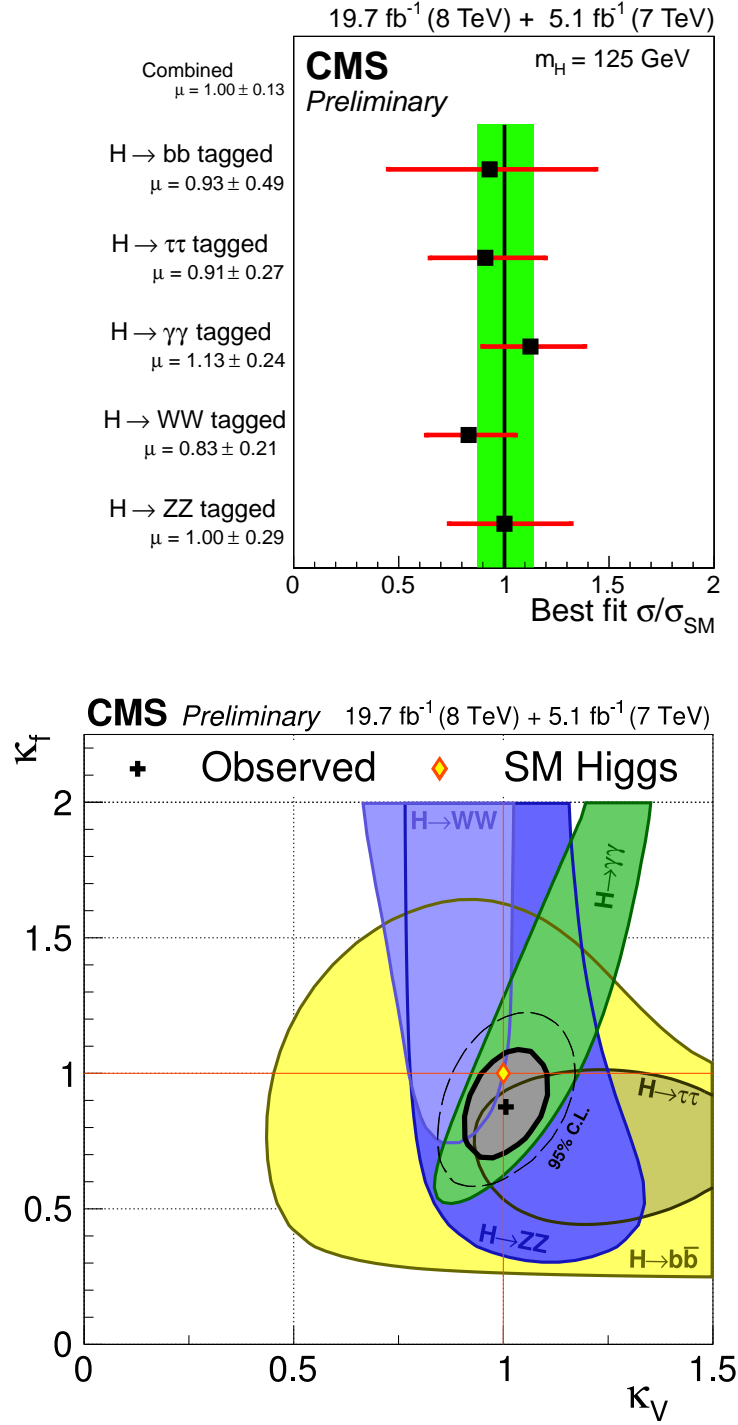


Figure 3.2: Upper plot: Values of the best fit σ/σ_{SM} for the combination (solid vertical line) and by predominant decay mode. The vertical band shows the overall σ/σ_{SM} uncertainty. Lower plot: 68% CL contours for individual channels and for the overall combination (thick curve) for the (κ_V, κ_f) parameters. The cross indicates the global best-fit values. The dashed contour bounds the 95% CL region for the combination. The yellow diamond represents the SM expectation. Results from the CMS collaboration. The shown parameter space was here restricted to the first quadrant where the global minimum of the fit was found. A second minimum was also obtained for $\kappa_f < 0$ (see also Fig. 3.3). Images reproduced from Ref. [11].

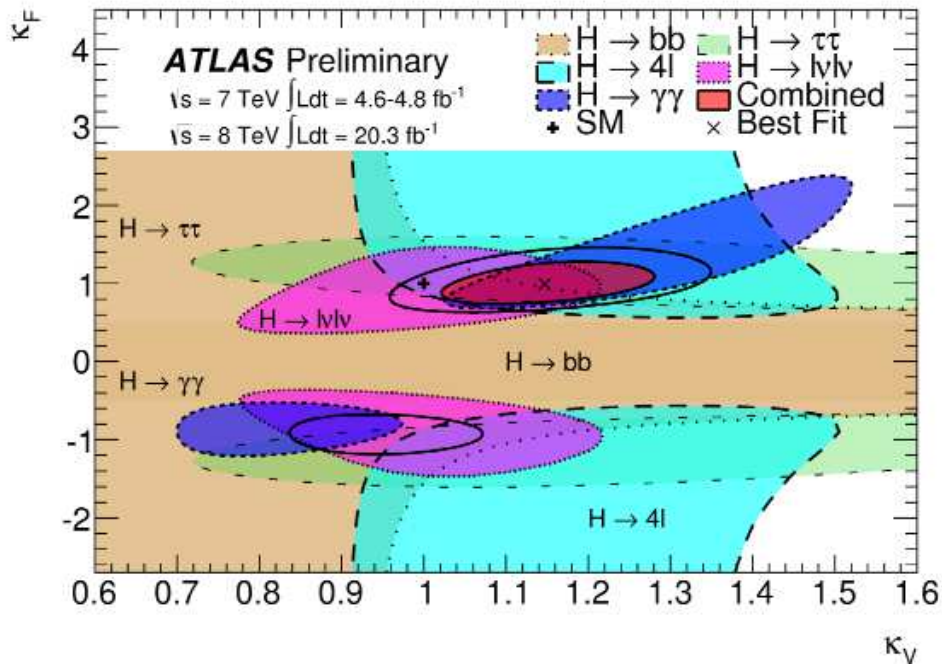
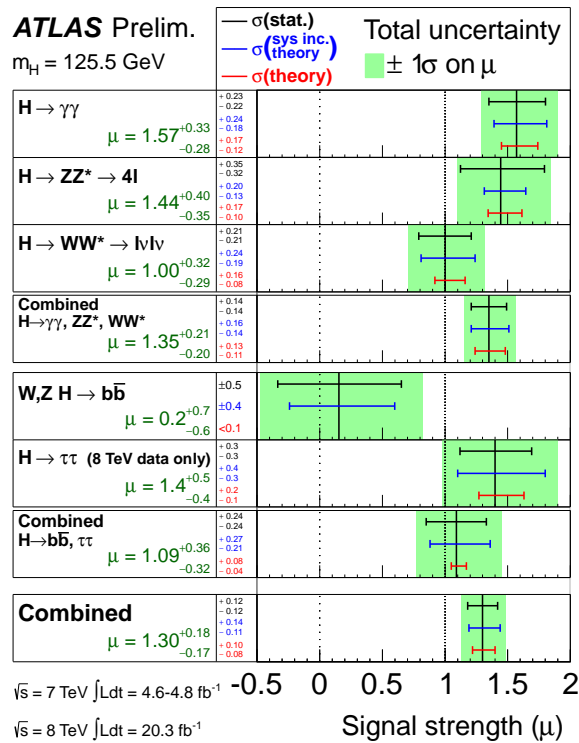


Figure 3.3: Upper plot: The measured signal strengths normalized to SM expectations for the individual final states and various combinations. The best-fit values are shown by solid vertical lines. The total $\pm 1\sigma$ uncertainties are indicated by green shaded bands, with the individual contributions from the statistical, systematic (including theory) and theoretical uncertainties (from QCD scale, PDF, and branching ratios) are shown as superimposed error bars. Lower plot: Results of fits that probe different coupling strength scale factors for fermions and vector bosons, assuming only SM contributions to the total width: 68% CL contours from individual decay channels and their combination. Results from the ATLAS collaboration. Images reproduced from Ref. [12].

From such fits, CMS obtained [11] both scale factors, κ_V and κ_f , consistent with unity within 1σ ; the accuracy is roughly $\sim 10\%$ for κ_V and $\sim 20\%$ for κ_f (see Fig. 3.2). From one-dimensional parameter scans (in which the other coupling was set to its SM value), one gets the following 95% CL intervals: $\kappa_V \in [0.88, 1.15]$ and $\kappa_f \in [0.64, 1.16]$. A similar analysis was done by ATLAS [12] (see Fig. 3.3).

It should be stressed here that this procedure is not completely model-independent because the content of the loops in gluon fusion and in $H \rightarrow \gamma\gamma$ decays must be explicitly assumed in order to relate production mechanisms with decay modes via the same parameters: in the SM, the loops are dominated by respective contributions from the top quark and from the W boson. Agreement with the SM of the total Higgs signal strength, in particular in the dominant “untagged” category, as well as that of the $H \rightarrow \gamma\gamma$ signal strength, justifies the approach. More generally, the procedure can be regarded self-consistent for any model that does not involve significant contributions from unknown heavy particles within the present energy reach. This may in fact be the case in an interesting wide class of theories beyond the SM, known as SILH models, that we will discuss further on. The procedure itself of scaling the Higgs couplings by only two independent factors, κ_V and κ_f , is likewise consistent with the expected low-energy phenomenology of these models. Therefore, the above result is of special interest from this point of view. A dedicated test for the presence of BSM particles was carried based on $\gamma\gamma$ data. A fit to the data where all tree-level couplings were assumed equal to their SM values, $\kappa_V = \kappa_f = 1$, and varied freely were the effective Higgs couplings to gluons and photons, κ_g and κ_γ , revealed consistency with the SM within 1σ .

By reverting the procedure, the top coupling is probed by assigning a common signal strength factor for the gluon fusion production mechanism, with addition of the little $t\bar{t}H$ production mode, because they both scale predominantly with the Yukawa coupling of the top quark in the SM. The assumption that the Higgs couples proportionally to the fermion mass has been indirectly supported by the data.

Other tests included modified up-type to down-type fermion couplings, motivated by SUSY models, and modified independently top, bottom and τ couplings. No deviations from the SM were observed.

3.1.4 Searches for a non-SM Higgs

By contrast, all dedicated searches for a non-Standard Higgs to date gave negative results.

Additional, heavy SM-like Higgses were excluded at the 95% CL or more up to the mass of 710 GeV from a combination of data from ZZ and WW decays [26]. Likewise, no additional resonances have been observed in the $\gamma\gamma$ spectrum between 150-850 GeV [27].

Dedicated searches were carried for neutral and charged Higgses within the framework of the Minimal Supersymmetric extension of the Standard Model (MSSM). The most stringent exclusion limits come from the search for the MSSM decay $h, H, A \rightarrow \tau^+\tau^-$ [28] for which the standard $\tau^+\tau^-$ analysis was modified so as to maximize the sensitivity to BSM effects. An MSSM scalar Higgs differs from the SM Higgs in terms of the relative contributions from different production mechanisms and decay branching fractions. In particular, $b\bar{b}$ -associated production followed by decay into a $\tau^+\tau^-$ pair gets enhanced because Higgs couplings to down-type fermions and third generation fermions increase

with $\tan\beta$. Additional exclusions were obtained from searches for the MSSM-specific effects affecting the decays into $b\bar{b}$ and $\mu^+\mu^-$. Charged Higgses, predicted by the MSSM, were searched for in the decay channels $H^\pm \rightarrow \tau^\pm\nu$, $H^\pm \rightarrow cs$ and $H^\pm \rightarrow tb$ [29]. The combination of all these results severely constrain the available MSSM parameter space in the Higgs sector, although the hypothesis that the only discovered boson so far is in fact the lighter of the two scalar Higgses of the MSSM cannot be ruled out completely.

Other, non-minimal supersymmetric models have been constrained as well. This includes in particular the Next-to-Minimal Supersymmetry (NMSSM), predicting a light Higgs scalar decaying into a pair of light Higgs pseudoscalars, with a final state consisting of 4 muons, $h \rightarrow aa \rightarrow 4\mu$. Such decay chain, once thought to be an alternative to the SM/MSSM scenario that should attract physicists' main attention in case the LHC fails to observe Higgs signal in one of its mainstream SM channels, is inconsistent with the data [30]. An upper limit has been set on the cross section for standalone light pseudoscalar Higgs production via gluon fusion followed by decay into a muon pair, $\sigma(pp \rightarrow a)Br(a \rightarrow \mu^+\mu^-)$, which translates into further limits in the NMSSM parameter space [31].

Explicit searches for Higgs anomalous couplings have been carried. Higgs production in association with a single top quark (and a light quark jet) is particularly sensitive to the relative sign of the Higgs boson coupling to fermions and bosons and to the value itself of the Higgs to top coupling. Such studies were carried independently based on the $b\bar{b}$ and $\gamma\gamma$ decay modes, but their results were inconclusive [25].

Inconsistency of the Higgs boson with models assuming the existence of a fourth lepton generation, as well as fermiophobic Higgs models, was shown early on [32]. Other dedicated searches include heavy scalar and pseudoscalar Higgses in a general two-doublet model (2HDM), doubly charged Higgses, invisible decays of the SM-like Higgs and lepton flavor violating decays and were translated into respective exclusion limits [33].

To summarize, consistency of all the data with the Standard Model holds invariably in what regards Higgs physics. Most key analyses have already been performed on the whole 7+8 TeV dataset and so the main conclusions are unlikely to change significantly anytime before late 2015. No hints of new physics have been observed, whether in the Higgs sector, or for that matter in the many non-Higgs related searches carried at both ATLAS and CMS (for a review of the latter the reader is referred elsewhere [34] [35]). On the other hand, plenty of room for new physics is still there to be unraveled at some higher energy, or even possible to show up eventually at the currently available energy if only more LHC luminosity was available. There are no clear indications so far as to what this physics beyond the Standard Model might be. Contrary to SUSY, which may not provide any measurable hints of new physics unless by an increase of energy, SILH models in general predict new physics in both ways. The second phase of the LHC, due to start in 2015, will increase both the energy and the luminosity and has chances to solve the puzzle.

There is one more important thing to learn from the spin-parity analyses in particular. Since the $H \rightarrow W^+W^-$ channel offers relatively little sensitivity to the Higgs spin-parity, the same weakness is bound to apply to measurements of W helicity in the final state. Even more difficult this will become in the most interesting high mass region where the W 's are more boosted. Separation of W helicities in WW scattering requires other techniques to be used.

3.2 Electroweak physics results

Both ATLAS and CMS have produced a large number of results concerning gauge boson production in general [36]. The most directly relevant for us are those concerning diboson and triboson production. Their importance for the study of VV scattering is twofold. Measurements of total cross sections for diboson production cross check our calculations of irreducible background. More specific analyses of the respective kinematic distributions allow to place limits on anomalous triple and quartic vector boson couplings.

In what regards triboson production, 95% CL limits were set at CMS on anomalous quartic couplings for $WW\gamma\gamma$, $WWZ\gamma$ [37]. These were based by searches for the $WW\gamma$ and $WZ\gamma$ final states, respectively. There is no directly equivalent limit so far on the $WWWW$ coupling, i.e., based on a measurement of triboson WWW production, either from ATLAS or CMS.

Results abound as far as diboson production is concerned. Let us review the most important of them. The total inclusive W^+W^- cross section at 7 TeV as measured by CMS was found to be [38]

$$\sigma(pp \rightarrow W^+W^-)|_{7TeV} = 52.4 \pm 2.0(stat) \pm 4.5(syst) \pm 1.2(lumi)^2 \text{ pb},$$

which is consistent within the errors with Standard Model predictions in the next-to-leading order, including the two main production mechanisms of quark-antiquark annihilation and gluon-gluon fusion. That the measured value is actually marginally higher than the prediction can be ascribed to other production mechanisms such as: diffractive production, double parton scattering, QED exclusive production, and Higgs boson production with decay to W^+W^- , expected to yield additional contributions up to about 5% altogether. The ATLAS Collaboration measured [39]

$$\sigma(pp \rightarrow W^+W^-) = 51.9 \pm 2.0(stat) \pm 3.9(syst) \pm 2.0(lumi) \text{ pb}.$$

The total $pp \rightarrow ZZ$ cross section at $\sqrt{s} = 7$ TeV was measured to be

$$\begin{aligned} \sigma(pp \rightarrow ZZ)|_{7TeV} &= 6.24 \pm_{0.80}^{0.86}(stat) \pm_{0.32}^{0.41}(syst) \pm 0.14(lumi) \text{ pb (CMS) [40], and} \\ \sigma(pp \rightarrow ZZ)|_{7TeV} &= 6.7 \pm 0.7(stat) \pm_{0.3}^{0.4}(syst) \pm 0.3(lumi) \text{ pb (ATLAS) [41].} \end{aligned}$$

The inclusive $W^\pm Z$ production cross section from CMS was [42]

$$\sigma(pp \rightarrow WZ)|_{7TeV} = 20.76 \pm 1.32(stat) \pm 1.13(syst) \pm 0.46(lumi) \text{ pb},$$

and from ATLAS it was [43]

$$\sigma(pp \rightarrow WZ)|_{7TeV} = 19.0 \pm_{1.3}^{1.4}(stat) \pm 0.9(syst) \pm 0.4(lumi) \text{ pb}.$$

All the ZZ and WZ cross sections are consistent with Standard Model NLO predictions.

Sadly, there is no dedicated measurement of the much lower same-sign WW production, although some bounds on it can be in principle indirectly inferred using a combined measurement of $WW + WZ$ based on events with a W decaying leptonically and two jets. Unfortunately, these measurements [44] are of not enough precision to extract the tiny same-sign WW contribution.

²Errors labeled *lumi* are those related to the LHC luminosity measurement.

Finally, the $W\gamma$ and $Z\gamma$ cross sections are [45]:

$\sigma(pp \rightarrow W\gamma)|_{7TeV} \times Br(W \rightarrow l\nu) = 37.0 \pm 0.8(stat) \pm 4.0(syst) \pm 0.8(lumi)$ pb (CMS), and

$\sigma(pp \rightarrow Z\gamma)|_{7TeV} \times Br(Z \rightarrow ll) = 5.33 \pm 0.08(stat) \pm 0.25(syst) \pm 0.12(lumi)$ pb (CMS).

The ATLAS collaboration does not quote their total cross section values, but restricts the measurements to a predefined fiducial region. In any case, no deviations from the SM were observed [46].

At 8 TeV, CMS measured [47]:

$\sigma(pp \rightarrow W^+W^-)|_{8TeV} = 69.9 \pm 2.8(stat) \pm 5.6(syst) \pm 3.1(lumi)$ pb,

$\sigma(pp \rightarrow ZZ)|_{8TeV} = 8.4 \pm 1.0(stat) \pm 0.7(syst) \pm 0.4(lumi)$ pb, and

$\sigma(pp \rightarrow WZ)|_{8TeV} = 24.61 \pm 0.76(stat) \pm 1.13(syst) \pm 1.08(lumi)$ pb [42].

The W^+W^- value is slightly higher than the Standard Model NLO prediction of $57.3^{+2.3}_{-1.6}$ pb, but again an extra 5% increase of this value is expected from the additional contributions calculated at the next-to-next-to-leading order, chiefly from Higgs boson production. Explanations in terms of new physics have also been suggested, but are not quite convincing. The ZZ and WZ values agree with Standard Model NLO predictions within the errors. ATLAS showed:

$\sigma(pp \rightarrow W^+W^-)|_{8TeV} = 71.4 \pm 1.2(stat)^{+5.0}_{-4.4}(syst) \pm 2.2(lumi)$ pb [48],

$\sigma(pp \rightarrow ZZ)|_{8TeV} = 7.1 \pm 0.5(stat) \pm 0.3(syst) \pm 0.2(lumi)$ pb [49], and

$\sigma(pp \rightarrow WZ)|_{8TeV} = 20.3 \pm 0.8(stat) \pm 1.2(syst) \pm 0.7(lumi)$ pb [50].

Limits on anomalous triple gauge couplings, and in particular the ones of most direct relevance for us, namely WWZ and $WW\gamma$, have been derived so far from the 7 TeV data. An up-to-date summary of these measurements, together with a set of references to the original papers, is available in Refs. [55]. Also included in the summary are the respective results from the TeVatron and LEP. In all these works, anomalous couplings were studied within the formalism known as the effective Lagrangian approach, in which the most general form of the WWZ/γ vertex is considered, including all terms that respect Lorentz invariance and conserve C and P . The couplings are taken to be constant parameters of the Lagrangian and therefore independent of the boson momenta. The conceptual basis of this approach is explained in detail in Ref. [61]. Accordingly, experimental limits are set on five quantities: Δg_1^Z , $\Delta\kappa_Z$, λ_Z , $\Delta\kappa_\gamma$ and λ_γ . The first three of these modify the WWZ vertex, the following two modify the $WW\gamma$ vertex. In the SM, $\lambda_Z = \lambda_\gamma = 0$ and $g_1^Z = \kappa_Z = \kappa_\gamma = 1$. Their actual values are determined from studies of diboson production processes for which these vertices play a primary role, namely WW , WZ and $W\gamma$. An anomalous triple gauge coupling would be manifest in the rate of diboson production at high boson p_T and invariant mass. Typically, it is ascertained in CMS by a one-dimensional evaluation of the p_T spectrum of the leading lepton or of the dijet (both from W/Z decay) or of the photon. For the theoretical calculation of the expected spectrum, either one or two anomalous parameters are varied at a time. Correlations between couplings that contribute to the same vertex are rather weak and so one-dimensional

limits are generally sufficient.

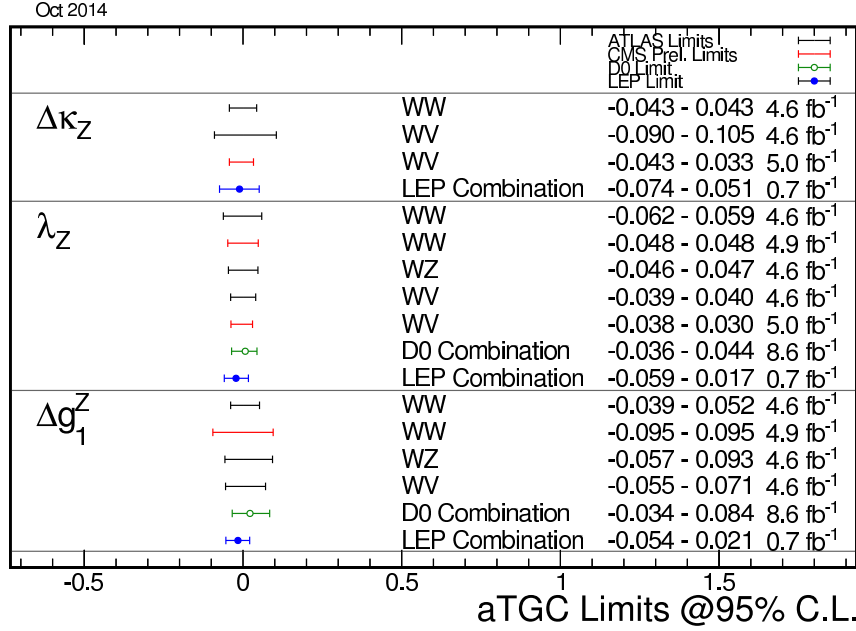


Figure 3.4: Current limits on the anomalous couplings that contribute to the WWZ vertex - compilation of results coming from LEP, TeVatron and LHC experiments. Image reproduced from Ref. [55].

While all these parameters may be probed independently in experiment, considerations of gauge symmetry induce additional relations between them:

$$\lambda_Z = \lambda_\gamma, \quad (3.1)$$

$$\Delta\kappa_Z = \Delta g_1^Z - \Delta\kappa_\gamma \tan^2\theta_W. \quad (3.2)$$

From this it follows that, e.g., measurement of WWZ couplings could be translated into $WW\gamma$ couplings on theoretical grounds.

3.3 Other results of relevance for the study of VV scattering

For the correct assessment of reducible backgrounds, several other measurements are as important. Let us only mention the ones we will directly refer to in this work.

Top production has been measured in several final states, including different W decay channels [51]. The most accurate inclusive $t\bar{t}$ production cross sections come from the dilepton final state. CMS reports [52]

$$\sigma(pp \rightarrow t\bar{t})|_{7TeV} = 162 \pm 2(stat) \pm 5(syst) \pm 4(lumi) \text{ and}$$

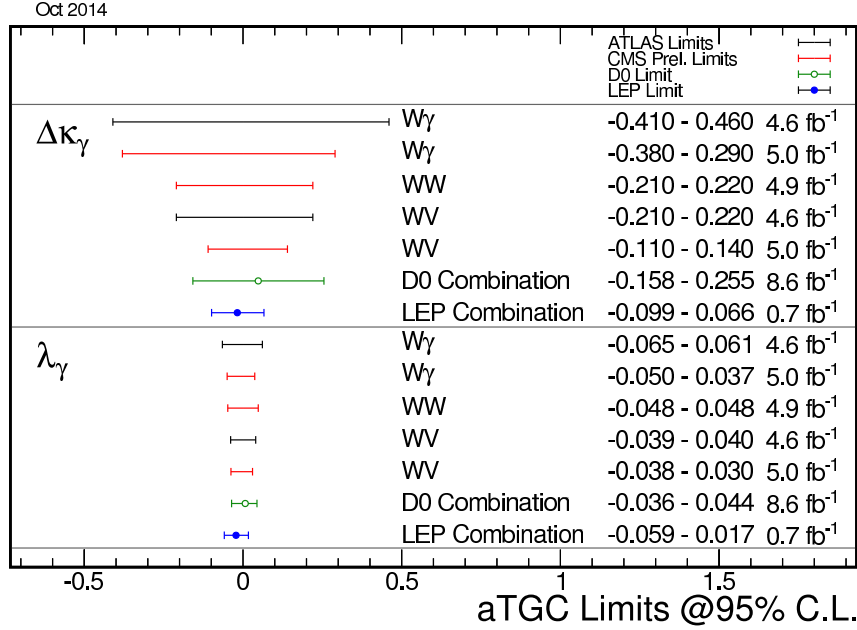


Figure 3.5: Current limits on the anomalous couplings that contribute to the $WW\gamma$ vertex - compilation of results coming from LEP, TeVatron and LHC experiments. Image reproduced from Ref. [55].

$$\sigma(pp \rightarrow t\bar{t})|_{8TeV} = 239 \pm 2(stat) \pm 11(syst) \pm 6(lumi) \text{ (from 5.3/fb of data).}$$

ATLAS measured [53]

$$\sigma(pp \rightarrow t\bar{t})|_{7TeV} = 177 \pm 3(stat) \pm_7^8(syst) \pm 7(lumi) \text{ and}$$

$$\sigma(pp \rightarrow t\bar{t})|_{8TeV} = 238 \pm 2(stat) \pm 7(syst) \pm 7(lumi).$$

The numbers are in good agreement with NNLO+NNLL calculations by Czakon et al. [54], where the quoted uncertainty of the latter is roughly the size of experimental errors.

A lot of other results indirectly relate to our subject. Important feedback is obtained in particular from forward physics where jet multiplicity and kinematics obtained from common event generators can be cross checked in detail against the data. These things however play a rather secondary role for us and we need not go through them here.

3.4 The VV interaction and why it is still interesting

In the previous chapter we have sketched the derivation of the Higgs boson using two independent approaches: from the principle of $SU(2) \times U(1)$ gauge invariance and from the requirement of tree level unitarity of all Standard Model processes. The paramount phenomenological manifestation of the underlying model is the existence of a physical scalar particle which couples to all known particles of non-zero mass in a completely determined way. Such particle manifests itself in a twofold way. At energies available in the LHC to date it should be produced in proton-proton collisions via different physical

mechanisms, each of them yielding partly identifiable experimental signatures, and decay into known Standard Model particles, with both production cross sections and branching fractions completely determined by its mass. A good candidate for such particle has indeed been found. The other manifestation will become available at higher energy and help answer the main question: is this the same particle?

3.4.1 Higgs mass and couplings in VV scattering

The second phenomenological manifestation of the Standard Model Higgs boson resides in the high energy behavior of the VV scattering amplitudes. In the Standard Model the HWW coupling is chosen such that it fully cancels the quadratic divergencies that appear after combining photon and Z exchange graphs with the four- W contact interaction. Thus, it is precisely the same particle which has been discovered at the LHC that is supposed to provide these *exact* cancelations. Violation of unitarity at some high enough energy will be the most extreme (and unrealistic) manifestation of the still existing problem should this cancelation not be the case. But let us put questions of unitarity aside, as they in fact represent a technical issue. The entire high energy behavior of the VV scattering amplitude is a fully quantitative question and depends on many inputs. Total and differential cross sections for the scattering of longitudinally polarized W and Z gauge bosons, at energies much larger than the masses of the latter, are a major experimental field where consistency of the Standard Model has to be tested. To this date we have practically no experimental data to confirm that the Higgs boson indeed does its job, assigned to it by the Standard Model.

A simple tree level calculation of the process $W_L^+ W_L^+ \rightarrow W_L^+ W_L^+$ reveals two basic facts. The total cross section as a function of the center of mass energy behaves differently depending on both the Higgs mass and Higgs couplings. As long as the HWW coupling is exactly 1, expressed in units of the value predicted by the Standard Model, the amplitude keeps rising up to the energy equivalent to the Higgs mass (notice that for $M_H < 2M_W$ it in practice never does so), then stays approximately flat. Phase space causes the cross section fall for higher energies. In the absence of a Higgs boson the amplitude rises indefinitely and so does the cross section. It can be calculated that unitarity violation occurs at about a 1.2 TeV energy and thus some new physics is bound to enter before this scale. Put in a more physical language, unless the scattering amplitude receives new contributions that reduce the amplitude way before this point, the WW interaction before the scale of 1.2 TeV inevitably becomes strong. The term “strong” specifically means that multiple rescattering is likely to occur. This means a difference in the basic dynamics of electroweak symmetry breaking compared to the Standard Model case where it is supposed to be “soft” and a single Higgs boson exchange takes place instead. We would talk then of a strongly interacting gauge sector. An even more interesting scenario occurs if the HWW coupling is different from 1. As we already know, in such case the quadratic terms in the amplitude are not completely canceled and this incomplete cancelation must show up at a high enough energy. In general, the total cross section will rise up to the Higgs mass (not if $M_H < 2M_W$), fall past the Higgs mass and rise up again at some energy. The situation again calls for new physics as the unitarity limit would be still inevitably hit at some energy whose precise value depends on the value of the coupling. The unrealistic by now, extreme case of no Higgs boson at all is technically equivalent to setting either an

infinite Higgs mass or a zero coupling. Relative to the SM prediction, the cross section will be enhanced at all energies as long as the HWW coupling is lower than the SM one and will reveal an energy pattern consisting of a depletion followed by a turning point and an enhancement if the HWW coupling is larger than the SM one. This is because in the latter case there is an overcancelation of the quadratic divergence by the Higgs graph which subtracts from the constant term in the total amplitude. At a certain energy the quadratic term becomes dominant anyway and asymptotically the cross sections for a given g_{HWW} and for $1 - g_{HWW}$ become the same.

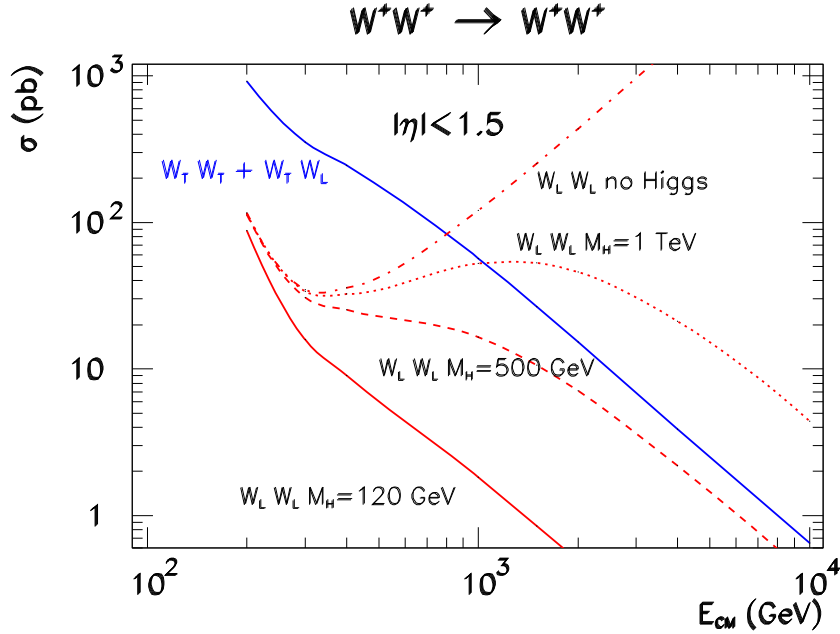


Figure 3.6: The total W^+W^+ scattering cross sections as a function of the center of mass energy for different final (and initial) state polarizations and for different Higgs masses, including the limiting Higgsless case. Assumed are two on-shell, unpolarized, colliding W^+ beams. A cut on the scattering angle that corresponds to pseudorapidity of ± 1.5 with respect to the incoming W direction was applied. The individual $W_T W_T + W_T W_L$ curves for each Higgs mass value coincide within the width of the blue line. Results of MadGraph [121] calculations.

Angular distributions of the scattered W 's are also sensitive to the mass and couplings of the Higgs boson. In the Standard Model with a light Higgs, the scattering occurs predominantly at small angles. A signature of any rise of the total cross section at some high energy is visible as the appearance of an additional component that tends to favor large scattering angles, with a local maximum at 90° . Thus any deviation from the Standard Model in terms of the Higgs couplings would be, quite similarly like different Higgs masses, observable as a correspondent excess in the rate of $W_L W_L$ scattered at large angles. The excess is the more pronounced the higher the energy. In the above demonstration of the principles, we have arbitrarily chosen same-sign WW scattering (in the next chapters we will see that this choice is in fact well motivated), but the same basic qualitative features are expected of the other scattering processes, involving W^+W^- , WZ

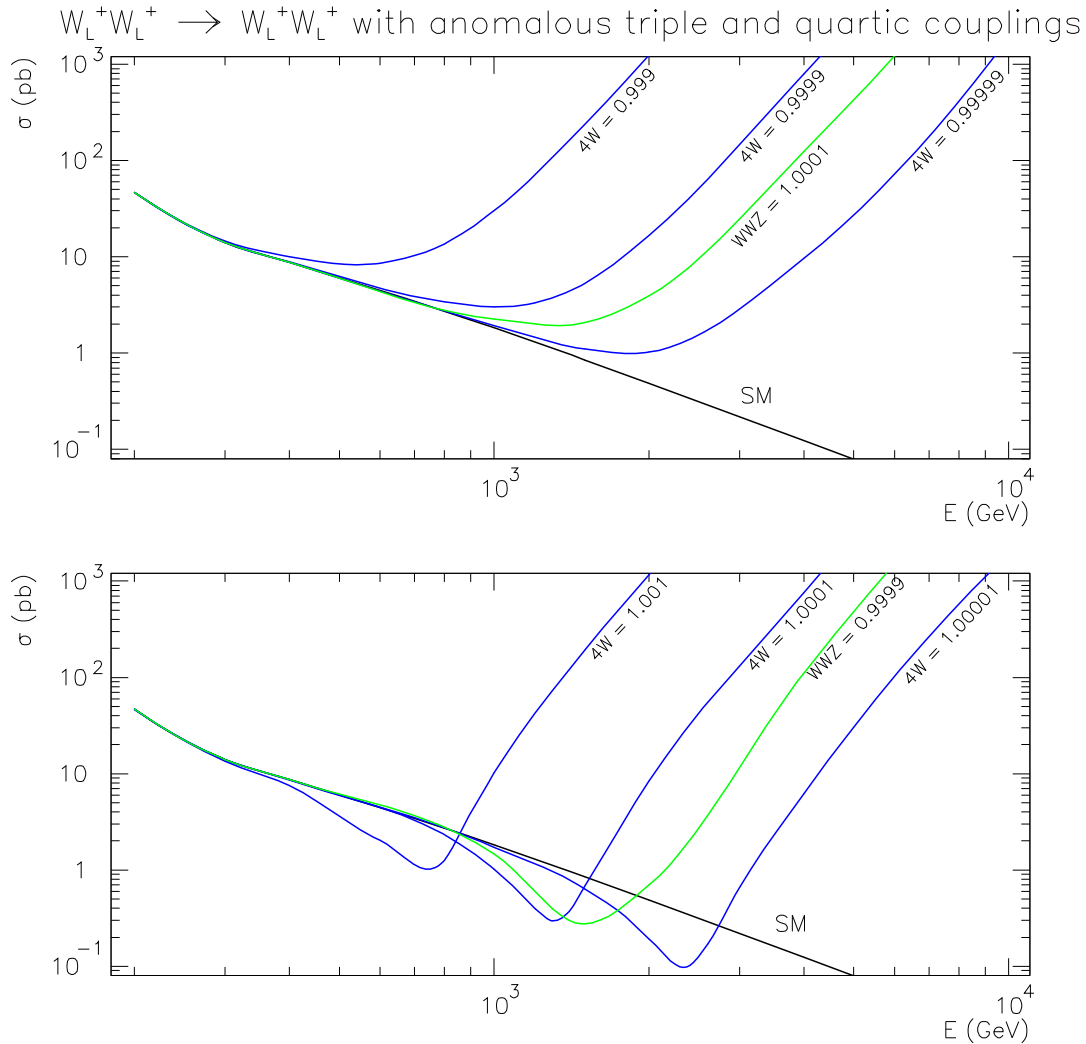


Figure 3.8: Total $W_L^+ W_L^+$ scattering cross section as a function of the center of mass energy for different values of the $WWWW$ quartic coupling (labeled $4W$, blue curves) and the WWZ triple coupling (labeled WWZ , green curves). The corresponding couplings are scaled by a constant factor relative to their respective Standard Model values. Assumed here are two colliding on-shell, unpolarized W^+ beams and a 120 GeV Higgs boson. A cut on the scattering angle that corresponds to pseudorapidity of ± 1.5 with respect to the incoming W direction was applied. Results of MadGraph calculations.

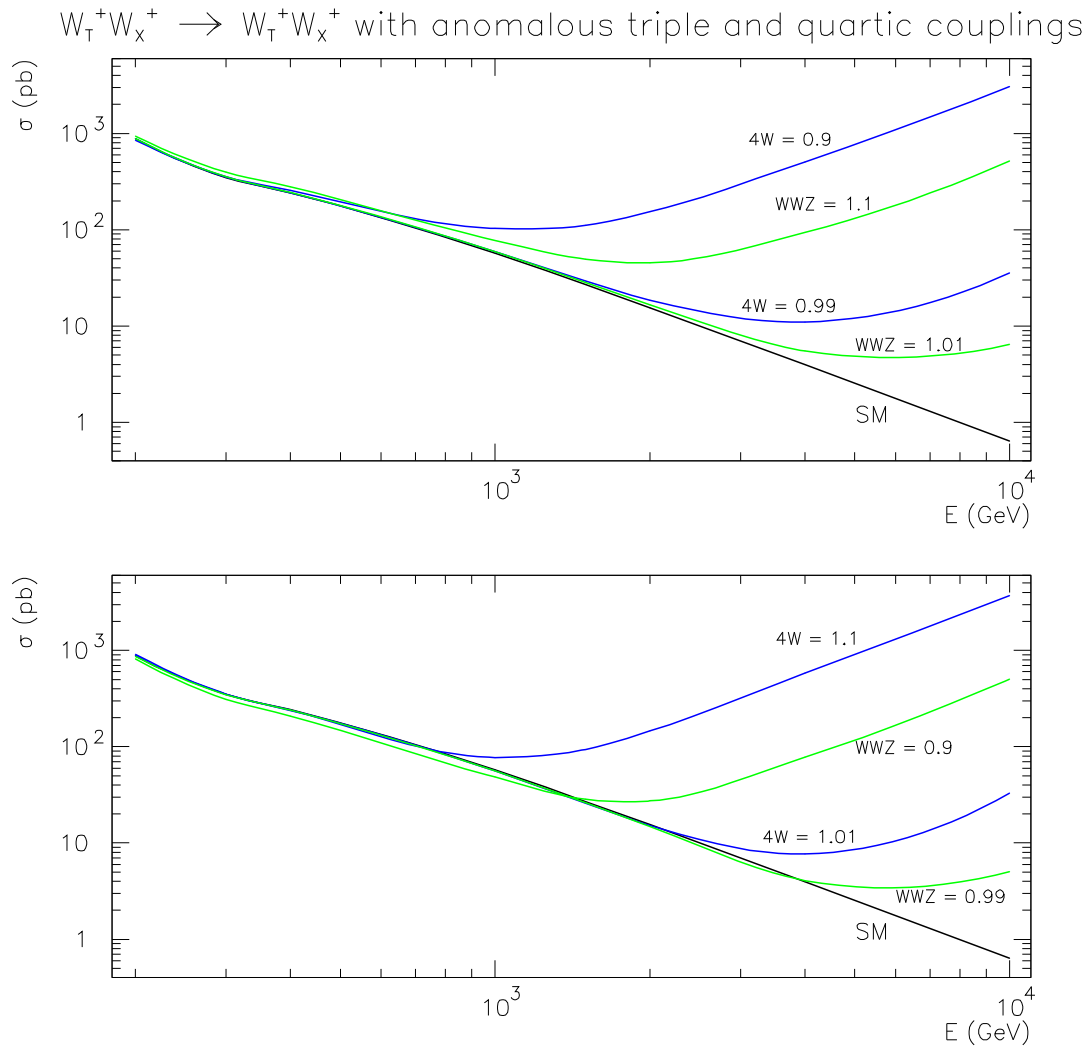


Figure 3.9: The total $W_T^+ W_X^+$ scattering cross section as a function of the center of mass energy for different values of the $WWWW$ quartic coupling (labeled $4W$, blue curves) and the WWZ triple coupling (labeled WWZ , green curves). The corresponding couplings are scaled by a constant factor relative to their respective Standard Model values. Assumed here are two colliding on-shell, unpolarized W^+ beams and a 120 GeV Higgs boson. A cut on the scattering angle that corresponds to pseudorapidity of ± 1.5 with respect to the incoming W direction was applied. Results of MadGraph calculations.

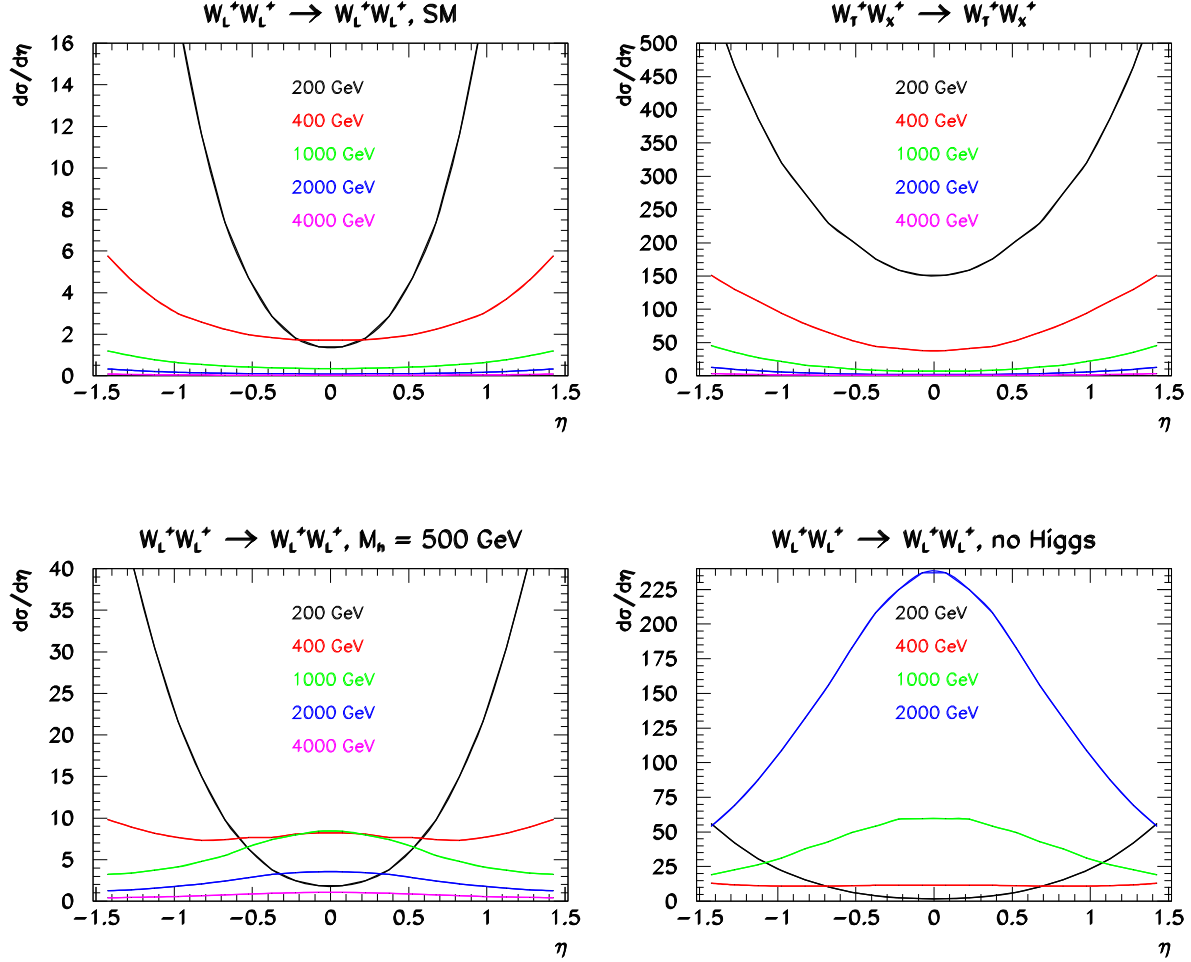


Figure 3.10: Examples of angular distributions of the scattered W^+W^+ pairs (pseudorapidities with respect to the incoming W^+W^+ direction) at different center of mass energies, depending on the value of the Higgs mass. SM-like couplings were assumed in all the cases. **Top left:** $W_L^+W_L^+$ with a 120 GeV Higgs. **Top right:** $W_T^+W_X^+$ (here subscript X denotes any polarization, T or L). **Bottom left:** $W_L^+W_L^+$ with a 500 GeV Higgs. **Bottom right:** $W_L^+W_L^+$, Higgsless case. The blue curve in the last plot already involves unitarity violation and therefore is unphysical. Results of MadGraph calculations.

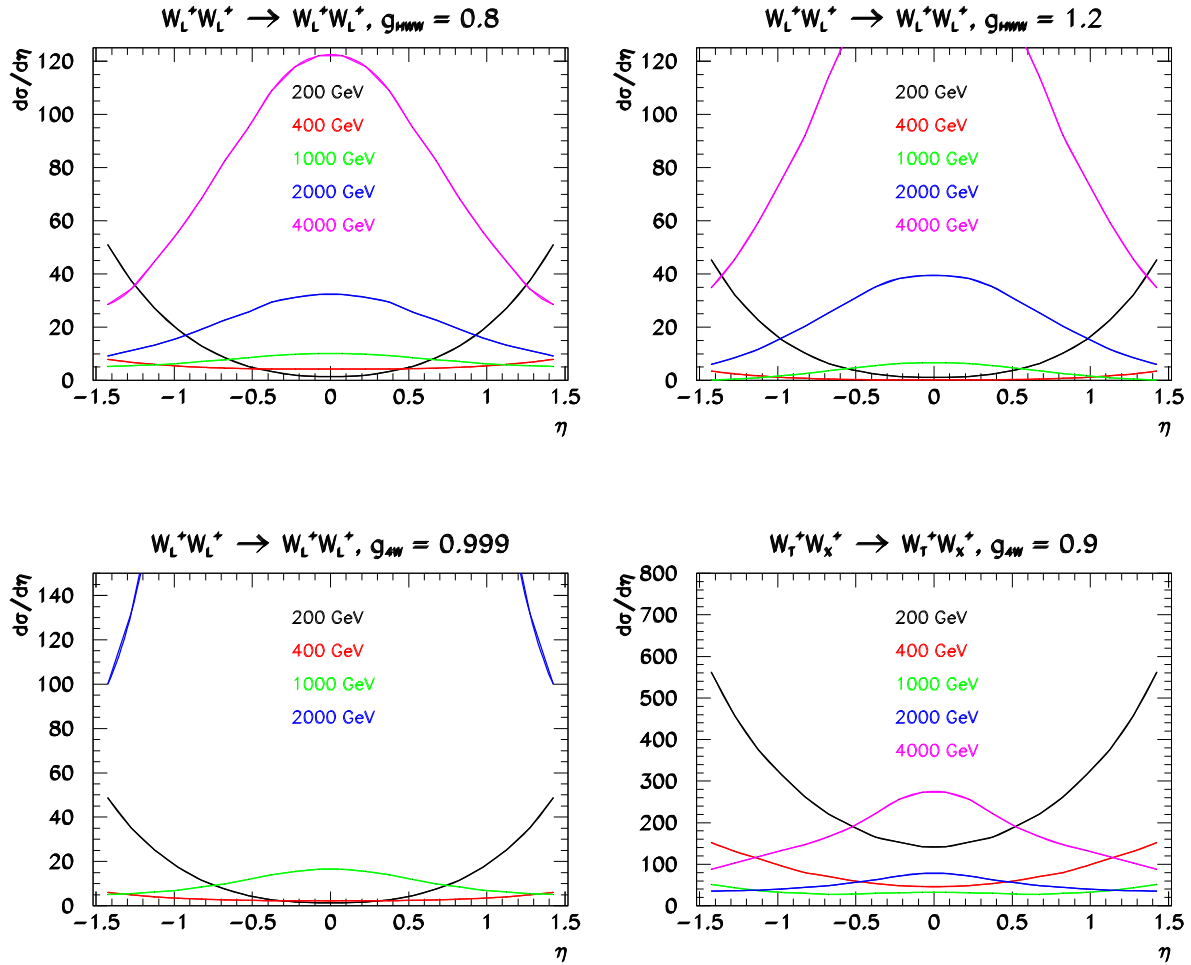


Figure 3.11: Examples of angular distributions of the scattered W^+W^+ pairs (pseudorapidities with respect to the incoming W^+W^+ pair direction) at different center of mass energies, depending on the Higgs and gauge couplings. A 120 GeV Higgs boson was assumed in all the cases. **Top left:** $W_L^+W_L^+$ with the HWW coupling equal to 0.8 times its SM value. **Top right:** $W_L^+W_L^+$ with the HWW coupling equal to 1.2 times its SM value. **Bottom left:** $W_L^+W_L^+$ with the SM $WWWW$ coupling scaled by a factor of 0.999 (the partially visible blue curve involves unitarity violation and therefore is unphysical). **Bottom right:** $W_T^+W_X^+$ with the SM $WWWW$ coupling scaled by a factor of 0.9. Results of MadGraph calculations.

measured via Higgs partial width measurements, the latter can be probed independently via measurements of diboson and triboson production. Consistency of the three types of measurements: Higgs couplings, multiboson production and vector boson scattering at high energy is an important closure test for any consistent physical theory and should be rigorously tested.

There is at least one fundamental difference between the phenomenology of scaled Higgs couplings and that of non-SM gauge couplings. The former manifests solely in $W_L W_L$ pairs, ultimately as an enhancement with energy. In the latter, there is always a combination of two effects. One is still the energy dependence of $W_L W_L$, which in this case is even steeper because the leading divergence now goes like the fourth power of energy (to begin with, we are assuming a simple scaling of the SM couplings by a constant factor), the other is the overall energy-independent normalization constant which affects in principle all helicity combinations in the same way. This will be mainly observable in $W_T W_T$ pairs, because they are the most abundant. Because however such normalization shifts will be much better measurable in the total diboson production than in boson-boson scattering, this effect is of lesser interest for us. Mixed $W_T W_L$ pairs will be modified in both ways: in the overall normalization and as a rise at high energy (remember that each W_L intrinsically carries energy dependence!). Therefore, in the general case, both $W_T W_X$ as well as $W_L W_L$ may be of interest. Moreover, angular distributions in vector boson scattering (VBS) processes exhibit similar qualitative features for $W_T W_X$ and $W_L W_L$ pairs in the scenario with a modified quartic coupling. The leading divergence in a VBS process is the same in case of an anomalous quartic coupling as for an anomalous triple gauge coupling. Put another way, for every anomalous quartic coupling, there is an equivalent value of the triple couplings that asymptotically produces the same effect. As long as we restrict ourselves to pure VBS processes and scaling individual SM couplings by constant factors, energy dependence of $W_L W_L$ pairs still carry the most information. This is because of their much steeper energy dependence which very quickly dwarfs any effects in $W_T W_X$. But, as we will see in the next chapter, a clean VBS sample is impossible to isolate in a real experiment. And new physics is likely to modify different couplings in a correlated way.

New physics may manifest itself in new interactions between gauge bosons. These interactions should show up indirectly as certain combinations of modified effective gauge boson couplings and Higgs to gauge couplings. We don't know the underlying new physics, but we do have a theoretical machinery to parametrize it in a model independent way. This is where Effective Field Theory comes back. Once again, this general framework has enough flexibility to describe the low energy phenomenology of new physics regardless of what it really is.

A modern effective quantum field theory for physics beyond the Standard Model can be written down in terms of an extended Lagrangian [57]

$$\mathcal{L} = \mathcal{L}_{SM} + \sum_i \frac{c_i}{\Lambda^2} \mathcal{O}_i + \sum_j \frac{f_j}{\Lambda^4} \mathcal{O}_j + \dots \quad (3.3)$$

where \mathcal{O}_i are dimension-six operators, \mathcal{O}_j are dimension-eight operators, the coefficients c_i, f_j are dimensionless and Λ is the energy scale of new physics. The Standard Model is recovered in the limit $\Lambda \rightarrow \infty$ and the entire model is bound to capture all the low-energy effects of physics beyond the Standard Model. By dimensional analysis one expects

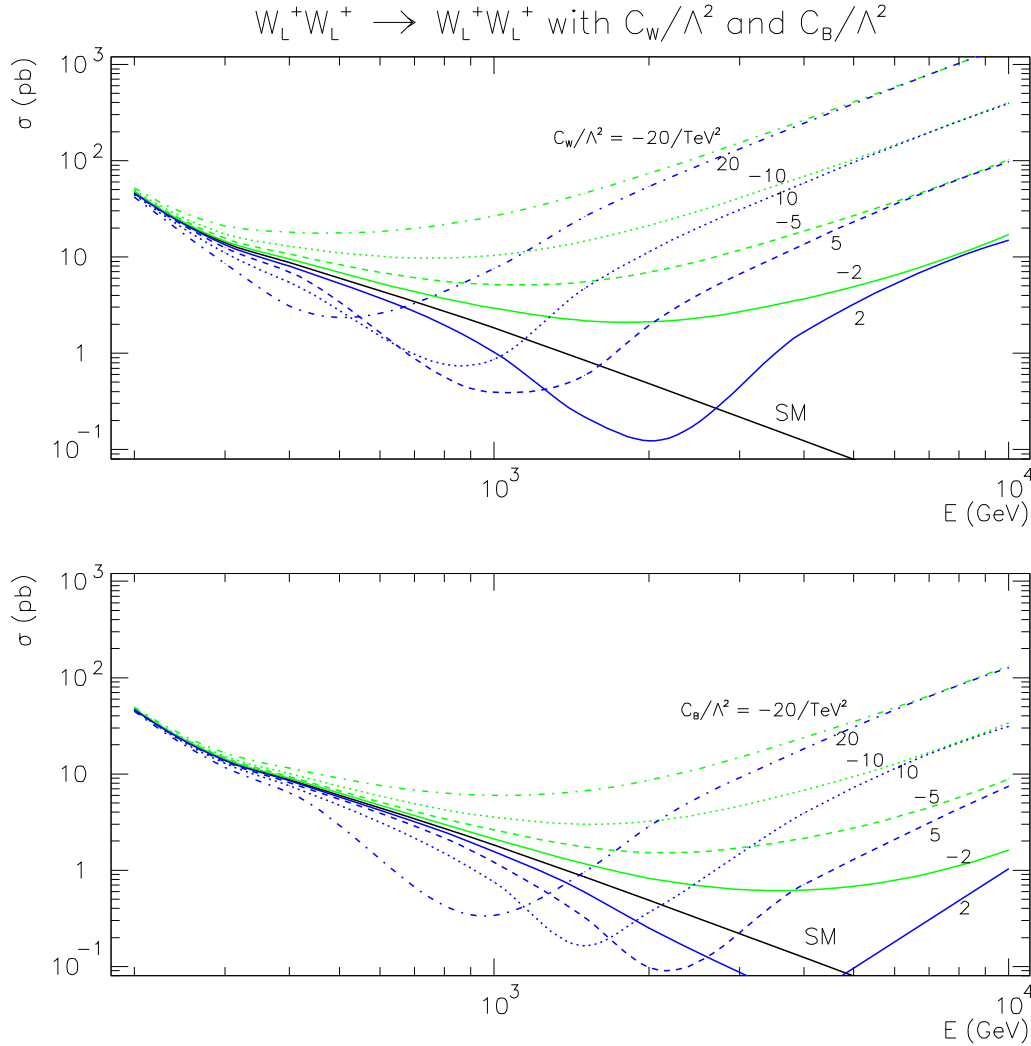


Figure 3.12: The total $W_L^+ W_L^+$ scattering cross section as a function of the center of mass energy for different values of the relevant dimension-6 operators in the W Effective Field Theory approach. Varied are: C_W/Λ^2 (upper plot) and C_B/Λ^2 (lower plot). Assumed here are two colliding on-shell, unpolarized W^+ beams and a 120 GeV Higgs boson. A cut on the scattering angle that corresponds to pseudorapidity of ± 1.5 with respect to the incoming W direction was applied. Results of MadGraph calculations.

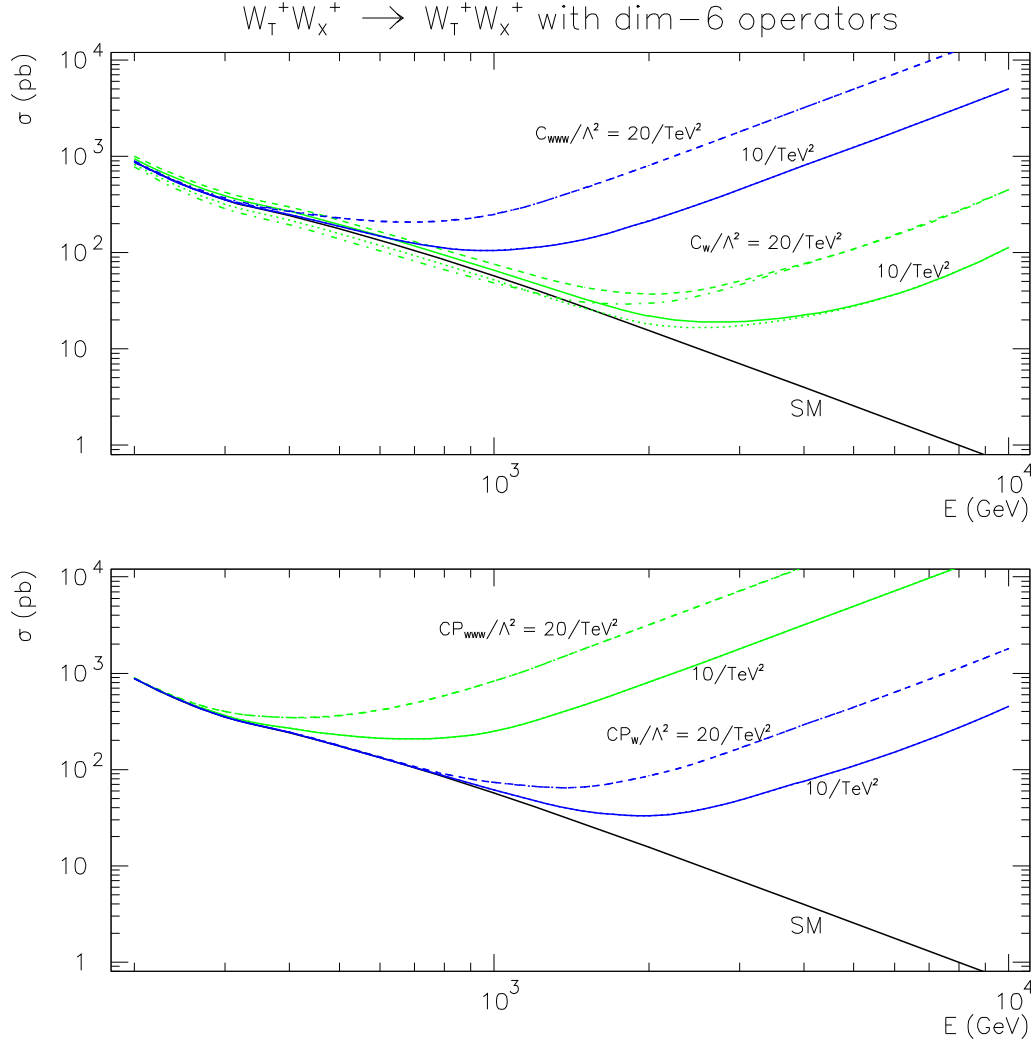


Figure 3.13: The total $W_T^+ W_X^+$ scattering cross section as a function of the center of mass energy for different values of the relevant dimension-6 operators in the W Effective Field Theory approach. Varied are: C_W/Λ^2 , C_{WWW}/Λ^2 (upper plot), CP_W/Λ^2 and CP_{WWW}/Λ^2 (labeled CP_W and CP_{WWW} , lower plot). Assumed here are two colliding on-shell, unpolarized W^+ beams and a 120 GeV Higgs boson. The rises at high energy are due to the $W_T^+ W_L^+$ combination, total normalization effects are predominantly due to $W_T^+ W_T^+$. A cut on the scattering angle that corresponds to pseudorapidity of ± 1.5 with respect to the incoming W direction was applied. Results of MadGraph calculations.

the lowest dimensional, hence dimension-6, operators to be dominant, since all higher dimension operators are suppressed by higher powers of Λ . However, different gauge boson interactions may or may not probe some or any of these operators, and so going to dimension 8 is necessary for a more complete description (only even-dimensional operators conserve lepton and baryon number). Operators $\mathcal{O}_i, \mathcal{O}_j$ are constructed from known fields, that is, particles of the Standard Model. Discovery of a new particle should result in revision of the model and inclusion of additional operators.

All related BSM phenomenology is described in a way which depends only on the ratios c_i/Λ^2 or f_j/Λ^4 . However, practical usefulness of an effective quantum field theory is restricted up to energies of order Λ . At energies higher than that, operators of arbitrary high dimension become important, because they are no longer suppressed. The quantity Λ characterizes a particular theory. While we don't know the scale at which new physics sets in, parameters of the form c_i/Λ^2 and f_j/Λ^4 have calculable intrinsic validity bounds defined by the unitarity condition. These bounds fix the maximum allowed value of the scale Λ that is relevant should new physics arise from any particular higher dimension operator. In an alternative formulation, sometimes called the Lagrangian approach [58], the anomalous couplings are taken to be constant Lagrangian parameters. There is no explicit relation to the scale of new physics and this formalism is applicable in the approximation in which these parameters do not depend on energy.

The Effective Field Theory approach has been gaining wide recognition in recent time, with more and more studies of sensitivity to BSM being expressed in this language. All possible independent dimension-6 operators constructed from the known fields have been catalogued [59]. There are just three dimension-6 operators that conserve both C and P and affect the interactions of gauge bosons. Following the notation used elsewhere in literature, these can be written as:

$$\mathcal{O}_{WWW} = \text{Tr}[W_{\mu\nu}W^{\nu\beta}W_{\beta}^{\mu}], \quad (3.4)$$

$$\mathcal{O}_W = (D_{\mu}\Phi)^{\dagger}W^{\mu\nu}(D_{\nu}\Phi), \quad (3.5)$$

$$\mathcal{O}_B = (D_{\mu}\Phi)^{\dagger}B^{\mu\nu}(D_{\nu}\Phi). \quad (3.6)$$

In the above, Φ is the Higgs doublet field and

$$W_{\mu\nu} = \frac{ig}{2}\sigma^a(\partial_{\mu}W_{\nu}^a - \partial_{\nu}W_{\mu}^a + g\epsilon_{abc}W_{\mu}^bW_{\nu}^c), \quad (3.7)$$

$$B_{\mu\nu} = \frac{ig'}{2}(\partial_{\mu}B_{\nu} - \partial_{\nu}B_{\mu}); \quad (3.8)$$

σ^a are Pauli matrices and g, g' are the SU(2) and U(1) gauge couplings, respectively. Two additional operators appear if we do not assume C and P conservation:

$$\mathcal{O}_{\tilde{W}WW} = \text{Tr}[\tilde{W}_{\mu\nu}W^{\nu\beta}W_{\beta}^{\mu}], \quad (3.9)$$

$$\mathcal{O}_{\tilde{W}} = (D_{\mu}\Phi)^{\dagger}\tilde{W}^{\mu\nu}(D_{\nu}\Phi). \quad (3.10)$$

Here the dual field strengths are defined as $\tilde{V}_{\mu\nu} = \frac{1}{2}\epsilon_{\mu\nu\rho\sigma}V^{\rho\sigma}$.

Typically, one such operator modifies more than one interaction vertex and vice-versa, each interaction receives the contributions from more than one higher-dimension operator. There is some arbitrariness in the way all these operators are defined. Recently it was noted [60] that the most useful formulation, at least from an experimental point of view, could be one obtained by choosing a basis of higher-dimension operators such that they match closely the measured processes, ideally in a one-to-one correspondence. Such approach would allow to study one vertex at a time and spare from the additional work of combining data from different processes in order to study the potential effects of a single operator. This interesting approach is still in the lounge, waiting for being implemented in commonly accessible event generators and used in data analyses, and hence will not be applied in this work.

It is transparent that VV scattering processes are not the best channels to study operators involving modifications of triple gauge couplings. Much better statistical significance can be obtained by measuring the total diboson production, i.e., not necessarily in the VBS mode. It is actually non-VBS diboson production that produces the most stringent limits on these parameters to present day, with currently existing data coming from LEP [61] and TeVatron experiments, as well as from Run 1 of the LHC. However, it is vital to know how these operators will affect the VBS measurements.

All of the above operators modify triple vector boson couplings, in addition of some of them modifying the Higgs couplings and/or the quartic vector boson couplings. Namely, \mathcal{O}_{WWW} modifies also the quartic $WWWW$ coupling, while \mathcal{O}_W modifies both the quartic and the HWW coupling. By contrast, operator \mathcal{O}_B affects neither, but it may affect other couplings, like HZZ or $HZ\gamma$. The key point that we want to emphasize and elaborate further on in this work is that each of these operators affects W_LW_L and W_TW_X pairs differently. This fact will have a paramount importance in order to interpret correctly the results of future measurements, which will - most probably - reveal a complicated combination of many effects (if anything!).

It is not difficult to tell which operators can affect W_LW_L , W_TW_T or W_TW_L vertices straight from their definition, even without deep knowledge of quantum field theory. A W field can be obtained either via a field strength $W_{\mu\nu}$ or via a Higgs field derivative. Every appearance of the field strength in the operator corresponds to transverse helicity. Longitudinal helicities enter via covariant derivatives of the Higgs field ($D_\mu\Phi$). Consequently, \mathcal{O}_B can affect only the scattering of W_LW_L pairs, while \mathcal{O}_W affects all possible helicity combinations. Operator \mathcal{O}_{WWW} has only field strengths in it, hence it affects directly only vertices involving W_TW_T . However, mixed pairs W_TW_L get also affected indirectly, via the t -channel scattering process with a Z_T exchange, in which one vertex is bound to comprise only transverse helicity states.

Although a simple scaling of a triple or quartic gauge coupling by a constant factor produces a divergence that goes like s^2 , gauge invariance enforces cancelation of the $\sim s^2$ terms for all the dimension-6 operators [62]. Consequently, the leading divergences are always proportional to s .

In the language of higher dimensional operators, the Higgs to gauge couplings can be furthermore modified via:

$$\mathcal{O}_{\Phi d} = \partial_\mu(\Phi^\dagger\Phi)\partial^\mu(\Phi^\dagger\Phi), \quad (3.11)$$

$$\mathcal{O}_{\Phi W} = (\Phi^\dagger \Phi) \text{Tr}[W^{\mu\nu} W_{\mu\nu}]. \quad (3.12)$$

Both modify HWW and HZZ vertices, but not pure gauge couplings. The first of them affects only $HW_L W_L$ vertices and will be further considered by means of a simple scaling of the HWW coupling by a constant for better transparency. The second one generates anomalous $HW_T W_X$ vertices and has no impact on $W_L W_L$. In addition, operator

$$\mathcal{O}_{\Phi B} = (\Phi^\dagger \Phi) B^{\mu\nu} B_{\mu\nu} \quad (3.13)$$

affects only HZZ , $HZ\gamma$ and $H\gamma\gamma$ of all the triple vertices and so it can be probed via ZZ scattering.

Here and in the remainder of this work we are assuming that the Higgs boson is a pure scalar. Possible admixtures from non-scalar components can be parameterized by means of an additional set of higher dimension operators. They have been constrained by the LHC Higgs data at 7 and 8 TeV, using a combination of the most sensitive Higgs decay channels. The limits were mainly driven by the ZZ and $\gamma\gamma$ channels, while standalone limits from WW in the purely leptonic decay mode are actually the weakest because in this case crucial kinematic information escapes with the two undetected neutrinos. In fact, the entire visible WW phenomenology very weakly depends on non-scalar admixture effects within the limits driven by the other decay modes. Although not necessarily negligible on their own and although potentially important from the interpretative point of view, such effects cannot make any major impact on our considerations.

Vertex, helicities	\mathcal{O}_{WWW}	\mathcal{O}_W	\mathcal{O}_B	$\mathcal{O}_{\Phi d}$	$\mathcal{O}_{\Phi W}$	$\mathcal{O}_{\Phi B}$
$HWW, W_L W_L$	-	v	-	v	-	-
$HWW, W_T W_X$	-	v	-	-	v	-
$WWZ, W_L W_L$	-	v	v	-	-	-
$WWZ, W_T W_X$	v	v	-	-	-	-
$WW\gamma, W_L W_L$	-	v	v	-	-	-
$WW\gamma, W_T W_X$	v	(v)	-	-	-	-
$WWWW, W_L W_L$	-	v	-	-	-	-
$WWWW, W_T W_X$	v	v	-	-	-	-

Table 3.1: Sensitivity to dimension-6 operators of the individual gauge and Higgs to gauge couplings that contribute to WW scattering, decomposed into helicity combinations of the interacting (initial and final) WW pair. Note that these are not necessarily the helicities at a single vertex. Helicity-flip contributions ($W_L W_L \rightarrow W_T W_X$ and $W_T W_X \rightarrow W_L W_L$) have been ignored in this table. For the $W^\pm W^\pm$ process these effects are only relevant at center of mass energies near the WW mass threshold and do not get enhanced by any of the dimension-6 operators. The same is not necessarily true for the $W^+ W^-$ process. The entry marked as (v) stands for marginally sensitive, but not measurable.

It is also possible to reinterpret the anomalous couplings quoted in section 3.2 in the language of the coefficients of dimension-6 operators. Based on Ref. [57], one gets the

following relations:

$$c_{WWW}/\Lambda^2 = \frac{2\lambda_\gamma}{3g^2m_W^2} = \frac{2\lambda_Z}{3g^2m_W^2}, \quad (3.14)$$

$$c_W/\Lambda^2 = 2\frac{\Delta g_1^Z}{m_Z^2}, \quad (3.15)$$

$$c_B/\Lambda^2 = 2\left[\frac{\Delta\kappa_\gamma}{m_W^2} - \frac{\Delta g_1^Z}{m_Z^2}\right] = 2\frac{\Delta\kappa_\gamma - \Delta\kappa_Z}{m_Z^2}. \quad (3.16)$$

It should be stressed that the above relations hold so long as we expect the dimension-6 operators be dominant. Consideration of dimension-8 operators would generally render them not valid anymore.

Precise determination of the corresponding limits on these coefficients from the most up-to-date combination of all the existing LHC, Tevatron and LEP data is a complicated task that surpasses the scope of this work. It is also inessential for us in this moment. In fact, most of these limits so far have not changed dramatically since LEP times. Their improvement will be possible with an order of magnitude increase in integrated luminosity and doubled beam energy planned for LHC Runs 2 and 3. Without getting into too much detail and in accordance with the quoted relations, we can safely assume the allowed dimension-6 operator coefficients c_{WWW}/Λ^2 , c_W/Λ^2 and c_B/Λ^2 still be of order ± 1 -10 TeV^{-2} .

On the other hand, a clean study of quartic gauge boson couplings can be carried with interactions that do not have a triple vertex associated to it. These are described using dimension-8 effective operators. Dimension-8 operators are not necessarily just a higher order correction to dimension-6 operators. Likely, they probe different physics. Anomalous triple couplings can result from averaging out unknown heavy particles in loops. Quartic couplings can be regarded as a window to electroweak symmetry breaking. They arise as a contact interaction manifestation of heavy particle exchange. It is quite possible that quartic couplings deviate from the SM, but triple couplings do not. The operators of direct relevance for us are:

$$\mathcal{O}_{S,0} = [(D_\mu\Phi)^\dagger D_\nu\Phi] \times [(D^\mu\Phi)^\dagger D^\nu\Phi] \quad (3.17)$$

and

$$\mathcal{O}_{S,1} = [(D_\mu\Phi)^\dagger D^\mu\Phi] \times [(D_\nu\Phi)^\dagger D^\nu\Phi], \quad (3.18)$$

because they only modify the $WWWW$ and $WWZZ$ vertices. A combination $8\frac{c-1}{v^4}(\mathcal{O}_{S,0} - \mathcal{O}_{S,1})$, where v is the Higgs vacuum expectation value and c is a dimensionless number, corresponds to a simple rescaling of the Standard Model quartic coupling by a factor c .

The above are the only two independent operators constructed solely from Higgs field derivatives, and hence affecting only W_LW_L pairs. Additional dimension-8 operators can be constructed from field strength tensors and field derivatives or from field strength tensors alone. These are:

$$\mathcal{O}_{M,0} = \text{Tr}[W_{\mu\nu}W^{\mu\nu}] \times [(D_\beta\Phi)^\dagger D^\beta\Phi], \quad (3.19)$$

$$\mathcal{O}_{M,1} = \text{Tr}[W_{\mu\nu}W^{\nu\beta}] \times [(D_\beta\Phi)^\dagger D^\nu\Phi], \quad (3.20)$$

$$\mathcal{O}_{M,6} = (D_\mu\Phi)^\dagger W_{\beta\nu}W^{\beta\nu}D^\mu\Phi, \quad (3.21)$$

$$\mathcal{O}_{M,7} = (D_\mu\Phi)^\dagger W_{\beta\nu}W^{\beta\mu}D^\nu\Phi, \quad (3.22)$$

$$\mathcal{O}_{T,0} = \text{Tr}[W_{\mu\nu}W^{\mu\nu}] \times \text{Tr}[W_{\alpha\beta}W^{\alpha\beta}], \quad (3.23)$$

$$\mathcal{O}_{T,1} = \text{Tr}[W_{\alpha\nu}W^{\mu\beta}] \times \text{Tr}[W_{\mu\beta}W^{\alpha\nu}], \quad (3.24)$$

$$\mathcal{O}_{T,2} = \text{Tr}[W_{\alpha\mu}W^{\mu\beta}] \times \text{Tr}[W_{\beta\nu}W^{\nu\alpha}]. \quad (3.25)$$

We have only listed here the operators that affect the same-sign $W^\pm W^\pm$ scattering process. A full list of dimension-8 operators that can modify quartic gauge couplings, including those which can produce anomalous quartic vertices involving only Z 's and γ 's, that do not exist in the SM, can be found in Ref. [63]. Numerical coefficients behind these operators (usually denoted as f with the appropriate subscripts) are largely unconstrained by experiment. The possibilities to study quartic couplings at LEP were very limited, while the TeVatron did not offer enough energy and luminosity. Vector Boson Scattering (VBS) at the LHC is the right place to probe them.

3.5 Beyond the Standard Model?

Upon discovery of the Higgs boson, the Standard Model has been completed. Is this really the end of the story? Voluminous of theoretical papers have been written to explain why the Standard Model cannot be the ultimate theory and we will not repeat these arguments here. And yet, for improbable this may seem at first glance, the bare truth is that hardly any experimental result in particle physics to the present date can be said to support the idea that the Standard Model needs any major change anywhere below the Planck scale! Let us critically review what we currently have. The muon magnetic dipole moment may be one such indication [64]. The magnetic dipole moment is a measure of quantum effects that modify the effective strength of a charged particle interaction with a photon. These quantum corrections can be very precisely predicted in the framework of Quantum Electrodynamics (QED). Such calculations consistently reveal a lower value than the experimental world average, the discrepancy is currently at the level of 3.6σ . This result, while very interesting, is still not significant enough, as well as too isolated and indirect to be convincing on its own right. The last 15-20 years brought an explosion of neutrino physics projects, following the observation of neutrino oscillations by Kamiokande. But neutrino masses, regardless of what they ultimately are, including Dirac or Majorana, can be in principle accommodated within the Standard Model if only we relax the massless

neutrino prejudice which used to be sort of imposed by hand to the theory before 1996. In a minimalistic scenario it would only require giving neutrinos what they always *could* have within the Standard Model framework and not make any impact on the rest of the theory. Finally, the much celebrated naturalness problem, i.e., keeping the Standard Model Higgs boson light despite its quadratically divergent radiative corrections from fermionic loops, is possible simply by invoking some kind of anthropic principle (technically by assuming an enormous amount of fine tuning between the “naked” mass and the radiative mass shift). Whether or not we find such solutions satisfactory from the purely aesthetic point of view is, alas, a different question. Yet other claims for the necessity of physics beyond the Standard Model have been made on purely theoretical grounds, like within the frameworks of Grand Unification Theories, Superstrings, etc., but they all lack any experimental evidence.

More suggestive in this respect are in fact astrophysical observations. Evidence of Dark Matter in the Universe is firmly established and does call for new physics. It could be argued, though, that in principle nothing forbids adding extra particles to the Standard Model Lagrangian that would completely decouple from the known particles except via gravitation, without adding anything to our understanding of the known part of the world. Overwhelming excess of matter over anti-matter in the Universe cannot be explained by Standard Model physics, either, at least in its presently known form. But it is still an open question whether this asymmetry can be explained in terms of leptogenesis in the scenario of a strongly CP -violating neutrino sector. And that’s really all we have.

Of the proposed extensions of the Standard Model, Supersymmetry (SUSY) represents the best known class of models. Originally proposed to tackle the technical problem of loop corrections to the Higgs mass, over thirty years later it still offers a wide range of valid models which to this date are neither confirmed nor excluded experimentally. Results of the LHC Run 1 have rendered the simplest SUSY models, such as the MSSM or the NMSSM, less popular, but more generalized models are still in the mainstream of BSM searches. SUSY has been said to be the only known class of models that reduce *exactly* to the Standard Model at low energy, so as to possibly reveal no hints of itself whatsoever at the presently reachable energies. Depending on one’s point of view, this can be found as much an advantage as a weakness. In fact, if SUSY is true, there is not much to expect in the foreseeable future from WW scattering, either, in terms of deviations from the Standard Model.

A separate wide class of alternative candidates for physics Beyond the Standard Model is known as the Strongly Interacting Light Higgs (SILH) models [65]. They are generally based on the assumption that electroweak symmetry breaking is triggered by a light *composite* Higgs, which emerges from a new strongly-interacting sector as a pseudo-Goldstone boson. This implies the existence, at some higher energy scale, of an additional particle spectrum, characterized by a typical mass parameter $M \gg M_H$ and a coupling constant g , with $g_{SM} \ll g < 4\pi$. The Higgs multiplet is assumed to belong to this “strong” sector. In the limit $g_{SM} = 0$ the Higgs becomes an exact Goldstone boson. Ordinary Standard Model particles couple weakly to the strong sector. Models known as Little Higgs [66], Littlest Higgs [67], Holographic Higgs [68], etc., are particular variations of this general idea.

The effective Lagrangian corresponding to this class of models can again be written down in a parametric form, where different physical scenarios correspond to different val-

ues of the parameters in the Lagrangian. In the low energy approximation, corresponding to the energies accessible in the LHC, the Lagrangian can be symbolically rewritten as a sum

$$\mathcal{L} = \mathcal{L}_{SM} + \mathcal{L}_H + \mathcal{L}_V, \quad (3.26)$$

where \mathcal{L}_{SM} is our familiar Standard Model Lagrangian, \mathcal{L}_H describes additional interactions involving the Higgs boson and \mathcal{L}_V describes additional interactions involving gauge bosons only. These new interactions imply modifications of the cross sections and branching fractions of the Higgs boson relative to the predictions of the Standard Model. In particular, Higgs couplings to known fermions and bosons are somewhat different than in the Standard Model. In an effective formulation, the whole Higgs-related phenomenology of SILH models can be described via the choice of a few numbers that parameterize our ignorance of the underlying physics. It was shown that general rules of SILH select just three of them as the most important ones for LHC studies, which govern the leading effects expected in Higgs physics. In the following these are denoted as $\xi = (vg/M)^2$ ($v = 246$ GeV is the Higgs vacuum expectation value), c_y and c_H . In terms of these parameters, the Higgs partial widths are modified with respect to the Standard Model as follows:

$$\Gamma(h \rightarrow f\bar{f})_{SILH} = \Gamma(h \rightarrow f\bar{f})_{SM}[1 - \xi(2c_y + c_H)], \quad (3.27)$$

$$\Gamma(h \rightarrow W^+W^-)_{SILH} = \Gamma(h \rightarrow W^+W^-)_{SM}[1 - \xi(c_H - \mathcal{O}(g_{SM}^2/g^2))], \quad (3.28)$$

$$\Gamma(h \rightarrow ZZ)_{SILH} = \Gamma(h \rightarrow ZZ)_{SM}[1 - \xi(c_H - \mathcal{O}(g_{SM}^2/g^2))], \quad (3.29)$$

$$\Gamma(h \rightarrow \gamma\gamma)_{SILH} = \Gamma(h \rightarrow \gamma\gamma)_{SM}[1 - \xi Re(\frac{2c_y + c_H}{1 + J/I} + \frac{c_H}{1 + I/J} + \mathcal{O}(g_{SM}^2/g^2))]. \quad (3.30)$$

Here I and J are loop functions describing Higgs radiative decays whose numerical values depend mostly on the top quark mass. Their full definitions can be found in Ref. [65]. The ξ parameter naturally ranges between 0 and 1, the two limiting cases corresponding to the Standard Model and technicolor theories, respectively. Note that to the lowest order it is correct to say that SILH phenomenology in comparison with the Standard Model can be described as an overall modification of all the Higgs couplings to fermions and another overall modification of all the Higgs couplings to gauge bosons. For example, the ‘‘fermiophobic Higgs’’ scenario is obtained by setting $c_H=0$ and $\xi c_y=1/2$. Extraction of c_y and c_H is a main task for precision measurements of the Higgs production rate and branching fractions. Given that c_y and c_H are typically numbers of the order of unity, the size of possible deviations from the Standard Model in terms of Higgs production cross sections times branching fractions can amount even to $\sim 30\%$. Such effects are not excluded in the light of present data and their existence will be subject to verification at the LHC with $\sqrt{s} = 13$ TeV.

As we already know, an HWW coupling different from the Standard Model one reflects in the predicted high energy behavior of WW scattering amplitudes. Indeed, in SILH

models the light Higgs unitarizes the amplitudes only partially or, better saying, it only defers the unitarity crisis to higher energies. We talk then of a partially strong WW scattering. Relevant cross sections still grow above the Higgs mass, albeit slower, with an asymptotic behavior given in the lowest order of $g^2/M^2 s$ by

$$A(W_L^\pm W_L^\pm \rightarrow W_L^\pm W_L^\pm) = -\frac{c_H g^2}{M^2} s, \quad (3.31)$$

$$A(W_L^+ W_L^- \rightarrow W_L^+ W_L^-) = \frac{c_H g^2}{M^2} (s + t), \quad (3.32)$$

$$A(W_L^\pm Z_L \rightarrow W_L^\pm Z_L) = \frac{c_H g^2}{M^2} t, \quad (3.33)$$

$$A(W_L^\pm W_L^\pm \rightarrow Z_L Z_L) = \frac{c_H g^2}{M^2} s, \quad (3.34)$$

$$A(Z_L Z_L \rightarrow Z_L Z_L) = 0, \quad (3.35)$$

and up to scale of M , where new physical states are bound to appear and do the rest of the unitarization. Notice that the above amplitudes are proportional to the ones obtained within the framework of a Higgsless Standard Model and in fact, up to the energy M :

$$\sigma(pp \rightarrow jj W_L W_L)_{SILH} = (c_H \xi)^2 \sigma(pp \rightarrow jj W_L W_L)_{Higgsless}. \quad (3.36)$$

The immediate conclusion that can be drawn at this point is that all the previous studies of WW scattering, which assumed a pure Higgsless Standard Model as a phenomenological laboratory, are not entirely obsolete even once the Higgs has been discovered. Their results remain completely valid as long as the predicted signal sizes are scaled by an appropriate factor dependent on the actual value of the $HWLW$ coupling.

The following toy model well illustrates the phenomenological complementarity between SILH and SUSY. The most straightforward example of a general framework in which partially strong WW scattering can take place is the two-doublet model (2HDM). In this framework, couplings of the light and heavy Higgs scalars to the W boson are given by $g_{SM} \sin(\beta - \alpha)$ and $g_{SM} \cos(\beta - \alpha)$, respectively, where α is the Higgs mixing angle and $\tan\beta$ is the usual ratio of vacuum expectation values. If the factor $\sin(\beta - \alpha)$ is sufficiently small and the heavy Higgs sufficiently heavy, the relevant amplitudes can rise significantly in between the energies corresponding to the masses of the light and heavy Higgses for partially strong WW scattering to take place. The heavy Higgs will ultimately unitarize this growth. This, however, is generally not the case in models involving SUSY, e.g., in the MSSM the heavier the heavy Higgs is the closer to unity the factor $\sin(\beta - \alpha)$ will be and vice-versa. Thus no appreciable WW scattering can be expected in the MSSM.

Finally, it is always important to realize that different phenomenological features may be directly linked to each other within certain classes of models, but need not be so in general. Searches for anomalous quartic couplings should be still carried. Measurement of Higgs couplings that deviate from the Standard Model values does not automatically imply the existence of partially strong WW scattering. The dynamics of electroweak symmetry breaking ultimately still will remain an open question and can be possibly concluded only via direct measurement of the WW scattering cross section at high energy.

For the sake of completeness one should mention also another predicted signature of SILH models, namely enhanced production of Higgs pairs at high energy [69]. Measurement of double Higgs production can have important implications for spotting out our position on the electroweak phase diagram [70], but such effects can be hard to detect in practice and do not belong to our main topic.

Chapter 4

VV scattering at the LHC

This chapter provides a comprehensive overview of the VV scattering process at the LHC from a phenomenological point of view.

Longitudinal VV scattering carries the most direct, quantitative information about the details of the actual mechanism of electroweak symmetry breaking. The practical challenge lies in digging that information out. As we have no W beams, in any real experiment we have no control over the polarizations of the interacting pair. This means, assuming every helicity state is taken with equal probability, that a $V_L V_L$ initial pair happens in only 1/9 of all the VV cases. The majority of initial pairs are $V_T V_T$ and $V_T V_L$ states, of little sensitivity to the Higgs parameters and indeed to the Higgs existence at all. Furthermore, because of the matrix element, interacting $V_L V_L$ pairs make up no more than 5% of the total interacting VV pairs, assuming the Standard Model is approximately correct and the Higgs boson light. Variations of the $V_T V_T$ and $V_T V_L$ scattering cross sections as a function of the Higgs mass and HVV couplings amount to some $\sim 3\%$ in total and moreover the potential excesses or deficits have no clearly defined preferred kinematic signature, making their isolation impracticable. Thus the biggest part of all VV interacting pairs is merely a potential background in our search. One way to proceed is to look for specific kinematic signatures associated to a hard $2 \rightarrow 2$ scattering process and compare the yield of selected events to the Standard Model expectation. The underlying *assumption* is then that any possible excess over the prediction is due to the additional $V_L V_L$ component. This indeed was the approach taken in many early phenomenological papers on the subject. It is clear that such approach requires very good control over the systematic errors related to the theoretical prediction. Measurement of V polarization based on the decay products is especially difficult for the WW process where crucial information escapes along with two neutrinos, although the methodology is in principle known and applied in some analyses [71]. But in our kinematic regime of interest measurement of the final state polarizations will be a challenge. In what follows we will show that we can, nonetheless, to some extent measure the polarizations of the initial state. More often than not polarizations are actually conserved in the scattering process, at least in what regards $W_L W_L$ versus all the rest. And this conservation holds most strictly in the $W^\pm W^\pm$ process. This means, in particular, that $W_L^\pm W_L^\pm$ pair in the final state can be produced almost exclusively from an initial $W_L^\pm W_L^\pm$ pair (see Fig. 4.1). The only exception to this rule lies in the region of center of mass energies just above the double W mass threshold, where helicity-flip effects are more likely to occur, above all

$W_T W_X \rightarrow W_L W_L$. In the other direction, these effects are negligible altogether because of the relative smallness of $W_L W_L$. In any case, for center of mass energies above 400 GeV, the admixture from helicity-flip effects is completely negligible. This is the prime reason why it makes sense to separate $W_L W_L$ pairs in the final state from the bulk of WW interactions and study their distinctive kinematic properties.

It is much more complicated to separate a clean $W_L W_L$ scattering process in $W^+ W^-$, for which still at an energy of a TeV about 20% of $W_L W_L$ pairs come from the process $W_T W_X \rightarrow W_L W_L$.

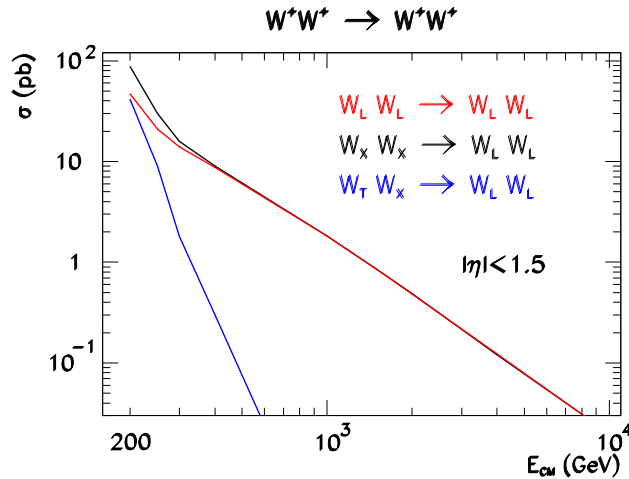


Figure 4.1: Total $W^+ W^+ \rightarrow W_L^+ W_L^+$ scattering cross sections in the SM as a function of the center of mass energy. Shown are the individual contributions of different initial polarization states to the final state consisting of purely longitudinal $W_L^+ W_L^+$ pairs. Subscript X denotes any polarization (T or L). Assumed are two on-shell, unpolarized, colliding W^+ beams. A cut on the scattering angle that corresponds to pseudorapidity of ± 1.5 with respect to the incoming W direction was applied. Results of MadGraph calculations.

4.1 Formal signal definition

In a hadron collider, WW scattering can occur via W emission off two colliding quarks. A lowest order diagram of the process is shown in Fig. 4.2 (left).

The final state is characterized by the presence of two W bosons (more precisely: their respective decay products) and two jets. Regardless of how we technically define signal and background, it is clear that in practice we have no control over whether a specific pair of vector bosons has indeed interacted or not. A whole other class of events in which two W bosons are produced and do not interact will inevitably be present and separable from the signal process on a statistical basis only, thus becoming the bulk of irreducible background. There are two different approaches often adopted in literature regarding how the signal can be formally defined. The kinematic approach defines the signal in terms of the expected kinematics of a hard $2 \rightarrow 2$ scattering process and considers explicitly as signal events all those which fall into a predefined kinematical (multidimensional) window. As the kinematic limits are not sharp, the boundaries are by necessity somewhat

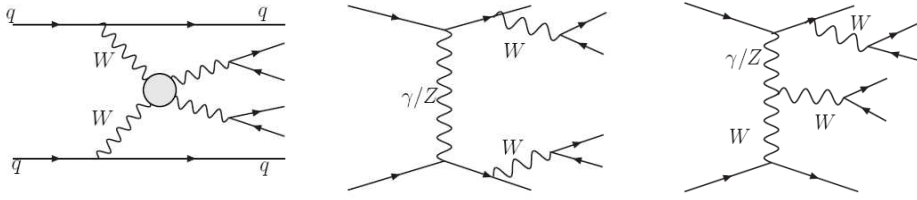


Figure 4.2: Feynman diagrams of WW scattering at the LHC (left) and examples of graphs contributing to the irreducible background (middle and right). The scattering graph contributes to the signal as long as $W = W_L$, otherwise it contributes to the irreducible background as well.

arbitrary and so no definition is really unique. Indeed, many different signal definitions have been in use by experimentalists. Moreover, by the same token, it is assumed that the part that does not fall into the signal window and hence formally defines the irreducible background does not depend on the Higgs sector parameters, which in general need not be exactly true. A feature of this approach is that the Standard Model predicts some signal, too. Deviations from the Standard Model will usually lead to different signal predictions; consistency of each prediction with real data in the predefined kinematic window can be assessed.

A second, more generic approach defines the signal explicitly as the excess of WW pairs over the prediction of the Standard Model, apparently regardless of the actual physical mechanism that leads to such excess. The Standard Model in itself, regardless of the actual physical process, is then the formal definition of the total irreducible background. As we saw, this background will be composed mainly of $W_T W_T$ and $W_T W_L$ pairs. To reemphasize this point, the Standard Model signal is equal to zero *by construction*. Signal is BSM. The first approach is of course closer to what eventually will be done in a real experiment. However, to study the problem from a conceptual point of view, the second definition has at least two important advantages. First of all, it is unique as long as we fix the Standard Model Higgs mass that we use to define irreducible background. Second, it does not rely on any particular kind of interaction and there is no signal region defined a priori. The fact that we know what process is responsible for the possible appearance of signal is a bonus we can make use of at a later stage, but not a prerequisite. Note that *some* $W_L W_L$ scattering is naturally predicted even in the Standard Model and so the signal graph in itself is not fully equivalent to what we are for. The correspondence between the two approaches is clear and the translation of respective results into each other is conceptually more or less obvious, although it has been sometimes the source of some confusion.

For a better understanding of the full process from a theoretical point of view, one can decompose its complete parton level description into three distinct, intrinsically connected parts involving W emission, interaction and decay. However, one should always keep in mind that such factorization is approximative, its practical applicability is a subject of study and any potential conclusions we would like to draw require independent confirmation in the exact evaluation of the full process.

4.2 Computational issues and methods

Factorization of the signal process into the subsequent steps of W emission, interaction and decay, as we would herewith like to do, is a useful means to study certain features, but not always a satisfactory way of quantitative description. Quantum-mechanically, it is clear that all paths leading from the initial pp state (which can be decomposed into the many possible sub-states at the quark and gluon level) to any specific final state, say, $jj\mu^+\mu^+\nu\nu$, must be considered for the correct evaluation of the process. Clearly, the irreducible background must include not only graphs identical with the signal graph, with a dominant contribution from transverse W 's, but likewise a large number graphs not involving any WW interaction. Either of the two categories of events is not gauge-invariant on its own. Strong interference effects may occur, depending on the gauge, and so not only they cannot be treated separately, but neither can the signal. Correct calculation of signal and irreducible background from first principles (i.e., Feynman rules) requires all these processes added at the level of amplitudes. Signal must be defined using the “subtraction method” which technically requires the computation of two total cross sections for (e.g.) $pp \rightarrow jj\mu^+\mu^+\nu\nu$: one corresponding to the Standard Model, another one to the alternative scenario. The signal ultimately comes from subtracting the former from the latter. Note that in general the signal can be positive inasmuch as it can be negative and that both make physical sense. And indeed, the signal *is* negative in certain regions of phase space. In addition to pure electroweak diagrams, $\sim \alpha^6$ in the lowest order (up to the level of W decay), background also includes mixed, electroweak-QCD processes, $\sim \alpha^4\alpha_s^2$. The minimal collection of those correspond to gluon exchange graphs between the two interacting quarks. Depending on the chosen final state, the number of additional electroweak-QCD diagrams can vary widely and so does therefore the total background cross section. All in all, the lowest order calculation of the $pp \rightarrow jj\mu^+\mu^+\nu\nu$ process, which is the simplest from the computational point of view, requires consideration of 5656 Feynman diagrams.

The signal in the lowest order is a purely electroweak process. However, interference between scattering and non-scattering diagrams applies in principle also for electroweak-QCD ones. The fact that signal (understood as BSM!) can indeed be calculated ignoring any QCD contributions, regardless of the relative amounts of the pure electroweak and electroweak-QCD processes, is a present from nature rather than a rule of thumb. Interference effects can be shown to cancel out to a good accuracy in the difference through which we define the signal¹. This is because electroweak-QCD events populate mostly a different region of kinematic phase space than the purely electroweak signal events - the respective transverse momenta of scattered W 's are nearly clean separated - and this conclusion holds even for W^+W^- scattering where the total signal+background cross section is dominated by QCD contributions by an order magnitude. In our example process $pp \rightarrow jj\mu^+\mu^+\nu\nu$, this allows to reduce the number of Feynman diagrams necessary for the calculation of the signal to 5208 (however, another dedicated calculation is then needed to determine the term to subtract, which is not equal to the total irreducible background anymore).

¹Bear in mind of course that what we are for in this chapter is an estimate of the magnitudes of signal and background, not a precision measurement

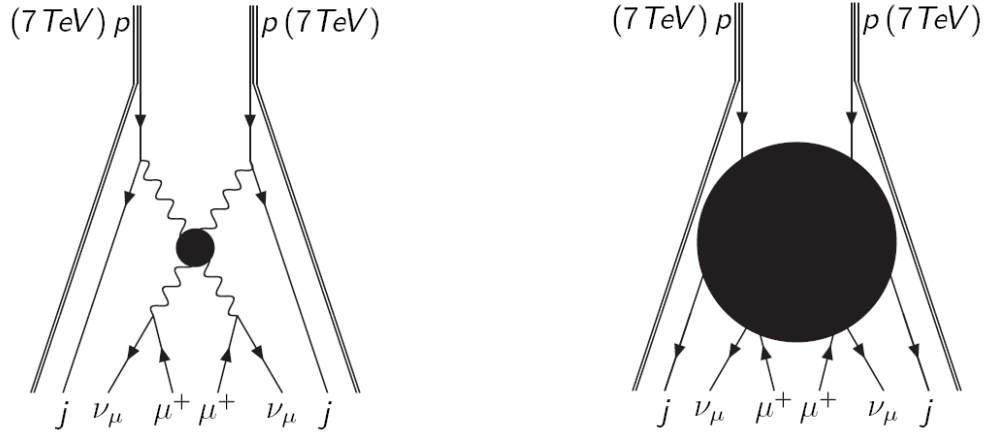


Figure 4.3: Schematic representation of the signal process (left) and of the entire set of processes which need be taken into account for the correct evaluation of the signal (right). Drawings by J. Kuczmariski.

4.2.1 Effective W Approximation and the Equivalence Theorem

Older literature made extensive use of the so called Effective W Approximation [72], with its nice acronym EWA (or more generally, Effective Vector Boson Approximation, EVBA). Its main advantage is that it renders the lowest order signal graph gauge invariant on its own, under some approximative assumptions. The idea is similar to that of factorization for parton distribution functions. The total cross section is described in terms of density functions for a polarized W being radiated by a fermion with a given momentum fraction, times the scattering amplitude for two bosons carrying these momentum fractions. The boson is assumed to be radiated approximately collinearly at a high center of mass energy, so it is close to the mass shell and we can neglect the fermion masses. In the amplitude of the scattering process it is then taken to be on shell. This means that the treatment will only necessarily be valid when $\sqrt{s} \gg M_W$ and so small virtualities of the gauge boson may be neglected. The explicit expression for the density function can be derived from the matrix element calculated for an on-shell boson being emitted off a fermion as a function of the fermion initial four-momentum and the momentum fraction carried by the boson. The total process cross section to the level of the scattered gauge bosons is finally given by integrating the scattering amplitude with the appropriate density function over the full range of the momentum fraction. The EWA provides an effective way to calculate the signal-like graphs standalone to a typical accuracy of 20-30%. A substantial literature exists on the accuracy and conditions of applicability of the EWA. Although the validity of the approximations does not explicitly exclude any helicity states, the EWA by construction disregards non-scattering contributions and is therefore not able to predict the total irreducible background levels. The latter still requires computation of the full set of diagrams.

The EWA technique is often coupled with the evaluation of gauge boson interaction done using the Equivalence Theorem [73]. The Equivalence Theorem states that at an

energy much larger than the vector boson mass, the amplitude for a process involving interaction of longitudinally polarized vector bosons on the mass shell is given by the amplitude in which these vector bosons are replaced by the corresponding unphysical Goldstone bosons. Intuitively this is understandable as a consequence of the Higgs mechanism. The vector bosons get their masses via absorbing the Goldstone bosons and so their longitudinal components retain the properties of the scalar interactions. Whether this naive intuition is really correct or not, the approximation is valid up to the leading energy term and it is applicable in every order of perturbation theory. The approximation is very useful because it is technically much easier to calculate amplitudes involving massless scalars than those involving massive vectors. The ratio of the actual vector boson mass to the center of mass energy of the interaction defines its practical accuracy.

However, several authors emphasized the importance of using full matrix element calculations in order to correctly reproduce the entire kinematics of the final state, which lies at the basis of defining optimum selection criteria for the isolation of longitudinal signal from transverse background. The advantages of the EWA and the Equivalence Theorem naturally waned once full matrix element generation tools became available to the public and fast computer clusters alike. Approximative techniques to evaluate the WW interactions are rarely used in modern studies.

4.2.2 The “production \times decay” approximation

In quantum physics, full calculation of the process, say, $pp \rightarrow jj\mu^+\mu^+\nu\nu$ involves summing over all the possible paths leading to the final state. Note that in such, formally fully correct, treatment information on the individual W helicities is lost. We don’t even know whether there was a W^+W^+ intermediate state at all at any time in the process. As a matter of principle, helicity is well defined only for *on-shell* bosons. To what extent the W ’s after interaction are on-shell and hence to what extent they can be sensibly assigned longitudinal or transverse polarizations at all, is a crucial issue. Experimentally, W helicity manifests itself in angular distributions of the decay products - for example the charged lepton from W decay with respect to the mother W direction. It cannot be deduced on an event by event basis.

The full process $pp \rightarrow jj\mu^+\mu^+\nu\nu$ can be reasonably expressed as a coherent sum of its W_LW_L and $W_TW_T + W_TW_L$ contributions only so long as we can assign two W helicities to each event, even if only on paper. This is possible if and only if the scattered W ’s are produced near enough the mass shell, or equivalently, off-shell effects, including graphs in which a W boson is exchanged in the t -channel, do not lead to significant changes of the measurable kinematics of the final state. Only under this assumption can the process be approximately factorized into steps consisting of WW production and decay. It was shown that in the kinematic region of interest for us, this approximation indeed holds to better than 10% both in shapes and normalizations, which is quite enough for our purposes. Because of this lucky fact, the characteristic features of final states associated to W_LW_L and $W_TW_T + W_TW_L$ can be studied separately of each other. One can also hope for a more detailed signal event selection that will be based not solely on the scattering kinematics, but also on the preferred W helicities. The on-shell approximation for the scattered bosons is sometimes referred to as the “production \times decay” approximation, as it technically

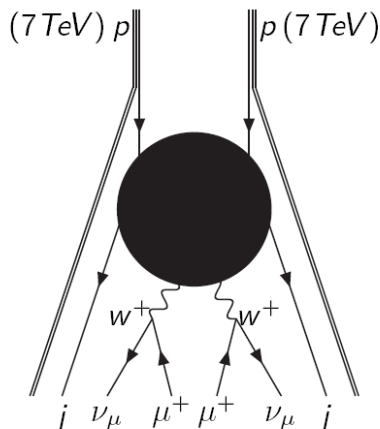


Figure 4.4: Schematic representation of the full set of processes which need be taken into account for the evaluation of the signal in the “production \times decay” approximation; cf. Fig. 4.3. Drawing by J. Kuczmarski.

allows to reduce computational work to the reduced process $pp \rightarrow jjW^+W^+$ (where the two bosons are *assumed* to be exactly on-shell) in the first step and thus decrease the number of Feynman diagrams to consider from 5656 to 1428. Similar conclusions hold for W^+W^- and ZZ if only applied far enough from the Higgs resonance region where the agreement expectedly breaks down.

Since in principle we can indeed sensibly assign specific polarizations to WW final states, it is legitimate to restrict the formal signal definition explicitly to W_LW_L pairs in all the computations, at least in studies concerning the source of electroweak symmetry breaking. The practical advantage is one of avoiding large cancelations in the signal definition coming from the dominant and largely BSM-insensitive $W_TW_T + W_TW_L$ states.

In literature one also finds a similar approach under the name of Narrow Width Approximation. Generally it has been shown to work for Standard Model processes with a typical accuracy of Γ/M , the ratio of the total width to the mass of the particle involved [74]. However, some implementations of the Narrow Width Approximation in event generators consist merely of neglecting the non-resonant graphs, but with off-shell effects and spin correlations kept, and thus are not fully equivalent to our approach.

4.3 Emission of a gauge boson off a quark

The characteristic difference in the kinematics of the final states associated to the emission of W_L and W_T off a quark are their different angular distributions. The W_LW_L and W_TW_T luminosity spectra calculated from pure emission probabilities from two quarks colliding head-on at a fixed energy and without any further interaction assumed, already reveal interesting differences in their kinematic features - see Fig. 4.6.

The longitudinally polarized W tends to be emitted at a smaller angle (hence smaller

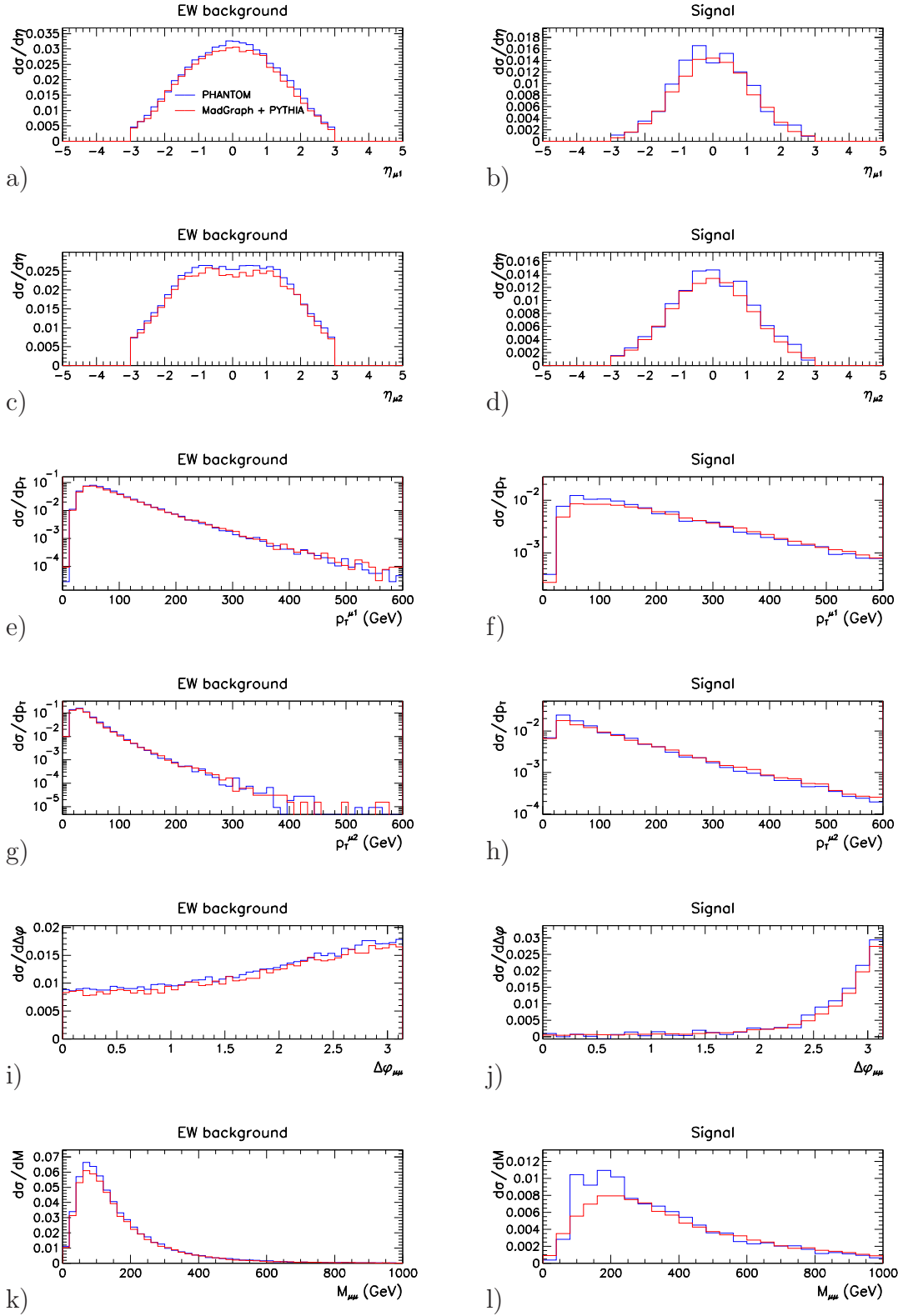


Figure 4.5: Kinematic distributions of final state muons from the $pp \rightarrow jj\mu^+\mu^+\nu\nu$ process at 14 TeV, obtained using the W on-shell approximation (labeled MadGraph+PYTHIA) and exact matrix element calculations (labeled PHANTOM). Shown are: pseudorapidities of the two muons (a-d), their transverse momenta (e-h), distances in the azimuthal angle (i,j) and invariant masses (k,l). VBF topological cuts were applied, including $|\eta_{\mu}| < 3$ and $\Delta\eta_{jj} > 4$. In background calculations only electroweak processes were taken into account and the Higgs mass was set 200 GeV.

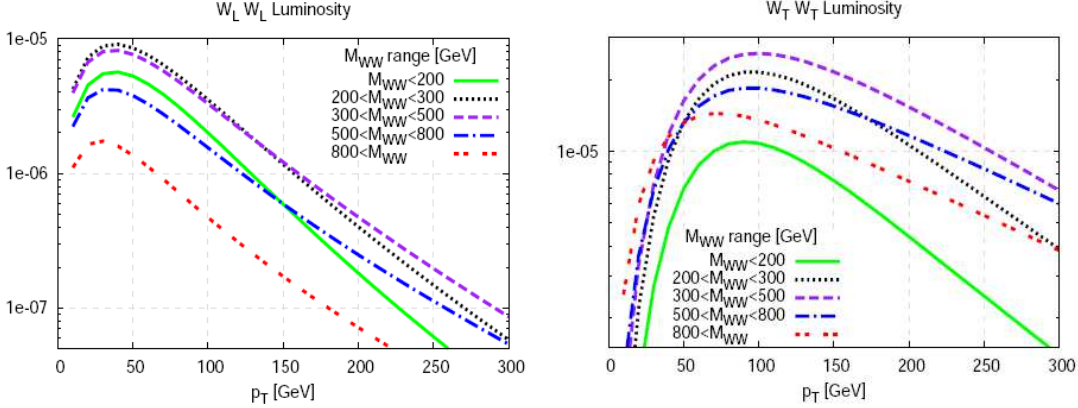


Figure 4.6: Distributions of transverse momenta of the outgoing quarks after the emission of a W_L (left) and of a W_T (right) in intervals of the WW invariant mass. Assumed is a pair of colliding quarks, each emitting a W boson, no WW interaction is taken into account. Calculation done within the Effective W Approximation.

transverse momentum) with respect to the incoming quark direction than the transversely polarized W . As a consequence, the final quark accompanying a longitudinal W is more forward than the one accompanying a transverse W . This effect is more pronounced the larger the invariant mass of the WW pair, M_{WW} . The transverse momentum distributions of quarks associated with W_L emission become narrower as M_{WW} increases and the peak of the distribution gradually moves to lower values. No such trend is associated with W_T emission, except for very large M_{WW} , where in case of a fixed incoming quark energy the effects of overall energy and momentum conservation become a limiting factor. These observations suggest that our potential to separate the $W_L W_L$ signal from the $W_T W_T$ background increases with M_{WW} already at the level of emission. Tagging two opposite forward jets in a relatively narrow band of transverse momentum for a fixed value of M_{WW} is the ideal technique to be used. The practical problem in implementing this conclusion in an experiment is that the absolute scale of transverse momentum of the emitted W is defined by the mother quark energy. Events can be efficiently discriminated based on the transverse momenta of the outgoing jets so long as we have monochromatic quark beams².

4.4 Interaction of two gauge bosons

Total cross sections and angular distributions in the scattering process of two on-shell W bosons, depending on their energies and polarizations, were already discussed in the previous chapter. Here we have just learned that in addition, since W_L 's tend to be emitted from a quark line in a more collinear way than W_T 's, the $W_L W_L$ rest frame will be approximately equivalent to the lab frame as long as we disregard highly asymmetric quark-quark collisions. Excess over the predictions of the Standard Model is therefore expected in the central region of the detector, as far as the scattered W directions are

²Obviously, we would be doing much better in a lepton collider, if only it had a similar energy reach!

concerned. Let us now build a naive toy model of such process. For a WW pair coming from nearly collinear emissions and scattered back-to-back at a large angle, we can approximate

$$M_{WW} \approx 2\sqrt{M_W^2 + p_T^{(1)} p_T^{(2)}}, \quad (4.1)$$

where $p_T^{(1)}$ and $p_T^{(2)}$ are the transverse momenta of the scattered W 's understood as unsigned scalar quantities. The product $p_T^{(1)} p_T^{(2)}$ (or its square root, to be more precise) is a measure of M_{WW}^2 and this equivalence naturally works better for large M_{WW} .

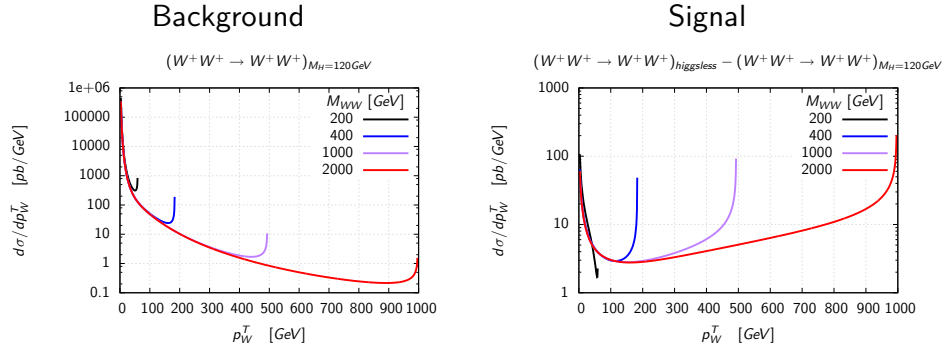


Figure 4.7: The W^+W^+ scattering cross sections for background and signal as a function of the transverse momenta of the outgoing W , for different center of mass energies (M_{WW}). Calculation done within the Effective W Approximation.

A large value of $p_T^{(1)} p_T^{(2)}$ is not only the kinematic region where deviations from the Standard Model are supposed to emerge (because of the s -divergence), but also independently where W_L -associated jet kinematics is more easily distinguishable from the W_T -associated jet kinematics.

4.5 Gauge boson decay and possible final states

The branching fraction of W decay into any of the charged leptons with a corresponding neutrino is $(10.80 \pm 0.09)\%$. The Z boson decays into an oppositely charged lepton pair of a given flavor in $(3.366 \pm 0.002)\%$ of the cases and in $(20.00 \pm 0.06)\%$ into neutrinos. The rest are hadronic decays. From an experimental point of view, this gives potentially many possible final states of interest, depending on the particular scattering process and the decay modes of the two bosons.

- Purely leptonic

$$pp \rightarrow jjW^+W^- \rightarrow jjl^+\nu l^-\nu$$

$$pp \rightarrow jjW^\pm W^\pm \rightarrow jjl^\pm\nu l^\pm\nu$$

$$pp \rightarrow jjW^\pm Z \rightarrow jjl^\pm \nu l^{+\mp}$$

$$pp \rightarrow jjZZ \rightarrow jjl^+ l^- \nu \nu$$

$$pp \rightarrow jjZZ \rightarrow jjl^+ l^- l^+ l^-$$

Leptonic W and Z decays are the preferred decay modes for a wide range of measurements involving gauge bosons, and among other things, provide some of the most sensitive means for Higgs studies. Their main limiting factor is low statistics induced by the small individual branching fractions. Practical viability of these modes crucially depends on our background rejection capability. This in general favors the non-zero total charge states $W^\pm W^\pm$, $W^\pm Z$, and the four-lepton final state (ZZ), which is the only one where the full kinematics of the process can be measured. On the other hand, both the Z production cross section and its leptonic branching fraction are lower than those of a W , hence production rates favor W^+W^- followed by $W^\pm W^\pm$. The purely leptonic channels are often regarded as the “gold-plated” modes in phenomenological literature because of their clean, distinctive signatures and because the rough magnitudes of both the signal and the main backgrounds can usually be reasonably estimated without involving a full detector simulation.

- Semi-leptonic

$$pp \rightarrow jjWW \rightarrow jjjjl\nu$$

$$pp \rightarrow jjZW \rightarrow jjjjl\nu$$

$$pp \rightarrow jjWZ \rightarrow jjjjl^+ l^-$$

$$pp \rightarrow jjZZ \rightarrow jjjjl^+ l^-$$

These processes combine a hadronic decay of one gauge boson with a leptonic decay of the other. They are characterized by reasonable statistics and higher reducible backgrounds. Typically, control of the latter requires full detector simulation to handle, e.g., the dominant backgrounds from processes involving production of W/Z +jets with a jet misidentified as a lepton. Additionally, at large W/Z energies, the two jets originating from a hadronic decay tend to merge in the detector which further reduces the signal isolation efficiency and adds extra backgrounds to be considered. Early studies usually revealed these channels be somewhat less promising, overall, than purely leptonic. However, improvements in event reconstruction in LHC experiments and in particular the use of novel techniques of “jet pruning” [75] that allow to determine the mass of the original object producing the jet and therefore distinguish QCD jets from W jets to a large accuracy, bring new interest to the semi-leptonic channels again. These techniques have been demonstrated to be applicable in the k_T and Cambridge-Aachen jet reconstruction algorithms [76], but not in the default anti- k_T algorithm used in CMS and ATLAS. Since they have been shown to offer great promise, reconsideration of the jet reconstruction algorithm to be applied for VBS analyses is a potential possibility. Clearly a lot of rework needs to be done as dedicated reprocessing of all the past studies will be required, but in the end the semi-leptonic channels may prove very useful to increase the total significance of the signal.

- Purely hadronic

$$pp \rightarrow jjWW \rightarrow jjjjjj$$

$$pp \rightarrow jjWZ \rightarrow jjjjjj$$

$$pp \rightarrow jjZZ \rightarrow jjjjjj$$

Despite their large branching fractions, these processes are completely overwhelmed by the multi-jet QCD background and in addition their study requires full detector-dependent modeling of event reconstruction effects. The purely hadronic modes are therefore not considered for detailed studies at this time.

In the above we assume $l = e, \mu$. Decays into taus constitute yet a separate class of specific final states and signatures, but due to the relative complexity and lower identification efficiency they can be disregarded for the time being.

In the search for the most promising channels to begin with, the crucial point is the underlying physics and in particular existence or non-existence of heavy Higgs-like resonances within the energy range of the LHC. Their existence of course favors the W^+W^- and ZZ channels and indeed these usually have been given the most attention, also as a byproduct of Higgs physics. Further on however we will mainly focus on an alternative yet plausible scenario that such resonances, if any, are too heavy for direct detection at the LHC. In this case, the non-resonant³ modes $W^\pm W^\pm$ (and $W^\pm Z$, in some sense) acquire not only equal importance, but as we will further see, their relative exoticity can be well turned into an advantage.

4.6 The uniqueness of $W^\pm W^\pm$

It is now time to explain that the apparently arbitrary choice of the $pp \rightarrow jj\mu^+\mu^+\nu\nu$ process as a particular example in many of our earlier considerations was in fact well motivated. The $W^\pm W^\pm$ final state, with its ± 2 total electric charge carries unique features that make it of particular interest at the LHC. We have already seen that same-sign WW scattering is the only process for which the cross-talk amplitudes, $W_T W_X \rightarrow W_L W_L$ and $W_L W_L \rightarrow W_T W_X$, are completely negligible, mostly due to lack of any s -channel graphs that contribute to the process. The latter also has other consequences. Contrary to other diboson states with two accompanying jets, production of the $jjW^\pm W^\pm$ state in the lowest order is dominated by only one physical mechanism at the quark level, namely a quark-quark interaction associated with a W^\pm emission from each colliding quark. Whether or not these two W^\pm bosons do interact, information on their polarizations stays encoded in the kinematics of the two outgoing quarks (recall section 4.3), unless it is disturbed by a subsequent quark interaction. If only we knew the energies of the colliding quarks, appropriate cuts on the angles and transverse momenta of the two tagging jets would increase the probability of choosing a $W_L W_L$ state - regardless of their own final kinematics and the rest of the process. By the same token, the only QCD contributions to the irreducible background are graphs $\sim \alpha^2 \alpha_S^2$ of the form of internal gluon exchange between the two quarks. Not only they are negligible in the calculation of the BSM signal, as already shown, but their contribution to the background can be reduced to below 10%

³Strictly speaking, $W^\pm W^\pm$ is non-resonant as long as there are no bosonic isospin triplets, and hence doubly charged bosons, in nature.

after basic topological VBF cuts. Moreover, one can hope that existence of a single physical mechanism will facilitate the search for more advanced characteristic kinematic signatures of the signal. Conversely, there are many more ways to produce a jjW^+W^- final state at the LHC.

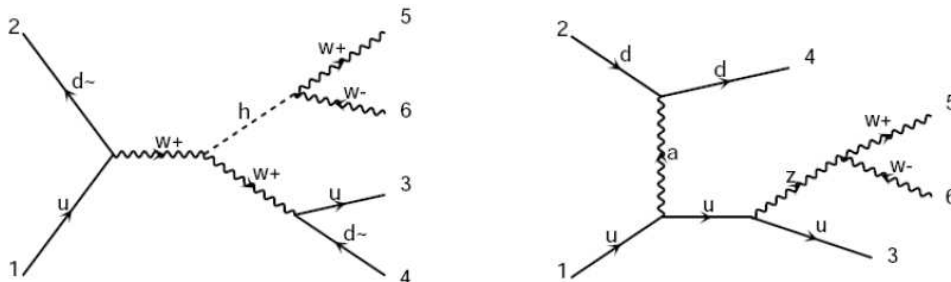


Figure 4.8: Examples of Feynman diagrams of purely electroweak processes that contribute to the process $pp \rightarrow jjW^+W^-$, but have no equivalent for jjW^+W^+ . Events where both W 's originate from a decay of a neutral particle contribute both to our definition of signal (left) and the irreducible background (right), but kinematicwise do not allow the distinction of W polarizations. The left graph is actually Higgs production via Higgsstrahlung and is of little relevance once VBF selection criteria are imposed. However, huge additional contributions to the irreducible background change significantly its overall kinematic distributions and mask the part of the background which is related to single W emissions from each colliding quark.

A W^+W^- pair can come from virtual Z decay, as well as two consecutive emissions off a single quark. Even more importantly, the electroweak-QCD background receives huge additional contributions from graphs involving gluon-gluon and quark-gluon interactions. In fact, processes $\sim \alpha^2\alpha_S^2$ dominate the total jjW^+W^- production by an order of magnitude, prior to kinematic cuts. Usual non-VBF Higgs production graphs, e.g., those involving Higgsstrahlung followed by Higgs decay into W^+W^- , also contribute to the signal according to our working definition, but are of little use kinematicwise when we go to higher energies. All in all, signal in the W^+W^- mode can be expected less well kinematically separated from background, and background much larger. Assuming the absence of new heavy Higgs-like resonances within the energy reach of the LHC at 13/14 TeV, W^+W^- is a more difficult choice. For completeness one should notice that the choice of same-sign W pair is also a powerful shield against the overwhelming reducible background originating from $t\bar{t}$ production. Only second order effects, like leptonic B decays or lepton charge misidentification can lead to a non-zero $t\bar{t}$ background. These aspects will be elaborated further on.

Assuming the pure Higgsless Standard Model scenario as the theoretical basis for the definition and numerical computation of the signal, the total signal cross section for $pp \rightarrow jjW^+W^+$ at $\sqrt{s} = 13/14$ TeV is roughly an order of magnitude smaller than the

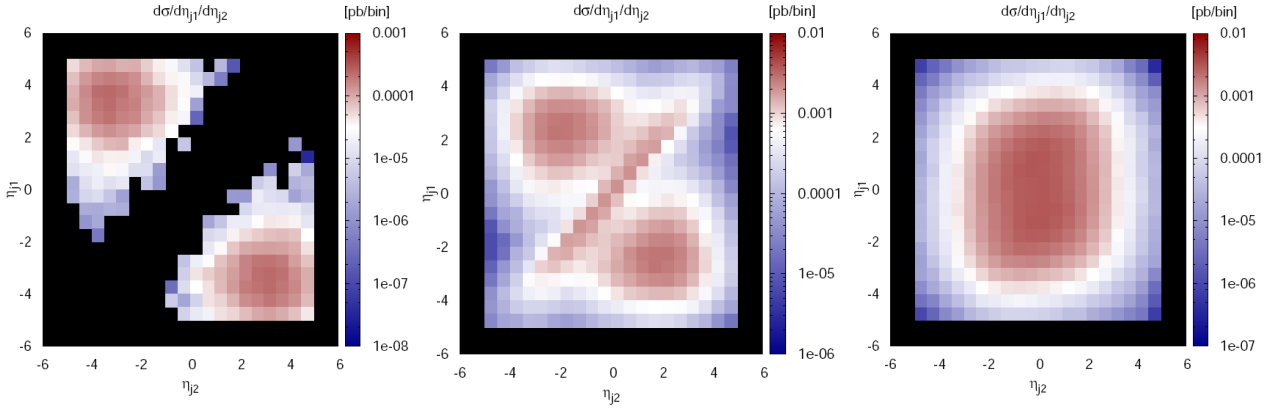


Figure 4.9: Distributions of signal (left), electroweak background (middle) and QCD background (right) for the process $pp \rightarrow jjW^+W^+$ at 14 TeV as a function of jet pseudorapidities. Results of parton-level MadGraph calculations involving all processes $\sim \alpha^4$ (left and middle) and all processes $\sim \alpha^2\alpha_S^2$ (right). Interference between the two classes was neglected for demonstration purposes.

irreducible background. Basic kinematic signatures of the signal and irreducible backgrounds in terms of angular distributions of the two outgoing jets, confirm the usefulness of the forward jet tagging technique (a basic VBF signature in the LHC) to isolate signal from background. The requirement of two opposite-sided, large pseudorapidity jets, $2 < |\eta_j| < 5$ and $\Delta\eta > 4$, suppresses the bulk of soft parton-parton collisions. It eliminates most of the electroweak background, and even more efficiently the electroweak-QCD background - for an illustration of the basic topologies of signal and backgrounds, see Fig. 4.9. This, together with another basic topological requirement of two W bosons within the acceptance of the detector (which can be approximated quantitatively as $|\eta_W| < 2$) has an important effect at the quark level as it effectively selects a very specific configuration of the colliding quarks. Not only we have a single production mechanism - residual processes in which both outgoing W 's originate from the same quark line, or not from a quark at all, are now completely suppressed - but also a common production kinematics. Energy distributions of the two quarks *before* interaction, usually preferring the lowest energies, as dictated by proton PDF's, now begin to peak quite strongly around roughly $\sim 1/7$ of the proton energy, as shown in Fig. 4.10. At the quark level the whole process can now be reasonably approximated by considering a symmetric collision of two nearly monochromatic quark beams with $\sqrt{s} \approx 2$ TeV. For kinematic calculations, the complicated proton-proton process with its 1428 tree level Feynman diagrams can be reduced to the “only” 102 diagrams corresponding to a pure quark level process $uu \rightarrow ddW^+W^+$ at a fixed energy.

Comparison of the final state kinematics of the processes $pp \rightarrow jjW^+W^+$ at 14 TeV and $uu \rightarrow ddW^+W^+$ at 2 TeV, after no more than the basic VBF topological cuts defined above, is very telling. The kinematics of the outgoing W bosons are indeed very similar,

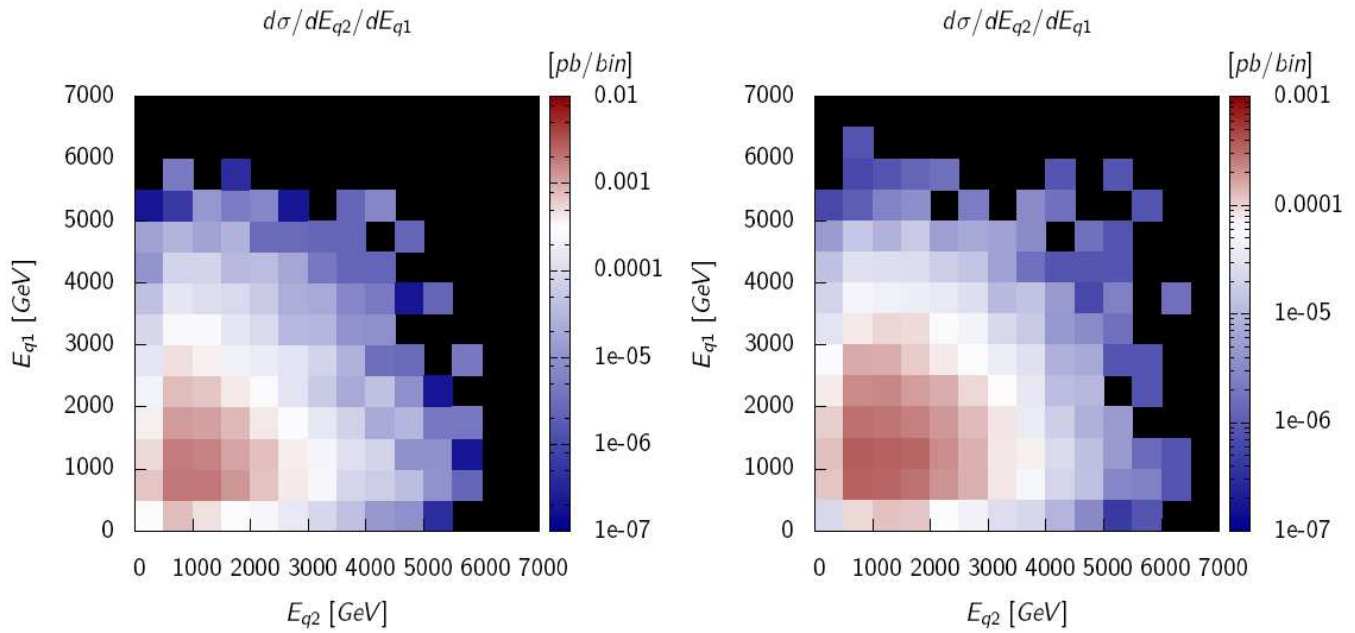


Figure 4.10: Background (left) and signal (right) for the process $pp \rightarrow jjW^+W^+$ at 14 TeV as a function of the energies of the two incident quarks after imposing basic topological cuts discussed in the text. Results of a parton-level MadGraph calculation.

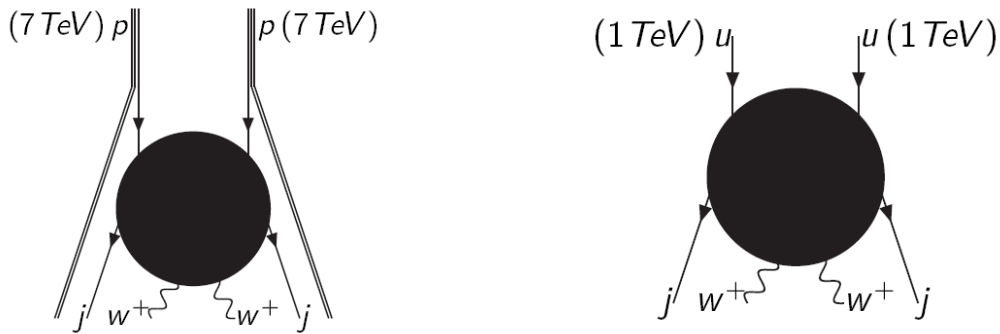


Figure 4.11: Schematic representations of the full set of processes which need be taken into account for the evaluation of the signal in the “production \times decay” approximation (left) and of the reduced set of processes which need be taken into account to learn the basic kinematics of the signal process and of the irreducible background (right). Drawings by J. Kuczmarski.

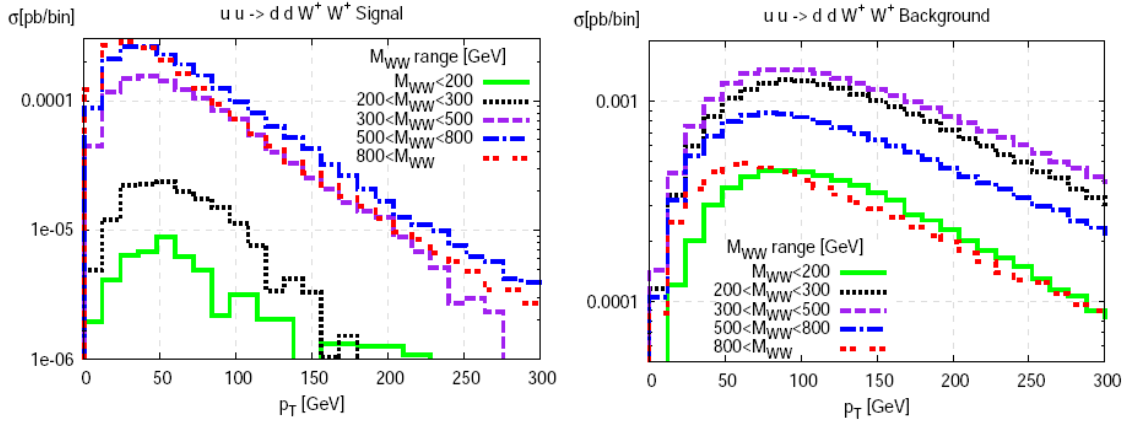


Figure 4.12: Distributions of transverse momenta of the jets associated to the emission of $W_L W_L$ signal (left) and $W_T W_T$ background (right) in the quark level process $uu \rightarrow dd W^+ W^+$ at an incident center of mass energy of 2 TeV. Results of MadGraph simulations. Note similarity in gross features to the distributions resulting from the pure emission process shown in Fig. 4.6.

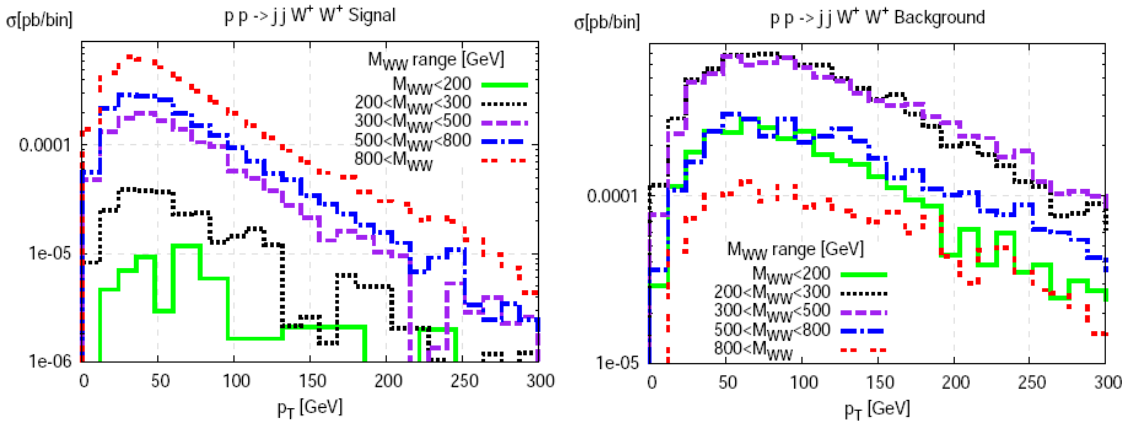


Figure 4.13: Distributions of transverse momenta of the jets associated to the emission of $W_L W_L$ signal (left) and $W_T W_T$ background (right) in the full process $pp \rightarrow jj W^+ W^-$ at 14 TeV (bottom row). Results of MadGraph simulations. Note similarity in gross features to the distributions resulting from the quark process shown in Fig. 4.12 and from the pure emission process shown in Fig. 4.6.

with the respective pseudorapidity and transverse momentum distributions merely being typically some 5-15% more smeared in the former. Larger differences affect only the tails of the transverse momenta of the jets and the two-jet invariant mass.

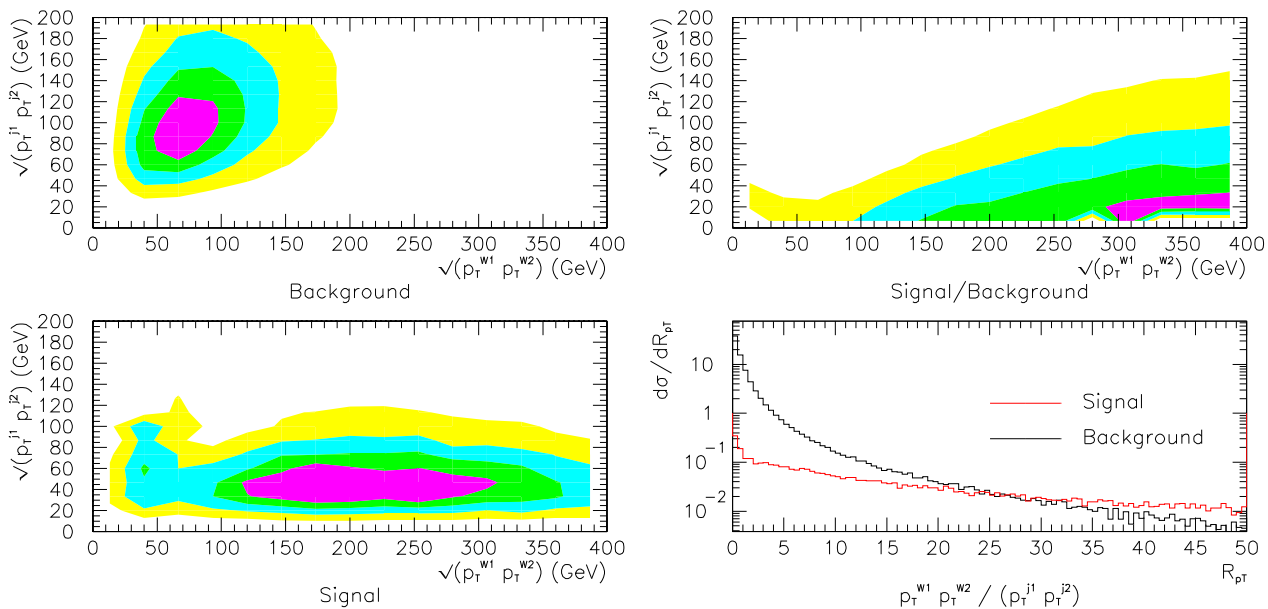


Figure 4.14: The kinematics of longitudinal signal and transverse background in the pure electroweak quark-level process $uu \rightarrow ddW^+W^+$ at 2 TeV. **Left:** the differential cross sections of background and signal in a two-dimensional space defined by the square roots of the transverse momentum products of the two outgoing d quarks and the two outgoing W 's, $\sqrt{p_T^{d1} p_T^{d2}}$ versus $\sqrt{p_T^{W1} p_T^{W2}}$; the color contours are equidistant and the scale ranges from zero (white) to 0.004 fb/GeV² for the background and to 0.0002 fb/GeV² for the signal (purple). **Upper right:** the signal to background ratio from dividing the two left plots; the vertical scale is logarithmic for better visualization and ranges from 0.03 (white) to 30 (purple). **Lower right:** the distributions of the ratio $p_T^{W1} p_T^{W2} / (p_T^{j1} p_T^{j2})$ for signal and background. No kinematic cuts were applied. Results of a MadGraph calculation. Signal was calculated by considering longitudinal W^+W^+ pairs only and subtracting the SM-based distributions from the Higgsless-based distributions.

The fact that most features of the final state kinematics can be approximated with a picture of two colliding monochromatic quark “beams” has a very important phenomenological consequence. Systematic differences in the kinematics of the tagging jets associated to the emission of longitudinally and transversely polarized gauge bosons can indeed be observed in an experiment. Partonic structure functions inside a proton in the first step inevitably smear out the measured transverse momentum distributions and hide the information on W polarity. Remarkably, after basic VBF topological cuts this information can

be unveiled again. Tree level calculations show that transverse momentum distributions of jets in signal and background events indeed follow the same qualitative trends as outlined before for the pure emission process of a longitudinal and transverse gauge boson, as well as in the signal and background in an ideal quark process, once VBF topological cuts are applied on the former - see in particular Figs. 4.12 and 4.13.

To summarize our findings, signal is characterized by emissions of longitudinal W 's followed by their hard interaction. Signatures of the first part are two opposite tagging jets at large pseudorapidities and with relatively *low* transverse momenta. The second part induces a large WW scattering angle which translates into small W pseudorapidities and large transverse momenta. Because their respective kinematics is severely constrained by the sole physical mechanism and the energies of the colliding quarks, signal and background events occupy rather restricted and largely separated regions in the phase space of the four final state particles, and in particular their transverse momenta. The signal cross section is nearly flat over a large range of the product $\sqrt{p_T^{W_1} \cdot p_T^{W_2}}$ and much more rapidly falling with $p_T^{j_1} \cdot p_T^{j_2}$. By contrast, the background cross section is much steeper in $\sqrt{p_T^{W_1} \cdot p_T^{W_2}}$ than $p_T^{j_1} \cdot p_T^{j_2}$. This is not unexpected, as we recall the expression $\sqrt{p_T^{W_1} \cdot p_T^{W_2}}$ directly correlates with the center of mass WW energy, M_{WW} . The region of phase space where all four transverse momenta are relatively low to moderate, typically $p_T^W \sim 100-200$ GeV and $p_T^j \sim 40-80$ GeV, is the region of largest kinematic overlap and thus is the most relevant for a successful signal isolation. In this region, the condition

$$p_T^{W_1} \cdot p_T^{W_2} / (p_T^{j_1} \cdot p_T^{j_2}) = \text{const} \quad (4.2)$$

to a fair accuracy corresponds to a line of constant signal to background ratio (S/B).

As already mentioned when discussing hadronic decays, decays of energetic W 's are highly boosted in the lab and decay products are emitted in a nearly collinear way. Our practical measure of M_{WW} in an experiment is then the product of the two transverse momenta of the visible charged leptons. Asymptotically for high energies, the latter is just a numerically scaled down (by a factor of 4) version of the former. We have hence arrived in a heuristic way to the definition of an experimental dimensionless variable

$$R_{p_T} = \frac{p_T^{l_1} \cdot p_T^{l_2}}{p_T^{j_1} \cdot p_T^{j_2}} \quad (4.3)$$

whose fixed value indeed represents a constant S/B to a good enough accuracy.

Correspondence between R_{p_T} and the typical VBF signature is straightforward. We recall that the latter includes two central back-to-back leptons (in case of leptonic decays) with high transverse momenta. Here however the specific cut value for these transverse momenta is now scaled with the values of transverse momenta of the jets, in a way that is based on background rejection grounds. Physically this can be said equivalent to adding the requirement of high M_{WW} and longitudinal polarizations. By contrast, the conventional VBF selection criteria are polarization-blind. This unique combination of the four transverse momenta is in fact more effective in separating signal from background than a combination of selection criteria imposed separately on the individual transverse momenta, because they scale with each other.

All the above considerations are equally true for W^-W^- as for W^+W^+ , although quantitative details differ due to the presence of two valence u quarks inside a proton.

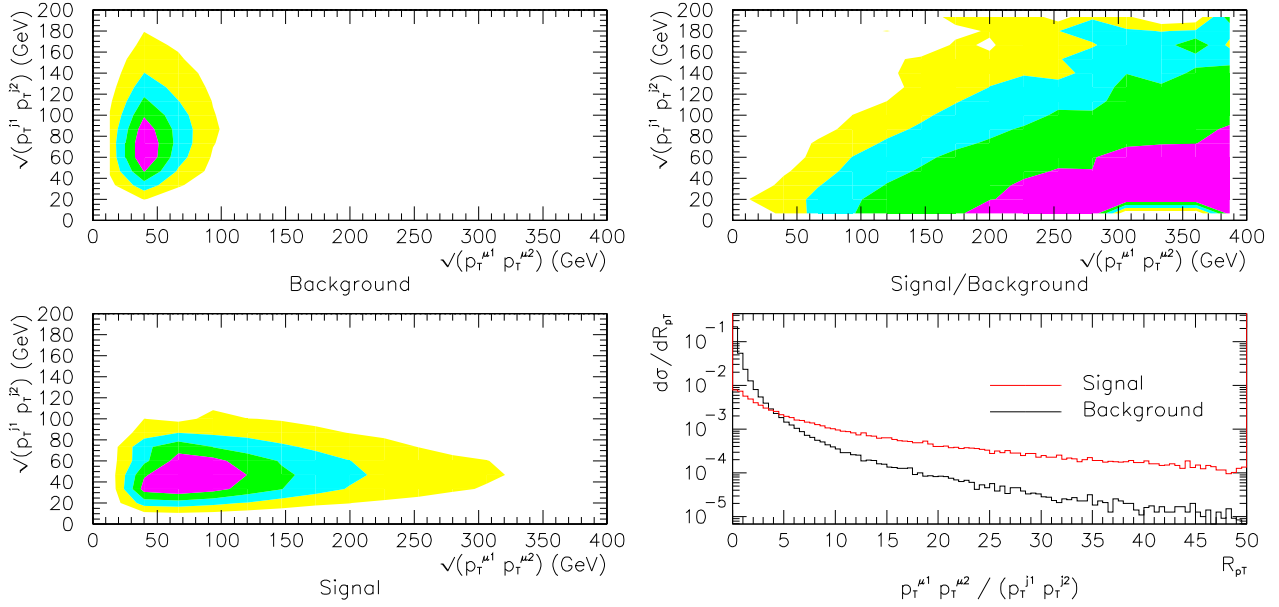


Figure 4.15: The kinematics of longitudinal signal and transverse background in the full process $pp \rightarrow jj\mu^+\mu^+$ at 14 TeV after applying basic topological VBF cuts only. **Left:** the differential cross sections of background and signal in a two-dimensional space defined by the square roots of the transverse momentum products of the two leading jets and the two outgoing muons, $\sqrt{p_T^{j1} p_T^{j2}}$ versus $\sqrt{p_T^{\mu1} p_T^{\mu2}}$; the color contours are equidistant and the scale ranges from zero (white) to $0.48 \cdot 10^{-4}$ fb/GeV² for the background and to $0.7 \cdot 10^{-5}$ fb/GeV² for the signal (purple). **Upper right:** the signal to background ratio from dividing the two left plots; the vertical scale is logarithmic for better visualization and ranges from 0.04 (white) to 40 (purple). **Lower right:** the distributions of the ratio $p_T^{\mu1} p_T^{\mu2} / (p_T^{j1} p_T^{j2})$ for signal and background. Results of a MadGraph simulation, processed by PYTHIA 6 [122] for the effects of parton showering, hadronization and jet reconstruction, and further processed by PGS 4 for the effects of finite resolution in the measurement of jet and muon p_T in a CMS-like detector. Signal was calculated by subtracting the SM-based distributions from the Higgsless-based distributions.

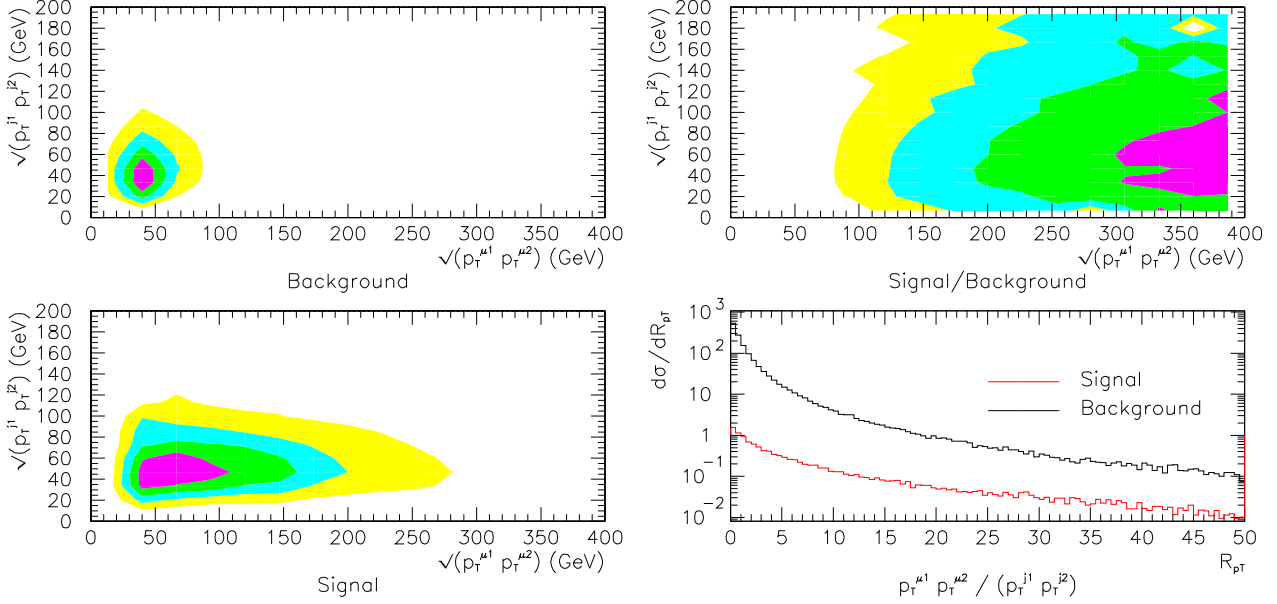


Figure 4.16: The kinematics of longitudinal signal and transverse background in the full process $pp \rightarrow jj\mu^+\mu^-$ at 14 TeV after applying basic topological VBF cuts only. **Left:** the differential cross sections of background and signal in a two-dimensional space defined by the square roots of the transverse momentum products of the two leading jets and the two outgoing muons, $\sqrt{p_T^{j1} p_T^{j2}}$ versus $\sqrt{p_T^{\mu+} p_T^{\mu-}}$; the color contours are equidistant and the scale ranges from zero (white) to 0.0011 fb/GeV^2 for the background and to $0.12 \cdot 10^{-4} \text{ fb/GeV}^2$ for the signal (purple). **Upper right:** the signal to background ratio from dividing the two left plots; the vertical scale is logarithmic for better visualization and ranges from 0.0025 (white) to 2.5 (purple). **Lower right:** the distributions of the ratio $p_T^{\mu+} p_T^{\mu-} / (p_T^{j1} p_T^{j2})$ for signal and background. Results of a MadGraph simulation of $pp \rightarrow jjW^+W^-$, processed by PYTHIA 6 for W decay into muons, the effects of parton showering, hadronization and jet reconstruction, and further processed by PGS 4 for the effects of finite resolution in the measurement of jet and muon p_T in a CMS-like detector. The original PYTHIA 6 source code was modified to account for the correct, polarization-dependent, angular distributions for the decays $W^\pm \rightarrow \mu^\pm \nu$. Signal was calculated by considering longitudinal W^+W^- pairs only and subtracting the SM-based distributions from the Higgsless-based distributions.

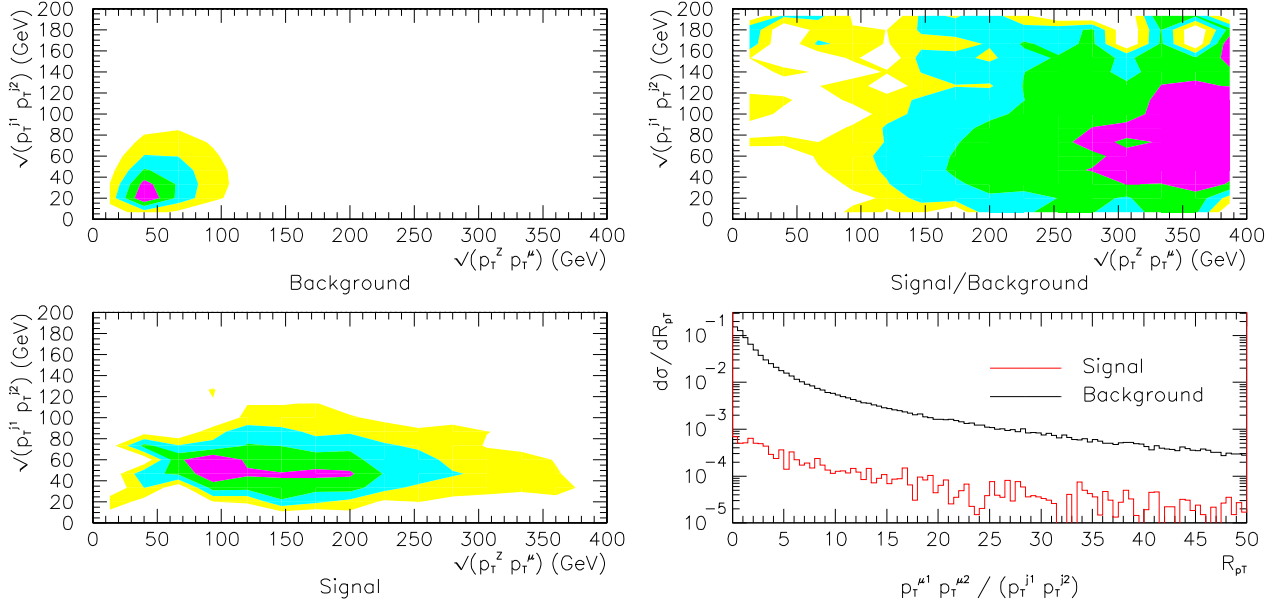


Figure 4.17: The kinematics of longitudinal signal and transverse background in the full process $pp \rightarrow jjW^+Z \rightarrow jj\mu^+\mu^+\mu^-$ at 14 TeV after applying basic topological VBF cuts only. **Left:** the differential cross sections of background and signal in a two-dimensional space defined by the square roots of the transverse momentum products, $\sqrt{p_T^{j1} p_T^{j2}}$ versus $\sqrt{p_T^{\mu^+} p_T^Z}$ where p_T^Z stands for the total transverse momentum of the two opposite-sign muons that reproduce the best Z mass. The color contours are equidistant and the scale ranges from zero (white) to $2 \cdot 10^{-4}$ fb/GeV² for the background and to $3 \cdot 10^{-6}$ fb/GeV² for the signal (purple). **Upper right:** the signal to background ratio from dividing the two left plots; the vertical scale is logarithmic for better visualization and ranges from 0.004 (white) to 4 (purple). **Lower right:** the distributions of the ratio $p_T^{\mu^+} p_T^Z / (p_T^{j1} p_T^{j2})$ for signal and background. Results of a MadGraph simulation, processed by PYTHIA 6 for parton showering, hadronization and jet reconstruction, and further processed by PGS 4 for the effects of finite resolution in the measurement of jet and muon p_T in a CMS-like detector. Signal was calculated by subtracting the SM-based distributions from the Higgsless-based distributions.

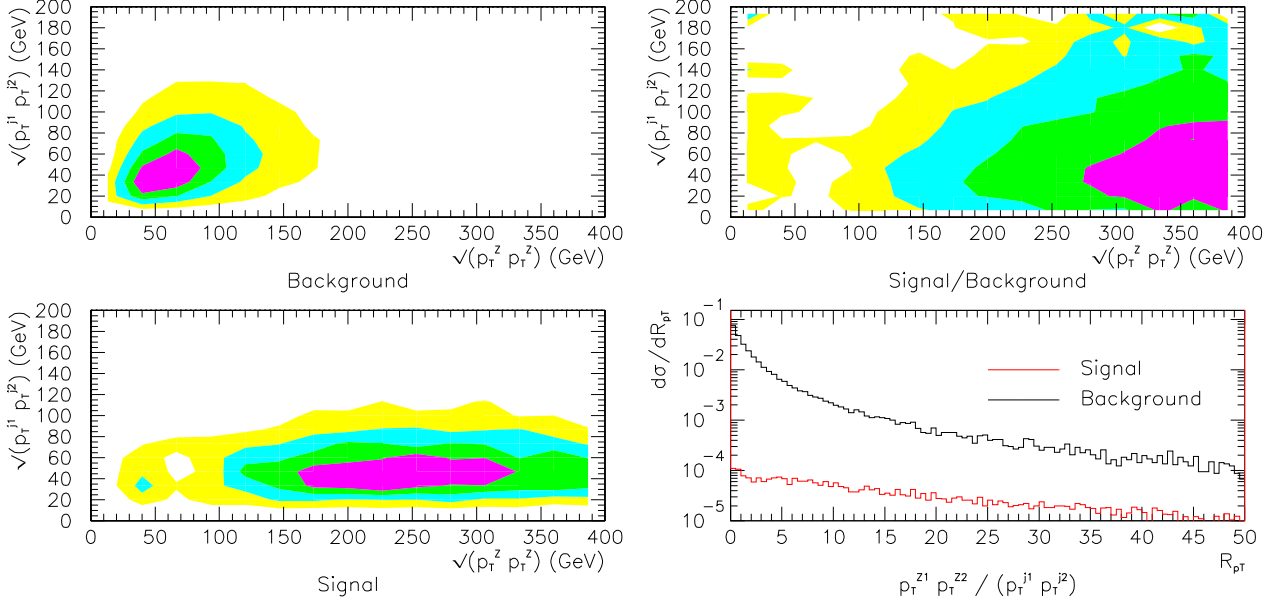


Figure 4.18: The kinematics of longitudinal signal and transverse background in the full process $pp \rightarrow jjZZ \rightarrow jj\mu^+\mu^-\mu^+\mu^-$ at 14 TeV after applying basic topological VBF cuts only. **Left:** the differential cross sections of background and signal in a two-dimensional space defined by the square roots of the transverse momentum products of the two leading jets and the two Z bosons, $\sqrt{p_T^{j1} p_T^{j2}}$ versus $\sqrt{p_T^{Z1} p_T^{Z2}}$ where the transverse momenta of the Z bosons were reconstructed from pairs of opposite-sign muons reproducing the best Z masses. The color contours are equidistant and the scale ranges from zero (white) to $3 \cdot 10^{-5}$ fb/GeV² for the background and to $4 \cdot 10^{-7}$ fb/GeV² for the signal (purple). **Upper right:** the signal to background ratio from dividing the two left plots; the vertical scale is logarithmic for better visualization and ranges from 0.0008 (white) to 0.8 (purple). **Lower right:** the distributions of the ratio $p_T^{Z1} p_T^{Z2} / (p_T^{j1} p_T^{j2})$ for signal and background. Results of a MadGraph simulation of $pp \rightarrow jjZZ$, processed by PYTHIA 6 for Z decay into muons, the effects of parton showering, hadronization and jet reconstruction, and further processed by PGS 4 for the effects of finite resolution in the measurement of jet and muon p_T in a CMS-like detector. Signal was calculated by considering longitudinal ZZ pairs only. This study did not include the correct, polarization-dependent, angular distributions for the decays $Z \rightarrow \mu^+\mu^-$. Such effects cannot nonetheless change any of our conclusions.

The total production rate of W^-W^- is approximately one fourth of that of W^+W^+ .

By the same arguments it should be clear that R_{p_T} is a specific variable suited for the study of same-sign WW scattering, but not of other VBS processes, W^+W^- in particular. For a comparative study of R_{p_T} usefulness in different VBS processes, see Figs. 4.14 thru 4.18. The meaning of R_{p_T} is not selection of a hard scattering process any more than conventional VBF selections are. Rather, it is rejection of background of a specific type: the one related to gauge boson emissions off two colliding quarks in which at least one of the bosons is transversely polarized. The uniqueness of same-sign WW is that it is the only process in which this type of background can be made its main component. This observation is very important. For the purely leptonic decay modes, the whole signal size, defined in terms of W_LW_L pairs and the unitarity limit is of order of 0.3 fb. This means in any realistic scenario a low number of signal events to begin with. Feasibility of signal detection, assuming luminosities measured in hundreds of inverse femtobarns, is thus mainly determined by the background rejection potential.

4.7 Reducible backgrounds and selected experimental issues

By reducible background is meant all contributions that can mimick the signal in a real experiment, but physically come from a different collection of particles in the final state. In other words, in an ideal detector the reducible background could be zero, but is not because of finite detector performance and event reconstruction capabilities. Following the standard background process classification used e.g. in CMS, the most important potentially dangerous reducible background sources in the study of WW scattering at high energies, for the purely leptonic decay modes, are: inclusive $t\bar{t}$ production, W +jets with a jet misidentified as a lepton and QCD multijet events with two jets misidentified as leptons. For the purely leptonic decay modes, the key detector features that determine the magnitude of the reducible background are the purities of lepton reconstruction, including the charge, and to a lesser degree the efficiency of b quark tagging.

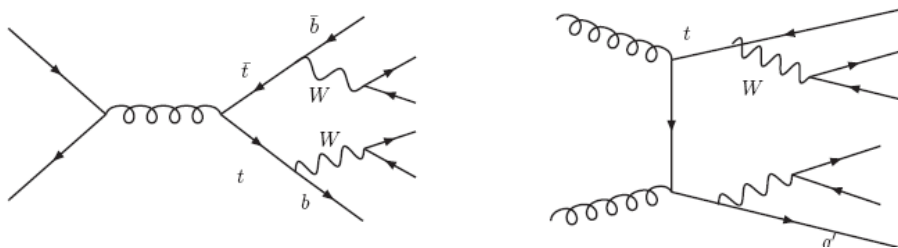


Figure 4.19: Two lowest order graphs for the inclusive $t\bar{t}$ background.

It must be stressed immediately at this point that we are considering the backgrounds

that can be significant at 13/14 TeV after imposing all the discussed selection criteria. It is an obvious fact that use of looser criteria, e.g., as a preselection for a multivariate type of analysis (MVA) will translate into additional and differently composed background to consider.

Top pair production at the LHC overwhelms the WW scattering signal by several orders of magnitude. We have already noted that the same-sign WW scattering mode is advantageous here in that a $t\bar{t}$ pair produces in principle always an opposite-sign gauge boson pair, along with two b -jets. However, the initial $t\bar{t}$ production cross section is so much larger than our potential signal that tiny effects associated to leptonic b decays or a charge mismeasurement of the lepton arising from W decay, can lead to measurable effects which cannot be disregarded. As each top quark decays into a W and a bottom quark, it is clear that b -tagging efficiency plays an important role. A typical b -tagging algorithm in a collider experiment is based on the most characteristic feature of B mesons, namely their short lifetimes, identifiable in the detector as subsequent decays occurring from a vertex which is displaced somewhat from the proton-proton interaction point. Many b -tagging algorithms have been developed and their performance studied in CMS, the most commonly accepted being the Combined Secondary Vertex (CSV) algorithm [77]. The algorithm relies on the reconstruction of secondary vertices together with the track-based lifetime information in a jet. For each track a 3-dimensional impact parameter is computed from its minimum distance of approach to the vertex, then tracks in a vertex are ranked based on a significance number equal to the value of the impact parameter expressed in units of its uncertainty. Likelihood discriminants to identify the jet as a b -quark are based on the significance of usually the second-ranked (“High Efficiency”) or sometimes the third-ranked (“High Purity”) tracks. The threshold value is, as always, arbitrary and allows to choose an optimum working point for each analysis based on the general performance curve that correlates the tagging efficiency with tagging purity, the latter determined in terms of the efficiency for tagging a u -, d -, s -, c - or gluon jet. Since tightening the tagging criterion quickly leads to an avalanche increase of light quark mistagging, the final b -tagging efficiency is determined mainly by the maximum acceptable tagging impurity. From the CSV performance curves we learn that signal losses can be kept up to or below 2% overall, while 50% of genuine b quarks get tagged. For a $t\bar{t}$ event, with two b quarks in it, this means a reduction factor of 0.25. Useful, but far insufficient to keep the $t\bar{t}$ background to manageable levels. Alternatively, a 0.10 reduction factor can be obtained by allowing of a 10% loss of the signal. The fact that b -tagging efficiencies decrease in the forward/regions regions is not very disturbing because tag jets usually do not originate from b quarks, as we will see further on. Because of steeply increasing impurity rates, further adjustments of these numbers leave rather little room for improvement.

The bulk of the $t\bar{t}$ background must be in any case eliminated kinematicwise. The top quark mass defines a natural upper bound for the invariant mass of its visible decay products, in our case the jet and the lepton. There is of course an ambiguity here related to correlating the proper jet with the proper lepton, overall kinematic constraints however favor a configuration in which relative ranks (defined by the respective p_T values) of the jets and the lepton anticorrelate. Which is to say, more often than not, the largest- p_T lepton with the second- p_T jet and the largest- p_T jet with the second- p_T lepton reproduce

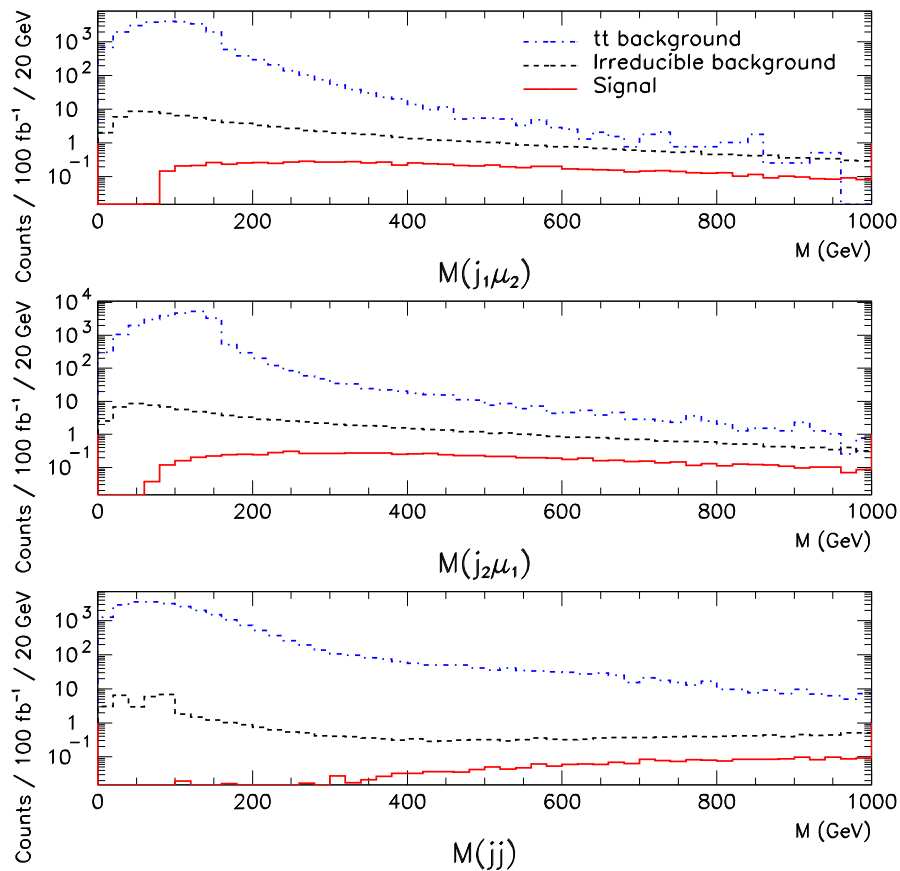


Figure 4.20: Distributions of the invariant mass of the two leading jets (top) and of combinations of jets and leptons (middle, bottom) for the signal, irreducible background and $t\bar{t}$ background in the $pp \rightarrow jjW^+W^+$ process at 14 TeV, after applying basic topological VBF cuts. Results of a MadGraph calculation, processed by PYTHIA 6 for W decay into muons, the effects of parton showering, hadronization and jet reconstruction. The original PYTHIA 6 source code was modified to account for the correct, polarization-dependent, angular distributions for the decays $W^\pm \rightarrow \mu^\pm\nu$.

the top mass constraint. Furthermore, as in a typical $t\bar{t}$ production event, the two b -jets do not undergo any hard interactions, the two-jet invariant mass strongly prefers much lower values than those typical of WW scattering. It was determined from simulation that the combination of simple cuts:

$$\begin{aligned} M_{l_1 j_2} &> 200 \text{ GeV}, \\ M_{l_2 j_1} &> 200 \text{ GeV}, \\ M_{jj} &> 500 \text{ GeV}, \end{aligned}$$

together with b -tagging already reduces the $t\bar{t}$ background to manageable levels as long as it is only driven via effects like charge mismeasurement or leptonic B decays. Commonly used for reduction of the $t\bar{t}$ background is the additional requirement of central jet veto. Its usual form is removal of events with any additional jets of p_T larger than a predefined threshold and anywhere between the two tagging jets in pseudorapidity. Because WW scattering is a pure electroweak process, little jet activity in between the two tagging jets is expected in signal. Note however that a certain form of the central jet veto is already applied via the requirement of two tagging jets. By construction we require them here to be the two leading jets in the event, hence “central jet veto” proper in practice means an additional cut only if at least one of the tagging jets has p_T below the chosen threshold. Such cut provides another factor ~ 0.25 in terms of $t\bar{t}$ background rejection.

Detector efficiencies in terms of lepton charge determination, especially at large transverse momenta ($p_T \sim 300$ GeV), are relatively poorly studied. This is because beam energies of 7 or 8 TeV do not provide much data in this region and most mainstream physics analyses are very little sensitive to such effects anyway. Finally, because evaluation of potential backgrounds related to charge misidentification is in practice done using various partly or wholly data-driven methods that do not require explicit knowledge of the misidentification probability per se. But the results from 7/8 TeV cannot be directly applied to 13/14 TeV because the relevant p_T and η distributions differ. Correct charge reconstruction is generally easier in the central barrel region of the detector, which is advantageous for us. A simulation-based study done in CMS, in which the rate of muons with the reconstructed charge not equal to the generated charge was measured, revealed charge misreconstruction be at the level of 10^{-3} for muon p_T up to 100 GeV and slowly rising above [78]. An earlier study of cosmic muons passing through the whole detector in which muon charges were reconstructed separately in the top and bottom halves and disagreed, revealed this disagreement be already at the 0.5% level for p_T of the order of 300 GeV [79]. The two results do not disagree badly and taking into account the improvements in muon reconstruction between the times of the two analyses, we can safely assume a 99.7% muon sign matching probability as fully realistic in our kinematic range of main interest.

The charge misreconstruction for electrons is known both from simulations and from data using a Tag-and-Probe technique to be well below 1% in the barrel region ($|\eta| < 1.5$) for relatively low p_T and gradually increasing with p_T [81] [82]. The use of independent methods to estimate the charge from a combination of various data from the central tracker detector and the electromagnetic calorimeter was shown to significantly reduce the inefficiencies of the standard Gaussian-Sum Filter (GSF) track curvature method. The efficiency still degrades somewhat with p_T , but 99% gives the right order of magnitude of what can be readily achieved as far as electron sign matching is concerned. ATLAS

also reports [82] sub-percent level inefficiencies of electron charge reconstruction for the barrel once their “tight identification” criteria are imposed, while at the same time the efficiency of electron-ID (reconstruction+identification) in the barrel region is larger than 85% for $p_T > 50$ GeV.

The jet \rightarrow electron or photon \rightarrow electron misidentification rates, commonly called “fake rates”, are usually determined using data driven methods. For an analysis of a given final state, a control sample is defined from data which differs from the signal data in that the quality criteria used to formally define an object of a certain kind, say, an electron or a muon, were loosened. The control sample is known to be composed mainly of “fakes”. The fake rate in the signal region is calculated by scaling the measured background distributions with the measured probabilities of each “fake” to pass the nominal quality criteria, usually as a function of its p_T and $|\eta|$. Results of such methods are directly applicable only in the context of their specific analyses. On the other hand, generic but simulation-based studies exist in which misidentification probabilities were measured relative to any random jet of a given p_T and $|\eta|$. The results naturally depend on the details of the electron selection criteria applied. In CMS, simulation work has shown [83] that a combination of stringent electron identification criteria based on:

- track, electromagnetic and hadronic isolation, each defined as the p_T/E_T sum of all tracks/clusters lying within a $\Delta R=0.5$ cone around the reconstructed electron, relative to the E_T of the electron,
- the geometrical matching of the track with the cluster in both pseudorapidity and the azimuthal angle,
- the ratio of the electromagnetic energy deposit to the electron momentum, E/p , or alternatively, $|1/E - 1/p|$,
- the electromagnetic cluster shape described in terms of the ratio of energy deposits within a 3×3 and 5×5 cell collection centered around the seed of the cluster,

makes the probability that a jet gets reconstructed as an electron possible to reduce to $(1.1 \pm 0.2) \cdot 10^{-4}$ on average and somewhat increasing with E_T , as far as can be judged from a rather low statistics. Moreover, due to the mechanisms of W +jets production at the LHC, in these events only 27% of those “fake electrons” have the same sign as the W . This translates into W +jets background rates being nearly 3 times lower in $W^\pm W^\pm$ than in $W^+ W^-$. The same study suggests that the electromagnetic cluster shape described in terms of the pseudorapidity spread of the shower in 5×5 cells around the seed has also a large discriminating power on top of the other criteria and can reduce the fake rate by a further half. The overall electron reconstruction efficiency using the identification criteria that were ultimately applied in this study was 74% overall, but larger than 80% for $E_T > 50$ GeV and larger than 90% for $E_T > 100$ GeV, which is of main interest for us. Given the large total W +jets and QCD multijet events cross sections, keeping the fake rates low is imperative for the electron decay channels and so even allowing a slight decrease in the reconstruction efficiency is the better choice. Similarly, fake rates of photons misreconstructed as electrons were determined from simulation to be $(0.7 \pm 0.1)\%$, with an additional factor 2 reduction accounting for a particular choice of sign.

It is worth noting that all the abovementioned variables, and a few additional ones, are used as discriminators in the standard electron-ID used in CMS analyses. Based on early simulation studies, ATLAS reported jet-to-electron fake rates of the order of $2 \cdot 10^{-4}$ for jet $p_T > 100$ GeV, with the Boosted Decision Tree techniques used for electron identification and isolation, while keeping high electron-ID efficiency in this kinematic region [84]. Since this study was based on a simulated dijet sample, it is not possible to derive the charge correlation factor. Another study [85] reports on the possibility of a further reduction down to the level of $\sim 10^{-5}$ at the expense of electron-ID efficiency decreasing to 67%. Unfortunately both numbers are p_T -averaged.

In view of everything above, we can tentatively assume for further considerations an average electron fake rate in our kinematic domain of $\sim 10^{-4}$, times the appropriate sign factor, with a 90% electron-ID efficiency and a 99% charge reconstruction efficiency. However, one cannot completely trust Monte Carlo programs to study effects related, e.g., to jet fragmentation at the LHC. Only real data in the appropriate kinematic domain will ultimately determine the impurities. Further improvements in electron purity and sign matching, keeping a reasonably high overall reconstruction and identification efficiency, must be particularly encouraged and followed with a special attention, since they can be the key for success in including the electron-electron and mixed muon-electron decay channels to the WW scattering search at 13 TeV and can prove vital for the observation of signal.

Fake rates of hadrons misreconstructed as muons in principle include two distinct effects. The first of them are punch-thru pions which reach the muon chambers. They are usually associated with hadronic activity around the fake muon track. The second class are real muons from pions or kaons decaying in the detector, often referred to as “non-prompt” muons. These are recognizable by a characteristic kink in the track, visible at the point of the pion or kaon decay. By choice of appropriate isolation criteria both effects can be suppressed to a negligible level. Measurements and simulations done within ATLAS [86] reveal a total fake rate for jets of less than $\sim 10^{-5}$ and dropping with jet p_T , and about 10^{-3} for single tracks. The latter however may be contaminated with real “prompt” muons from W and Z decays. In our further considerations we will disregard these backgrounds.

One last experimental issue that is definitely worth to mention at the present moment, particularly in the context of the planned future upgrades of LHC detectors, concerns jet reconstruction efficiency at large pseudorapidity. In Standard Model VBF processes at 14 TeV, pseudorapidity distributions for tagging jets peak between 2-3. This holds approximately equally true for $V_T V_X$ as for $V_L V_L$ pairs. This however does not imply that this region is of most interest for BSM search. Contrary, the best sensitivity to BSM effects is likely to be more forward. E.g., non-SM Higgs couplings will reflect in a wide pseudorapidity range for the tagging jets, going even all the way up to 5 for the subleading jet. It is therefore important to have a good jet reconstruction in the entire pseudorapidity range and keep high performance in the most forward region for the whole High Luminosity LHC program.

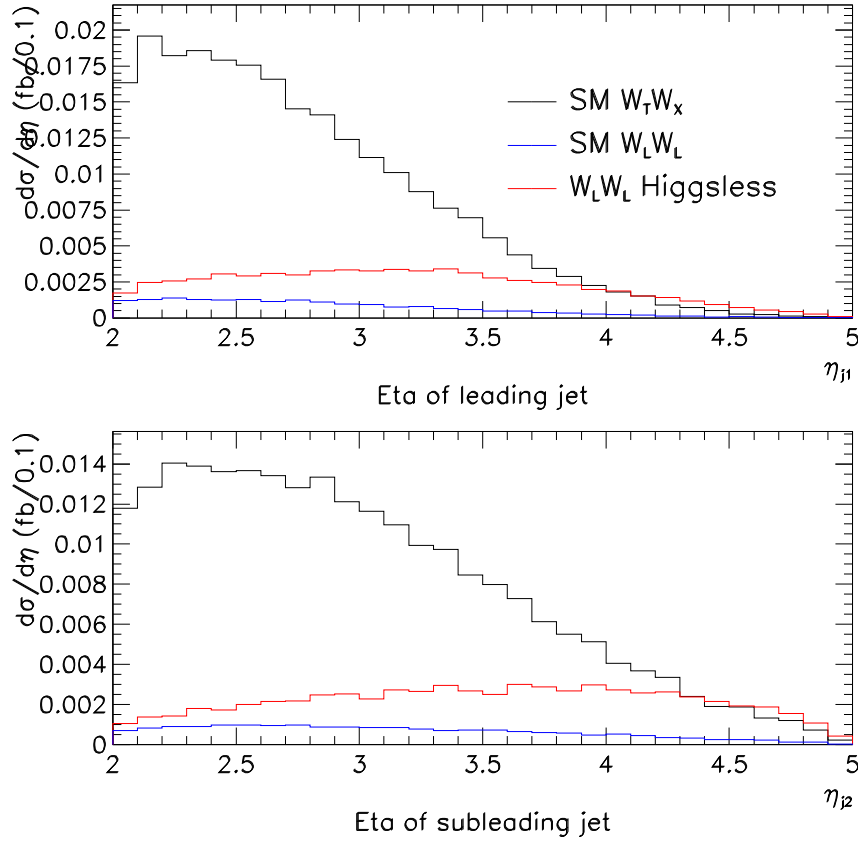


Figure 4.21: Pseudorapidity distributions for the leading (top) and subleading (bottom) tagging jets in the $pp \rightarrow jjW^+W^+$ process at 14 TeV, with leptonic W^+ decay, after applying basic topological VBF cuts, namely $\Delta\eta_{jj} > 4$ and $|\eta_l| < 2.1$. Shown are the SM spectra for $W_L W_L$ and $W_T W_X$ pairs and the $W_L W_L$ spectra for the Higgsless signal. Results of a MadGraph calculation, processed by PYTHIA 6 for W decay into muons, the effects of parton showering, hadronization and jet reconstruction. The original PYTHIA 6 source code was modified to account for the correct, polarization-dependent, angular distributions for the decays $W^\pm \rightarrow \mu^\pm \nu$.

Chapter 5

Simulation-based studies vs. experimental results

The processes of VV scattering have been lying in the interest of physicists for almost as long as the Standard Model itself. Despite of there being many simulation-based analyses of VV scattering at the LHC with 14 TeV, both at a phenomenological level or involving elements of a full experiment-specific detector simulation, a vast majority of them need critical revisiting in accordance to recent developments in our experimental knowledge and in the available simulation tools.

To begin with, in most older studies it was Higgs boson existence that was considered the biggest unknown of the model. Consequently, signal was calculated either in terms of a pure Higgsless Standard Model, or a Higgsless Standard Model where only the unitarity of scattering amplitudes was enforced by hand, or a Standard Model with a very heavy Higgs, or finally within the framework of a particular alternative model of electroweak symmetry breaking. Physicswise all these scenarios are now obsolete. This however does not imply that older studies should be sent to oblivion. It is rather straightforward to reinterpret the results of the former three classes of works in terms of a 125 GeV Higgs with different HWW or HZZ couplings. For that the relevant signal figures should to a good approximation only be scaled down by calculable, coupling-dependent factors. In a similar manner it has been shown that in the regime of the LHC at 14 TeV, the sole unitarity bound produces a 20-25% reduction of the signal figures compared to a pure Higgsless Standard Model. Moreover, in a non-resonant process like $W^\pm W^\pm$ this approach is in fact approximately equivalent to assuming a heavy Higgs (with $M_H \approx 1.2$ TeV), the one notable difference being that the latter must then have a very large width, which affects the scattered $W^\pm W^\pm$ mass spectrum in a non-trivial way. More problematic is only reinterpretation of results that were obtained by assuming particular alternative models of electroweak symmetry breaking, but even there some of the analysis methods that have been worked out may remain useful today.

Equally problematic are the old estimates of reducible backgrounds. In phenomenological studies such backgrounds are, more often than not, treated either qualitatively, e.g., by suggesting certain cuts to suppress them, or considered only partially. Optimistically, its supposedly largest component was studied in more detail (typically, inclusive $t\bar{t}$ production).

Results based of full detector simulations for a specific experiment often differed widely

from results of purely phenomenological analyses, especially in the semileptonic decay channels. The former have been evaluated using detector-specific simulation tools available at the time of their publication, which is, in the early stages of software development for ATLAS or CMS, to focus on these two. It is obvious that these tools have since improved paramountly. But the improvements are usually difficult to quantify without redoing the whole simulation. Unfortunately this means that these older studies that involved full detector simulation usually do not represent a valid reference to assess the best current experimental sensitivity in the search for physics beyond the Standard Model in WW scattering.

First, however, let us briefly recall and review the leading past works in the subject, focusing not that much on their numerical results, but rather with a special emphasis on what things of all those older studies remain completely valid today.

5.1 Early calculations

Physicists' interest in VV scattering clearly predates the LHC. Already in the early papers of Chanowitz et al. [89] it was noticed that scattering of same-sign longitudinally polarized W 's is the most sensitive probe of effects related to the mechanism of electroweak symmetry breaking. Several other authors, including Barger et al. [90] and independently Dicus et al. [91] studied in detail the process of W^+W^+ scattering in the context of the planned Superconducting Super Collider (SSC). Their numerical results do not have a direct importance for us, but some of their qualitative observations are strikingly up to date. Among other things, they proposed kinematic cuts to keep the $t\bar{t}$ background under control and stressed the importance of jet transverse momenta in the separation of the longitudinal WW signal from the transverse WW background. In particular, to tackle the latter, cuts on the *maximum* allowed jet p_T were discussed.

Systematic studies of the WW scattering phenomenology in the particular context of the LHC started later in the 1990's. Their main physical focus was observation of signal related to different scenarios of electroweak symmetry breaking on the assumed absence of a Higgs boson. Despite their main underlying physics assumptions are now implausible, a large amount of knowledge is still contained in these studies and a lot of this knowledge remains valid in the context, e.g., of searches for new heavy resonances or other experimental signatures in the absence of such resonances. To a large extent we can still follow the general guidelines presented in those papers.

The early paper of Barger et al. [90] provided the justification on theoretical grounds of some basic signal selection criteria in the context of heavy Higgs searches at the LHC. It is here that introduced and justified on theoretical grounds was the idea of a central jet veto as a primary criterion to distinguish QCD-related backgrounds from the purely electroweak signal.

Especially enlightening from the phenomenological point of view, although again focused on various Higgsless scenarios, are the works of Bagger et al. [92]. They developed the general methodology, introduced the "subtraction method" for the mathematical definition of the signal and recapitulated on the basic experimental signatures. They proposed original sets of kinematic cuts optimized for all the individual VBS processes separately and finally, they showed a comparative study of possible signals and backgrounds (not

only irreducible) after each step of the full event selection. They also noticed the experimental advantages of purely leptonic W and Z decay modes in their analyses and termed them as “gold-plated”. Let us recall some of their main conclusions that are still valid today. From the different analyses by Bagger et al. it follows that depending on the actual physics scenario, any of the different scattering processes: W^+W^- , $W^\pm W^\pm$, $W^\pm Z$ or ZZ , may turn out to be the most promising one, or even a combination of all of them could be required. Models which predict heavy scalar resonances were found most easy to study in the ZZ and W^+W^- processes (in agreement with everything we have said so far), heavy vector resonances should show up more efficiently in the WZ process, while very heavy resonances or scenarios with no such resonances at all would manifest only as an increase of the total event yield at large invariant mass and this increase is the most pronounced in no else than $W^\pm W^\pm$. The significance of the ZZ channel is driven mainly by the $l^+l^-\nu\nu$ final state rather than the cleaner, but lower rate $4l$ final state. The former is nonetheless contaminated by a detector dependent background coming from $Z + \text{QCD}$ jets events, which have not been explicitly taken into account in this analysis, except from assuming it be suppressable by applying a cut on missing transverse energy (MET). The significance of the W^+W^- process in its turn crucially depends on the efficiency of suppressing the overwhelming inclusive $t\bar{t}$ background using such techniques as b -tagging and central jet vetoing. In these works, the respective signals were calculated using the Effective W Approximation and the Equivalence Theorem, as well as assuming particular scenarios of electroweak symmetry breaking, alternative to the Higgs model. All the analyses were carried at a purely partonic level. Quantitative estimates of the required luminosity to observe a non-SM signal in the different channels vary from below 100 to 250/fb for the LHC running at 14 TeV, but because of the approximative character of the relevant calculations they should be taken with care. All the signal scenarios involve strong WW scattering, in which they resemble a Higgsless Standard Model with reinforced unitarity. Even though the authors perform an essentially counting experiment, with an analysis which is not optimized for resonance search (in most cases the resonance is very broad anyway), differences of more than a factor 3 in the required luminosities give a rough idea of the degree of model dependence of the signal significances and hence of all their quoted results. The process $ZZ \rightarrow 4l$ is perhaps the most interesting both because of its low background and because it offers the best event reconstruction and hence full determination of the nature of the heavy resonance, but it also requires the largest luminosity for observation. It was estimated to be around 300/fb of LHC running at 14 TeV to observe a 99% CL signal, which corresponds to roughly 4σ . The sensitivity of the $W^\pm Z$ process to non-SM physics was shown rather marginal. The authors suggest in fact focusing on the Drell-Yan process to enhance the significance of $W^\pm Z$ in the search for heavy vector resonances. Meanwhile, the $W^\pm W^\pm$ process fares poorly in scenarios with heavy scalars, but somewhat surprisingly turns to be the most efficient in scenarios with heavy vectors, in addition to non-resonant ones. Typical luminosities required to observe signal at a 99% CL oscillate roughly around 200/fb. Of other interesting observations that are worth recalling, the authors stress that signal is contained mainly at relatively low p_T of the tagging jets, typically $p_T \sim M_W/2$. Large jet p_T thresholds usually applied in various analyses of LHC data because of pile-up related background would therefore translate into low signal detection efficiency. As a possible alternative, single jet-tagging was proposed, which of course would come at the expense of background rejection effi-

ciency. However, good signal efficiency could be achieved with double-jet tagging if only the jet p_T threshold could be lowered to 15 GeV.

Unfortunately, the studies by Bagger et al. came too much ahead of their time and many of their important conclusions, perhaps because of the obsolete by now computational techniques they applied, got largely forgotten before the LHC started operation. It is time now to rediscover the findings of this work and reevaluate them with modern and fully up to date simulation tools.

Other classic works include the ones by Dobado et al. [93], focused specifically on ZZ and WZ production. Their studies were carried within the Electroweak Chiral Lagrangian approach. They mainly elaborated on a unitarization technique based on the Inverse Amplitude Method, in which new dynamic resonances appear in VV scattering and enforce unitarization. They also applied the Equivalence Theorem and used the Effective W Approximation in their calculations of the relevant VBS processes. A tentative analysis was presented at the level of undecayed gauge bosons, by further assuming a 100% efficiency in their reconstruction, and moreover only irreducible backgrounds were taken into account. Since both their signal and background treatments are highly approximative, their numerical results cannot be considered but purely qualitative. In what's important for us, however, they do confirm the importance of Drell-Yan production rather than VBS for the WZ process.

Chanowitz et al. [94] in a series of follow-up papers focused on W^+W^+ and WZ processes. The authors observed a complementarity of the W^+W^+ and WZ processes as a function of the mass scale of the hypothetical new, heavy vector resonances. The combination of the two was shown to guarantee the “no-lose theorem”, meaning that signal would be always observable one way or another, i.e., in at least one of the two processes. For the calculation of the WZ signals they considered Drell-Yan as well as VBS. Here too calculations were based on the Chiral Lagrangian Model and, as in the previous analyses, the Equivalence Theorem and the Effective W Approximation were used to evaluate VBS processes. Only irreducible backgrounds were explicitly considered. However, their work was the first to mention the potential importance of detector dependent backgrounds related to lepton sign mismeasurement. They also followed up on the issue of separating the final state polarizations, but focused on purely leptonic cuts for this purpose. The reason was simple: specific of their analysis was the treatment of VBS and Drell-Yan together. They omit some typical VBS cuts, like forward jet tagging, which would kill their Drell-Yan signal. Under these conditions, they finally found an LHC luminosity of 140/fb guarantee the “no-lose” condition with a significance of at least 3σ , which perphas does not have a direct meaning for us.

In a ground breaking paper, Butterworth et al. [95] found that semi-leptonic decay modes could be as promising as purely leptonic. They considered only the W^+W^- scattering process (note however than in semi-leptonic decays one of the W 's has no measured charge, so in reality a sum of W^+W^- and W^+W^+ is automatically implied) and calculated the signal in several models within the Electroweak Chiral Lagrangian approach, that corresponded to the existence of heavy scalar or heavy vector resonances, as well as no resonances at all. The calculation was done using a modified version of the PYTHIA generator which indirectly involves the Effective W Approximation. Background evaluation included $t\bar{t}$ production and radiative W +jets events, calculated likewise within PYTHIA. The authors concluded that signal could be measured after 100/fb of LHC

data, but stressed that the final word would only come from real measurements of the reducible backgrounds. Indeed, it was later shown that uncertainties related to background modelling in the semi-leptonic decay modes were tantalizing. Although this was probably the first simulation-based phenomenological analysis which involved a toy jet reconstruction procedure and envisaged the use of jet substructure to tackle the problem of jet merging from highly boosted W bosons decaying hadronically, the real performance of this procedure may depend on additional effects, e.g., detector resolution, not studied in this analysis. Using a newer PYTHIA version with improved parton showering and a dedicated event reconstruction software used by CMS at the time, it was found [96] that these predictions were way too optimistic. It also indicated that a lot of work was still required on the detector and reconstruction side.

Some of the many other studies of the phenomenology of VV scattering before Higgs discovery are listed under Ref. [97].

A lot of early simulation work, that in addition included simulated detector response and event reconstruction, was done within the ATLAS collaboration [98]. In these studies, signals were calculated using PYTHIA and the various backgrounds using such generators as MadGraph and MC@NLO. The main focus was WZ in different semi-leptonic and purely leptonic decay modes and WW in the semi-leptonic decay mode in which case the signal and backgrounds were evaluated together with WZ , where $W \rightarrow l\nu$ and $Z \rightarrow jj$ (in a real experiment, processes tend to be naturally grouped by final state as seen in the detector). They also produced a result for $ZZ \rightarrow l^+l^-\nu\nu$, but only in the scenario of a Higgs-like resonance with a mass of 500 GeV. Unfortunately, no results from purely leptonic decays of WW have been shown and no $W^\pm W^\pm$ in particular. Their analyses included standard VBS selection criteria, not specifically optimized for gauge boson polarization. However, their p_T threshold for the identification of tag jets vary between 10 and 20 GeV, ensuring reasonably high acceptance for longitudinal bosons. The study focused mainly on Higgsless, resonant scenarios, many of the considered resonances were relatively light and so the results must be regarded as out of date today. Interestingly, the only non-resonant scenario considered in this study (there is however no information about the exact parameter values used within PYTHIA to simulate this kind of signal) did not lead to promising results and was not even included in the table of results that concluded the study.

5.2 Recent works and post-Higgs discovery developments

A new generation of VV scattering studies commenced with the introduction of universal, commonly accessible physics calculation tools, like MadGraph, CompHEP, ALPGEN, PHASE/PHANTOM or VBFNLO, which calculate the full matrix elements for a given process. They replaced PYTHIA-based and other signal calculations done only in the Effective W Approximation. At the same time, since those generators often did not have any alternative models of electroweak symmetry breaking explicitly implemented, signal calculations necessarily required a more generic, model-independent approach. Such approach was in practice provided by considering a pure Higgsless Standard Model, or a Higgsless Standard Model with effective unitarization. This could be implemented either

as a sharp cutoff or else assuming that the relevant scattering amplitudes saturate just before reaching the unitarity limit. Incidentally, the latter is phenomenologically similar to non-resonant Higgsless models. Therefore many of these newer studies are directly relevant for the case of a light Higgs boson with modified couplings and no new resonances within the mass range of the LHC. They require in principle only a scale factor for an effective translation into a physically valid and up to date scenario.

One of the earliest WW scattering analyses that did not make use of approximative computation techniques was the work by Eboli et al. [108], in which purely leptonic decays were studied in the WW process and in all charge combinations. They find a full calculation of the scattering amplitudes necessary not only for a correct cross section evaluation, but also to describe accurately all correlations between final state particles. A notable feature of the presented analysis was the most complete available treatment of inclusive $t\bar{t}$ background, it included contributions from processes with up to two associated QCD jets computed at the matrix element level. The inadequacy of considering only pure $t\bar{t}$ production in the lowest order was shown. Conceptually the work was focused on a study of anomalous quartic vector boson couplings in which two exclusive working hypotheses were considered in what regards Higgs existence. For a discussion of the main concept and of the obtained results, we will still come back to this work in the next section.

Of the newer analyses at the phenomenological level, the works by Ballestrero et al. [99] clearly stand out and they also effectively triggered a lot of further, detector level work within the CMS collaboration. In a series of papers they studied both the semi-leptonic and purely leptonic decay channels. Calculations were done with the newly created PHANTOM program [123] which computes complete tree level matrix element amplitudes for $2 \rightarrow 6$ fermionic processes to the orders $\mathcal{O}(\alpha^6)$, $(\alpha^4\alpha_S^2)$ and $(\alpha^2\alpha_S^4)$, wherever appropriate. All the analyses were carried in a manner which closely resembles realistic experimental analyses. Scattering processes were grouped by final state. Signal was defined in terms of a VBF-like kinematics in the purely electroweak process where the final event yields were compared in the Higgsless and light Higgs cases. The fact that they typically assume $M_H = 200\text{GeV}$ for the Standard Model case is a rather minor issue. Additionally, processes $\mathcal{O}(\alpha^4\alpha_S^2)$ and $(\alpha^2\alpha_S^4)$ accounted for all the extra, non-scattering, background. In principle, the scope of background processes that can be taken into account in this way includes the most basic $t\bar{t}$ production process without additional quarks or gluons. But as we already mentioned as will further see in the next chapter, such treatment is insufficient for an accurate account of inclusive $t\bar{t}$ background for VBF processes, since the bulk of events that can survive VBF cuts comes in fact from higher order diagrams. The applied selection criteria selected general VBF events and were not optimized for longitudinal W/Z polarization. Moreover, a high p_T threshold for tag jets was used, as had become already routine e.g. in Higgs searches. All the analyses were carried at the partonic level and background treatment, as mentioned above, in practice included only irreducible backgrounds. The final sensitivity was evaluated from event counting or from a shape analysis of the invariant mass spectrum of the visible gauge boson decay products. Not surprisingly, the most interesting results came from the purely leptonic states. Again here the same-sign dilepton channel ($W^\pm W^\pm$) was shown to provide the best discrimination between different scenarios, closely followed by $ZZ \rightarrow l^+l^-\nu\nu$ and W^+W^- . Obviously, quantitative comparisons are subject to further change once all re-

ducible backgrounds are properly included. The analysis of semi-leptonic decays can only be treated as a demonstration because the jet merging issue which affects the decays of highly boosted gauge bosons in a real detector was not addressed in this study and because final state radiation, leading to additional jet combinatorics, was not simulated. Perhaps the most interesting result of Ballestrero et al. from our (biased) perspective resides in that their works were among the first ones to explicitly consider the Strongly Interacting Light Higgs models as an alternative to either Higgsless or the Standard Model. Their results suggested a decrease of the signal size (redefined here for our purposes as the enhancement with respect to the Standard Model) by a factor 3-4 when compared to a pure Higgsless scenario. Since effectively the only relevant feature of the considered SILH scenario was a modification of the HWW and HZZ couplings by a factor numerically close to 0.7, compared to the SM, their result presented in this way can be treated as model independent. It is in fact a particular example of a scale factor that is necessary to apply to all the former Higgsless-based studies to render them fully realistic.

The CMS collaboration produced a full set of results, corresponding to the many different final states, obtained using the general prescription of Ballestrero et al., with the addition of the dedicated CMS event reconstruction software [100]. The final states that were considered corresponded both to semi-leptonic and purely leptonic decay modes of W^+W^- , $W^\pm Z$, ZZ and $W^\pm W^\pm$. The results were admittedly not very encouraging. However, e.g., the analysis of the same-sign channel was clearly suboptimal. Moreover, as already stressed, the work was done at the time of rapidly changing CMS reconstruction and analysis tools and cannot be taken as the final word. Very derisible would be to have these data reanalyzed with the most recent versions of the CMS software and using the most efficient selection criteria for a complete and up to date evaluation.

In another analysis done at the phenomenological level, Zeppenfeld et al. [101] studied leptonic decays of the W^+W^- , ZZ and $W^\pm Z$ scattering pairs. They calculated signal and backgrounds using the VBFNLO generator program, where signal was defined in terms of a 1 TeV Standard Model Higgs or alternatively via a Warped Higgsless model with heavy vector resonances. Their most important conceptual innovation from today's perspective was that their background treatment included realistic modelling of $t\bar{t}$ +jets in addition to irreducible backgrounds. For the former they developed an original simulation-based approach which is suitable for VBF analyses. Initial and final state radiation processes were simulated and double counting was avoided by defining mutually exclusive topological requirements for processes with 0, 1 and 2 QCD jets generated at the matrix element level. Consequently, they found $t\bar{t}$ +jets the most important remaining background in the W^+W^- channel, in contrast to what was assumed in many other studies. We will review their method in further detail in the next chapter. A toy jet reconstruction by recombination of the final state partons was also applied. Quite consistently with most previous studies, they found $W^\pm Z$ the preferred channel for the vector resonance scenario and W^+W^- closely followed by $ZZ \rightarrow l^+l^-\nu\nu$ for the heavy Higgs scenario. They finally found a very high signal significance after collecting 300/fb of data at 14 TeV within the considered scenarios. This analysis also lacks separate consideration of the $W^\pm W^\pm$ process.

The importance of the $W^\pm W^\pm$ process as the one which guarantees the best realistic signal to background ratios, and the possibility to further improve signal selection criteria by careful study of specific signatures of $W_L W_L$ and $W_T W_X$ separately, including lower

thresholds on the p_T of tag jets, was rediscovered in the paper by Doroba et al. [102]. Many of the old observations of Bagger et al. were reconfirmed using a full tree level matrix element calculation of signal and backgrounds, including $t\bar{t}$ +jets, and including rough estimates of some additional detector effects related to jet reconstruction and lepton charge misidentification. Signal in this work was defined in terms of a Higgsless Standard Model with the unitarity condition implemented by applying appropriate weight factors to generated events with a WW mass larger than 1.2 TeV. Translation of all the results into the case of a light Higgs boson with modified couplings is straightforward.

From 2012 onwards it has become clear that all we can realistically hope for in VV scattering are the effects of non-SM Higgs (and gauge) couplings. Some general guidelines for a rough recomputation of all the predicted signal sizes were presented by Cheung et al. [103]. They considered all the different VV scattering processes and calculated scale factors to be applied to results of former Higgsless studies as a function of the actual HWW and HZZ couplings. Only purely leptonic W and Z decays were taken into account. However, all the signal sizes in this work were calculated in the Effective W Approximation and more importantly, the signal definition and selection criteria applied for this calculation involved two experimentally unmeasurable quantities, namely the WW scattering angle and the WW invariant mass. Hence, this work should be considered primarily a demonstration of principles rather than exact numerical results.

Most recently, various studies have been concentrated on possible methods to enhance signal significance via improvement of data analysis techniques as well as event reconstruction tools. Improvements in the analysis can be expected by means of applying novel techniques to explore the full shapes of signals and backgrounds in the multidimensional phase space spanned by the entire kinematics of visible particles in the final state. Measured multidimensional distributions can be compared to predictions arising from particular theoretical models calculated from the matrix elements. A likelihood function can then be defined to quantify the consistency of data with a predefined model. Such approach was used in a study by Freitas and Gainer [104]. The analysis they propose falls into the category of Multivariate Analyses (MVA), which have become the standard in contemporary experiments like ATLAS or CMS, supplementing or in many cases completely superseding the respective cut-based analyses. In fact, most Higgs related results published by CMS or ATLAS to date have versions of MVA's at their bases. The potential of discerning various theoretical models is quantified by a $\Delta\chi^2$ calculated for any two hypotheses. Focusing on W^+W^+ scattering at $\sqrt{s} = 14$ TeV, the authors found a significant improvement in the LHC potential to discern SILH models from the Standard Model by using their own version of the Matrix Element Method (MEM). The reference in this study was a one-dimensional analysis of the lepton-lepton invariant mass spectrum, as is routinely practiced in data analyses in HEP experiments. Expressed directly as a function of the SILH parameter ξ_{c_H} which governs the modification of Higgs couplings to gauge boson in the lowest order, the expected $\Delta\chi^2$ rises approximately linearly from 0 to 10 as the value of ξ_{c_H} increases from 0 to 1. Note that effectively $\xi_{c_H}=0$ is equivalent to the Standard Model, while $\xi_{c_H}=1$ is equivalent to no Higgs. Meanwhile, a similar $\Delta\chi^2$ obtained by considering solely the two-lepton invariant mass spectrum was found larger than 1 only for unrealistically large deviations from the Standard Model, beyond $\xi_{c_H} > 0.7$. A purely counting experiment offers of course yet lower sensitivity. However, one should remember that $\Delta\chi^2$ in a counting experiment is bound to depend on the selec-

tion criteria and $\Delta\chi^2$ in any analysis that does not exploit the full final state kinematics is bound to depend on the event preselection used to measure the analyzed spectrum. For further discussion on the correspondence of counting experiments with MVA's in the analysis of VV scattering, see next chapter.

Also in the context of MVA's, the subject of semi-leptonic decay modes was recently revitalized by Cui and Han [105]. Their main theoretical focus was also SILH models versus the Standard Model. They considered WW scattering, with all charge combinations included, and explored the jet substructure to separate the signal from various background processes, including reducible backgrounds such as $t\bar{t}$ +jets and W +jets. A detailed study of jet substructure provides an effective means not only to distinguish boosted W jets from QCD jets to a large accuracy, but also to account for the different W polarizations between signal and irreducible background. Wherever signal consists of longitudinally polarized gauge bosons, the two partons from hadronic W decay tend to be emitted more perpendicularly with respect to the W direction than in background events. Put another way, the p_T ratio of the two partons from signal events tends to be larger than the corresponding ratio from background events. For the purely electroweak processes of the Standard Model, the p_T share of the two partons is usually highly asymmetric, while it is typically more balanced in the signal. In order to distinguish boosted W jets from QCD jets, the authors use the current state-of-the-art methods. They are based on the fact that a boosted W has two hard subjets (i.e., geometrical regions where hadronic energy is concentrated), while a QCD jet has a single hard subjet. Subjets can be identified using dedicated techniques known as filtering, pruning or trimming. Additionally, W decay products have no color altogether. On the other hand, QCD jets carry color charge and are color-connected to other partons in the event. This reflects in different transverse jet profiles - QCD jets are typically much more diffuse. The most powerful way of separating signal from background is to combine different variables describing jet substructure: the masses and transverse momenta after jet pruning, planar flows, jet cone size dependencies, etc., to form an effective discriminator for the Boosted Decision Tree method. Overall, they found signal for the simplest Higgsless case possible to observe at more than 5σ (from $S/\sqrt{S+B}$) after 100/fb of data at 14 TeV, which is better than reported for the purely leptonic decay modes. The corresponding result for SILH models scales like $(c_H\xi)^2$. There is however considerable uncertainty related to their quantitative background evaluation. Although they considered both $t\bar{t}$ +jets and W +jets, as well as the irreducible $jjWW$ background from processes $\sim \alpha^4\alpha_S^2$, to demonstrate the principles of operation of the W -jet tagging procedure, their final background numbers are likely to be underestimated. This is because these backgrounds were obtained solely via parton showering from the basic $t\bar{t}$, $W + 1$ jet and WW processes, respectively, generated with PYTHIA, when this approach is known to be insufficient. The efficiency of the W -jet tagging algorithm may also depend on detector resolution and pile-up. Nevertheless, this work clearly indicates the direction. It proves that with the current reconstruction and analysis tools, and envisaging possible further refinements in the coming years, semi-leptonic decay channels will offer additional discovery potential and should not be neglected.

5.3 The quartic coupling perspective

Three leading order graphs contribute to $W^\pm W^\pm$ scattering in the Standard Model (five to W^+W^-), including Z/γ exchange, the $WWWW$ (quartic) contact interaction and Higgs exchange. Before Higgs discovery, and even later until Higgs couplings were known to enough precision, it was the Higgs exchange graph that represented the major puzzle in the entire picture and so a measurement of WW scattering could be practically considered equivalent to Higgs probing. As the by now discovered Higgs boson continues to fit Standard Model predictions with better and better precision, a shift of viewpoint is gradually taking place in what regards the physical motivation of studying VV scattering processes at the LHC. By assuming Higgs couplings known, e.g., exactly equal to their values predicted in the SM or to the values measured in the LHC, and by moreover assuming that no new physics be directly observed within the energy range at consideration, we can revert this reasoning and reformulate the problem in terms of the quartic $WWWW$ coupling. Indirect signs of new physics may include a modification of the effective four- W interaction term, leading to an anomalous coupling value. Such deviation would violate the cancelation of the leading $\sim s^2$ terms in the WW scattering amplitudes between the contact interaction graph and the Z/γ exchange graph, producing a divergence proportional to the fourth power of energy. The observed energy dependence would therefore in principle be different than in the case of modified Higgs couplings. However, deviations from the SM are likely to show up in more complicated forms than as a simple scaling factor applied on the SM value. Generally, anomalous quartic couplings may be generated as a contact interaction approximation of heavy particle exchange. The specific form of the operator that effectively contributes to the quartic vertex, plus the energy scale at which new physics sets in and places a natural cutoff for the relevant calculations, is a key question in order to assess the expected energy dependence. The actual value of the $WWWW$ quartic coupling is currently very poorly constrained by experiment. As we noticed before, VV scattering, along with triboson production, provide the most direct probes of the quartic couplings.

Interestingly, prior to Higgs discovery some authors studied Higgsless models in the language of effective anomalous quartic couplings. The correspondence is straightforward. Deviations from a pure Higgsless SM, possibly arising from heavy particle exchange or some kind of strong dynamics, were effectively parameterized as an anomaly in the quartic gauge vertex. As an example, based on such approach Godfrey [106] noticed early on that for the lowest dimension operators that do not include photons the LHC will provide the most constraining measurements compared to e^+e^- , e^-e^- , $\gamma\gamma$ or $e\gamma$ colliders. Furthermore, he found same-sign $W^\pm W^\pm$ scattering be the best process to study the quartic couplings. A similar approach was taken by Belyaev et al. [107], who basically redid the work of Bagger et al. in the language of anomalous quartic couplings. Today these studies are however of historical interest only.

By contrast, the work of Eboli et al. [108] retains its actuality because they have considered the case of a 120 GeV Higgs as one of their two reference scenarios in the study of quartic couplings. It was also one of the earliest papers where the full analysis was carried within the language of the Effective Field Theory with higher dimension (dimension-8 in this case) operators. As already mentioned, these authors considered the $W^\pm W^\pm$ and W^+W^- processes and purely leptonic decays. The analogy to former

Higgsless studies is evident. They propose a full collection of selection criteria, which is in fact a variation of the familiar Higgsless selection criteria. They included: $|\eta_j| < 4.9$ and $\Delta\eta_{jj} < 3.8$, $\eta_j^{min} < \eta_l < \eta_j^{max}$, $MET > 30$ GeV and $p_T^l > 30$ (100) GeV for same-sign (opposite-sign) leptons. Additional cuts: $M_{jj} > 1000$ GeV, a central jet veto and $\phi_{e\mu} > 2.25$ rad, were applied for W^+W^- only. W helicities were not distinguished, but a moderate jet p_T threshold for the tag jets (20 GeV) ensured good acceptance for W_LW_L pairs. Signals were calculated using the MadGraph generator with self-added modifications to include the anomalous terms. It must be stressed that in this analysis background evaluation included only irreducible background and inclusive $t\bar{t}$ production for W^+W^- and irreducible background only for $W^\pm W^\pm$. Moreover, all the analysis was done essentially at the parton level, with some experimental resolutions and estimates of reconstruction efficiencies simulated on top. The results are therefore likely to be too optimistic as far as overall background rejection is concerned. Unitarity constraints were satisfied by imposing a sharp cutoff at $M_{WW} = 1.25$ TeV. Final results were extracted by merely counting the total event yield in the signal window. From a combination of both processes and assuming an integrated LHC luminosity of 100 fb^{-1} , they came to predict the following 99% CL limits:

$$\begin{aligned} -22 &< \frac{f_{S,0}}{\Lambda^4} \text{ TeV}^{-4} < 24, \\ -25 &< \frac{f_{S,1}}{\Lambda^4} \text{ TeV}^{-4} < 25, \end{aligned}$$

under the assumption of only one non-vanishing coefficient at a time. In practice, combination of $W^\pm W^\pm$ and W^+W^- is crucial, because the two coefficients studied from each process separately show strong anticorrelation, especially in the same-sign process. This was the first such detailed study that explicitly focused on the LHC sensitivity to anomalous quartic couplings and used the language of higher-dimension operators. Although it may need minor updates in several places, it still remains the most complete phenomenological analysis of its kind.

5.4 VV scattering in LHC measurements at 8 TeV

Practically no simulation-based studies of VV scattering on a detector-independent level exist for pp collisions at 7 or 8 TeV. This is not just because these beam energies were not really considered at the early stages of LHC planning, but rather decided later on as a compromise between current technical possibilities and physics needs. The main reason is that it was known from rough order of magnitude estimates that 7/8 TeV would in fact not suffice to carry a truly conclusive measurement in terms of possible physics beyond the SM. After Higgs discovery, this became even more clear. This is why existing VBS-like measurements done at 8 TeV are still largely disconnected conceptually from all the simulation work presented above and it is not always a trivial task to realize how they in fact relate. Here we will examine first results from ATLAS and CMS concerning VV scattering that were obtained from an analysis of the 8 TeV data. In doing this our main point of interest will not be what the results tell us about physics, but rather what we can learn for future analyses at a higher beam energy.

Preliminary results on vector boson scattering at 8 TeV have been produced both by ATLAS [109] and CMS [110]. As the main ideas behind these two studies are closely

related and both analyses came out at a similar time (as usual, though, the ATLAS paper came first), we will discuss both of them simultaneously, making appropriate distinctions only when relevant. In both cases searches were carried for a loosely defined VBS-like signature in the same-sign WW scattering process and the purely leptonic decay channel. To partially tackle the inescapable problem of low statistics, applied VBS-like selection was in both cases minimal. The signature consisted of two reconstructed same-sign leptons (each of which could be either an electron or a muon) passing all the respective “high-quality” criteria and at least two jets within detector acceptance. The definitions of detector acceptance were marginally different for ATLAS and CMS, but could not play any major role in the final result. Minimum p_T of 20 (25) GeV was required in ATLAS (CMS) for the leptons and of 30 GeV for the jets. In addition, a minimum missing transverse energy of 40 GeV was required to account for the two neutrinos. The only additional selection criteria applied on the data in order to separate pure electroweak $jjW^\pm W^\pm$ production from processes involving gluon exchange was a cut on the jet-jet invariant mass, $M_{jj} > 500$ GeV, and rapidity separation $|\Delta y_{jj}| > 2.4$ (ATLAS) or 2.5 (CMS). Subscript jj refers always to the two leading (highest- p_T) jets in the event. These criteria are also instrumental in suppressing various sources of reducible background, chiefly inclusive $t\bar{t}$ production. At an average lepton p_T that corresponds to the beam energy of 8 TeV, the charge of the muon is measured accurately to negligible levels. However, inefficiency of electron charge determination can produce non-negligible detector background coming from e^+e^- pairs copiously produced at the Z boson peak. For this reason, the ee invariant mass was required to lie outside a band of 10 (ATLAS) or 15 (CMS) GeV around the Z mass. This cut affected only the electron-electron decay channel. Moreover, for any lepton pair its mass had to be larger than 20 GeV in ATLAS and 50 GeV in CMS. This is perhaps the most significant difference between the two analyses and was dictated by the respective detector capabilities in what concerns in particular the contamination from jets misreconstructed as leptons. Remaining inclusive $t\bar{t}$ background, entering via both lepton sign-flip effects and leptonic b quark decays, was effectively eliminated by standard b quark vetoing. Details of the b -tagging techniques were developed independently by the two collaborations, but both are based on combining the information from impact parameter significance of the individual tracks with explicit secondary vertex reconstruction. The bulk of background coming from WZ or ZZ +jets production was reduced by a veto on a third lepton. Here the cut depends on the efficiency and purity of lepton reconstruction and must be optimized in a detector-dependent manner. Consequently, it was somewhat stricter in ATLAS than in CMS: it involved any additional reconstructed leptons with $p_T > 6/7$ GeV or 10 GeV, respectively. In addition to the above, the ATLAS analysis used minimum angular separation criteria between the two leptons and between leptons and jets, the meaning of which is rather marginal.

Signal is defined as electroweak $jjW^\pm W^\pm$ production within a kinematic region consistent with vector boson scattering. There is no explicit distinction between WW scattering and non-scattering WW production at any stage of the two analyses. In fact, the ATLAS paper is conservatively entitled “*Evidence of Electroweak Production...*” and makes no mention of VBS anywhere in the paper abstract. Naturally, signal definition includes SM contributions and so it contains what in all our previous considerations has been called irreducible background. There is a subtle way in which signal is not exactly the same thing in the two analyses. In the CMS analysis, there is no distinction between pure electroweak

$jjW^\pm W^\pm$ production and QCD mediated (gluon exchange) processes within the selected kinematic window. Both are treated as an integral part of the signal. The ATLAS analysis explicitly separates QCD production of $jjW^\pm W^\pm$ as another class of background, as opposed to a purely electroweak process. How much of each we have in the sample is deduced from simulation. The question is not completely straightforward because the two types of processes interfere constructively, i.e., the total cross section is larger than the sum of the individual pure cross sections. This interference is of about 15% of the electroweak signal and depends on the choice of scale. ATLAS calculates the contribution from the interference terms by subtracting the coherent sum of pure electroweak and QCD process from the complete calculation including the interference. It is then added to the pure electroweak process as part of the signal prediction. They define a wider “inclusive” kinematic region in order to verify that QCD contributions are indeed suppressed in the proper signal region. In the signal region, the QCD contribution amounts to roughly 10% of the total $jjW^\pm W^\pm$ production. Such differences are in fact within the statistical errors of the signal sample collected in these studies. The future practical solution to the above problems would be in applying selection criteria tight enough so that any QCD contribution, including the interference, would become negligible altogether. This is, however, not a viable option for the present energy and the accumulated statistics.

For the background estimates both collaborations developed original methods which differ rather widely. Whenever simulations are used, typically, leading order generators were applied (MadGraph, POWHEG, SHERPA or ALPGEN), and the results were normalized in terms of a constant factor to the next-to-leading order in QCD cross sections obtained, e.g., with VBFNLO. Uncertainties of the order of 10% were found within the signal kinematic window for the main backgrounds. Differences in the respective LO generators used by ATLAS and CMS are unlikely to play a major role, but the respective PDF and QCD scale choices are in fact one of the main components of the systematic errors. CMS background predictions are for the most part data-driven. The so-called “non-prompt” lepton backgrounds, originating from leptonic decays of heavy quarks, hadrons misidentified as leptons (W +jets), and electrons from photon conversions in the detector were deduced from a control sample defined by one lepton which passes the full lepton selection criteria and another lepton which fails these criteria, but passes a “loose lepton” selection. Fake rates for such loose leptons to pass the nominal lepton criteria were then calculated and applied to the signal region. Similarly, the WZ background with two accompanying jets is predicted from a data control region requiring an additional lepton with $p_T > 10$ GeV. Other background sources included triboson production, sign-flip effects and double parton scattering. They amounted to less than 10% of the total background and were estimated from simulation. ATLAS background predictions for WZ and ZZ +jets (labeled “prompt”), as well as photon conversion background, were driven from full detector simulations and cross checked with the data in several same-sign dilepton control regions. Sign-flip backgrounds (part of which they include in the “conversion” category) and backgrounds involving leptons reconstructed from jets (collectively denoted as “other non-prompt”) were estimated directly from data.

Interesting is the significant difference in the final background composition between ATLAS and CMS. “Prompt” backgrounds, composed in 90% of WZ production with a lost third lepton (either not reconstructed or falling outside detector acceptance), amount to as much as two thirds of the total background at ATLAS. By contrast, it is less

than 20% in CMS. In absolute numbers, the remaining WZ background is over 7 times higher in ATLAS than it is in CMS (7.5 ± 1.1 vs. 1.0 ± 0.1 (stat.) events, respectively). Moreover, the effect is present consistently in all the lepton flavor combinations: $e^\pm e^\pm$, $\mu^\pm \mu^\pm$ and $e^\pm \mu^\pm$. Such difference cannot be explained solely by physics, i.e., details of the applied selection criteria, although stronger cuts on $|\Delta y_{jj}|$ and M_u adopted by CMS contribute in the right direction. We recall that the third lepton veto used to suppress WZ was stricter in ATLAS than in CMS in terms of the p_T threshold. However, different efficiencies of lepton reconstruction and third lepton veto, connected to the respective “tight” and “loose” lepton identification criteria applied by the two experiments, must be doubtlessly causing the resulting discrepancy. By contrast, the amounts of “non-prompt” (including conversion) background predicted in the two experiments are roughly similar: 6.3 ± 1.1 events in ATLAS, 4.2 ± 0.8 (stat.) events in CMS. We recall here that CMS used a stricter cut on the minimum lepton-lepton mass to protect from this kind of backgrounds. Different fake rates of hadrons misidentified as leptons may explain the observed differences. One thing is evident from this comparative study. Background levels and compositions crucially depend on tiny detector-specific effects related to the reconstruction and identification algorithms of different physics objects. They are difficult to predict from pure physics principles, unless in restricted kinematic regions chosen so to render most of these effects negligible. We will recall this when trying to draw updated predictions for 14 TeV.

Predicted signal levels are calculated from full detector simulations that use the MadGraph generator for CMS and POWHEG-BOX for ATLAS. Signal predictions in the SM amount to 8.8 ± 0.2 (stat.) events for CMS and 15.2 ± 0.8 for ATLAS, where we have redefined the ATLAS signal to include QCD for better consistency with CMS. As before, the difference may be at least partly due to signal selection criteria, in particular different cuts on M_u and $|\Delta y_{jj}|$; to a lesser degree $|M_{ee} - M_Z|$ and $|\eta_e|$ which affect only the electron decay channels. A 5% difference exists in the total integrated luminosity recorded by the two detectors (20.3 fb^{-1} ATLAS vs. 19.4 fb^{-1} CMS). The rest of the difference is nailed down to be due to theoretical uncertainties, reconstruction efficiencies and resolutions. In particular, the most important systematic uncertainties in the signal predictions are those related to the choice of PDF’s (7.7%) and the QCD scale (5%), jet energy scale and resolution (5%) and lepton efficiency (3%).

To quantify the statistical significance of the signal, events yields were examined in eight separate intervals formed by 4 bins of M_{jj} times two lepton charges. The observed (expected) signal significance in CMS is 2.0σ (3.1σ). In ATLAS, the corresponding numbers are 3.6σ (2.8σ). The apparently large discrepancy between the actually observed numbers of events in the signal region: 12 events in CMS vs. 34 events in ATLAS is consistent within the errors with all the earlier predictions.

It is trivial to convince oneself that ATLAS and CMS 8 TeV results neither confirm nor disconfirm Higgs existence, let alone give any clue of the relevant Higgs coupling. Likewise, they are hardly sensitive to anomalous triple gauge couplings within their present experimental bounds. Instead, they can be interpreted in terms of the first experimental bounds on the quartic $WWWW$ coupling. The fact that both analyses used a relatively high jet p_T threshold to protect from pile-up jets means that $W_L W_L$ pairs were disfavored. This additionally reduces the sensitivity to the HWW coupling and also to those higher dimension operators which modify only longitudinal gauge boson interactions. The

CMS collaboration obtained 95% CL limits on all nine dimension-8 operators that lead to anomalous contributions to the $WWWW$ coupling. Respective signal predictions were derived from MadGraph-generated samples in which one anomalous parameter was varied at a time. Limits were based on the measured lepton-lepton invariant mass spectrum of events that pass the full selection. Other considered spectra included the jet-jet invariant mass the four-body mass and the leading lepton p_T , but did not reveal improvements in sensitivity to the parameters in question. Here there was no specific optimization with the respect to the individual anomalous parameters, e.g., in what concerns the WW helicity combinations they directly affect. The effect of these parameters on the background is marginal and was neglected. This concerns also the WZ background, since in our signal window it is dominated by QCD contributions rather than WZ scattering. In addition to the uncorrelated limits on individual parameters, limits were derived in the two-dimension space of $f_{S,0}/\Lambda^4$ vs. $f_{S,1}/\Lambda^4$. Obtained contours show a strong anticorrelation between these parameters. Because of this the limits on individual parameters obtained by one-dimensional projections of the correlated limits are weaker than their uncorrelated limits by at least a factor of ~ 5 . The reason is straightforward. Each scattering process probes in fact specific combinations of anomalous parameters. And the other way around, improvement on the correlated limits can be only achieved by combining data from different scattering processes: W^+W^- , WZ and ZZ , which probe different combinations of the same parameters. Data at 8 TeV are however of not enough statistical power to study the other processes.

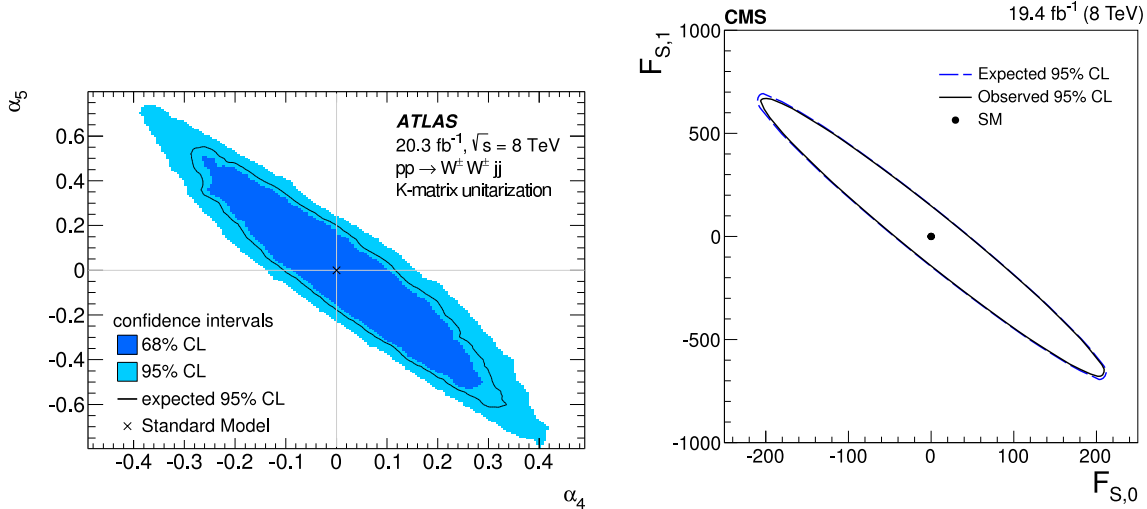


Figure 5.1: Left: observed and expected two-dimensional limits on the operator coefficients a_4 and a_5 from an analysis of the process $pp \rightarrow jjW^\pm W^\pm$ at 8 TeV done by the ATLAS collaboration - image reproduced from Ref. [109]. Right: observed and expected two-dimensional limits on the operator coefficients $f_{S,0}$ and $f_{S,1}$ from an analysis of the process $pp \rightarrow jjW^\pm W^\pm$ at 8 TeV done by the CMS collaboration - image reproduced from Ref. [110].

The ATLAS collaboration derived limits on the $WWWW$ coupling expressed in terms

of the a_4 and a_5 parameters of the Electroweak Chiral Lagrangian. The underlying model, as currently implemented in the WHIZARD generator, includes a 125 GeV Higgs boson in addition to the traditional dimension-4 operators foreseen within the framework of the EWChL, and so non-zero values of a_4 and a_5 can be in principle reinterpreted as equivalent to anomalous quartic couplings. While formally data may still be interpreted in this language, such treatment has not gained wide recognition in the physicists' community. A more practical problem is that non-zero a_4 and a_5 still induce unitarity violation and provide no built-in mechanism to restore unitarity. Results do depend on the arbitrarily chosen unitarization scheme, which is an intrinsic uncertainty of the model. ATLAS used the K-matrix unitarization procedure and did not quantify the theoretical uncertainties related to this particular choice. Effective equivalence of the phenomenological impact of non-zero (a_4, a_5) with that of dimension-8 operators from the Effective Field Theory approach was demonstrated. The relationships for the $jjW^\pm W^\pm$ process are supposedly the following [63]:

$$a_4 = \frac{v^4 f_{S,0}}{8\Lambda^4}, \quad (5.1)$$

$$a_5 = \frac{v^4 (f_{S,1} - f_{S,0})}{16\Lambda^4}, \quad (5.2)$$

where v is the usual Higgs vacuum expectation value. With the above one can verify that the far endpoints of the 95% CL contours from ATLAS, approximately $a_4 = \pm 0.4$ and $a_5 = \mp 0.7$, correspond to $f_{S,0}/\Lambda^4 \approx \pm 870 \text{ TeV}^{-4}$ and $f_{S,1}/\Lambda^4 \approx \mp 2180 \text{ TeV}^{-4}$, several times weaker bounds than from the CMS analysis. Why such discrepancy? Partly because ATLAS does see an excess of events with respect to SM predictions, while CMS sees a deficit. Another reason is that the CMS methodology does not assume any physical cutoff Λ for the evaluation of the anomalous signals. The underlying assumption that new physics does not directly show up to the presently available energy is natural in the light of no new physics having been actually observed in the LHC so far. However, $f_{S,0}/\Lambda^4$ and $f_{S,1}/\Lambda^4$ may lead to unitarity violation within the quoted limits. Put another way, even a BSM signal equivalent to hitting the unitarity limit at the highest available energy could not be observed with the present data. By saying earlier on that the results neither confirm nor disconfirm Higgs existence, we effectively meant exactly the same thing. Data at 8 TeV do not provide enough sensitivity to establish really physically meaningful limits on the studied parameters. Formally calculable limits reflect the applied unitarization procedure or lack of it and one should be extremely careful in drawing physics conclusions. The exercises done by ATLAS and CMS serve as a demonstration of principles and technical preparation for future measurements at higher energies. They set up and test the methodology. They reveal the main experimental and theoretical issues to be addressed in such measurements. But their physics meaning on its own is for the time being quite limited.

The CMS collaboration derived also limits on the production cross section times branching fraction of a doubly charged Higgs decaying into $W^\pm W^\pm$. Doubly charged Higgs bosons are expected in models that contain a Higgs triplet field. In such models, the $W^\pm W^\pm$ scattering process would be a resonant one, in contrast to the SM and its most popular proposed extensions.

Chapter 6

What can the LHC measure

After delivering 5 fb^{-1} of proton-proton data at 7 GeV and 20 fb^{-1} at 8 TeV, the LHC entered the first long shutdown (LS1) phase from 2013 till the end of 2014 and has been due to upgrades. LS1 included a large number of simultaneous activities concerning both the injectors and LHC itself, aimed to ensure reliable operation at nominal parameters from 2015. Most importantly the center of mass energy will now be nearly doubled and become 13 TeV. Early plans assumed a center of mass energy of 14 TeV and a lot of earlier simulation work was in fact done under this assumption. As physics is unlikely to change significantly between 13 and 14 TeV, these studies are mostly still valid and in this work we will discuss 13/14 TeV simulation results in a complementary way, without making clear distinctions. The main priorities of LS1 are to repair and consolidate the interconnects, bring all necessary equipment up to the level needed for 6.5 TeV per beam, repair leaks and other maintenance work required after 3 years of operation. Upgrade and maintenance activities in the machine are accompanied by concurrent upgrade and maintenance activities on part of the individual detectors.

The LS1 will be the first long shutdown of the LHC, part of a long term draft plan which foresees operation until 2035, with several subsequent operation periods and long shutdowns. Run 2 of the LHC is due to start early in 2015 and last for the next 3 years with an intermediate luminosity of $10^{34} \text{ cm}^{-2}\text{s}^{-1}$. Long shutdown 2 (LS2) is planned from mid-2018 until the end of 2019. After that, Run 3 of the LHC will proceed with nominal energy and nominal luminosity of $2 \times 10^{34} \text{ cm}^{-2}\text{s}^{-1}$. The amount of proton-proton data collected in Runs 2 and 3 is conservatively expected to be 300 fb^{-1} . Given the experience from Run 1 and the excellent machine operation which surpassed conservative expectations already in the second year of running, it may possibly turn out even larger. After 2022, the machine will be due for another major upgrade for an order of magnitude increase of luminosity, while keeping the same beam energy. This future phase is referred to as the High Luminosity LHC (HL-LHC). Long shutdown 3 (LS3) is planned to last from 2023 until late 2025 for the LHC and from 2024 until mid-2025 for the injectors. The following three machine operation periods, interspaced with long shutdowns 4 and 5, aim at delivering 3000 fb^{-1} of proton-proton collisions until 2035. This is the ultimate aim of the LHC.

In this chapter we will try to answer the question of what can the LHC, operating at 13/14 TeV, measure in the various VV scattering processes, having in mind everything we have learned so far both on the theory side and from existing measurements. Because

the physics motivation to study VBS processes has significantly changed only in the last couple of years and is still in the process of reformulation, up to date analyses are not so abundant and a comprehensive review of fully valid predictions for the LHC is rather hard to find. In an attempt to fill the hole, we will herewith sketch some analyses which are supposed to be completely consistent with all our present knowledge, yet not involving anything more than common simulation tools. For full transparency and in order to avoid usage of any experiment specific software, the analysis will be kept as simple as possible from the point of view of the applied analysis tools. It will be a cut-based analysis. While we do not assume that the future final analyses by the ATLAS and CMS collaborations will indeed be done in this way, such simple analysis is accurate enough for our purpose, which is to evaluate the order of magnitude of possible signals from different BSM sources, shed light on the LHC potential to identify a physics scenario from the sole study of VBS processes, as well as to identify some of the main challenges and limiting factors in what concerns background rejection. Whenever possible and applicable, we will follow the ideas of earlier works by many authors, but all the results will be independently recalculated with modern simulation tools. This will include some detector resolution effects, so long as the latter do not involve full detector simulation.

Our main focus here will be on the purely leptonic decays. This choice is mainly motivated by pragmatism - these channels do not suffer from complicated, QCD-related systematic uncertainties in event reconstruction and, as we have seen, the final signal to background ratio, with all major detector dependent effects included, is driven by merely a few experiment-specific factors: the purity of electron reconstruction, charge measurement efficiency for electrons and muons at high p_T , and the efficiency of b -tagging. All these effects can be to a rough accuracy described in terms of simple numbers, without necessarily applying the entire methodology of event reconstruction used in a real experiment. All other systematics can be either assumed known or play a lesser role.

Our baseline to define the BSM signal and tune the necessary selection criteria will be the Higgsless Standard Model, as we inherit from most of the classic studies. However, the ultimate goal is to find how this translates into realistic scenarios with modified Higgs couplings and anomalous triple and quartic gauge boson couplings, with all the relevant similarities and differences being taken into account.

6.1 Modeling of the signal and irreducible background

In previous chapters we have discussed in detail the formal definitions, the computational methods and issues for the complete calculation of the signal and irreducible background. A full set of signal selection criteria that are applicable to future data at $\sqrt{s} = 14$ TeV follows directly from our previous considerations:

- at least two jets with $2 < |\eta_j| < 5$ and $\eta_{j_1}\eta_{j_2} < 0$,
- exactly two isolated same-sign/opposite-sign leptons with $\Delta\varphi > 2.5$,
- $M_{jj} > 500$ GeV,
- $M_{l_1j_2}, M_{l_2j_1} > 200$ GeV,

- b quark veto,
- optional: central jet veto,
- $R_{p_T} > 3.5$ or a suitable combination of cuts that selects large p_T^l , small $|\eta_l|$ and large M_{ll} .

We recall that the first two criteria are basic topological VBF cuts, the next four are dedicated $t\bar{t}$ suppression cuts (not exactly - requirement of large M_{jj} also suppresses the irreducible background) and only the *last* item represents cuts, only one in the same-sign case, that separate the longitudinal W signal from the transverse W background.

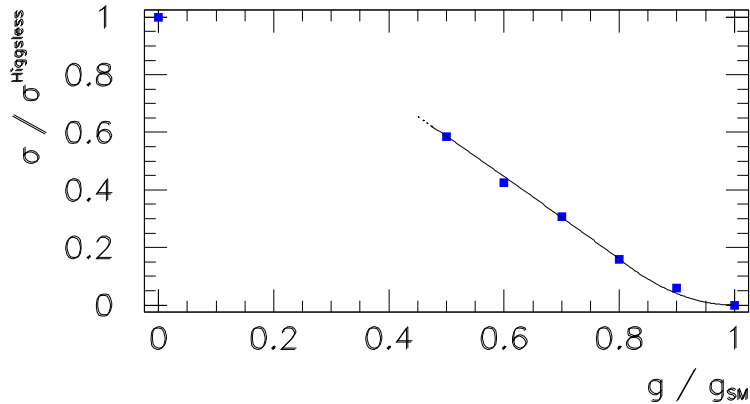


Figure 6.1: Actual signal cross section relative to the Higgsless cross section as a function of the actual HWW coupling relative to its Standard Model value. Signal sizes were determined after applying all the signal selection criteria discussed in the text. The points provide a good first approximation of how to scale the results of all the former WW scattering studies which used the Higgsless hypothesis to evaluate signals in order to reinterpret them in terms of a Higgs with modified couplings. Result of parton-level MadGraph calculations for the process $pp \rightarrow jjW^+W^+$ with $W^+ \rightarrow \mu^+\nu$.

From analyses available to date it can be inferred that the order of magnitude W^+W^+ signal cross section, where signal is defined in terms of a pure Higgsless Standard Model, and by further assuming purely leptonic decays ($l = e, \mu$), is close to 0.12 fb. This number has been recalculated using MadGraph 5. It includes effects associated to hadronization, final state radiation and jet reconstruction using an imitative simple jet cone algorithm. Sheer signal size is similar for W^+W^+ and for W^+W^- . Physically realistic scale factors range from 0.8 for a pure Higgsless with unitarity or a heavy Higgs, to 0.31, 0.16 and 0.06 for a light Higgs boson that couples to the W with a strength equal to, respectively, 0.7, 0.8 and 0.9 of what is predicted in the Standard Model [111] (see Fig. 6.1). Because of the amplitude interference patterns, signals for HWW couplings larger than unity (in

SM units) are generally lower than for their mirror values. Finite detector resolutions in the measurement of p_T or η of the leptons and jets effectively play the role of a further $\sim 10\%$ reduction. Signal in the anomalous gauge coupling scenarios must be calculated independently and will be shown later on. Irreducible background levels for W^+W^+ are of the order of 0.05 fb in a conventional cut analysis and can be shrunk at least to 0.02 fb by applying an R_{p_T} cut instead or even more sophisticated correlated variable techniques. The latter will be much closer to what eventually can be achieved using a Multivariate Analysis in which the entire final state kinematics is exploited. For W^+W^- the irreducible background amounts to about 0.11 fb and it is unlikely to improve in a significant way. Signal for W^-W^- is about a factor 4 lower than for W^+W^+ , but backgrounds are at similar levels.

Total cross sections for the signal (calculated within the Higgsless scenario) and irreducible background in the W^+W^+ and W^+W^- processes, after each subsequent class of selection criteria discussed in the text, are shown in Fig. 6.2.

6.2 Modeling of the inclusive $t\bar{t}$ production background

Reducible backgrounds in real experiments are typically determined using partly or wholly data-driven methods. This and the following sections discuss pure simulation-based results and are not intended as a model for a future analysis of experimental data. Their purpose is merely to establish a suitable methodology to estimate all these backgrounds in simulation-based studies, before they can be cross checked against the data. The methods described here should be accurate enough to assess the orders of magnitude of the relevant backgrounds and to study the main challenges related to background reduction.

Calculations of the $t\bar{t}$ background are affected by large QCD-related uncertainties. The inclusive $t\bar{t}$ production cross sections in proton-proton collisions at $\sqrt{s} = 7$ and 8 TeV has been measured by both ATLAS and CMS. These numbers provide the only currently available direct experimental bond to reduce the theory-based systematic uncertainties for the predicted $t\bar{t}$ cross sections at 14 TeV. As the number of relevant Feynman diagrams grows rapidly with the order in α_S , the whole process cannot be accurately modelled in the lowest order plus allowing initial and final state radiation. The leading parton level subprocesses that are complete missed in such approximative treatment are graphs leading to an additional quark-jet in the final state, $pp \rightarrow t\bar{t}q$ ¹. These two classes of events do not involve any double-counting. Their coherent sum reasonably reproduces the total cross sections at 7 or 8 TeV, as measured in the LHC. A more satisfactory description, developed especially for the study of inclusive $t\bar{t}$ production as a background to VBF processes, is based on explicitly considering three processes at the tree level: $pp \rightarrow t\bar{t}$, $pp \rightarrow t\bar{t}j$ and $pp \rightarrow t\bar{t}jj$ (j denoting quarks and gluons alike) plus initial and final state radiation. These processes represent the leading order contributing diagrams of inclusive $t\bar{t}$ production for the cases where 2, 1 or 0 tagging jets arise from b quarks, respectively. The three different topological configurations select three mutually exclusive subsamples and thus double-counting is automatically avoided. It is actually the latter two classes

¹Following the common convention, by pp we always mean the sum of all the corresponding interactions at the parton level, i.e., quark-quark, quark-gluon or gluon-gluon, while the remnants of the protons are ignored. Hence, e.g., $pp \rightarrow t\bar{t}$ does not mean baryon number violation.

that define the amount of $t\bar{t}$ background. The contribution from $pp \rightarrow t\bar{t}$ with both b quarks becoming tagging jets is minimal. That the two abovementioned methods produce consistent results for 14 TeV has been verified.

From completed simulation-based studies, that include also CMS-like detector resolution effects, it can be inferred that the total top production background falling within the kinematic phase space defined by all the abovementioned signal selection criteria: basic VBF cuts, $t\bar{t}$ suppression cuts and the R_{p_T} cut, can be roughly parameterized as

$$B_{t\bar{t}} = 12 \text{ fb} \cdot (1 - \epsilon_{b\text{-tag}})^2 \cdot (1 - \epsilon_{\text{sign}}) \cdot \epsilon_{CJV}. \quad (6.1)$$

Here the normalization factor includes the branching fractions of W decaying into electrons or muons and the proper selection efficiency, $\epsilon_{b\text{-tag}}$ is the average efficiency of b -tagging, ϵ_{sign} is the average efficiency of lepton charge reconstruction and ϵ_{CJV} is the central jet veto factor, if applied. For example, setting $\epsilon_{b\text{-tag}}=0.5$, $\epsilon_{\text{sign}}=0.995$ and $\epsilon_{CJV}=1$, as expected for the same-sign mode, one gets $B_{t\bar{t}} \sim 0.015$ fb. It should be noted that with the above numbers the predominant contribution indeed comes from charge misreconstruction. Leptonic B decays are suppressed by a combination of kinematics and isolation criteria to much below this level. Another subclass of the inclusive $t\bar{t}$ production background that affects the same-sign mode is $W^+t\bar{t}$ production, where one lepton comes from W decay, another from top decay. This background was shown negligible after applying standard signal selection cuts. For $\epsilon_{\text{sign}} \sim 0$ and $\epsilon_{CJV} \sim 0.25$, as is in the opposite-charge mode, $B_{t\bar{t}} \sim 0.75$ fb, and more stringent cuts on the lepton transverse momenta can reduce this number by perhaps an additional factor 2 while leaving a major part of the signal intact. It is clear at this point that, unless heavy resonances are present within the reach of $\sqrt{s} = 14$ TeV, only W^+W^+ carries the potential of signal levels above background fluctuations assuming luminosities measured in hundreds of inverse femtobarns.

The total $t\bar{t}$ cross section after each of the analysis cuts discussed in the text is shown in Fig. 6.3 (top plot).

6.3 Modeling of the W +jets backgrounds

Jets misreconstructed as electrons are the primary source of these backgrounds. The lowest order process of this kind that can mimic the signal is $W + 3$ jets, where in principle any of the three jets can be the fake electron. The kinematic regime we are probing by applying the signal selection cuts strongly favors large- p_T leptons. As a direct consequence, events in which the leading jet (where, as usual, we rank objects in a given class according to their p_T) is the one that gets misreconstructed make up over 90% of all the cases of W +jets events falling kinematically within the signal phase space. The subleading jet as the fake electron accounts for just about the rest of it. For the same reasons, it is inessential to consider additional samples with more than three jets at the generation level. Given the large total cross section for W +jets at the LHC, the purity of electron reconstruction is a crucial number. The final amount of W^+ +jets events mimicking the signal can be predicted as being roughly

$$B_{W^++\text{jets}} = 5 \text{ pb} \cdot \epsilon_{j\text{-fake}} \cdot f_{+/-}, \quad (6.2)$$

in total, where ϵ_{fake} is the overall probability of a jet being reconstructed as an electron satisfying all the quality selection criteria and $f_{+/-}$ is the sign matching factor. For $\epsilon_{fake} \sim 1.1 \cdot 10^{-4}$ and $f_{+/-}=0.27$ (W^+W^+), this gives 0.08 fb. For $f_{+/-}=0.73$ (opposite-sign), it is about 0.2 fb. It is not a negligible number and, not so unexpectedly, it is a more important background source than top production for the same-sign mode. However, this background is bound to affect different final states differently. Half of the total B_{W+jets} is due in the $jjee$ final state, the other half in the $jj\mu\mu$ final state (where signal is twice the size of the $jjee$ signal) and no contribution is possible to the $jj\mu\mu$ final state.

The W^-+jets background is typically a factor 2 lower due to the charge asymmetry in W production at the LHC. We assume then additional contributions of 0.1 fb for the opposite-sign and 0.04 fb for W^-W^- .

Another class of background is related to a fake electron being reconstructed from a photon with an associated track. The leading order process that can generate such events is $Wjj\gamma$. Its total cross sections is much lower than for $W + 3$ jets and additional kinematic and combinatorial factors make it in fact negligible. This background is of the order of

$$B_{Wjj\gamma} = 0.18 \text{ fb} \cdot \epsilon_{\gamma-fake}. \quad (6.3)$$

where $\epsilon_{\gamma-fake}$ is the overall probability of a photon misreconstructed as an electron satisfying all the quality selection criteria and of the required charge. For $\epsilon_{\gamma-fake} \sim 0.0035$ we get $B_{Wjj\gamma} < 0.001$ fb.

The total $W+jets$ cross section after each of the analysis cuts discussed in the text is shown in Fig. 6.3 (second plot).

6.4 Modeling of the QCD multijet background

The leading order background process of this kind is $jjjj$ with two of the four jets misreconstructed as electrons. Huge cross sections for QCD processes at the LHC compensate the low probability of having two simultaneous fakes and so this background can prove overwhelming. This result may seem surprising at first glance, but in fact it is dictated by the very specific kinematic correlations we are looking for, significantly different from the ones typically observed in regular gauge boson physics analyses done on the 7 and 8 TeV data. Again here, the kinematic regime we probe favors large p_T and therefore fakes generated by the two leading jets account for 80-90% of all events satisfying the complete selection criteria, while the rest to a sub-percent level comes from the combination of the first with the third jets being reconstructed as fake electrons. For the same reasons it is also here inessential to consider higher order processes. In order to render the QCD multijet background manageable, we further assume the following combination of cuts to be applied in the $jjee$ final state only:

$$\begin{aligned} MET &> 60 \text{ GeV}, \\ M_{ee} &> 250 \text{ GeV}, \\ p_T^{j_1} &> 30 \text{ GeV}. \end{aligned}$$

The meaning of the first two cuts is straightforward. For the third cut, note that here in most cases j_1 denotes really the *third* jet. Extra cuts bring a substantial reduction of

the background while keeping 70% of the $jjee$ signal, or equivalently well over 90% of the total signal. In total,

$$B_{jjjj} = 6.5 \text{ nb} \cdot \epsilon_{j\text{-fake}}^2 \cdot f_{+/-}, \quad (6.4)$$

where $\epsilon_{j\text{-fake}}$ is the probability of a jet being reconstructed as an electron satisfying all the quality selection criteria and $f_{+/-}$ is a combinatorial factor equal to 0.25 for each same-sign mode and 0.5 for opposite-sign. By assuming $\epsilon_{j\text{-fake}} \sim 10^{-4}$ we end up at $B_{jjjj} \sim 0.016$ fb for same-sign and 0.032 fb for opposite-sign, still not negligible numbers. However, knowing that this background only concerns the $jjee$ final state, as does the W +jets background concern the $jjee$ and $jje\mu$ final states in fixed proportions, comparison of the selected event yields will be an additional tool to disentangle the various background sources and isolate the signal (provided enough statistical power). Yet another piece of valuable information will be provided by the study of the W^-W^- mode.

The total QCD multijet cross section after each of the analysis cuts discussed in the text is shown in Fig. 6.3 (third plot).

6.5 *WZ and ZZ as backgrounds to WW*

Several previous analyses, in particular the ones by Chanowitz et al. [94], hinted on the possibility that continuum WZ production with one lepton which escaped detection, could be as well an additional significant background to $W^\pm W^\pm$. The subject was brought up again in the recent analyses by ATLAS [109] and CMS [110]. The validity of this assertion strongly depends on the applied selection criteria. In our case, the amount of remaining W^+Z background with at least two associated jets after cuts gets reduced to about 0.04 fb altogether, i.e., regardless of whether the negatively charged lepton from Z decay gets reconstructed or not. The geometrical condition of this third lepton falling outside of the accepted pseudorapidity range of $|\eta| < 2.1$, translates into a further suppression by more than an order of magnitude, to about 0.003 fb, and this number gives the final estimate of the W^+Z background in the analysis of W^+W^+ . For W^-W^- , the relative contamination from W^-Z is about a factor 2 larger from pure combinatorics. Similar is the WZ contamination to W^+W^- , here however both W^+Z and W^-Z can contribute. Signal from $W^\pm Z$, if any, eventually adding up to signal from WW is of course a bonus rather than a problem.

The total WZ cross section after each of the analysis cuts discussed in the text is shown in Fig. 6.3 (bottom plot). Contaminations from ZZ are still smaller.

6.6 *WZ and ZZ as signals*

To estimate the amount of BSM signal for the WZ and ZZ processes, we follow existing literature on the subject, and the work of Bagger et al. [92] in particular. We can recall and confirm here some of their most elaborated and relevant signal selection criteria that were shown to exploit specific kinematic features of each of these processes in order to enhance S/B. In addition to requiring standard VBF topology and applying cuts against inclusive $t\bar{t}$ background (for ZZ only a cut on $M_{jj} > 500\text{GeV}$ applies), the process specific cuts are the following. For WZ :

- $M_Z - 10 \text{ GeV} < M_{l+l^-} < M_Z + 10 \text{ GeV}$,
- $M_T(WZ) > 500 \text{ GeV}$,
- $p_T^Z > \frac{1}{4}M_T(WZ)$,
- $MET > 50 \text{ GeV}$,
- $p_T^l > 40 \text{ GeV}$.

For $ZZ \rightarrow 4l$:

- $M_Z - 10 \text{ GeV} < M_{l+l^-} < M_Z + 10 \text{ GeV}$ for both lepton pairs,
- $M_{4l} > 500 \text{ GeV}$,
- $p_T^Z > \frac{1}{4}\sqrt{M_{4l}^2 - 4M_Z^2}$ for each Z ,
- $p_T^l > 40 \text{ GeV}$.

For $ZZ \rightarrow l^+l^-\nu\nu$:

- $M_Z - 10 \text{ GeV} < M_{l+l^-} < M_Z + 10 \text{ GeV}$,
- $M_T(ZZ) > 500 \text{ GeV}$,
- $p_T(ll) > \frac{1}{4}M_T(ZZ)$,
- $MET > 250 \text{ GeV}$,
- $p_T^l > 40 \text{ GeV}$.

In the above, M_Z is the PDG Z mass, while all other symbols refer to reconstructed quantities. The transverse masses are defined as follows:

$$M_T^2(WZ) = [\sqrt{M^2(lll) + p_T^2(lll) + MET^2} - [p_T^{\vec{}}(lll) + M\vec{E}T]^2], \quad (6.5)$$

$$M_T^2(ZZ) = [\sqrt{M_Z^2 + p_T^2(ll) + \sqrt{M_Z^2 + MET^2}} - [p_T^{\vec{}}(ll) + M\vec{E}T]^2]. \quad (6.6)$$

Background is expected to be dominated by irreducible SM background for ZZ and additionally $Zt\bar{t}$ +jets production for WZ . Under these assumptions and applying the cuts described above, background levels amount approximately to 0.027 fb for $W^\pm Z$, 0.003 fb for $ZZ \rightarrow 4l$ and 0.009 fb for $ZZ \rightarrow 2l2\nu$. Higgsless signals would be of the order of 0.009 fb, 0.005 fb and 0.012 fb, respectively. For WZ , background is relatively large and its kinematic separation from the signal, if by the latter we understand non-SM Higgs couplings, is marginal. This forces to use strict selection criteria which in turn would require very high luminosity to be successfully applied. The ZZ modes are relatively clean, especially the $4l$, but clearly suffer of low statistics.

The total cross sections of the signal and irreducible background for WZ and ZZ after each of the analysis cuts discussed in the text are shown in Fig. 6.4. In the event of absence of new heavy resonances within reach, these processes are unlikely to improve our knowledge of the Higgs sector.

6.7 Key uncertainties

A phenomenological analysis based on signal and background calculations done by matrix element generators at the tree level is affected by specific uncertainties. These come partly from theory itself and partly from imperfect knowledge of detector related effects. A detailed analysis of all the systematic errors is rather inessential at this point, but we can outline the most important limitations to the accuracy of our predictions. Not accidentally, some of them will translate into the limiting factors at the time of carrying the real measurement.

Total cross sections for proton-proton processes calculated in a given order in perturbative expansion are sensitive to the choice of such things as the set of parton distribution functions (PDF's) and the QCD factorization and renormalization scales. Typically, the choice of PDF's by itself does not change numerical results by more than 5%. The factorization scale corresponds to the resolution at which the proton is being probed. When calculated to all orders in perturbative QCD, the hadronic cross section is independent of the scale. But at any finite order it must depend logarithmically on it [112]. Moreover, the dependence is usually significant at low orders in perturbation theory. The way to obtain a reliable prediction is to calculate higher-order corrections until the factorization scale dependence is reduced. It was shown that calculations of diboson production in the vector boson scattering configuration carried at the next-to-leading order (NLO) in QCD are very weakly dependent on the scale. The residual uncertainty is of 2.5% in a typical VBF kinematics (for W^+W^+). Meanwhile, results of leading order (LO) calculations can be made coincide with the former by a choice of the factorization scale equal to the momentum transfer of the t -channel electroweak boson [114]. This solution has recently been implemented as an option in MadGraph 5. Deviations induced by setting the scale to a fixed value, e.g., the Z mass are of order of 10%. Even more sophisticated recipes are currently devised [115]. These will allow further reduction of scale related uncertainties for future studies and data analyses.

Furthermore, a key problem in making precise perturbative QCD predictions is to set the proper renormalization scale of the running coupling. A poor choice of the renormalization scale can manifest itself as a strong dependence on the ratio of the NLO cross section to the LO cross section (the so called K-factor) [113]. As our process of interest is of purely electroweak nature, the signal predictions are affected only via uncertainties in the modeling of parton hadronization and final state radiation. In studies that do not involve detailed detector simulation, these are anyway dwarfed by imperfect modeling of jet reconstruction procedures, calorimeter efficiencies and resolutions. In the prediction of QCD-related background, variations depending on the scale can easily amount to 30% without dedicated hard work. In our case we take clear advantage of the fact that these backgrounds are expected to be small after all cuts. For inclusive $t\bar{t}$ production we have also an experimental ansatz since the total cross sections have been measured at 7 and 8 TeV by both ATLAS and CMS. It is in any case the inclusion of $t\bar{t}j$ and $t\bar{t}jj$ processes in the first place that ensures the total cross sections are consistent with the measurements within the errors of the latter. These errors are of the order of 5-10%.

The overall smallness of background in the same-sign process is an advantage at the time of the measurement, but a relative disadvantage for phenomenological studies. The background is difficult to predict because it depends primarily on a combination of tiny

detector effects rather than physics calculable from first principles. In case of $t\bar{t}$ this is not only knowledge of exact b -tagging efficiencies as a function of jet p_T and η , but as we saw in the same-sign WW channel, the result is mainly driven by the efficiency of lepton charge identification. At the present moment this is only taken into account as an order of magnitude estimate. Surely, a small change in efficiency can produce a significant effect on the S/B ratio. Likewise, W +jets and QCD multijet backgrounds enter via the tiny effects of jets misidentified as leptons. These are strongly detector- and software-dependent and only an order of magnitude estimate can again be made at this point. And in any case they must be considered in simultaneous relation with the efficiency of lepton-ID for genuine leptons. It is of little use to evaluate such effects in more detail on purely phenomenological grounds. However, we can at least define kinematic conditions under which the abovementioned backgrounds are small enough that their precise values can be measured using data-driven methods at the proper time, but will not jeopardize the entire analysis. Ultimately, exact background levels and compositions will differ from experiment to experiment (in our case from ATLAS to CMS).

In all the numerical predictions that are presented in this section, things like detector efficiencies, if only different from unity by more than a few per cent, were taken into account by simply scaling the final cross sections. Basic detector resolutions [80] [81] [88] can be simulated with dedicated simulation tools, namely the PGS program [124]. In general, PGS-level results are over 10% lower than PYTHIA-level (generator+hadronization) results. Meanwhile, results in the electron decay channels are consistent with those in muon decay channels, from which they differ only in the assumed resolution, to a few per cent and hence this number can be used as a rather conservative upper limit of the resolution-related uncertainty. Differences between jet reconstruction algorithms and the effects of choosing a cone/cluster size parameters R are negligibly small. We recall that although the current standard jet definition used, e.g., in CMS is set by the anti- k_T algorithm [87], which is not an available option in PYTHIA 6, but has been implemented in PGS 4, it is likely to be changed in the future for specific analyses in order to improve W tagging in hadronic decays. For the purpose of the studies presented here, either the k_T or a simple cone algorithm [76] with $R = 0.5$ was used. High pile-up conditions may additionally degrade the efficiency of tag-jet selection. The issue of lowering the tag-jet p_T threshold, important from the point of view of W_L selection, requires a dedicated study within a fully realistic pile-up simulation. Such study is currently under preparation. Triggering efficiencies are not taken into account anywhere in this study, but purely leptonic decay modes are obviously advantageous in this respect. They do not require any dedicated VBF trigger based on hadronic signals. Instead, triggering on a single lepton should be quite enough and the fact that any of the two required leptons may fire the trigger makes trigger efficiency a minor issue. Since we want high- p_T leptons, trigger thresholds should not be a problem, either.

6.8 Higgs couplings in VV scattering

The lepton-lepton invariant mass or transverse mass spectra (where applicable) of the signal and backgrounds, after applying all the selection criteria, are shown for all the VV scattering processes in Figs. 6.5 thru 6.10. Respective signals were calculated within the

Higgsless SM scenario. Assuming optimistically the HWW coupling be 0.7, 0.8 or 0.9 of its SM value, which is still not ruled out by experiment, for W^+W^+ in the purely leptonic decay we can hope for a signal size of the order of 0.040, 0.020 or 0.008 fb, respectively, after all selection criteria; similar for W^+W^- , and about a quarter of that for W^-W^- . Total background levels may amount to 0.1 fb, 1.1 fb and 0.07 fb, respectively. Sticking to W^+W^+ alone, this means roughly 12, 6 or 2 signal events after collecting 300 fb^{-1} of data over 30 Standard Model events. In terms of anomalous Higgs-to-gauge couplings and having in mind the present experimental bounds derived from Higgs measurements from LHC Run 1, it already looks unlikely that WW scattering could provide a quantitative measurement on its own right. In order to observe frail hints of BSM anytime before the LHC enters in its High Luminosity regime (2025), it will be necessary to combine different processes and different decay channels. Nonetheless, consistency cross checks to $\sim 20\%$ with precision measurements of Higgs production rates and decays will certainly be attainable and they should still be considered an important part of the physics program for LHC Runs 2 and 3. Variations of the HWW coupling of less than 20% will only be accessible with 3000 fb^{-1} of data. And of course, the more the Higgs boson appears SM-like, the more confined gets WW scattering to the role of a consistency cross check with limited precision, as opposed to a true BSM search.

In the ZZ channel, the primary focus will be direct search for new resonances. On the absence of such, BSM signal arising from a scaled HZZ coupling may consist of a handful of events even after 3000 fb^{-1} . Not unexpectedly, the $l^+l^-\nu\nu$ final state offers in principle more statistics than $4l$, but is harder to analyze. Here, however, special effort is required to include the semileptonic decays into the game. Under strict requirements of two tagging jets in the endcaps, two additional jets in the barrel that reproduce the Z mass and no additional jet activity, QCD background levels may turn out controlable. Dedicated simulations are missing at the present moment.

The WZ channel probes in principle both HWW and HZZ couplings in a combined way, but its sensitivity is marginal. BSM signal levels are insufficient to be measurable even with 3000 fb^{-1} .

It is clear that the application of MVA's enhances the possibilities to carry an optimal analysis and isolate the signal. The final sensitivity depends on the kinematic separation of signal and background in the multidimensional phase space and on the overall signal statistics, to a lesser degree on the amount of background. As long as the full kinematic information on each event is taken into account, quantitative results should in principle not depend on the applied preselection of events, unless the latter suppresses too much of the proper signal. It is therefore preferable to reduce signal losses to minimum. A cut-based analysis, such as outlined in this work, represents in fact the current *lower limit* in the achievable sensitivity. In any case, what we have learned from the present studies, and will emphasize this point once again, is that a conventional analysis that consists of applying polarization-blind VBF selection criteria plus a shape analysis of the lepton-lepton invariant mass spectrum is suboptimal and should be replaced by a more sophisticated analysis that explores the full kinematics of the final state to deliver the best final result. A lot of valuable information sits in particular in the jet spectra, far more than whether the process was VBF or not. Correlated variables like R_{p_T} can be thought of as a first effective step towards fuller exploration of the entire kinematic phase of the four particles in the final state. Given that BSM effects in WW scattering may sit at the

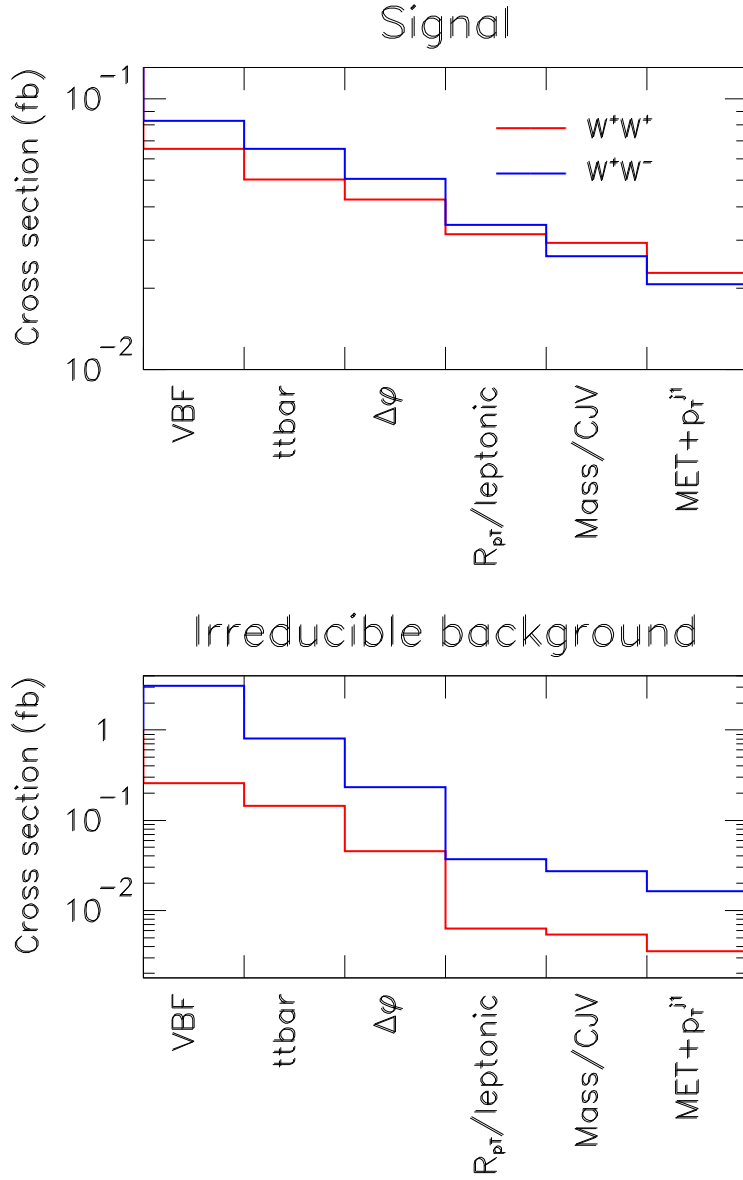


Figure 6.2: Total cross sections for the signal and irreducible background after each subsequent class of cuts proposed in the analysis. Red histograms are for $pp \rightarrow jjW^+W^+$, blue histograms for $pp \rightarrow jjW^+W^-$; in both cases W decay into muons is assumed. The signal is calculated under the Higgsless hypothesis. Results reflect pure event kinematics, all detector efficiencies and inefficiencies (where appropriate) are assumed 100%. The meaning of the cut labels is the following: • **VBF**: $2 < |\eta_j| < 5$, $\eta_{j1}\eta_{j2} < 0$ and $|\eta_\mu| < 2.1$, • **ttbar**: $M_{jj} > 500$ GeV and $M_{j1\mu2}, M_{j1\mu2} > 200$ GeV, • **$\Delta\varphi$** : $\Delta\varphi > 2.5$, • **$R_{p_T}/\text{leptonic}$** : $R_{p_T} > 3.5$ for W^+W^+ or $p_T^{\mu1} + p_T^{\mu2} > 300$ GeV and $M_{\mu\mu} > 300$ GeV for W^+W^- , • **Mass/CJV**: $M_{\mu\mu} > 250$ GeV for W^+W^+ or central jet veto with $p_T > 25$ GeV for W^+W^- , • **MET+ p_T^{j1}** : missing $E_T > 60$ GeV and $p_T^{j1} > 30$ GeV. Results of a MadGraph calculation, processed by PYTHIA 6 for W decay into muons (jjW^+W^- only), the effects of parton showering, hadronization and jet reconstruction and further processed by PGS 4 for the effects of finite resolution in the measurement of jet and muon p_T in a CMS-like detector. The original PYTHIA 6 source code was modified to account for the correct, polarization-dependent, angular distributions for the decays $W^\pm \rightarrow \mu^\pm\nu$. The corresponding results for the decays of W into electrons are typically consistent within a few per cent and/or statistical fluctuations and are not shown here.

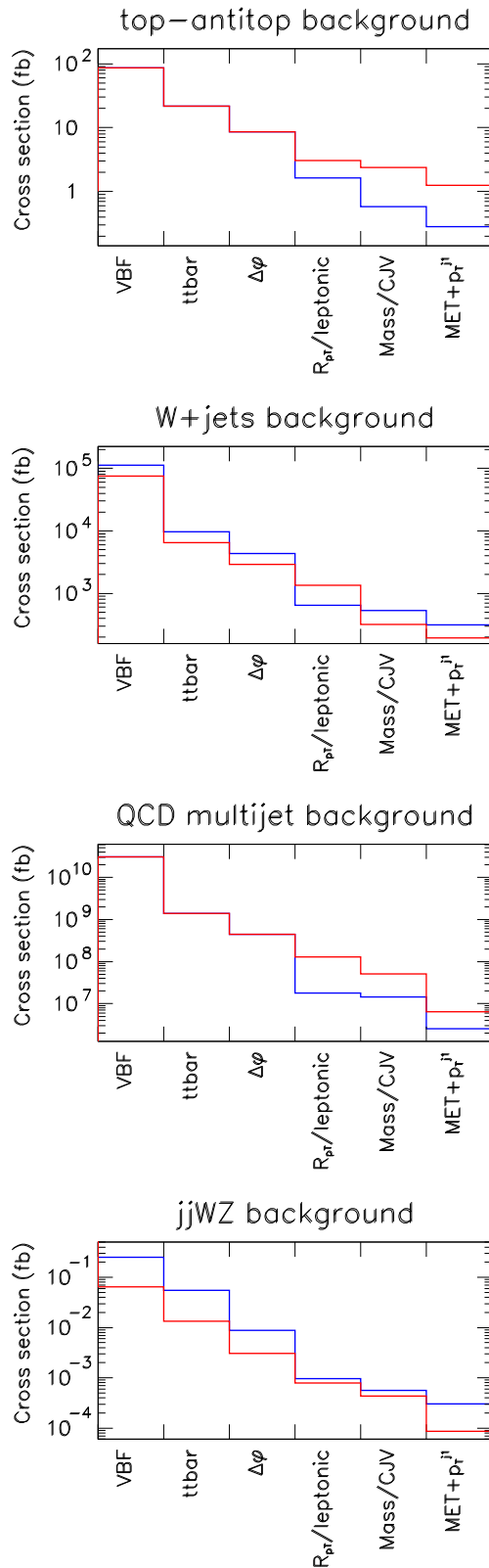


Figure 6.3: Total cross sections for the different main kinds of reducible background: inclusive $t\bar{t}$, W +jets, QCD multijet and WZ , after each subsequent class of cuts proposed in the analysis. Red histograms are for $pp \rightarrow jjW^+W^+$, blue histograms for $pp \rightarrow jjW^+W^-$; in both cases W decay into muons is assumed. Results reflect pure event kinematics, all detector efficiencies and inefficiencies (where appropriate) are assumed 100%. For details regarding this calculation and the precise meaning of cut labels see caption of Fig. 6.2.

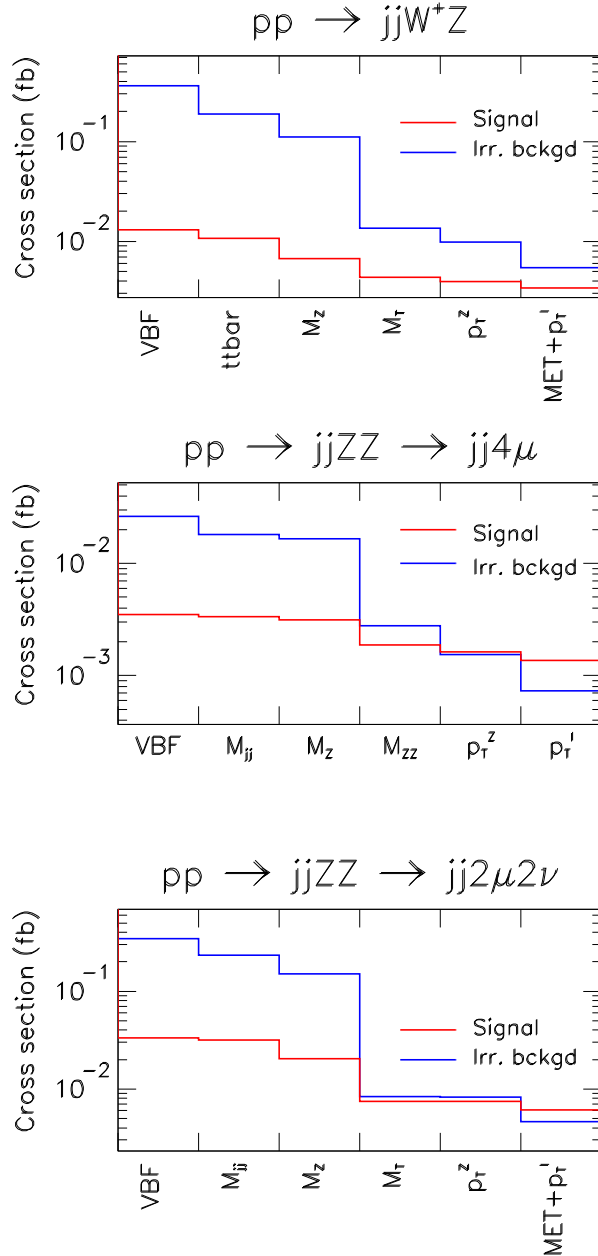


Figure 6.4: Total cross sections for the signal (red histograms) and irreducible background (blue histograms) after each subsequent class of cuts proposed in the analysis for the processes $pp \rightarrow jjW^+Z \rightarrow jj\mu^+\mu^+\mu^-$ (top), $pp \rightarrow jjZZ \rightarrow jj\mu^+\mu^-\mu^+\mu^-$ (middle) and $pp \rightarrow jjZZ \rightarrow jj\mu^+\mu^-\nu\nu$ (bottom) at 14 TeV. The signal is calculated under the Higgsless hypothesis. The meaning of the cut labels is the following: • **VBF**: $2 < |\eta_j| < 5$, $\eta_{j1}\eta_{j2} < 0$ and $|\eta_\mu| < 2.1$, • **ttbar**: $M_{jj} > 500$ GeV and $M_{j1\mu2}, M_{j2\mu1} > 200$ GeV, • **M_{jj}** : $M_{jj} > 500$ GeV, • **M_Z** : reconstructed Z mass(es) within 10 GeV, • **M_T** : transverse mass (defined in detail in section 6.6) > 500 GeV, • **M_{ZZ}** : $M_{4\mu} > 500$ GeV, • **p_T^Z** : $p_T^Z > \frac{1}{4}M_T$ for jjW^+Z and $jjZZ \rightarrow jj2l2\nu$ or $> \frac{1}{4}\sqrt{M_{4\mu}^2 - 4M_Z^2}$ for $jjZZ \rightarrow jj4l$, • **MET**: missing $E_T > 50$ GeV for jjW^+Z or 250 GeV for $jjZZ$, • **p_T^l** : $p_T^l > 40$ GeV. Results of a MadGraph calculation, processed by PYTHIA 6 for W decay into muons ($jjZZ$ samples only), the effects of parton showering, hadronization and jet reconstruction and further processed by PGS 4 for the effects of finite resolution in the measurement of jet and muon p_T in a CMS-like detector.

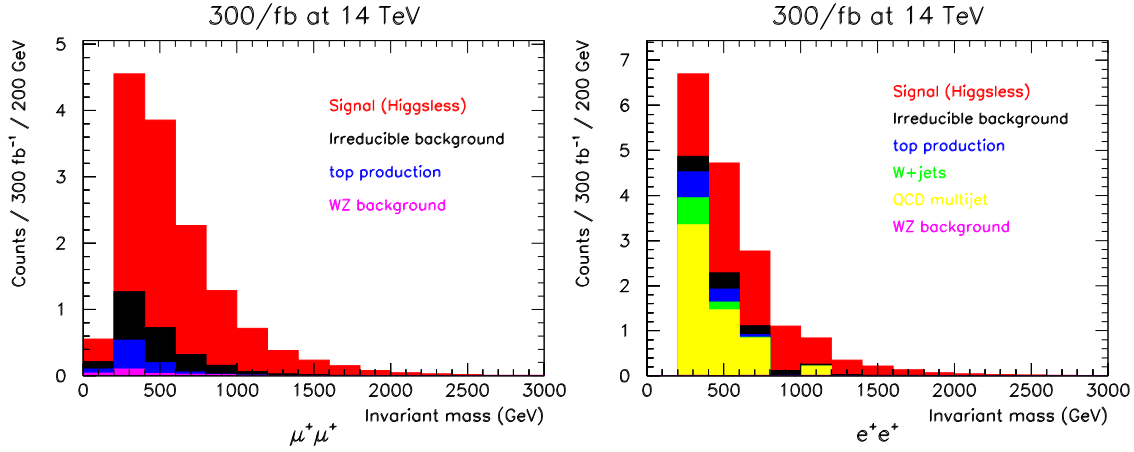


Figure 6.5: Invariant mass distributions of the two leptons resulting from the process $pp \rightarrow jjW^+W^+$ at 14 TeV, with $W^+ \rightarrow \mu^+\nu$ (left) and with $W^+ \rightarrow e^+\nu$ (right). Shown are the signal calculated under the Higgsless hypothesis and various contributions to the background, normalized to 300/fb of data. Applied were respectively all the signal selection criteria foreseen for the same-sign muon channel (cuts 1-4 from Fig. 6.2, up to and including R_{p_T}) and for the same-sign electron channel (all cuts 1-6 listed in Fig. 6.2). Signal was calculated by subtracting the SM jjW^+W^+ sample (by definition also identical with irreducible background) from the Higgsless jjW^+W^+ sample. The top production background was simulated as described in section 6.2. The WZ background was obtained from a dedicated jjW^+Z sample with subsequent W and Z decays into muons. The b -tagging efficiency was assumed 50% for a single b quark, for the muon charge mis-ID probability a constant value of 0.3% was taken, all other efficiencies and purities were assumed 100%. The W +jets background was deduced from dedicated $jjjW^+$ and $jjW^+\gamma$ samples, where either any of the jets or the photon was assumed to be misidentified as an electron. The QCD multijet background was deduced from a dedicated $jjjj$ sample where any pair of jets was assumed to be simultaneously misidentified as electrons. The probability of a jet faking an electron was assumed $1.1 \cdot 10^{-4}$ with a further 27% probability of sign matching and that for a photon 0.7% with a 50% probability of sign matching. For a more detailed explanation of the procedure see sections 6.3 and 6.4. The electron charge mis-ID probability for the evaluation of the top background was assumed to be 1%. Results of MadGraph simulations, processed by PYTHIA 6 for W decay into leptons (top production only), the effects of parton showering, hadronization and jet reconstruction and further processed by PGS 4 for the effects of finite resolution in the measurement of jet and lepton p_T in a CMS-like detector. The original PYTHIA 6 source code was modified to account for the correct, polarization-dependent, angular distributions for the leptonic W decays.

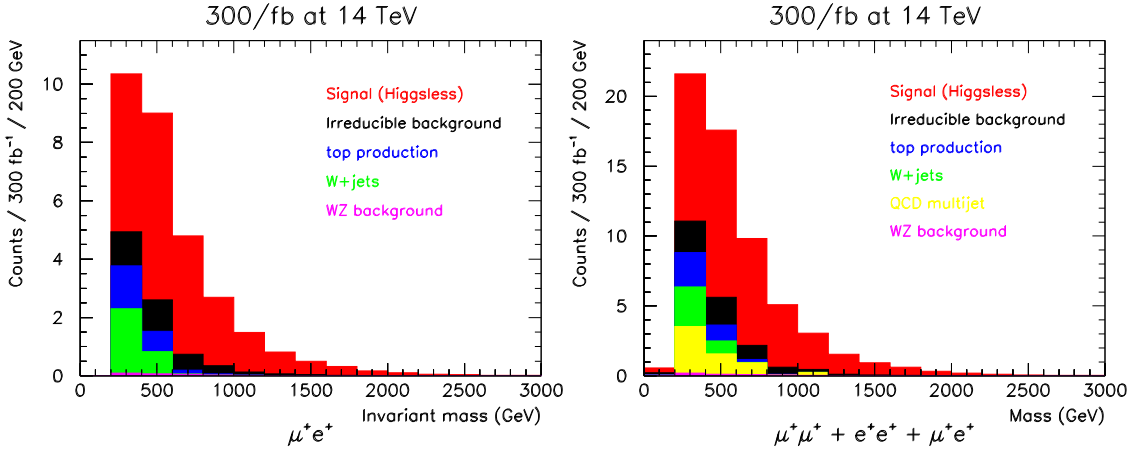


Figure 6.6: Invariant mass distributions of the two leptons resulting from the process $pp \rightarrow jjW^+W^+$ at 14 TeV, with one W decaying into a muon and another decaying into an electron (left) and with each W decaying either into a muon or an electron (right). Shown are the signal calculated under the Higgsless hypothesis and various contributions to the background, normalized to 300/fb of data. For the left plot, applied were all the signal selection criteria foreseen for the same-sign mixed muon+electron channel (cuts 1-5 listed in Fig. 6.2). The W +jets background was deduced from dedicated $jjjW^+$ and $jjW^+\gamma$ samples, where either any of the jets or the photon was assumed to be misidentified as an electron. The electron charge mis-ID probability for the evaluation of the top background was assumed to be 1%. The final μ^+e^+ kinematics was deduced by averaging out the distributions obtained in $\mu^+\mu^+$ and the e^+e^+ channels, which differed only due to different detector resolution effects assumed during processing by PGS 4. All the remaining procedures and assumptions were identical as described in the caption of Fig. 6.5. The right plot was obtained by summing up the individual W decay channels.

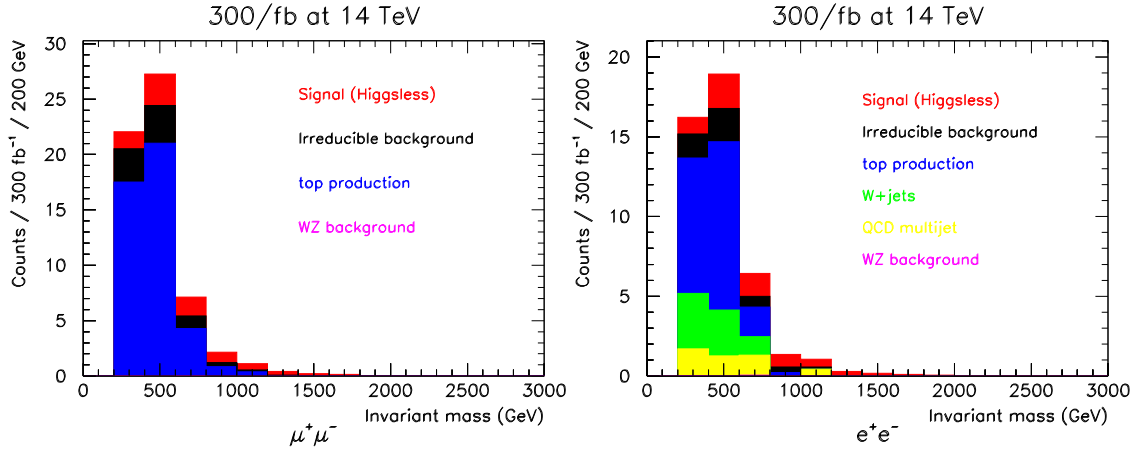


Figure 6.7: Invariant mass distributions of the two leptons resulting from the process $pp \rightarrow jjW^+W^-$ at 14 TeV, with $W^\pm \rightarrow \mu^\pm\nu$ (left) and $W^\pm \rightarrow e^\pm\nu$ (right). Shown are the signal calculated under the Higgsless hypothesis and various contributions to the background, normalized to 300/fb of data. Applied were respectively all the signal selection criteria foreseen for the opposite-sign muon channel (cuts 1-5 from Fig. 6.2, up to and including CJV) and for the opposite-sign electron channel (all cuts 1-6 listed in Fig. 6.2). Signal was calculated by subtracting a SM $jjW_L^+W_L^-$ sample from a Higgsless $jjW_L^+W_L^-$ sample. Irreducible background was calculated from a SM jjW^+W^- sample. The top production background was simulated as described in section 6.2. The WZ background was obtained from a dedicated jjW^+Z sample with subsequent W and Z decays into muons and an additional factor 1.5 was assumed to account for jjW^-Z (not simulated). The b -tagging efficiency was assumed 50% for a single b quark, all other efficiencies and purities were assumed 100%. The W +jets background was deduced from a dedicated $jjjW^+$ sample, where any of the jets was assumed to be misidentified as an electron. An additional factor 1.5 was assumed to account for $jjjW^-$ (not simulated). The QCD multijet background was deduced from a dedicated $jjjj$ sample where any pair of jets was assumed to be simultaneously misidentified as electrons. The probability of a jet faking an electron was assumed $1.1 \cdot 10^{-4}$ with a further 73% probability of sign matching. For a more detailed explanation of the procedure see sections 6.3 and 6.4. Results of MadGraph simulations, processed by PYTHIA 6 for W decay into leptons (for signal, irreducible background and top production), the effects of parton showering, hadronization and jet reconstruction and further processed by PGS 4 for the effects of finite resolution in the measurement of jet and lepton p_T in a CMS-like detector. The original PYTHIA 6 source code was modified to account for the correct, polarization-dependent, angular distributions for the leptonic W decays.

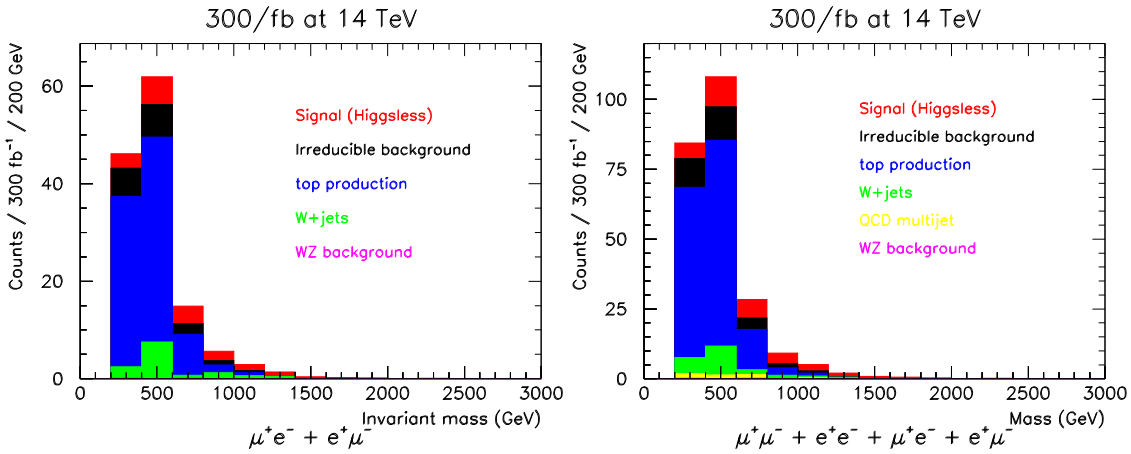


Figure 6.8: Invariant mass distributions of the two leptons resulting from the process $pp \rightarrow jjW^+W^-$ at 14 TeV, with one W decaying into a muon and another decaying into an electron (left) and with each W decaying into either a muon or an electron (right). Shown are the signal calculated under the Higgsless hypothesis and various contributions to the background, normalized to 300/fb of data. For the left plot, applied were all the signal selection criteria foreseen for the opposite-sign mixed muon+electron channel, i.e., cuts 1-5 from Fig. 6.2 (up to and including CJV). The final μe kinematics was deduced by averaging out the distributions obtained in $\mu^+\mu^-$ and the e^+e^- channels, which differed only due to different detector resolution effects assumed during processing by PGS 4. All the remaining procedures and assumptions were identical as described in the caption of Fig. 6.7. The right plot was obtained by summing up the individual W decay channels.

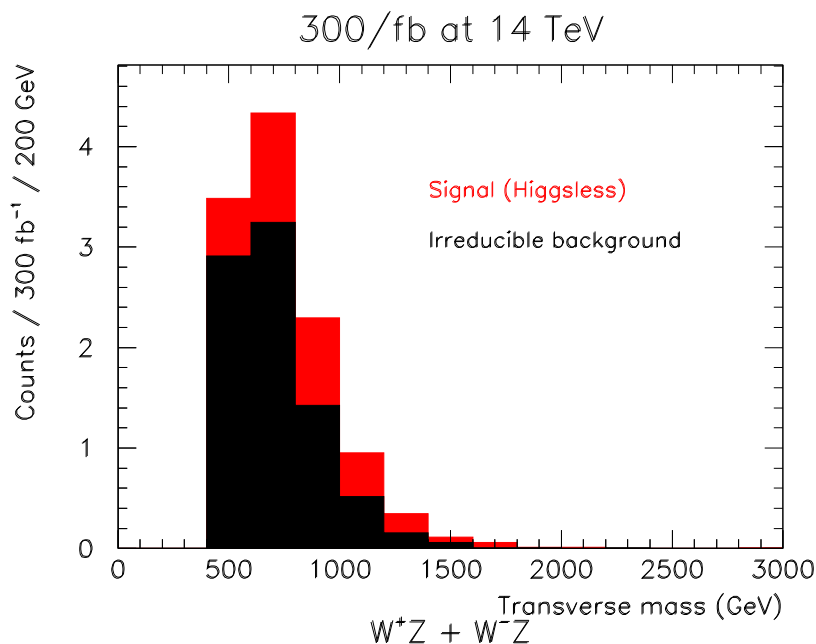


Figure 6.9: Distribution of the transverse mass (defined in detail in section 6.6) calculated for the process $pp \rightarrow jjW^\pm Z$ at 14 TeV, with subsequent leptonic decays of the gauge bosons. Shown are the signal calculated under the Higgsless hypothesis and the irreducible background, normalized to 300/fb of data. Applied were all the signal selection criteria foreseen for the WZ leptonic channel, no distinction was made between lepton flavors (e or μ). Signal was calculated by subtracting the SM jjW^+Z sample (by definition also identical with irreducible background) from the Higgsless jjW^+Z sample. The cross sections were obtained by scaling the simulated jjW^+Z sample by a factor of 1.5 to account for jjW^-Z (not simulated). All the relevant efficiencies and purities were assumed 100%. Results of MadGraph simulations, processed by PYTHIA 6 for parton showering, hadronization and jet reconstruction and further processed by PGS 4 for the effects of finite resolution in the measurement of jet and lepton p_T in a CMS-like detector.

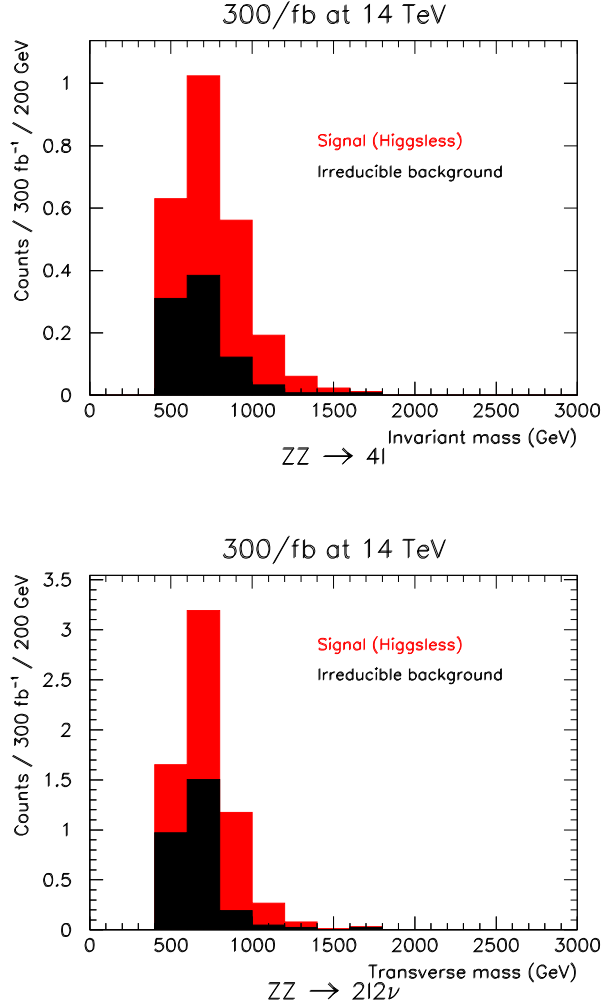


Figure 6.10: Invariant mass distribution of the four leptons resulting from the process $pp \rightarrow jjZZ \rightarrow jjl^+l^-l^+l^-$ (upper plot) and transverse mass distribution (defined in in section 6.6) from the process $pp \rightarrow jjZZ \rightarrow jjl^+l^-\nu\nu$ (lower plot) at 14 TeV. Shown are the signal calculated under the Higgsless hypothesis and the irreducible background, normalized to 300/fb of data. Applied were all the signal selection criteria foreseen for the ZZ four-lepton channel and for the $ZZ \rightarrow l^+l^-\nu\nu$ channel, respectively; no distinction was made between lepton flavors (e or μ). Signal was calculated by subtracting the SM jjZ_LZ_L sample from the Higgsless jjZ_LZ_L sample. All the relevant efficiencies and purities were assumed 100%. Results of MadGraph simulations, processed by PYTHIA 6 for Z decay into leptons, the effects of parton showering, hadronization and jet reconstruction and further processed by PGS 4 for the effects of finite resolution in the measurement of jet and lepton p_T in a CMS-like detector. This study did not include the correct, polarization-dependent, angular distributions for the leptonic Z decays. Such effects are nonetheless unlikely to change any of our conclusions.

edge of statistical significance for the LHC, application of the best analysis techniques may play a vital role.

6.9 Anomalous triple gauge couplings

Whether or not we will be able to observe *any* BSM signal is one question. Another one is whether we will be able to correctly interpret the result in an independent and standalone way, that is, not having to rely on other concurrent measurements and assume consistency within a given physics scenario.

New physics may manifest itself e.g. in anomalous triple gauge couplings which may likewise show up as an enhancement of WW scattering at high invariant mass. Details of the shapes of kinematic distributions of the final state particles depend on the physics scenario, but in general will also depend on specific values of the anomalous couplings, giving rise to annoying interpretative ambiguities. It is vital to study the dependencies of the individual kinematic variables and single out those of them that are mostly sensitive to the scenario but not to numerical values and vice-versa.

Updated 90% CL limits on the dimension-6 operators that lead to anomalous triple gauge couplings have been recently calculated [62]. We take the following values:

$$\begin{aligned} c_{WWW}/\Lambda^2 &\in [-15, 3.9] \text{ TeV}^{-2}, \\ c_W/\Lambda^2 &\in [-5.6, 9.6] \text{ TeV}^{-2}, \\ c_B/\Lambda^2 &\in [-29, 8.9] \text{ TeV}^{-2}. \end{aligned}$$

The above limits come from a combination of LEP, the TeVatron and the LHC Run 1 data. They are asymmetric because in each case the central values of the relevant couplings were determined.

It happens that anomalous couplings of roughly this size can produce BSM signals in WW scattering of the same order of magnitude as would be produced by a HWW coupling set to, e.g., 0.8 of its SM value. Assuming that the scale of new physics, Λ , is beyond direct LHC reach and therefore that no cutoff is necessary in evaluating signal rates, the expected amount of signal for W^+W^+ in the purely leptonic decay modes is close to 0.050 fb for $c_{WWW}/\Lambda^2 = -10/\text{TeV}^2$, 0.016 fb for $c_W/\Lambda^2 = -10/\text{TeV}^2$ (this includes 0.011 fb of W_LW_L and 0.005 fb of W_TW_X signal) and 0.003 fb for $c_B/\Lambda^2 = -10/\text{TeV}^2$. In deriving these numbers we have applied exactly the same signal selection criteria as we used before, although W_TW_X signals may be possible to further improve with dedicated optimizations. As it was with HWW , the LHC sensitivity to triple gauge couplings in W^+W^+ scattering is again at the very limit of present experimental bounds.

The most important point is that signal in general, understood as a sum of all possible BSM effects, may be as much manifest in W_LW_L pairs alone (if $c_B \neq 0$), as in W_TW_X alone (if $c_{WWW} \neq 0$), both W_LW_L and W_TW_X in roughly similar amounts (if $c_W \neq 0$), or any combination of the above cases. Any of the above scenarios ultimately manifests in an enhancement of WW scattering at high invariant mass, the latter being correlated with high lepton transverse momenta. Therefore, the R_{pT} variable is still a good BSM probe owing to its numerator. Because of the denominator, however, it always favors W_LW_L pairs over W_TW_X pairs. Without prior knowledge of the helicity composition

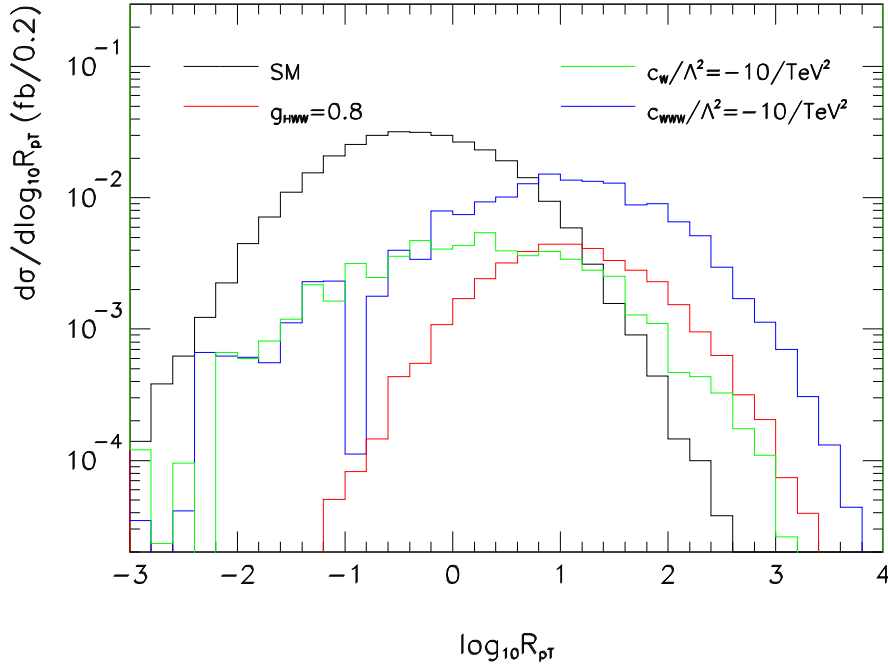


Figure 6.11: Distributions of $\log_{10} R_{pT}$ in the process $pp \rightarrow jjW^+W^+$ at 14 TeV, with leptonic W^+ decay ($l = e, \mu$) in different physics scenarios: Standard Model (black histo) and BSM signals for $g_{HWW} = 0.8$ (red histo), $c_W/\Lambda^2 = -10/\text{TeV}^2$ (green histo) and $c_{WWW}/\Lambda^2 = -10/\text{TeV}^2$ (blue histo). Applied were VBF topological cuts, including $\Delta\varphi_U > 2.5$. Result of MadGraph 5 simulations, processed by PYTHIA 6 for W^+ decay, parton showering, hadronization and jet reconstruction; no detector effects were included. The original PYTHIA 6 source code was modified to account for the correct polarization-dependent angular distributions for the W decays. Signals were calculated by subtracting the SM sample from the corresponding BSM sample. In calculating the BSM distributions it was assumed that the scale of new physics, Λ , is higher than the accessible energies and hence no cutoff was applied.

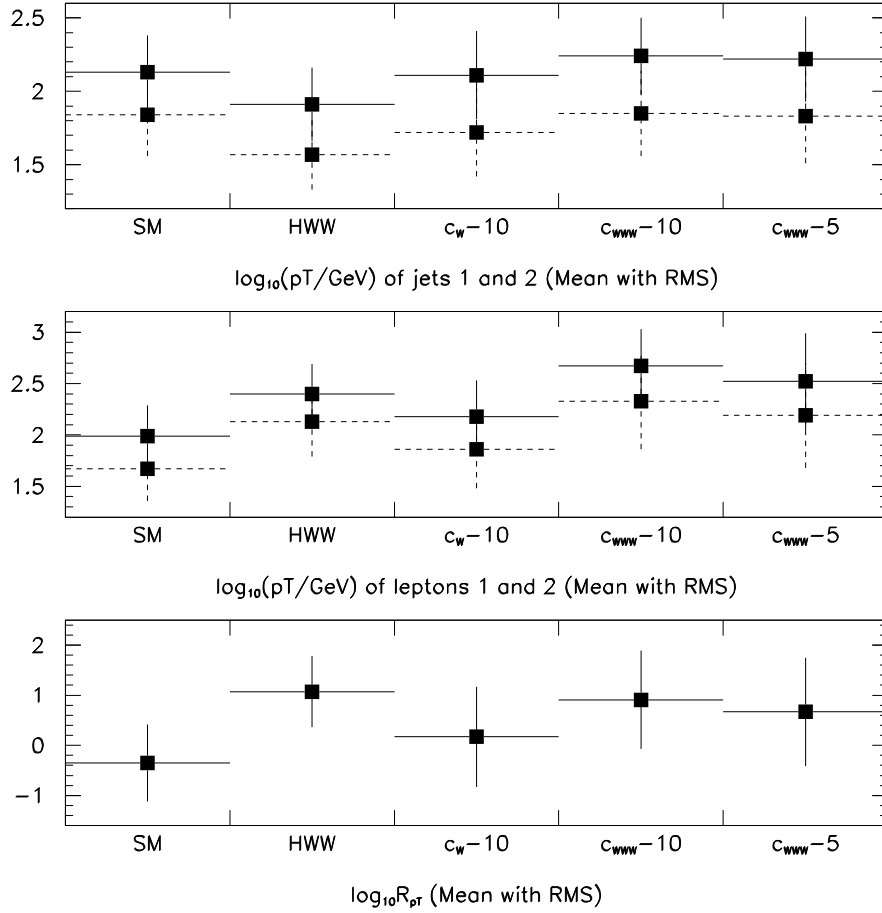


Figure 6.12: Mean values and RMS of the individual transverse momenta of the two jets (upper plot) and the two leptons (middle plot), and of the resulting R_{p_T} distribution (bottom plot) in the process $pp \rightarrow jjW^+W^+$ at 14 TeV, with leptonic W^+ decay ($l = e, \mu$) in different physics scenarios. On the two upper plots, solid lines represent the leading jet and lepton, respectively, and dashed lines represent the sub-leading jet and lepton, respectively. Vertical error bars represent the RMS. Each bin on the horizontal axis represents a physics scenario; from left to right: the Standard Model and BSM signals for $g_{HWW} = 0.8$, $c_W/\Lambda^2 = -10/\text{TeV}^2$, $c_{WWW}/\Lambda^2 = -10/\text{TeV}^2$ and $c_{WWW}/\Lambda^2 = -5/\text{TeV}^2$. Results of MadGraph 5 simulations, all conditions and assumptions as for Fig. 6.11.

of the signal, an enhancement in the numerator may be just compensated by a larger denominator. For a complete understanding of a future experimental result we need to examine the individual transverse momenta of the four final state objects.

What follows is a “quick and dirty” demonstration of principles how to extract the most physics information based on no more than four transverse momenta. Expressed in a logarithmic scale, individual p_T distributions in any given physics scenario, as well as the corresponding R_{p_T} distributions, can be to a first rough approximation described in terms of two parameters: the mean value and the RMS, see Fig. 6.11. This allows first simple studies of kinematic separation between different scenarios, before more detailed analyses become available. Since the expected signal statistics is anyway bound to be small, any more detailed shape spectrum may not be even plausible in practice. From such comparisons (see Fig. 6.12 bottom) we infer that R_{p_T} by itself will be enough to distinguish the SM scenario from BSM with a handful of events, as long as the overall signal size is significant enough. But it does not suffice to identify a BSM scenario. In particular, a pure c_{WW} scenario can produce an R_{p_T} spectrum indistinguishable from the one produced by an anomalous HWW scenario, despite the two signal samples consisting of different W polarizations. Moreover, outgoing lepton spectra are sensitive both to the physics scenario and to the numerical values of the anomalous coefficients and this interplay is very sophisticated (see Fig. 6.12 middle). Consequently, e.g., numerical variations within the c_{WW} scenario may be larger than differences between scenarios (cf., e.g., “ HWW ” with “ $c_{WW} - 10$ ” and “ $c_{WW} - 5$ ” in Fig. 6.12 bottom).

Fortunately, jet transverse momenta are a direct measure of helicity composition of the WW sample and nothing else. They do not depend on values of the anomalous coefficients (see Fig. 6.12 top). The trend is clear: the more W_T the higher jet p_T . A pure $W_L W_L$ (“ HWW ”) signal gives

$$\begin{aligned}\log_{10} p_T^{j1} &= 1.91 \pm 0.25 \text{ (RMS)}, \\ \log_{10} p_T^{j2} &= 1.57 \pm 0.24 \text{ (RMS)},\end{aligned}$$

while for a pure $W_T W_X$ signal (e.g. “ $c_{WW} - 10$ ”) it is

$$\begin{aligned}\log_{10} p_T^{j1} &= 2.24 \pm 0.26 \text{ (RMS)}, \\ \log_{10} p_T^{j2} &= 1.85 \pm 0.29 \text{ (RMS)}.\end{aligned}$$

Combined the information from the two jets, the two extreme cases can be distinguished at a 3σ level with as few as 7 isolated signal events and at 5σ with 20 events. This will be possible with 3000 fb^{-1} , unfortunately not with 300 fb^{-1} . Approximately four times this statistics is required to perform similar with a mixed helicity signal like in the case of $c_W \neq 0$. From a back of the envelope calculation it follows that with 20 isolated signal events (e.g., with $g_{HWW} = 0.9$ and 3000 fb^{-1}), the helicity composition of the signal can be determined to better than 20%. With 60 events (e.g., $g_{HWW} = 0.8$, 3000 fb^{-1}), it can be known to $\sim 10\%$. It should be kept in mind that average jet p_T does increase with M_{WW} for transverse polarization. This is why the leading jet p_T of the c_W signal is hardly different from the one in the SM, although the former has a relatively larger $W_L W_L$ component. But for any BSM scenario that manifests as a steady enhancement at high M_{WW} up to the kinematic limit of available phase space, differences in the jet p_T spectra for $W_T W_X$ are effectively a second order effect. On the other hand, jet p_T

spectra for $W_L W_L$ are very much independent of anything and are a unique signature of longitudinal polarization.

Once we have measured the helicity composition and hence settled which BSM effect plays the dominant role (at least within the limited scope of scenarios considered here), the numerical value of the leading anomalous coefficient can be deduced by studying the lepton transverse momenta (or alternatively the lepton-lepton invariant mass, which is quite the same thing).

In the above studies we have considered explicitly only negative values of the anomalous coefficients. Positive values of c_{WWW} or c_W happen to be more bound experimentally and in addition the interference with SM diagrams is in this case destructive. The signal will then consist of a slight depletion followed by very little enhancement within the allowed phase space, likely beyond LHC sensitivity.

Variations of c_B within the presently allowed range produce too little signal to be detected at the LHC. As a matter of principle, c_B affecting only $W_L W_L$ pairs cannot be distinguished from pure HW scaling by means of the methodology proposed here.

6.10 Anomalous quartic couplings

Some of the dimension-6 operators discussed above modify also the gauge quartic couplings. It is conceivable that their values will be eventually determined by non-VBS processes at the LHC and applied as background in more dedicated VBS analyses. On the other hand, quartic couplings can best be determined via VBS processes, along with triboson production. Since sensitivity of VBS processes to anomalous triple couplings, including Higgs to gauge couplings, within their present bounds is rather slim, a large deviation from SM predictions could in fact signal non-trivial contributions from physics related to operators of yet higher dimension than 6, namely dimension 8. For this reason it makes sense to go directly to the presently unbounded dimension-8 operators and study their potential consequences. These operators may affect VBS and triboson production, but not other processes. Such studies are currently in progress, some have already been shown.

In section 5.3 we have already discussed the LHC sensitivities to anomalous quartic couplings based on an early study of $W^\pm W^\pm$ carried at the phenomenological level. Most recently, sensitivity to quartic couplings in VBS processes has been studied by the Snowmass 2013 study group [116]. Results were presented in the language of higher-dimension operators in Effective Field Theory. Studied were the respective sensitivities of the ZZ process to parameters $f_{T,8}/\Lambda^4$ and $f_{T,9}/\Lambda^4$, of WZ to $f_{T,1}/\Lambda^4$ and of $W^\pm W^\pm$ to $f_{T,1}/\Lambda^4$. In Effective Field Theory, these coefficients scale dimension-8 operators $\mathcal{L}_{T,8}$, $\mathcal{L}_{T,9}$ and $\mathcal{L}_{T,1}$, respectively. In the same work, total cross sections for $W^\pm W^\pm WZ$ and ZZ were calculated varying many anomalous coefficients one at a time. Reportedly, $f_{T,1}/\Lambda^4$ and $f_{T,0}/\Lambda^4$ were the parameters that all the total cross sections were found most sensitive to. The choice of $f_{T,8}/\Lambda^4$ and $f_{T,9}/\Lambda^4$ for ZZ was motivated by the fact that these parameters are built uniquely from the neutral field strengths $B_{\mu\nu}$ and so they can only be probed in this process. Note that all these operators are built from field strengths only ($B_{\mu\nu}$ or $W_{\mu\nu}$) rather than Higgs field derivatives, and consequently affect directly only the vertices involving transversely polarized states. The various anomalous coefficients were

implemented in MadGraph matrix element calculations. Simulations included typical detector resolutions parameterized in the DELPHES program. Only irreducible backgrounds were considered, except for the $W^\pm W^\pm$ process for which the analysis included the WZ background scaled by an additional factor 2 to account for other backgrounds. Applied were minimal selection criteria which consisted in principle of a jet-jet invariant mass cut, $M_{jj} > 1$ TeV, in addition to the requirement of the proper final state for each scattering process, assuming purely leptonic decays. Signal, understood as the total electroweak production rate, was calculated using the alternative hypotheses of the SM and of non-zero value of the relevant anomalous coefficients (hence it is the difference between the two that defines signal in the understanding used throughout this work). The final results were obtained by evaluating the one-dimensional spectrum of the reconstructed VV mass (for ZZ and WZ) or of the 4-body invariant mass, M_{jjll} (for $W^\pm W^\pm$). Different pile-up conditions were simulated for the $W^\pm W^\pm$ process, but results reportedly did not vary much. The authors calculated also for each process the corresponding unitarity bounds as a function of the respective coefficient values. Results were presented with and without applying a sharp unitarity violation cutoff. Snowmass study results for 14 TeV are summarized in Table 6.1. One notices in particular that an order of magnitude increase in integrated luminosity, between 300 and 3000 fb^{-1} , translates into an increase of merely a factor ~ 2 in the expected sensitivities.

Process, parameter	Luminosity	5σ	95% CL
$ZZ, f_{T,8}/\Lambda^4$	300 fb^{-1}	5.5 (8.4) TeV^{-4}	3.2 (5.3) TeV^{-4}
$ZZ, f_{T,8}/\Lambda^4$	3000 fb^{-1}	2.9 (4.7) TeV^{-4}	1.7 (2.4) TeV^{-4}
$ZZ, f_{T,9}/\Lambda^4$	300 fb^{-1}	8.7 (9.0) TeV^{-4}	6.2 (6.7) TeV^{-4}
$ZZ, f_{T,9}/\Lambda^4$	3000 fb^{-1}	5.7 (6.3) TeV^{-4}	3.9 (4.6) TeV^{-4}
$WZ, f_{T,1}/\Lambda^4$	300 fb^{-1}	1.1 (1.6) TeV^{-4}	0.7 (1.0) TeV^{-4}
$WZ, f_{T,1}/\Lambda^4$	3000 fb^{-1}	0.6 (0.9) TeV^{-4}	0.4 (0.5) TeV^{-4}
$W^\pm W^\pm, f_{T,1}/\Lambda^4$	300 fb^{-1}	0.2 (0.4) TeV^{-4}	0.1 (0.2) TeV^{-4}
$W^\pm W^\pm, f_{T,1}/\Lambda^4$	3000 fb^{-1}	0.1 (0.2) TeV^{-4}	0.06 (0.1) TeV^{-4}

Table 6.1: The 5σ significance discovery values and 95% CL limits for coefficients of dimension-8 operators with 300 and 3000 fb^{-1} of data at 14 TeV using different VBS process. Numbers in brackets correspond to imposing a unitarity violation cutoff. Results of the Snowmass13 study [116].

Some other studies exist that include full detector simulation and improved background evaluation. The ATLAS collaboration presented a new set of simulation-based studies for 14 TeV, reformulated and updated after Higgs discovery [117]. Under the assumption that each scattering process will be mainly sensitive to new physics arising from just one of those higher order operators, sensitivities to new physics have been evaluated for ZZ , WZ and $W^\pm W^\pm$ in the purely leptonic decay modes. These studies were based on fully simulated events, including detector effects related to jet clustering, pile-up, as well as parameterized reconstruction efficiencies and resolutions for the different physics objects.

Early work was based on the EWChL approach and amplitude unitarization according to the model of Dobado et al. [93] to evaluate gauge boson scattering signals, and results

were given in terms of the EWChL parameters a_4 and a_5 . More recently, a newer set of analyses was presented with all the results translated into the language of Effective Field Theory.

The quartic $WWWW$ coupling was studied in terms of the $f_{S,0}/\Lambda^4$ coefficient that scales the effective operator $\mathcal{O}_{S,0}$ and is best probed via the same sign $W^\pm W^\pm$ channel. Otherwise, the analysis was akin to the one carried by the Snowmass study. Various reducible backgrounds were estimated using a combination of simulation work with existing experimental data. The most important of them were reportedly total $jjWZ$ production, $jjW^\pm W^\pm$ production via gluon exchange (QCD) graphs and several detector-dependent backgrounds generally termed “mis-ID’s”. The latter class included photon conversion, jets faking leptons and lepton charge flips.

Results were presented in terms of the 5σ discovery reach and 95% confidence level exclusion limits for expected luminosities of 300/fb and 3000/fb. With 300/fb, the 5σ discovery limit was obtained at 10 TeV^{-4} , while the expected 95% CL exclusion limit is 6.8 TeV^{-4} . An order of magnitude increase in luminosity was found to translate into nearly an order of magnitude improvement of the exclusion limit, but only slightly more than a factor 2 in the discovery reach. This is due to a non-trivial relation between $f_{S,0}/\Lambda^4$ and the signal size. However, in the event of BSM observation with 300 fb^{-1} , the anomalous coefficient could be measured with a precision better than 5% with 3000 fb^{-1} , which fully qualifies for the term precision measurement.

Based on earlier studies at the phenomenological level, similar limits can be also expected on $f_{S,1}/\Lambda^4$. It is important to realize that all these studies assume just one non-vanishing anomalous parameter at a time. It was also shown that $f_{S,0}$ and $f_{S,1}$ produce similar signal and so are in fact anticorrelated. This anticorrelation is especially strong for $W^\pm W^\pm$. Combination of different scattering processes, in particular $W^\pm W^\pm$ and $W^+ W^-$, is instrumental in restricting the allowed ranges of both parameters at a time so to be comparable with limits obtained from considering just one parameter at a time.

The ATLAS study is the first complete detector-specific study of the unique physics capabilities of $W^\pm W^\pm$ scattering after Higgs discovery (unique in the sense that the same cannot be measured with possibly better precision in any other processes). Since a sizeable fraction of the background is comprised by the various detector-specific “mis-ID’s”, ATLAS results cannot be directly transferred to CMS, but one can safely assume that more important at this stage is further detector-independent analysis optimization. The published study most certainly keeps much room for improvements. First and foremost, it is polarization-blind. Moreover, a high p_T threshold of 50 GeV for both tag jets was used to protect against pile-up jets. This however at 14 TeV means automatical loss of two thirds of the $W_L W_L$ sample. It should be noted that $f_{S,0}$ produces BSM effects only in $W_L W_L$. Any lowering of the jet p_T thresholds will reflect in improved sensitivities. For example, with the p_T threshold applied on only one tag jet the $W_L W_L$ scattering statistics increases by a factor 2. A one-dimensional evaluation of the 4-body invariant mass does not exploit the full relevant details of the final state kinematics. Lack of explicit consideration of $\Delta\varphi_{ll}$ allows a lot of unnecessary non-VBS contributions, in particular $jjWZ$, without practically any gain in terms of signal. Finally, since $f_{S,0}$ enhances high WW masses for $W_L W_L$ pairs, it is plain to see that R_{p_T} will be as efficient a criterion to extract the BSM signal as it was for the case of a scaled HWW coupling. The above remarks become even more important when one notices that the Snowmass study [116] revealed

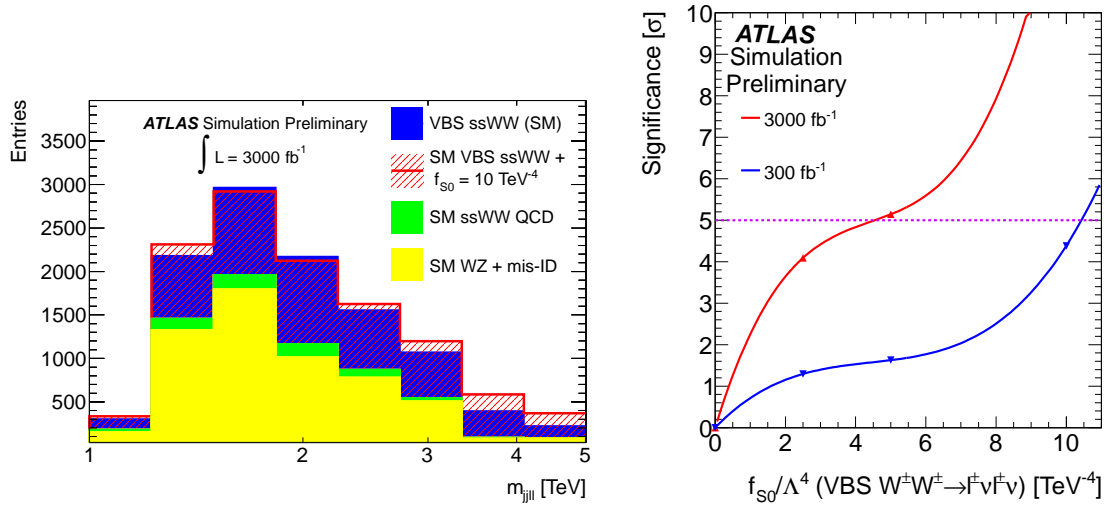


Figure 6.13: Reconstructed 4-body mass spectrum in the SM and in the scenario with $f_{S,0}/\Lambda^4 = 10 \text{ TeV}^{-4}$ (left) and BSM signal significance in standard deviations as a function of $f_{S,0}/\Lambda^4$ (right) from the $pp \rightarrow jjl^\pm l^\pm \nu \nu$ process at 14 TeV. Results of simulations done by the ATLAS experiment, images reproduced from Ref. [117].

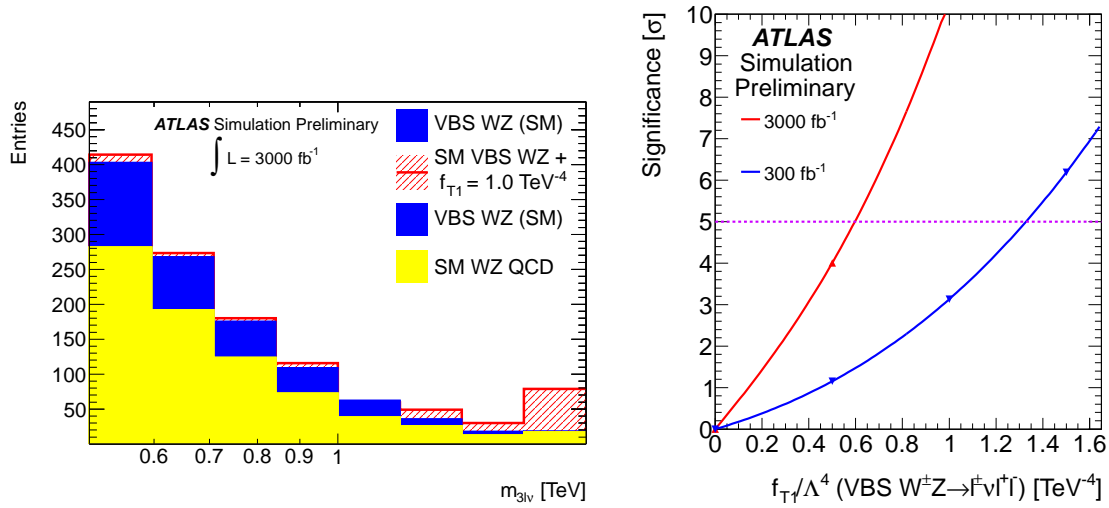


Figure 6.14: Reconstructed WZ mass spectrum in the SM and in the scenario with $f_{T,1}/\Lambda^4 = 1 \text{ TeV}^{-4}$ (left) and BSM signal significance in standard deviations as a function of $f_{T,1}/\Lambda^4$ (right) from the $pp \rightarrow jjl^\pm l^\pm l^\pm \nu$ process at 14 TeV. Results of simulations done by the ATLAS experiment, images reproduced from Ref. [117].

a much better sensitivity of the total $W^\pm W^\pm$ rate to $f_{T,1}/\Lambda^4$ than to $f_{S,0}/\Lambda^4$ or $f_{S,1}/\Lambda^4$. There may be no other way than to go to lower jet p_T in order to conclude anything about $f_{S,0}/\Lambda^4$ or $f_{S,1}/\Lambda^4$ proper.

Discovery reaches and expected exclusion limits for other dimension-8 operators were also obtained from $W^\pm Z \rightarrow W^\pm Z$ and $Z\gamma\gamma$ production. From a study of WZ scattering expected limits and discovery reaches were derived on $f_{T,1}/\Lambda^4$, for which this process is supposed to be most suited. It must be stressed however that the Snowmass study revealed $W^\pm W^\pm$ be actually much more sensitive to this parameter than WZ . Again here, selection criteria were reduced to a suitable combination of 3 leptons and a high jet-jet invariant mass. The expected 95% CL limits were found to be 0.7 TeV^{-4} and 0.3 TeV^{-4} for 300 fb^{-1} and 3000 fb^{-1} , respectively, while 5σ discovery reaches were 1.3 TeV^{-4} and 0.6 TeV^{-4} , respectively. The results are in fact in full agreement with those of the Snowmass study. Because $f_{T,1}$ directly affects only transversely polarized pairs, high jet p_T threshold may not be a problem here. However, drawing the result from a one-dimensional analysis of the reconstructed WZ mass spectrum is beyond doubt suboptimal.

A similar study for the WZ channel was recently presented by the CMS collaboration [118]. This analysis included fast simulation of detector response at high luminosity, with dedicated CMS-specific packages developed for the planned low luminosity and high luminosity phases of the LHC. More restrictive selection criteria than applied in the ATLAS study included most of the typical VBF criteria for WZ , namely $\Delta\eta_{jj} > 4$, minimum MET, high jet-jet invariant mass and a reconstructed Z mass. In addition, cuts were applied on the lepton-lepton and jet-lepton separation. The final result was obtained from a shape analysis of the reconstructed one-dimensional WZ transverse mass spectrum. This produced similar, if only slightly better, sensitivities than those reported by ATLAS. A 5σ discovery is expected for $f_{T,1}/\Lambda^4$ down to 1 TeV^{-4} with 300 fb^{-1} and to 0.55 TeV^{-4} with 3000 fb^{-1} . This study too used a conservative jet p_T threshold and made no specific selection as to separate W/Z polarizations. Another interesting result is that the Standard Model process of WZ scattering after the proposed preselection can be visible at 5σ after collecting $185/\text{fb}$ of data. Hence, consistency with the SM can be precisely tested in the event of absence of new physics.

Once again it is important to realize the arbitrariness of such analyses in terms of the assumed choice of the appropriate parameter or parameters to be studied in relation to a particular scattering process. Strictly speaking, $f_{S,0}$ and $f_{S,1}$ modify also the $WWZZ$ vertex. Likewise, both vertices are sensitive to other dimension-8 operators, constructed either from field strength tensors and Higgs field derivatives or from field strength tensors alone. Most of these dependencies have not been explicitly studied so far. They may not even add up coherently, but involve non-trivial interference effects. The task of disentangling the different contributions will be a long and complicated one. It will certainly require a combination of all scattering processes. We are only at the beginning of the real work. The good news is that we can at least partly help this task with a technique to separate different polarization states via their respective jet transverse momentum spectra.

Finally, even if we understand the VBS measurements as purely Standard Model measurements, aimed solely at setting limits on various anomalous contributions (for the LHC such scenario cannot be disregarded), application of dedicated techniques to separate

longitudinal from transverse gauge bosons will certainly result in better experimental limits - at least for those operators which affect mainly $V_L V_L$ pairs.

Chapter 7

Beyond the LHC

According to the European Strategy for Particle Physics, update of 2013, *Europe's top priority should be the exploitation of the full potential of the LHC, including the high-luminosity upgrade of the machine and detectors with a view to collecting ten times more data than in the initial design, by around 2030.* The ultimate goal of the LHC is to deliver 3000 fb^{-1} of proton-proton data within the next 15-20 years, but until then beam energy will stay at 13/14 TeV. For beyond the High Luminosity LHC timescale, the next priority outlined by the European Strategy for Particle Physics is pushing the energy frontier. A “High Energy LHC” option has been studied as a possible next step after 2035. The replacement of the NbTi dipole magnets with 20 T dipoles based on the novel High Temperature Superconductor (HTS) technology would allow reaching as high as 33 TeV in the very same LHC ring. Meanwhile, a yet more ambitious project has been gaining momentum and attracting the attention of particle physicists. On February 12-15, 2014, a kick-off meeting took place of the Future Circular Collider (FCC) Study group in Geneva [119]. A total number of 341 physicists from all over the globe met to discuss the rationale and perspectives to build a new, more powerful collider that one day may possibly become the LHC successor. The main aim of the project is building a new ring in the area of Geneva that will eventually collide protons at a center of mass energy of 100 TeV. The process of setting up a new international collaboration was initiated.

7.1 General features of VV scattering at the FCC

The subject of Vector Boson Scattering is widely considered as one of the key physics topics for the FCC (here and in what follows, we will refer as FCC to specifically the proton-proton option, more exactly known as FCC-hh - there exist also electron-electron and electron-hadron options that are being considered in parallel, possibly to be realized some day in the very same FCC tunnel).

Producing any realistic simulation-based predictions for WW scattering in proton-proton collisions at 100 TeV is connected to several theoretical issues. Event topology changes as all the outgoing products of a collision get generally boosted more forward than they are in the LHC. This means in particular that the typical signature of a VBS event is now modified so to extend to higher pseudorapidity of the two tagging jets. Early studies indicate that the minimum jet pseudorapidity range to be covered extends at least up to $|\eta| < 6$. From the experimental point of view it is unlikely that useful jet reconstruction

can be extended to yet higher $|\eta|$ in a real detector, and so we will assume this minimum coverage as a reasonable compromise between physics needs and technical possibilities. Leading order calculations of the process, say, $pp \rightarrow jjW^+W^+$ with the required kinematic coverage may not be of enough accuracy for 100 TeV and use of NLO generators is officially encouraged and recommended by the FCC-hh group. However, because of relatively little QCD contamination, the same-sign channel in the purely leptonic decay mode is the least affected by this uncertainty. Preliminary studies with the VBFNLO generator indicate that LO versus NLO differences amount here to less than 10% [120]. The applicability of currently available PDFs constitute a source of additional uncertainty. All these issues need to be aggressively addressed. Furthermore, little is known at the present moment of the particle detectors and their performances for the FCC, although some first intelligent guesses as to what these potential detectors may (are bound to?) look like have already been presented. In any case, development of complete, realistic simulations for the FCC is a task for many years and many people. Nonetheless, it is already possible to get a rough glimpse of the possibilities and main advantages over the LHC. And once again here, we will make the claim that a traditional analysis consisting of selecting VBF-topology events and studying the lepton-lepton invariant mass spectrum is by far a suboptimal strategy.

The total cross section for $pp \rightarrow jjW^+W^+$ with two forward “tagging” jets is over 40 times larger at 100 TeV than at 14 TeV. A hint of the FCC physics capabilities can be grasped by simply repeating quite the same analysis we have outlined in previous sections for the LHC, with the slight alteration of the basic topological cuts which now will read:

$$\begin{aligned} 2.5 < |\eta_j| < 6, \\ \eta_{j1}\eta_{j2} < 0, \\ |\eta_l| < 2.1. \end{aligned}$$

Detailed simulation of inclusive $t\bar{t}$ background for 100 TeV is currently missing; there is however much to suppose that this background can be kept at a manageable level here too. The kinematic bounds from the top quark mass, which we have previously quantified as $m_{j1j2} < 200$ GeV and $m_{j2j1} < 200$ GeV are valid here as well, while the signal region in 100 TeV collisions starts typically at significantly higher values. Stringent cuts like $m_{jl} > 400$ or 500 GeV can be readily imposed if necessary to suppress the $t\bar{t}$ background to the desired level without being too costly to the signal. In all the following considerations we will only discuss the signal and irreducible background, the latter being defined, as usual, as the Standard Model total WW production.

It is plain to see that all the kinematic features that distinguish the BSM signal from the SM background are qualitatively still the same as we saw for 14 TeV. In particular, W_LW_L signal clearly populates a region of lower jet transverse momenta than W_TW_X background. The median of the leading jet p_T distribution of the signal is found around 100 GeV which poses no problems from the detector point of view. The sub-leading jet distribution, however, has a median around 50 GeV. This means that requiring two tagging jets with $p_T > 50$ GeV, as is assumed by default in some studies, automatically means an unacceptable 50% signal loss in every study where we are interested in W_LW_L . Special effort must be dedicated in order to keep the machine pile-up under reasonable control and make the low p_T jets accessible to physics analysis. A machine operating in a 5 ns mode (option considered as a possible backup solution), and therefore having a 5 times lower pile-up, would be clearly advantageous from this point of view. Ideally,

reaching the $p_T > 20$ GeV level would be the goal that best corresponds to the physics needs. Alternatively, one should reconsider the concept of tagging only one forward jet and setting an algorithm to find the second jet off line. Such studies however have not been seriously started to the present moment. The leading lepton p_T for the signal ranges virtually from around 100 GeV above, hence triggering on a single lepton will not be a problem ¹.

7.2 Higgs to gauge couplings at the FCC

At the level of basic topological cuts, the two kinematic variables that offer the best sensitivity to the HWW coupling are still $\Delta\varphi_{ll}$ and R_{p_T} . The former, as usual, selects hard scattering events, the latter separates BSM from SM contributions, the more effectively if BSM manifests in $W_L W_L$ pairs. Since we are working here with energy-independent variables, the respective signal and background regions can be taken to a first approximation the same as we had before, before more detailed, dedicated optimization is done. Simple cuts like $\Delta\varphi_{ll} > 2.5$ and $R_{p_T} > 3.5$ already suffice to isolate significant amounts of signal in a scenario with the HWW coupling being as close to the SM one as to a few per cent. The amount of irreducible background left will be close to 0.66 fb, while signal ranges from 2.54 fb to 0.69 fb, to 0.26 fb and to 0.06 fb for the scenario of the HWW coupling being equal to 0.8, 0.9, 0.95 and 0.98 times its Standard Model value, respectively. For details, see Figs. 7.1 thru 7.4. Assuming an integrated luminosity of 1000 fb^{-1} (the order of magnitude that is usually considered for the FCC-hh), a 3-4% deviation from the Standard Model coupling will be measurable with a 5σ significance. Assuming 3000 fb^{-1} , we reach a 2% sensitivity. A combined shape analysis of the two respective distributions will ultimately produce even more accurate results. As long as we can restrict our analysis to the case of $g_{HWW} < 1$, shape analysis in the lepton-lepton invariant mass distribution gives little improvement in this measurement and is not much more efficient than a simple counting experiment as we have just done. Nonetheless, an interpretative ambiguity may still exist between $g_{HWW} < 1$ and $g_{HWW} > 1$ cases. The lepton-lepton invariant mass spectrum, or equivalently lepton transverse momenta, solve this puzzle unambiguously, since they directly reflect the interference pattern between the Higgs exchange graph on the one hand and the sum of the Z/γ exchange and the 4- W contact graphs on the other. To be more explicit, the spectrum monotonously rises with respect to the SM if $g_{HWW} < 1$, while it initially falls and ultimately rises if $g_{HWW} > 1$. The turning point lies well within the allowed kinematic phase space of the FCC if only the HWW coupling differs from unity enough to produce a statistically significant signal. Past it the $g_{HWW} > 1$ spectrum tends to catch up with its mirror $g_{HWW} < 1$ spectrum and the two become asymptotically identical.

¹If any triggering will still be used at all - some authors predict, based on the so called Moore's law, that the need to have a first level trigger will disappear altogether by the time FCC-hh is starting.

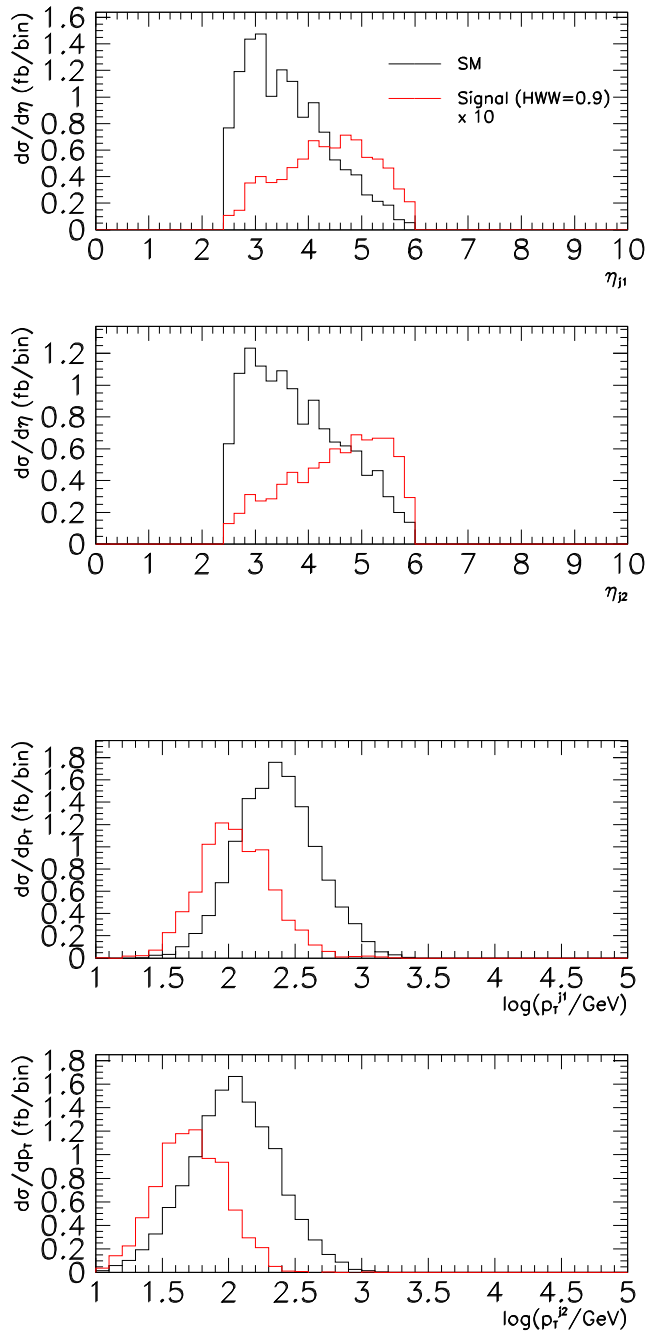


Figure 7.1: Distributions of pseudorapidities (two upper plots) and transverse momenta (two lower plots) of the leading and sub-leading jets from the $pp \rightarrow jjW^+W^+$ process at 100 GeV, with leptonic W^+ decay ($l = e, \mu$). Shown are the distributions for the Standard Model irreducible background (black histograms) and the BSM signal (red histograms). BSM was defined in terms of the HWW coupling set to 0.9 of its SM value. Signal was calculated by subtracting the SM sample from the BSM sample and multiplied by a factor 10 for better visibility. Only basic topological cuts were applied (see text). Result of MadGraph simulations, processed by PYTHIA 6 for parton showering, hadronization and jet reconstruction. No detector effects were taken into account.

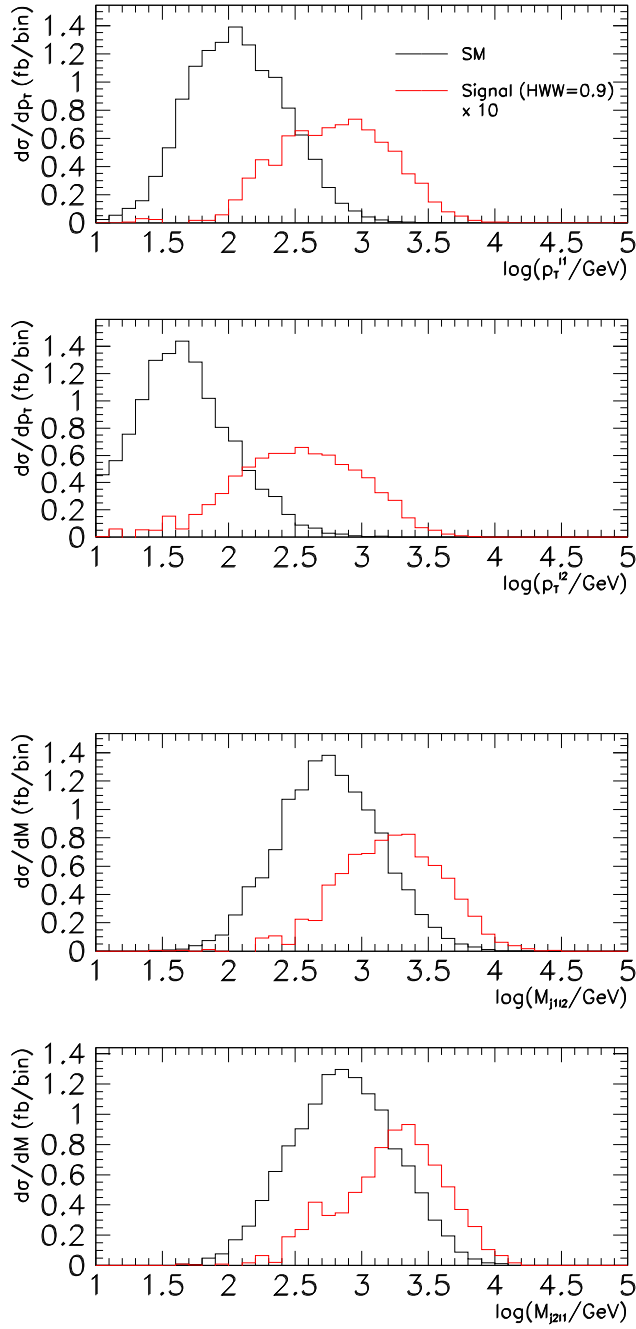


Figure 7.2: Distributions of transverse momenta of the leading and sub-leading (two upper plots) leptons, and invariant mass distributions of combinations of jets and leptons (two lower plots) from the $pp \rightarrow jjW^+W^+$ process at 100 GeV, with leptonic W^+ decay ($l = e, \mu$). Shown are the distributions for the Standard Model irreducible background (black hists) and the BSM signal (red hists). BSM was defined in terms of the HWW coupling set to 0.9 of its SM value. Signal was calculated by subtracting the SM sample from the BSM sample and multiplied by a factor 10 for better visibility. Only basic topological cuts were applied. Result of MadGraph simulations, processed by PYTHIA 6 for W decay into leptons, parton showering, hadronization and jet reconstruction. The original PYTHIA 6 source code was modified to account for the correct, polarization-dependent, angular distributions for the W decays. No detector effects were taken into account.

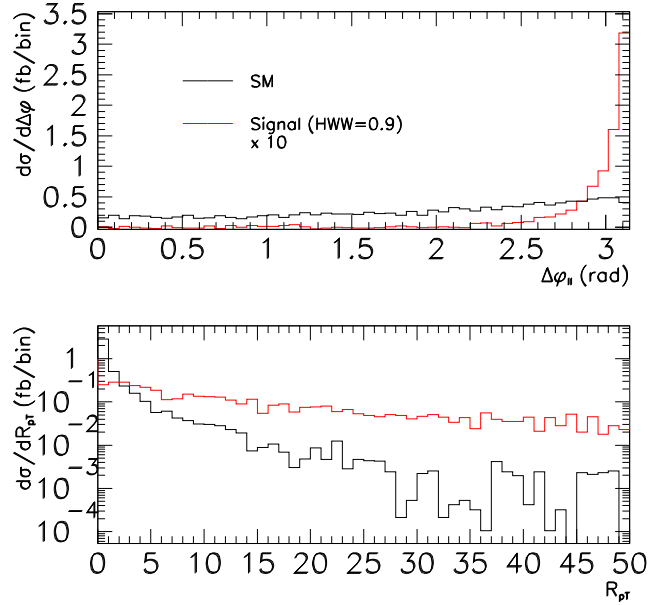


Figure 7.3: Top: distribution of the lepton-lepton azimuthal separation, $\Delta\varphi$, and bottom: distribution of the ratio $p_T^{l1} p_T^{l2} / (p_T^{j1} p_T^{j2})$, from the $pp \rightarrow jjW^+W^+$ process at 100 GeV, with leptonic W^+ decay ($l = e, \mu$). Shown are the distributions for the Standard Model irreducible background (black histos) and the BSM signal (red histos). All assumptions and conditions as in Fig. 7.2. For the lower plot, an additional cut on $\Delta\varphi > 2.5$ was applied.

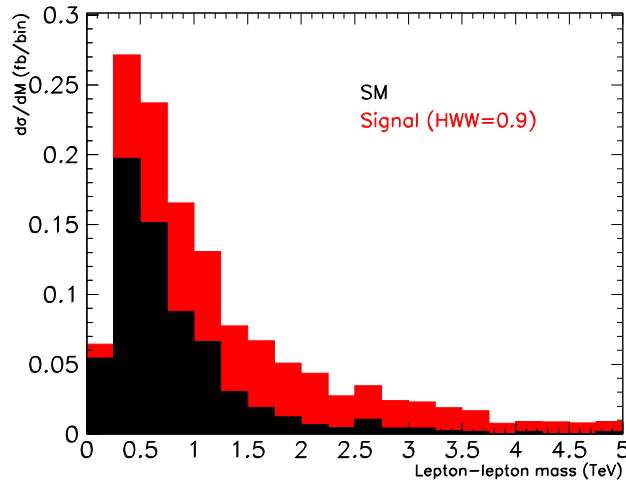


Figure 7.4: Lepton-lepton invariant mass in the $pp \rightarrow jjW^+W^+$ process at 100 GeV, with leptonic W^+ decay ($l = e, \mu$). Shown are the BSM signal (red histo) stacked on the Standard Model irreducible background (black histo). In addition to basic topological cuts, required was $\Delta\varphi > 2.5$ and $R_{pT} > 3.5$. All other assumptions and conditions as in Fig. 7.2.

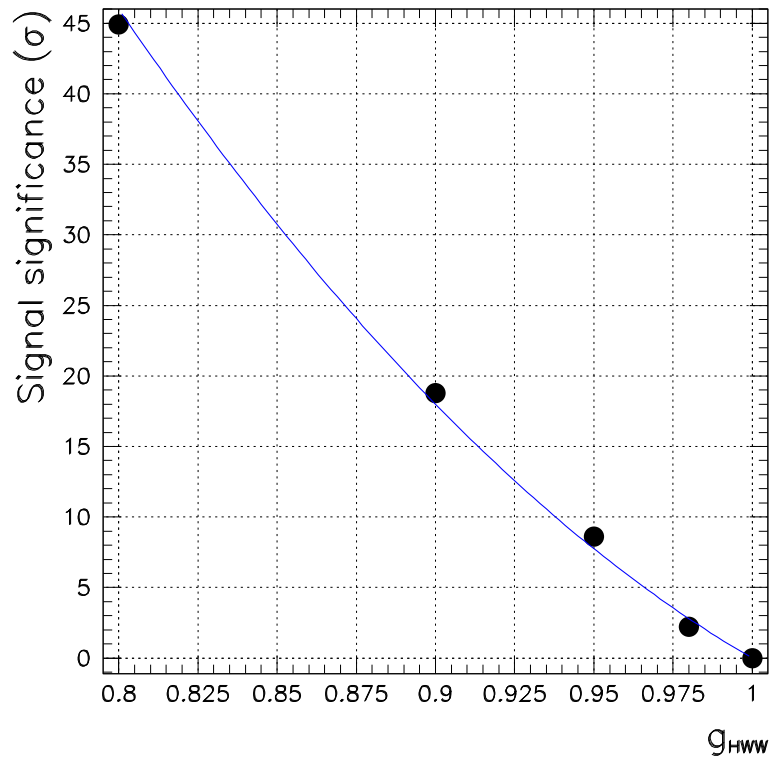


Figure 7.5: Signal significance, expressed in terms of the ratio $S/\sqrt{S+B}$ (S - BSM signal, B - SM irreducible background) as a function of the actual value of the HWW coupling relative to its SM value, simulated in the $pp \rightarrow jjW^+W^+$ process at 100 TeV, with leptonic W^+ decay ($l = e, \mu$), and assuming an integrated luminosity of 1000 fb^{-1} . All assumptions and conditions as in Fig. 7.4. In signal evaluation no unitarity cutoff was applied and so the leftmost points may be slightly overestimated.

7.3 Anomalous gauge couplings at the FCC

As mentioned before, the most sensitive probes of triple gauge couplings will come from measurements of total diboson production. Preliminary simulation work indicates that the relevant VBS modes will be able to independently cross check these results and push the sensitivity to well within the present limits in terms of anomalous operators \mathcal{O}_{WWW} , \mathcal{O}_W and even \mathcal{O}_B . Of course, these limits will be still improved by the LHC. More or less detailed quantitative estimates of such sensitivities are currently being worked out by many people, but perhaps are not the most urgent question at the present moment. In fact a far more important issue needs to be tackled. The analyses carried so far (like the one we have just reported on in the previous section!) usually focus on a single BSM effect or a single anomalous operator at a time. This is acceptable for LHC energies where the main question is whether we can observe *any* BSM effect given present bounds on anomalous couplings, but our ability to identify a physics scenario without relying on other measurements is limited. The aim of the FCC is however to identify a physics scenario. A single anomalous operator is unlikely what we will eventually observe in an experiment. The key question to address is whether we can disentangle the different effects for a correct interpretation of the experimental result. This requires a careful comparative study of the phenomenology associated to the possible different scenarios.

In the scenario with non-SM Higgs to gauge couplings, signal manifests solely in $W_L W_L$ pairs rising with energy above SM prediction. It happens that a quartic $WWWW$ coupling scaled by a constant factor will also be mostly observable in this way. The entire contribution of the quartic vertex to the dominant $W_T W_T$ scattering cross section is rather minute, so the total rate varies very little with it. Mixed $W_T W_L$ pairs get some energy dependence in addition to an overall normalization shift, but this last effect is even less appreciable than in $W_T W_T$ because of lower absolute rates, and the first effect is dwarfed by a much steeper energy dependence coming from $W_L W_L$ pairs. Consequently, it is the functional form of the $W_L W_L$ energy dependence through which one must distinguish a scaled HWW coupling from a scaled $WWWW$ coupling. Various anomalous contributions to the quartic coupling may however affect $W_T W_X$ as well as $W_L W_L$.

There is one result published from the Snowmass 2013 study [116] that is of direct interest for the FCC. The sensitivity of the $W^\pm W^\pm$ scattering process to the coefficient $f_{T,1}/\Lambda^4$, measured in terms of the expected 5σ discovery reach and 95% CL limit increases by an impressive factor of 100 between 14 and 100 TeV, assuming the same integrated luminosity and exactly the same data analysis. By comparison, sensitivities to anomalous coefficients studied in the WZ and ZZ processes were compared at beam energies of 14 and 33 TeV and revealed improvement by merely a factor 1.2-1.8, depending on the analysis. This already gives a glimpse of the superb physics capabilities of the FCC, but does not answer the question of being able to identify the scenario.

A yet different story is the one with triple gauge couplings WWZ and $WW\gamma$. They affect $W_L W_L$, $W_T W_T$ and $W_T W_L$ pairs in different ways, as well as they affect both VBS and non-VBS processes. Since the VBS sample is a fraction of the non-VBS sample in absolute counts and because the kinematics of their respective final states partly overlap, VBS signals can only be studied on their own right once stringent criteria are predefined to suppress the unavoidable non-VBS contamination to a negligible level. For a correct evaluation of pure VBS signals, the non-VBS contribution must be negligible not only

in the SM scenario, but in any arbitrary scenario with anomalous couplings within their present experimental bounds. In case of $W^\pm W^\pm$ this can be effectively achieved by tightening the lepton back-to-back requirement to $\Delta\varphi_{ll} > 2.8$. This is because of two classes of non-scattering processes. One involves a $u - u$ quark collision with one of the quarks interacting after W^+ emission, the other is $u - \bar{d}$ annihilation. They are negligible in the SM, but become part of the non-VBS signal with anomalous WWZ and $WW\gamma$ couplings. Luckily, tightening $\Delta\varphi_{ll}$ does not significantly reduce the VBS signal at 100 TeV. For the other VV scattering processes, the large number of diagrams potentially contributing to the non-VBS signal may prove this much more complicated.

In any BSM scenario, new physics ultimately ends up enhancing the VV scattering cross section at a sufficiently high invariant mass. It remains true regardless of whether or not this cross section gets depleted at some intermediate scale, depending on the signs of the anomalous coefficients and therefore the pattern of interference between the individual scattering diagrams. It is also true regardless of whether it is $W_L W_L$ or $W_T W_X$ the primary source of signal. It should be noted that even if $W_T W_X$ contribute to the VBS signal, it does not make $W_L W_L$ any less important. Quite the contrary, the \mathcal{O}_W operator produces a similar amount of VBS signal for both helicity combinations, in clear contrast with \mathcal{O}_{WWW} on one side and \mathcal{O}_B , $\mathcal{O}_{\Phi d}$, $\mathcal{O}_{\Phi W}$ and the relevant dimension-8 operators on the other. It makes the ability to separate the two samples experimentally a bonus of special interest.

As was the case for the LHC, use of the R_{p_T} variable, the way we did just above in the scenario with modified Higgs to gauge couplings, is effective for any BSM scenario that enhances high WW invariant masses. This is because of the still holding strong correlation between M_{WW} and the lepton transverse momenta. It is also always automatically more effective for $W_L W_L$ signals than for $W_T W_X$ signals because of the jet transverse momenta in its denominator. However, if we allow both $W_L W_L$ and $W_T W_X$ signals, there is no way to separate these by looking at R_{p_T} alone without a priori knowledge of the physics scenario. A study of respective signals associated to, e.g., the \mathcal{O}_W operator clearly shows this interpretative ambiguity: the entire shape of the R_{p_T} distribution for a pure $W_L W_L$ sample with, say, $C_W/\Lambda^2 = -10/\text{TeV}^2$ almost exactly coincides with that of a pure $W_T W_X$ sample with $C_W/\Lambda^2 = -20/\text{TeV}^2$ (see Fig. 7.6). The ambiguity is solved by looking at the individual jet transverse momenta, and chiefly the p_T of the leading jet. The separation of the two helicity sub-samples is much better for 100 TeV than for 14 TeV. The maximum of the leading jet p_T distribution is clearly shifted with respect to the SM to lower values for $W_L W_L$ signals and to higher values for $W_T W_X$ signals. A shape analysis of the leading jet p_T distribution, measured from the events that pass the standard R_{p_T} cut, should suffice to determine the helicity composition to a satisfactory accuracy, enough to resolve whether the signal is indeed $W_L W_L$ -driven (via \mathcal{O}_B , pure HWW or $WWWW$) or $W_T W_X$ -driven (via \mathcal{O}_{WWW}) or mixed (via \mathcal{O}_W or any suitable combination). A peak at around 100 GeV of the measured excess over the SM (itself having a median around 200 GeV) is an unequivocal sign of $W_L W_L$. A broader peak at around 300 GeV signals $W_T W_X$. The signal peak positions link directly to helicity and hardly vary with the actual physics scenario or specific values of the anomalous coefficients. The fact that

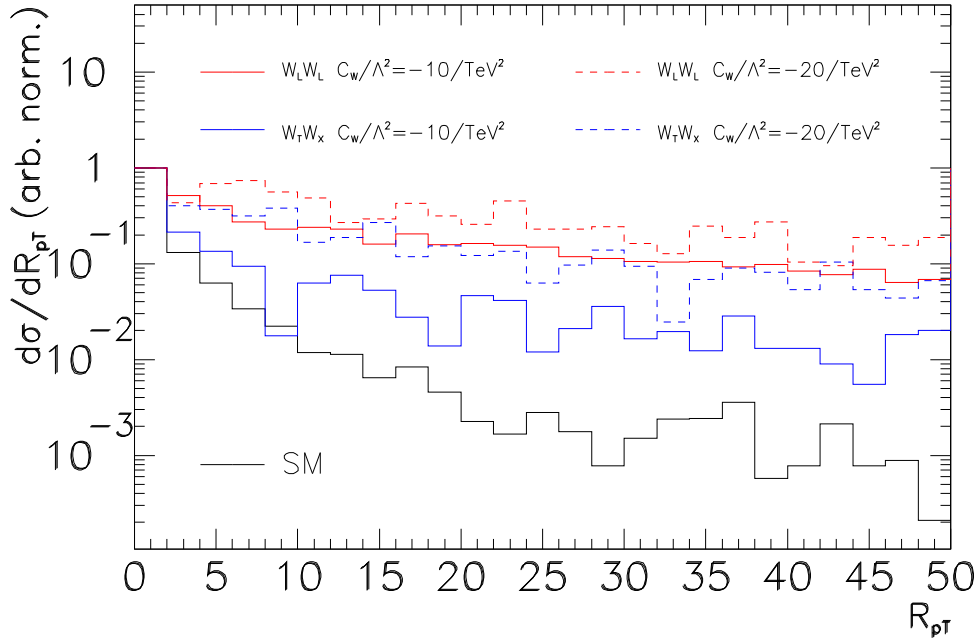


Figure 7.6: The shapes of R_{p_T} distributions resulting from the $pp \rightarrow jjW^+W^+$ process at 100 TeV with leptonic W^+ decay ($l = e, \mu$). Shown are: the Standard Model scenario (black histo, all helicity combinations summed up), the $C_W/\Lambda^2 = -10/\text{TeV}^2$ additive signals (blue solid histo - $W_T W_X$ pairs, red solid histo - $W_L W_L$ pairs) and the $C_W/\Lambda^2 = -20/\text{TeV}^2$ additive signals (blue dashed histo - $W_T W_X$ pairs, red dashed histo - $W_L W_L$ pairs). For the sake of a convenient comparison, each distribution was individually scaled to the contents of its first bin, $R_{p_T} < 2$. VBF topological cuts (see text) and a cut on $\Delta\varphi_U > 2.8$ were applied. Signals were evaluated without applying any Λ cutoff. Results of MadGraph simulations, all assumptions and conditions as in Fig. 7.4.

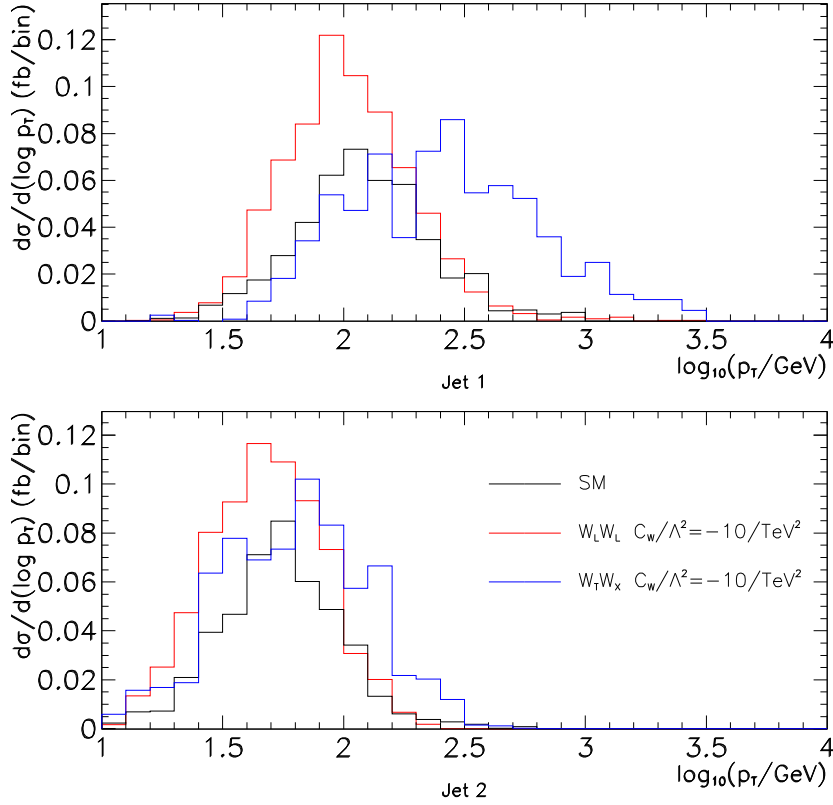


Figure 7.7: Transverse momentum distributions of the leading and subleading jets in the $pp \rightarrow jjW^+W^+$ process at 100 TeV with leptonic W^+ decay ($l = e, \mu$). Shown are the Standard Model scenario (black histo, all helicity combinations summed up), and the additive signals of $C_W/\Lambda^2 = -10/\text{TeV}^2$ (blue histo - $W_T W_X$ pairs, red histo - $W_L W_L$ pairs). Applied were all signal selection criteria discussed in the text. Results of MadGraph simulations, all assumptions and conditions as in Fig. 7.6.

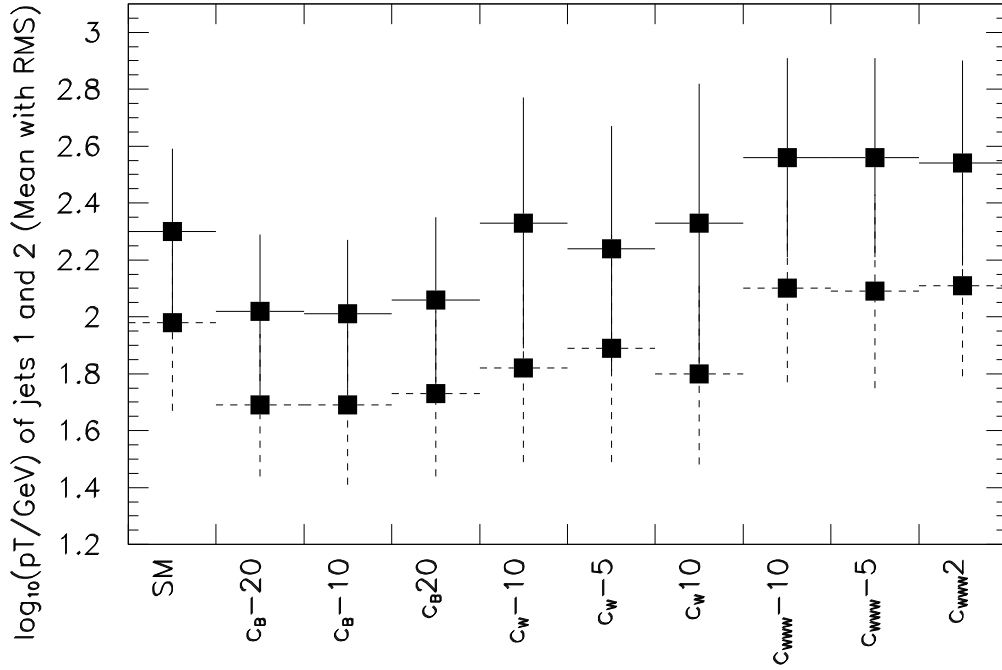


Figure 7.8: Mean values and RMS of the individual transverse momenta of the two jets in the process $pp \rightarrow jjW^+W^+$ at 100 TeV, with leptonic W^+ decay ($l = e, \mu$) in different physics scenarios. Solid lines represent the leading jet and dashed lines represent the sub-leading jet. Vertical error bars represent the RMS. Each bin on the horizontal axis represents a physics scenario; from left to right: the Standard Model and BSM signals for $c_B/\Lambda^2 = -20/\text{TeV}^2$, $c_B/\Lambda^2 = -10/\text{TeV}^2$, $c_B/\Lambda^2 = 10/\text{TeV}^2$, $c_W/\Lambda^2 = -10/\text{TeV}^2$, $c_W/\Lambda^2 = -5/\text{TeV}^2$, $c_W/\Lambda^2 = 10/\text{TeV}^2$, $c_{WWW}/\Lambda^2 = -10/\text{TeV}^2$, $c_{WWW}/\Lambda^2 = -5/\text{TeV}^2$ and $c_{WWW}/\Lambda^2 = 2/\text{TeV}^2$. Applied were VBF selection criteria, including $\Delta\varphi_{ll} > 2.8$. Results of MadGraph 5 simulations, all conditions and assumptions as for Fig. 7.6.

the peak position slightly shifts for different values of c_W/Λ^2 (see Fig. 7.8), is because the proportion of the selected W_LW_L and W_TW_X pairs changes likewise. The RMS of the $\log_{10}(p_T^{j1})$ distributions are close to 0.3 and 0.4 for W_LW_L and W_TW_X , respectively, making a clear distinction possible whenever signal itself becomes statistically significant. Larger widths are already a clear indication that signal is in fact a mixture of W_LW_L and W_TW_X , with two distinct sub-samples vaguely emerging from the spectrum. The sub-leading jet is a less powerful discriminator on its own because it receives a substantial W_L contribution from W_TW_L pairs. Nonetheless it can be used as an additional consistency cross check. Once combined the information from the two jets, it turns out that as few as 10 events suffice to distinguish a pure W_LW_L from a pure W_TW_X signal at the 5σ level. In other words, with an isolated signal sample of N events, the helicity composition can be deduced to a precision of $\sim 1/\sqrt{2.5 N}$. That makes, e.g., for $HWW = 0.95$ and no other anomalous couplings (260 signal events in 1000 fb^{-1}) a 4% measurement.

In a given physics scenario, W_LW_L and W_TW_X signals do not differ significantly in terms of the outgoing lepton kinematics. Somewhat different widths of the respective p_T distributions (larger for W_TW_X than for W_LW_L) are expected as a simple consequence of the angular distributions in W decay. These differences alone may however easily prove not significant enough or too entangled with other effects to be of much practical use unless we know beforehand the helicity composition of the selected sample from other sources. But once we have independently established the helicity composition, leptons in the final state help resolve the remaining ambiguities concerning the physical scenario and the sign of the anomalous coefficients. The W_LW_L -driven scenarios clearly differ in the lepton transverse momenta and/or invariant mass distributions. For example, the median of the leading lepton p_T distribution is around 600 GeV for a purely HWW -driven signal, but may become larger with new physics manifesting itself in modified $WWWW$ or WWZ couplings. These numbers are a direct consequence of the s -dependences of the relevant amplitudes plus a common phase space factor, and so they have also very little sensitivity to the actual values of the parameters in question. It is the total signal rate that determines the coefficient values. The lepton-lepton invariant mass also unambiguously fixes the sign of the relevant anomalous parameter in case an ambiguity exists on measuring the signal rate alone. Because of the sign of the interference terms between the three basic graphs contributing to $W^+W^+ \rightarrow W^+W^+$, any of the following scenarios: $g_{HWW} < 1$, $C_W < 0$ and $C_B < 0$, produces a steady enhancement in the M_{ll} spectrum, ultimately suppressed by phase space. By contrast, $g_{HWW} > 1$, $C_W > 0$ and $C_B > 0$ are bound to produce a moderate depletion at intermediate masses, followed by a rise at larger values, eventually catching up asymptotically with the former. For C_{WWW} , the sign may be more difficult to determine. In any case, there is a strong correspondence between invariant mass distributions and transverse momenta distributions of the outgoing leptons and detailed simulation work will ultimately have to tell which approach is preferable.

There are however also ambiguities that would take more effort to resolve. For example, the signal of $C_B < 0$ coincides with that of scaling the Higgs to WW coupling by an appropriately chosen constant, although the former does not modify the HWW coupling at all. Such ambiguities may be ultimately solvable only in the context of combining data from different processes.

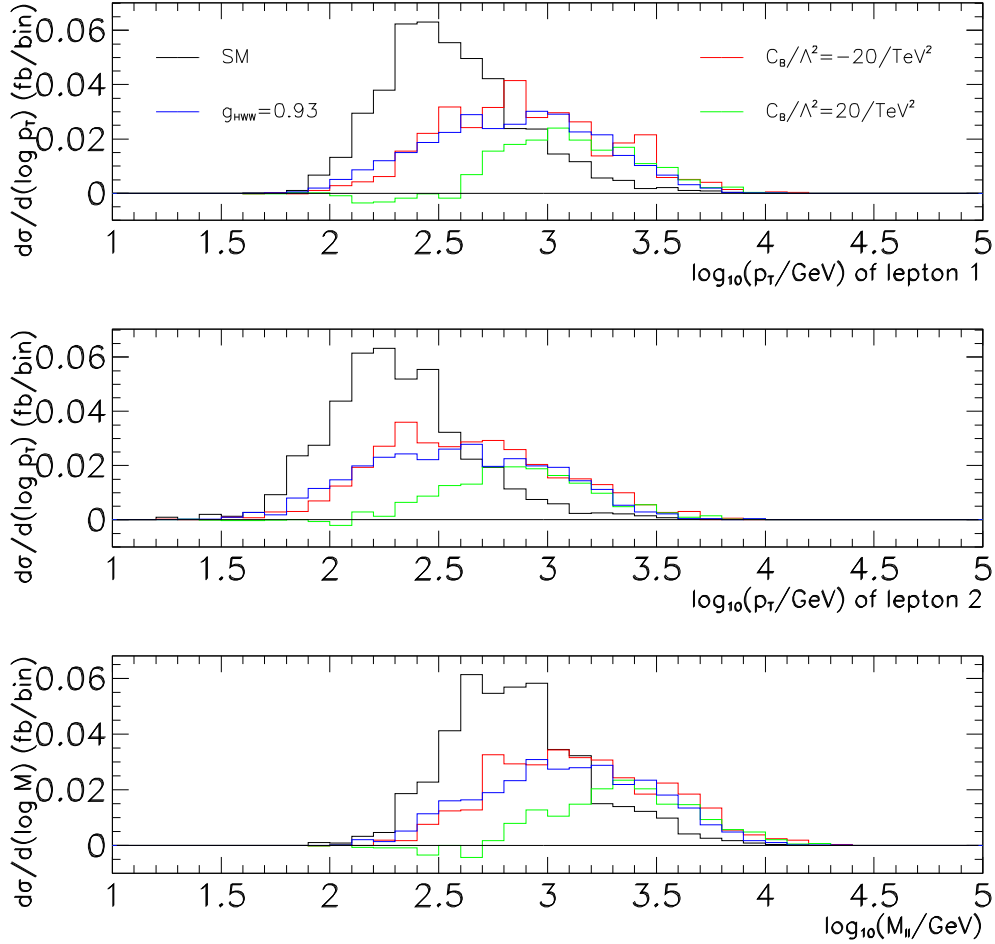


Figure 7.9: Transverse momentum distributions of the leading and subleading leptons (upper and middle plots) and lepton-lepton invariant mass distribution (lower plot) in the $pp \rightarrow jjW^+W^+$ process at 100 TeV with leptonic W^+ decay ($l = e, \mu$). Shown are the Standard Model scenario (black histo, all helicity combinations summed up), and the additive W_LW_L signals of $C_B/\Lambda^2 = -20/\text{TeV}^2$ (red histo), $C_B/\Lambda^2 = 20/\text{TeV}^2$ (green histo) and $g_{HWW} = 0.93$ (blue histo). Applied were all signal selection criteria discussed in the text. Results of MadGraph simulations, all assumptions and conditions as in Fig. 7.6.

Another source of complication in this type of analyses arises from the unknown scale of new physics, Λ . In the Effective Field Theory approach, values of the anomalous coefficients are intimately connected to the value of Λ . Theoretical predictions depend only on the ratio c/Λ^2 or c/Λ^4 , but one cannot separate the coefficient from the energy. However, if the data fit the theoretical curve in the entire kinematic phase space covered by the experiment, then Λ must be at least equal to the WW invariant mass of the highest data point. Otherwise, data would indicate the appropriate cutoff value. On the other end, the value of Λ must be lower than a calculable upper limit defined by the unitarity condition. Hence one could at least bound Λ from above and below. Nevertheless, for practical purposes the unitarity condition may be completely irrelevant in terms of evaluating the expected sensitivity limits, because the FCC sensitivity reaches to anomalous coefficient values that do not lead to unitarity violation within the available energy scale [116].

All in all, we have emphasized the primary importance of studying same-sign WW interactions at the FCC. Moreover, it is the full event kinematics studied from a clean W^+W^+ scattering sample with leptonic W decay, and most of all the transverse momenta of all four final state particles, that carry the bulk of the necessary information in order to disentangle the underlying physics scenario and correctly interpret the results.

Chapter 8

Summary

The Higgs boson is an empirical fact. Moreover, based on all the data collected at Run 1 of the LHC, it looks by all means consistent with the Standard Model one. In particular, Higgs couplings to vector bosons are consistent with SM ones to an accuracy of roughly $\sim 20\%$. No other hints of physics BSM have been observed so far, either. This does not preclude that the dynamics of electroweak symmetry breaking may still be partially strong. Whether or not we observe Higgs couplings deviate from their SM predictions in future measurements, only direct observation of VV scattering at high energies will ultimately tell if this is indeed the case.

The full phenomenology of VV scattering at high energy depends on the Higgs mass, Higgs to gauge couplings, gauge boson triple couplings and gauge boson quartic couplings. With the present experimental bounds on these inputs, only the Higgs mass can be considered definitely fixed for VBS studies. Effects from non-SM Higgs couplings and triple couplings can still be observed at the LHC with $\sqrt{s} = 13$ TeV with hard work and some luck and consistency checks can be done with new, more precise measurements of all the relevant quantities that will come directly from Higgs physics on one side and total di-boson production on the other. Agreement between these three classes of measurements can be translated into the first real experimental limits on anomalous quartic gauge couplings. Alternatively, disagreement may signal existence of the latter. In the event of absence of direct observation of new resonances, the best process to study VBS-related physics is same-sign WW scattering in the purely leptonic decay mode, but with further improvements the semi-leptonic decay modes may prove equally important. However, with 300 fb^{-1} VBS processes on their own offer little possibilities to interpret the results in a standalone way, i.e., without relying on concurrent measurements. This is because the BSM effects are bound to be tiny and statistics too low to carry more precise studies. The 300 fb^{-1} program is likely to end up as a Standard Model measurement, of a similar philosophy as the ones already carried by ATLAS and CMS from 8 TeV data. However, the focus for the High Luminosity LHC program should be BSM and it is time now to plan an analysis strategy different from a Standard Model analysis. The High Luminosity program has chances to provide enough data for at least some physics scenarios be distinguished from others based on studies of VBS processes alone. Among other things, this can be done by applying novel techniques to separate different helicity combinations in the selected samples of VV pairs that we advocate in this work. In particular, should an excess over SM predictions be observed, it should be possible to tell whether this ex-

cess is related to the mechanism of electroweak symmetry breaking or to other physics. Improvement in the sensitivity to new physics, and especially to those effects that affect mainly $V_L V_L$ pairs, should be sought at low transverse momenta and large pseudorapidities of the tagging jets. This should be taken into account in planning future machine and detector upgrade activities for the HL-LHC phase. Not least, even in the absence of new physics, application of analysis techniques that fully exploit vector boson helicities will result in better exclusion limits, at least for those scenarios that do not modify the dominant transverse polarizations.

A qualitative improvement in sensitivity to BSM effects in VBS processes can only be achieved via further increase in beam energy. The FCC with its $\sqrt{s} = 100$ TeV has all the potential to observe many BSM effects in VV scattering and to identify the physical sources of these effects. Consistency of VBS measurements with Higgs physics, diboson production and triboson production measurements at the FCC will provide an ultimate closure test of the Standard Model or the theory that will replace it.

Chapter 9

Acknowledgments

The list of people I feel indebted to is long and, as always, subjective. But there are a few names I definitely must mention here.

First and foremost, I thank Profs. Stefan Pokorski, Jan Kalinowski and Sławek Tkaczyk for their long collaboration, countless meetings and discussions throughout the years, always inspiring and enlightening. The complicated interplay between theory and experiment, the conceptual feedback I have received on the theory side (SP, JK) and the support on the practical, experimental side (ST), was a very stimulating experience and crucial to complete this work. To Jan and Sławek I am also grateful for kindly agreeing to review parts of this work before publication and sending me their valuable comments. Any remaining mistakes, typos and other shortcomings that no doubt can still be found, are of course my fault.

I thank my CMS colleagues from the NCBJ and the University of Warsaw for their tolerance and patience to put up with me during all this time, as well as for all their intellectual feedback. In particular, I am indebted to Prof. Krzysztof Doroba for his pioneering role in starting up the *WW* related activities within the Warsaw CMS group, and to Prof. Jan Królikowski, Michał Bluj, Artur Kalinowski, Marcin Konecki, Piotr Zalewski and many others for sharing their wisdom and experience in our group meetings and informal discussions.

And I thank Mayda Velasco, my former boss at Northwestern, for it is there that my adventure with CMS has started.

Bibliography

- [1] ATLAS and CMS Collaborations, “*Birth of a Higgs boson*”, CERN Courier 53N4 (2013) 21,
CMS Collaboration, “*Observation of a new boson at a mass of 125 GeV with the CMS experiment at the LHC*”, Phys. Lett. B716 (2012) 30 [arXiv:1207.7235 [hep-ex]],
ATLAS Collaboration, “*Observation of a new particle in the search for the Standard Model Higgs boson with the ATLAS detector at the LHC*”, Phys. Lett. B716 (2012) 1 [arXiv:1207.7214 [hep-ex]],
“*A particle consistent with the Higgs Boson observed with the ATLAS Detector at the Large Hadron Collider*”, Science 338 (2012) 1576.
- [2] P. W. Higgs, “*Broken symmetries, massless particles and gauge fields*”, Phys. Lett. 12 (1964) 132,
“*Broken Symmetries and the Masses of Gauge Bosons*”, Phys. Rev. Lett. 13 (1964) 508.
- [3] F. Englert, R. Brout, “*Broken Symmetry and the Mass of Gauge Vector Mesons*”, Phys. Rev. Lett. 13 (1964) 321.
- [4] G. S. Guralnik, C. R. Hagen, T. W. B. Kibble, “*Global Conservation Laws and Massless Particles*”, Phys. Rev. Lett. 13 (1964) 585.
- [5] S.-Z. Wang, Q. Wang, “*Electroweak Chiral Lagrangian for Neutral Higgs Boson*”, Chin. Phys. Lett. 25, No.6 (2008) 1984,
J. R. Peláez, “*Strong WW Scattering, Chiral Lagrangians, Unitarity and Resonances*”, arXiv:hep-ph/9608371,
“*Strong WW scattering and resonances at LHC*”, arXiv:hep-ph/9705301,
T. Appelquist, G.-H. Wu, “*Electroweak chiral Lagrangian and new precision measurements*”, Phys. Rev. D48 (1993) 3235,
A. A. New, “*WW scattering using Electroweak Chiral Lagrangian*”, MPhil Thesis, University of Manchester, September 2001.
- [6] M. J. Herrero, E. R. Morales, “*The Electroweak Chiral Lagrangian as an Effective Field Theory of the Standard Model with a Heavy Higgs*”, arXiv:hep-ph/9412317.
- [7] S. Weinberg, “*A model of leptons*”, Phys. Rev. Lett. 19 (1967) 1264. A nice and comprehensive historical account of the origins of the Standard Model can be found in: F. Close, “*The Infinity Puzzle: Quantum Field Theory and the Hunt for an Orderly Universe*”, Basic Books, 2011.

- [8] T. W. B. Kibble, “*Englert-Brout-Higgs-Guralnik-Hagen-Kibble mechanism*”, *Scholarpedia*, 4(1):6441.
- [9] J. Horejsi, “*Introduction to Electroweak Unification*”, World Scientific, 1994.
- [10] B. W. Lee, C. Quigg, H. B. Thacker, “*Weak interactions at very high energies: The role of the Higgs-boson mass*”, *Phys. Rev. D* 16, No.5 (1977) 1519,
“*Strength of Weak Interactions at Very High Energies and the Higgs Boson Masss*”, *Phys. Rev. Lett.* 38, No.16 (1977) 883.
- [11] The most up-to-date Higgs related results from CMS are always available on: <https://twiki.cern.ch/twiki/bin/view/CMSPublic/PhysicsResultsHIG>.
- [12] The most up-to-date Higgs related results from ATLAS are always available on: <https://twiki.cern.ch/twiki/bin/view/AtlasPublic/HiggsPublicResults>.
- [13] CMS Collaboration, “*Precise determination of the mass of the Higgs boson and studies of the compatibility of its couplings with the standard model*”, CMS Public Analysis Summary, CMS-PAS-HIG-14-009,
“*Measurement of the properties of a Higgs boson in the four-lepton final state*”, *Phys. Rev. D* 89 (2014) 092007 [arXiv:1312.5353 [hep-ex]],
“*Measurement of Higgs boson production and properties in the WW decay channel with leptonic final states*”, *JHEP* 1401 (2014) 096 [arXiv:1312.1129 [hep-ex]],
“*Observation of the diphoton decay of the Higgs boson and measurement of its properties*”, arXiv:1407.0558 [hep-ex].
- [14] ATLAS Collaboration, “*Observation and measurement of Higgs boson decays to WW* with ATLAS at the LHC*”, ATLAS-CONF-2014-060,
“*Measurement of Higgs boson production in the diphoton decay channel in pp collisions at center-of-mass energies of 7 and 8 TeV with the ATLAS detector*”, arXiv:1408.7084 [hep-ex],
“*Measurements of Higgs boson production and couplings in the four-lepton channel in pp collisions at center-of-mass energies of 7 and 8 TeV with the ATLAS detector*”, arXiv:1408.5191 [hep-ex],
“*Measurement of the Higgs boson mass from the $H \rightarrow \gamma\gamma$ and $H \rightarrow ZZ^* \rightarrow 4l$ channels with the ATLAS detector using 25 fb^{-1} of pp collision data*”, *Phys. Rev. D* 90 (2014) 052004 [arXiv:1406.3827 [hep-ex]],
“*Measurements of Higgs boson production and couplings in diboson final states with the ATLAS detector at the LHC*”, *Phys. Lett. B* 726 (2013) 88 [arXiv:1307.1427 [hep-ex]].
- [15] ATLAS Collaboration, “*Evidence for Higgs boson Yukawa couplings in the $H \rightarrow \tau\tau$ decay mode with the ATLAS detector*”, ATLAS-CONF-2014-061,
“*Search for the Standard Model Higgs boson in the H to $\tau^+\tau^-$ decay mode in $\sqrt{s} = 7 \text{ TeV}$ pp collisions with ATLAS*”, *JHEP* 1209 (2012) 070 [arXiv:1206.5971 [hep-ex]].
- [16] CMS Collaboration, “*Evidence for the 125 GeV Higgs boson decaying to a pair of τ leptons*”, *JHEP* 05 (2014) 104 [arXiv:1401.5041 [hep-ex]].

- “Search for neutral Higgs bosons decaying to τ pairs in pp collisions at $\sqrt{s} = 7$ TeV”, Phys. Lett. B713 (2012) 68 [arXiv:1202.4083 [hep-ex]].
- [17] CMS Collaboration, “Search for the standard model Higgs boson produced in association with a W or a Z boson and decaying to bottom quarks”, Phys. Rev. D89 (2014) 012003 [arXiv:1310.3687 [hep-ex]],
“Search for a Higgs boson decaying into a b -quark pair and produced in association with b quarks in proton-proton collisions at 7 TeV”, Phys. Lett. B722 (2013) 207 [arXiv:1302.2892 [hep-ex]],
“Search for the standard model Higgs boson decaying to bottom quarks in pp collisions at $\sqrt{s} = 7$ TeV”, Phys. Lett. B710 (2012) 284 [arXiv:1202.4195 [hep-ex]],
ATLAS Collaboration, “Search for the bb decay of the Standard Model Higgs boson in associated (W/Z) H production with the ATLAS detector”, arXiv:1409.6212 [hep-ex],
“Search for the Standard Model Higgs boson decay to $\mu^+\mu^-$ with the ATLAS detector”, Phys. Lett. B738 (2014) 68-86 [arXiv:1406.7663 [hep-ex]],
“Search for the Standard Model Higgs boson produced in association with a vector boson and decaying to a b -quark pair with the ATLAS detector”, Phys. Lett. B718 (2012) 369 [arXiv:1207.0210 [hep-ex]].
- [18] CMS Collaboration, “Evidence for the direct decay of the 125 GeV Higgs boson to fermions”, arXiv:1401.6527 [hep-ex].
- [19] ATLAS Collaboration, “Search for Higgs boson decays to a photon and a Z boson in pp collisions at $\sqrt{s} = 7$ and 8 TeV with the ATLAS detector”, Phys. Lett. B732 (2014) 8 [arXiv:1402.3051 [hep-ex]],
CMS Collaboration, “Search for a Higgs boson decaying into a Z and a photon in pp collisions at $\sqrt{s} = 7$ and 8 TeV”, Phys. Lett. B726 (2013) 587-609 [arXiv:1307.5515 [hep-ex]].
- [20] F. Caola, K. Melnikov, “Constraining the Higgs boson width with ZZ production at the LHC”, Phys. Rev. D88 (2013) 054024 [arXiv:1307.4935],
N. Kauer, G. Passarino, “Inadequacy of zero-width approximation for a light Higgs boson signal”, JHEP 08 (2012) 116 [arXiv:1206.4803],
N. Kauer, “Inadequacy of zero-width approximation for a light Higgs boson signal”, Mod. Phys. Lett. A28 (2013) 1330015 [arXiv:1305.2092].
- [21] CMS Collaboration, “Constraints on the Higgs boson width from off-shell production and decay to Z -boson pairs”, arXiv:1405.3455 [hep-ex].
- [22] Y. Gao, A. V. Gritsan, Z. Guo, K. Melnikov, M. Schulze, N. V. Tran, “Spin determination of single-produced resonances at hadron colliders”, Phys. Rev. D81 (2010) 075022.
- [23] CMS Collaboration, “Constraints on the spin-parity and anomalous HVV interactions of the Higgs boson from the CMS experiment”, CMS Public Analysis Summary, CMS-PAS-HIG-14-018,
“Constraints on anomalous HVV interactions using $H \rightarrow 4l$ decays”, CMS Public Analysis Summary, CMS-PAS-HIG-14-014,

- “Study of the Mass and Spin-Parity of the Higgs Boson Candidate Via Its Decays to Z Boson Pairs”*, Phys. Rev. Lett. 110 (2013) 081803 [arXiv:1212.6639 [hep-ex]].
- [24] ATLAS Collaboration, *“Evidence for the spin-0 nature of the Higgs boson using ATLAS data”*, Phys. Lett. B726 (2013) 120 [arXiv:1307.1432 [hep-ex]].
- [25] CMS Collaboration, *“Search for $H \rightarrow bb$ in association with single top quarks as a test of Higgs boson couplings”*, CMS Public Analysis Summary, CMS-PAS-HIG-14-015,
“Search for associated production of a single top quark and a Higgs boson in events where the Higgs boson decays to two photons at $\sqrt{s} = 8$ TeV”, CMS Public Analysis Summary, CMS-PAS-HIG-14-001,
 ATLAS Collaboration, *“Search for $H \rightarrow \gamma\gamma$ produced in association with top quarks and constraints on the Yukawa coupling between the top quark and the Higgs boson using data taken at 7 TeV and 8 TeV with the ATLAS detector”*, arXiv:1409.3122 [hep-ex].
- [26] CMS Collaboration, *“Search for the Standard Model Higgs boson in the $H \rightarrow WW \rightarrow lvjj$ decay channel in pp collisions at the LHC”*, CMS Public Analysis Summary, CMS-PAS-HIG-13-027,
“Search for a standard-model-like Higgs boson with a mass in the range 145 to 1000 GeV at the LHC”, Eur. Phys.J. C73 (2013) 2469 [arXiv:1304.0213 [hep-ex]],
 ATLAS Collaboration, *“Search for a standard model Higgs boson in the mass range 200-600 GeV in the $H \rightarrow ZZ \rightarrow l^+l^-q\bar{q}$ decay channel with the ATLAS detector”*, Phys. Lett. B717 (2012) 70 [arXiv:1206.2443 [hep-ex]],
“Search for a heavy Standard Model Higgs boson in the channel $H \rightarrow ZZ \rightarrow llq\bar{q}$ using the ATLAS detector”, Phys. Lett. B707 (2012) 27 [arXiv:1108.5064 [hep-ex]].
- [27] CMS Collaboration, *“Search for new resonances in the diphoton final state in the range between 150 and 850 GeV in pp collisions at $\sqrt{s} = 8$ TeV”*, CMS Public Analysis Summary, CMS-PAS-HIG-14-006,
 ATLAS Collaboration, *“Search for Scalar Diphoton Resonances in the Mass Range 65-600 GeV with the ATLAS Detector in pp Collision Data at $\sqrt{s} = 8$ TeV”*, Phys. Rev. Lett. 113 (2014) 171801 [arXiv:1407.6583 [hep-ex]].
- [28] CMS Collaboration, *“Search for neutral MSSM Higgs bosons decaying to a pair of tau leptons in pp collisions”*, arXiv:1408.3316 [hep-ex],
“Search for Neutral MSSM Higgs Bosons Decaying to Tau Pairs in pp Collisions at $\sqrt{s} = 7$ TeV”, Phys. Rev. Lett. 106 (2011) 231801 [arXiv:1104.1619 [hep-ex]],
 ATLAS Collaboration, *“Search for neutral Higgs bosons of the Minimal Supersymmetric Standard Model in pp collisions at $\sqrt{s} = 8$ TeV with the ATLAS detector”*, arXiv:1409.6064 [hep-ex],
“Search for the neutral Higgs bosons of the Minimal Supersymmetric Standard Model in pp collisions at $\sqrt{s} = 7$ TeV with the ATLAS detector”, JHEP 1302 (2013) 095 [arXiv:1211.6956 [hep-ex]],
“Search for neutral MSSM Higgs bosons decaying to $\tau^+\tau^-$ pairs in proton-proton collisions at $\sqrt{s} = 7$ TeV with the ATLAS detector”, Phys. Lett. B705 (2011) 174 [arXiv:1107.5003 [hep-ex]].

- [29] CMS Collaboration, “*Search for charged Higgs bosons with the $H^+ \rightarrow \tau\nu$ decay channel in the fully hadronic final state at $\sqrt{s} = 8$ TeV*”, CMS Public Analysis Summary, CMS-PAS-HIG-14-020,
“*Search for a light charged Higgs boson in $H^+ \rightarrow c\bar{s}$ channel at CMS at $\sqrt{s} = 8$ TeV collisions*”, CMS Public Analysis Summary, CMS-PAS-HIG-13-035,
“*Search for a light charged Higgs boson in top quark decays in pp collisions at $\sqrt{s} = 7$ TeV*”, JHEP 1207 (2012) 143 [arXiv:1205.5736 [hep-ex]],
ATLAS Collaboration, “*Search for a light charged Higgs boson in the decay channel $H^+ \rightarrow c\bar{s}$ in $t\bar{t}$ events using pp collisions at $\sqrt{s} = 7$ TeV with the ATLAS detector*”, Eur. Phys. J. C73 (2013) 2465 [arXiv:1302.3694 [hep-ex]],
“*Search for charged Higgs bosons decaying via $H^+ \rightarrow \tau\nu$ in top quark pair events using pp collision data at $\sqrt{s} = 7$ TeV with the ATLAS detector*”, JHEP 1206 (2012) 039 [arXiv:1204.2760 [hep-ex]].
- [30] CMS Collaboration, “*Search for a non-standard-model Higgs boson decaying to a pair of new light bosons in four-muon final states*”, Phys. Lett. B726 (2013) 564 [arXiv:1210.7619 [hep-ex]].
- [31] CMS Collaboration, “*Search for a light pseudoscalar Higgs boson in the dimuon decay channel in pp collisions at $\sqrt{s} = 7$ TeV*”, Phys. Rev. Lett. 109 (2012) 121801 [arXiv:1206.6326 [hep-ex]].
- [32] CMS Collaboration, “*Searches for Higgs bosons in pp collisions at $\sqrt{s} = 7$ and 8 TeV in the context of four-generation and fermiophobic models*”, Phys. Lett. B725 (2013) 36 [arXiv:1302.1764 [hep-ex]],
“*Search for a fermiophobic Higgs boson in pp collisions at $\sqrt{s} = 7$ TeV*”, JHEP 1209 (2012) 111 [arXiv:1207.1130 [hep-ex]],
ATLAS Collaboration, “*Search for a fermiophobic Higgs boson in the diphoton decay channel with the ATLAS detector*”, Eur. Phys. J. C72 (2012) 2157 [arXiv:1205.0701 [hep-ex]].
- [33] CMS Collaboration, “*Search for a heavy charged Higgs boson in proton-proton collisions at $\sqrt{s} = 8$ TeV with the CMS detector*”, CMS Public Analysis Summary, CMS-PAS-HIG-13-026,
“*Searches for heavy scalar and pseudoscalar Higgs bosons and for flavor-violating decays of the top quark into a Higgs boson in pp collisions at $\sqrt{s} = 8$ TeV*”, arXiv:1410.2751 [hep-ex],
“*Search for lepton flavor violating decays of the Higgs boson*”, CMS Public Analysis Summary, CMS-PAS-HIG-14-005,
“*Search for invisible decays of Higgs bosons in the vector boson fusion and associated ZH production modes*”, arXiv:1404.1344 [hep-ex],
“*A search for a doubly-charged Higgs boson in pp collisions at $\sqrt{s} = 7$ TeV*”, Eur. Phys. J. C72 (2012) 2189 [arXiv:1207.2666 [hep-ex]],
ATLAS Collaboration, “*Search for charged Higgs bosons through the violation of lepton universality in $t\bar{t}$ events using pp collision data at $\sqrt{s} = 7$ TeV with the ATLAS experiment*”, JHEP 1303 (2013) 076 [arXiv:1212.3572 [hep-ex]],
“*Search for a light Higgs boson decaying to long-lived weakly-interacting particles in proton-proton collisions at $\sqrt{s} = 7$ TeV with the ATLAS detector*”,

- Phys. Rev. Lett. 108 (2012) 251801 [arXiv:1203.1303 [hep-ex]],
“Search for doubly-charged Higgs bosons in like-sign dilepton final states at $\sqrt{s} = 7$ TeV with the ATLAS detector”, Eur. Phys. J. C72 (2012) 2244 [arXiv:1210.5070 [hep-ex]],
“Search for Invisible Decays of a Higgs Boson Produced in Association with a Z Boson in ATLAS”, arXiv:1402.3244 [hep-ex].
- [34] CMS SUSY physics results are available on:
<https://twiki.cern.ch/twiki/bin/view/CMSPublic/PhysicsResultsSUS>.
- [35] CMS non-SUSY BSM searches are summarized on:
<https://twiki.cern.ch/twiki/bin/view/CMSPublic/PhysicsResultsEXO>.
- [36] The most up-to-date results on electroweak physics from CMS are always available on:
<https://twiki.cern.ch/twiki/bin/view/CMSPublic/PhysicsResultsSMP>. The most up to date results on electroweak physics from ATLAS are always available on:
<https://twiki.cern.ch/twiki/bin/view/AtlasPublic/StandardModelPublicResults>.
- [37] CMS Collaboration, “A search for $WW\gamma$ and $WZ\gamma$ production and constraints on anomalous quartic gauge couplings in pp collisions at $\sqrt{s} = 8$ TeV”, arXiv:1404.4619 [hep-ex].
- [38] CMS Collaboration, “Measurement of the W^+W^- Cross section in pp Collisions at $\sqrt{s} = 7$ TeV and Limits on Anomalous $WW\gamma$ and WWZ couplings”, Eur. Phys. J. C73 (2013) 2610 [arXiv:1306.1126 [hep-ex]].
- [39] ATLAS Collaboration, “Measurement of W^+W^- production in pp collisions at $\sqrt{s} = 7$ TeV with the ATLAS detector and limits on anomalous WWZ and $WW\gamma$ couplings”, Phys. Rev. D87 (2013) 112001 [arXiv:1210.2979 [hep-ex]].
- [40] CMS Collaboration, “Measurement of the ZZ production cross section and search for anomalous couplings in $2l2l'$ final states in pp collisions at $\sqrt{s} = 7$ TeV”, JHEP 1301 (2013) 063 [arXiv:1211.4890 [hep-ex]].
- [41] ATLAS Collaboration, “Measurement of ZZ production in pp collisions at $\sqrt{s} = 7$ TeV and limits on anomalous ZZZ and $ZZ\gamma$ couplings with the ATLAS detector”, JHEP 03 (2013) 128 [arXiv:1211.6096 [hep-ex]].
- [42] CMS Collaboration, “Measurement of the WZ production cross section in the $l^+l^-l'\nu$ decay channel at $\sqrt{s} = 7$ and 8 TeV at the LHC”, CMS Public Analysis Summary, CMS PAS SMP-12-006.
- [43] ATLAS Collaboration, “Measurement of WZ production in proton-proton collisions at $\sqrt{s} = 7$ TeV with the ATLAS detector”, Eur. Phys. J. C72 (2012) 2173 [arXiv:1208.1390 [hep-ex]].

- [44] CMS Collaboration, “*Measurement of the sum of WW and WZ production with W + dijet events in pp collisions at $\sqrt{s} = 7$ TeV*”, Eur. Phys. J. C73 (2013) 2283 [arXiv:1210.7544 [hep-ex]],
ATLAS Collaboration, “*Measurement of the $WW + WZ$ cross section and limits on anomalous triple gauge couplings using final states with one lepton, missing transverse momentum, and two jets with the ATLAS detector at $\sqrt{s} = 7$ TeV*”, arXiv:1410.7238 [hep-ex].
- [45] CMS Collaboration, “*Measurement of the $W\gamma$ and $Z\gamma$ inclusive cross sections in pp collisions at $\sqrt{s} = 7$ TeV and limits on anomalous triple gauge boson couplings*”, Phys. Rev. D89 (2014) 092005 [arXiv:1308.6832 [hep-ex]],
“*Measurement of the production cross section for $Z\gamma \rightarrow \nu\bar{\nu}\gamma$ in pp collisions at $\sqrt{s} = 7$ TeV and limits on $ZZ\gamma$ and $Z\gamma\gamma$ triple gauge boson couplings*”, JHEP 1310 (2013) 164 [arXiv:1309.1117 [hep-ex]].
- [46] ATLAS Collaboration, “*Measurements of $W\gamma$ and $Z\gamma$ production in pp collisions at $\sqrt{s} = 7$ TeV with the ATLAS detector at the LHC*”, Phys. Rev. D87 (2013) 112003 [arXiv:1302.1283 [hep-ex]].
- [47] CMS Collaboration, “*Measurement of W^+W^- and ZZ production cross sections in pp collisions at $\sqrt{s} = 8$ TeV*”, Phys. Lett. B721 (2013) 190 [arXiv:1301.4698 [hep-ex]],
“*Measurement of the $pp \rightarrow ZZ$ production cross section and constraints on anomalous triple gauge couplings in four-lepton final states at $\sqrt{s} = 8$ TeV*”, arXiv:1406.0113 [hep-ex],
“*Measurement of WZ and ZZ production in pp collisions at $\sqrt{s} = 8$ TeV in final states with b -tagged jets*”, arXiv:1403.3047 [hep-ex].
- [48] ATLAS Collaboration, “*Measurement of the W^+W^- production cross section in proton-proton collisions at $\sqrt{s} = 8$ TeV with the ATLAS detector*”, ATLAS-CONF-2014-033.
- [49] ATLAS Collaboration, “*Measurement of the total ZZ production cross section in proton-proton collisions at $\sqrt{s} = 8$ TeV in 20 fb^{-1} with the ATLAS detector*”, ATLAS-CONF-2013-020.
- [50] ATLAS Collaboration, “*A Measurement of WZ Production in Proton-Proton Collisions at $\sqrt{s} = 8$ TeV with the ATLAS Detector*”, ATLAS-CONF-2013-021.
- [51] ATLAS, CMS, CDF and D0 Collaborations, “*Top cross sections and single top*”, Int. J. Mod. Phys. Conf. Ser. 31 (2014) 1460277.
- [52] CMS Collaboration, “*Measurement of the $t\bar{t}$ production cross section in the dilepton channel in pp collisions at $\sqrt{s} = 8$ TeV*”, JHEP 02 (2014) 024 [arXiv:1312.7582 [hep-ex]],
“*Measurement of the $t\bar{t}$ production cross section in the dilepton channel in pp collisions at $\sqrt{s} = 7$ TeV*”, JHEP 11 (2012) 067 [arXiv:1208.2671 [hep-ex]],
“*Measurement of the $t\bar{t}$ production cross section and the top quark mass in the dilepton channel in pp collisions at $\sqrt{s} = 7$ TeV*”, JHEP 07 (2011) 049 [arXiv:1105.5661]

- [hep-ex]],
 The most up-to-date results on top quark physics from CMS are always available on:
<https://twiki.cern.ch/twiki/bin/view/CMSPublic/PhysicsResultsTOP>.
- [53] ATLAS Collaboration, “*Measurement of the top quark pair production cross section in pp collisions at $\sqrt{s} = 7$ TeV in dilepton final states with ATLAS*”, Phys. Lett. B707 (2012) 459 [arXiv:1108.3699 [hep-ex]],
 “*Top cross section measurements at ATLAS*”, arXiv:1108.6273.
- [54] M. Czakon, M. L. Mangano, A. Mitov, J. Rojo “*Constraints on the gluon PDF from top quark pair production at hadron colliders*”, arXiv:1303.7215 [hep-ph].
- [55] <https://twiki.cern.ch/twiki/bin/view/CMSPublic/PhysicsResultsSMPaTGC>,
 E. S. Protopapadaki, “*Diboson Higgs and EWK measurements and triple gauge couplings with ATLAS and CMS*”, ATL-COM-PHYS-2014-595.
- [56] <http://acfahep.kek.jp/acfareport/node182.html>.
- [57] C. Degrande, N. Greiner, W. Kilian, O. Mattelaer, H. Mebane, T. Stelzer, S. Wilenbrock, C. Zhang, “*Effective Field Theory: A Modern Approach to Anomalous Couplings*”, arXiv:1205.4231 [hep-ph].
- [58] K. Hagiwara, R. D. Peccei, D. Zeppenfeld, K. Hikasa, “*Probing the weak boson sector in $e^+e^- \rightarrow W^+W^-$* ”, Nucl. Phys. B282 (1987) 253,
 K. Hagiwara, S. Ishihara, R. Szalapski, D. Zeppenfeld, “*Low energy constraints on electroweak three gauge boson couplings*”, Phys. Lett. B283 (1992) 353,
 “*Low energy effects of new interactions in the electroweak boson sector*”, Phys. Rev. D 48 (1993) 2182.
- [59] B. Grzadkowski, M. Iskrzyński, M. Misiak, J. Rosiek, “*Dimension-Six Terms in the Standard Model Lagrangian*”, JHEP 1010 (2010) 085 [arXiv:1008.4884 [hep-ph]].
- [60] E. Massó, “*An Effective Guide to Beyond the Standard Model Physics*”, arXiv:1406.6376 [hep-ph].
- [61] G. Gounaris *et al.*, “*Triple Gauge Boson Couplings*”, arXiv:hep-ph/9601233.
- [62] T. Corbett, O. .J. .P. Éboli, M. C. Gonzalez-Garcia, “*Unitarity Constraints on Dimension-Six Operators*”, arXiv:1411.5026 [hep-ph].
- [63] M. Baak *et al.*, “*Study of Electroweak Interactions at the Energy Frontier*”, arXiv:1310.6708 [hep-ph].
- [64] A. Hoeck, W. J. Marciano, “*The Muon Anomalous Magnetic Moment*”
<http://pdg.lbl.gov/2013/reviews/rpp2013-rev-g-2-muon-anom-mag-moment.pdf>.
- [65] G. F. Giudice, C. Grojean, A. Pomarol, R. Rattazzi, “*The Strongly-Interacting Light Higgs*”, JHEP 0706 (2007) 045 [arXiv:hep-ph/0703164],
 G. F. Giudice, “*Theories for the Fermi Scale*”, arXiv:0710.3294 [hep-ph].

- [66] S. Chang, “A ”*Littlest Higgs*” Model with Custodial $SU(2)$ Symmetry”, JHEP 0312 (2003) 057 [arXiv:hep-ph/0306034].
- [67] N. Arkani-Hamed, A. G. Cohen, E. Katz, A. E. Nelson, “*The Littlest Higgs*”, JHEP 0207 (2002) 034 [arXiv:hep-ph/0206021].
- [68] K. Agashe, R. Contino, A. Pomarol, “*The Minimal Composite Higgs Model*”, Nucl. Phys. B719 (2005) 165 [arXiv:hep-ph/0412089],
R. Contino, L. Da Rold, A. Pomarol, “*Light custodians in natural composite Higgs models*”, Phys. Rev. D75 (2007) 055014 [arXiv:hep-ph/0612048].
- [69] R. Contino, Ch. Grojean, M. Moretti, F. Piccinini, R. Rattazzi, “*Strong Double Higgs Production at the LHC*”, JHEP 1005 (2010) 089 [arXiv:1002.1011 [hep-ph]].
- [70] A. Noble, M. Perelstein, “*Higgs Self-Coupling as a Probe of Electroweak Phase Transition*”, arXiv:0711.3018 [hep-ph].
- [71] CMS Collaboration, “*Measurement of the W -boson helicity in top-quark decays from $t\bar{t}$ production in lepton+jets events in pp collisions at $\sqrt{s} = 7$ TeV*”, JHEP 1310 (2013) 167 [arXiv:1308.3879 [hep-ex]].s,
“*Measurement of the Polarization of W Bosons with Large Transverse Momenta in W +Jets Events at the LHC*”, Phys. Rev. Lett. 107 (2011) 021802 [arXiv:1104.3829 [hep-ex]],
J. Marrouche, “*Vector boson polarisation at the LHC*”, April 2010.
- [72] R. N. Cahn and S. Dawson, “*Production of Very Massive Higgs Bosons*”, Phys. Lett. B136 (1984) 196 [Erratum-ibid. B138 (1984) 464],
S. Dawson, “*The Effective W Approximation*”, Nucl. Phys. B249 (1985) 42,
G. L. Kane, W. W. Repko and W. B. Rolnick, “*The Effective W^\pm, Z^0 Approximation for High-Energy Collisions*”, Phys. Lett. B148 (1984) 367,
S. Dawson, “*Radiative Corrections To The Effective W Approximation*”, Phys. Lett. B217 (1989) 347,
T. Veness, “*The effective W approximation*”, DESY Summer student program, 2012.
- [73] H. Veltman, “*The equivalence theorem*”, Phys. Rev. D41, No.7 (1990) 2294,
J. Barger, C. Schmidt, “*Equivalence theorem redux*”, Phys. Rev. D41, No.1 (1990) 264.
- [74] C. F. Uhlemann, N. Kauer, “*Narrow-width approximation accuracy*”, Nucl. Phys. B814 (2009) 195 [arXiv:0807.4112 [hep-ph]].
- [75] S. D. Ellis, C. K. Vermilion, J. R. Walsh, “*Recombination Algorithms and Jet Substructure: Pruning as a Tool for Heavy Particle Searches*”, arXiv:0912.0033 [hep-ph].
- [76] M. Zeinali, “*Jet Reconstruction Algorithms & Performances*”, talk given at IPM@CERN Meeting, September 2009,
CMS Collaboration, “*Performance of Jet Algorithms in CMS*”, CMS Public Analysis Summary, CMS PAS JME-07-003,
P. Scieferdecker, “*Jet Algorithms*”, April 2009,

- <https://twiki.cern.ch/twiki/pub/Sandbox/PhilippSTalk/>,
P.-A. Delsart, “*Jet Algorithms*”, February 2009,
http://www.pa.msu.edu/~yuan/ss2010/JetAlgorithms_lpssc2009.pdf.
- [77] CMS Collaboration, “*Identification of b-quark jets with the CMS Experiment*”, J. of Instr. 38 (2012) P04013 [arXiv:1211.4462 [hep-ex]],
“*b-Jet Identification in the CMS Experiment*”, CMS Public Analysis Summary, CMS PAS BTV-11-004,
“*Algorithms for b Jet Identification in CMS*”, CMS Public Analysis Summary, CMS PAS BTV-09-001,
I. Tomalin, “*b Tagging in CMS*”, J. Phys.: Conference Series 110 (2008) 092033
- [78] CMS Collaboration, “*Measurement of the charge asymmetry of atmospheric muons with the CMS detector*”, CMS Public Analysis Summary, CMS PAS MUO-10-001.
- [79] CMS Collaboration, “*Performance of CMS muon reconstruction in cosmic-ray events*”, JINST 5 T03022 (2010).
- [80] G. Abbiendi et al., “*Muon Reconstruction in the CMS Detector*”, CMS Analysis Note, CMS AN-2008/097,
M. Mulders et al., “*Muon Identification in CMS*”, CMS Analysis Note, CMS AN-2008/098,
L. Scodellaro, “*Performance of the CMS Muon Spectrometer, Muon Reconstruction and Identification Performance*”, talk given at *Physics at the Large Hadron Collider 2010*, DESY, Hamburg, June 2010.
- [81] CMS Collaboration, “*Electron reconstruction and identification at $\sqrt{s} = 7$ TeV*” CMS Public Analysis Summary, CMS PAS EGM-10-004,
W. Adam et al., “*Electron Reconstruction in CMS*”, CMS Analysis Note, CMS AN-2009/164,
R. Salerno, “*Electron reconstruction and identification in CMS at LHC*”, Nucl. Phys. B (Proc. Suppl.) 197 (2009) 230,
S. Baffioni et al., “*Electron reconstruction in CMS*”, Eur. Phys. J. C49 (2007) 1099,
P. Vanlaer, “*Electron and photon reconstruction in CMS*”, talk given at the *First IPM Meeting on LHC Physics*, Isfahan, April 2009.
- [82] ATLAS Collaboration, “*Electron performance measurements with the ATLAS detector using the 2010 LHC proton-proton collision data*”, arXiv:1110.3174 [hep-ex],
M. Wichmann, “*Electron Charge Misidentification in the ATLAS Detector*”, Diploma Thesis, Ludwig-Maximilians-Universität München, 2008.
- [83] W. Hintz, “*Electron identification with the CMS detector and applications for Higgs and W boson searches*”, PhD Thesis, ETH Zurich, 2010, CERN-THESIS-2010-219,
A. Palma, “*Studies on the dielectron spectrum with the first data of the CMS experiment at the Large Hadron Collider*”, PhD Thesis, Sapienza Università di Roma, 2009.
- [84] H.-J. Yang, “*Electron Identification Based on Boosted Decision Trees*”, Sept. 2008,
<http://gallatin.physics.lsa.umich.edu/~hyang/talks/e-ID-haijun.ppt>.

- [85] G. Wooden, “*Leptonic fake rates from jets at ATLAS*”, talk given at the *Berkeley workshop on physics opportunities with early LHC data*, May 2009.
- [86] J. Mellenthin, “*Measurement of muon misidentification rates in $Z \rightarrow \mu\mu$ events for the ATLAS detector*”, talk given at the *IMPRS Young Scientists’ Workshop, Ringberg*, July 2013.
- [87] M. Cacciari, G. P. Salam, G. Soyez, “*The anti- k_T jet clustering algorithm*”, JHEP04 (2008) 063.
- [88] A. Heister *et al.*, “*Jet Reconstruction and Performance in the CMS Detector*”, CMS Analysis Note, CMS AN-2005/005,
V. D. Elvira, “*CMS Jet and Missing E_T Commissioning*”, FERMILAB-CONF-09-745-CD-CMS.
- [89] M. S. Chanowitz, M. K. Gaillard, “*The TeV Physics of Strongly Interacting W ’s and Z ’s*”, Nucl. Phys. B261 (1985) 379,
M. S. Chanowitz, “*Electroweak Symmetry Breaking: Unitarity, Dynamics, and Experimental Prospects*”, Annu. Rev. Nucl. Part. Sci. 38 (1988) 38,
M. S. Berger, M. S. Chanowitz, “*Strong W^+W^+ scattering at the SSC*”, Phys. Lett. B263 (1991) 509.
- [90] V. Barger, K. Cheung, T. Han, R. J. N. Phillips, “*Strong W^+W^+ scattering signals at pp supercolliders*”, Phys. Rev. D42, No.9 (1990) 3052.
- [91] D. .A. Dicus, J. F. Gunion, R. Vega, “*Isolating the Scattering of Longitudinal W^+ ’s at the SSC using Like-Sign Dileptons*”, Phys. Lett. B258 (1991) 475.
- [92] J. Bagger, V. Barger, K. Cheung, J. Gunion, T. Han, G. A. Ladinsky, R. Rosenfeld, C. P. Yuan, “*Strongly interacting WW system: Gold-plated modes*”, Phys. Rev. D49 (1994) 1246 [arXiv:hep-ph/9306256v1]; “*LHC Analysis of the Strongly Interacting WW System: Gold-Plated Modes*”, Phys. Rev. D52 (1995) 3878 [arXiv:hep-ph/9504426].
- [93] A. Dobado, M. J. Herrero, J. Terron, “*The role of chiral Lagrangians in strongly interacting $W_L W_L$ signals at pp supercolliders*”, Z. Phys. C 50 (1991) 205; “ *$W^\pm Z^0$ signals from the strongly interacting symmetry breaking sector*”, Z. Phys. C 50 (1991) 465,
A. Dobado, M. J. Herrero, J. R. Peláez, E. Ruiz Morales, M. T. Urdiales, “*Learning about the strongly interacting symmetry breaking sector at LHC*”, Phys. Lett. B352 (1995) 400 [arXiv:hep-ph/9502309]; Phys. Rev. D62 (2000) 055011.
- [94] M. S. Chanowitz, W. B. Kilgore, “*Complementarity of Resonant and Non-resonant Strong WW Scattering at the LHC*”, Phys. Lett. B322 (1994) 147 [arXiv:hep-ph/9311336]. “ *W^+Z and $W^+\gamma$ Backgrounds to Strong W^+W^+ Scattering at the LHC*”, Phys. Lett. B347 (1995) 387 [arXiv:hep-ph/9412275],
M. S. Chanowitz, “*Strong WW scattering in unitary gauge*”, arXiv:hep-ph/9512358; “*The No-Higgs Signal: Strong WW Scattering at the LHC*”, eScholarship Repository, <http://repositories.cdlib.org/lbnl/LBNL-56734> (2004).

- [95] J. M. Butterworth, B. E. Cox, J. R. Forshaw, “*WW scattering at the LHC*”, Phys. Rev. D65 (2002) 096014.
- [96] P. Zych, “*Observation of the strongly-coupled Higgs sector in the CMS detector at the LHC*”, PhD Thesis, Warsaw University, 2007.
- [97] A. Alboteanu, W. Kilian and J. Reuter, “*Resonances and Unitarity in Weak Boson Scattering at the LHC*”, JHEP 0811 (2008) 010 [arXiv:0806.4145 [hep-ph]],
M. Fabbrichesi, L. Vecchi, “*Possible experimental signatures at the LHC of strongly interacting electro-weak symmetry breaking*”, arXiv:hep-ph/070326,
H.-J. He, Y.-P. Kuang, Y.-H. Qi, B. Zhang, A. Belyaev, R. Sekhar Chivukula, N. D. Christensen, A. Pukhov, E. H. Simmons, “*LHC Signatures of New Gauge Bosons in the Minimal Higgsless Model*”, arXiv:0708.2588 [hep-ph],
A. Birkedal, K. Matchev, M. Perelstein, “*Collider Phenomenology of the Higgsless Models*”, arXiv:hep-ph/0412278,
A. Birkedal, K. Matchev, “*Phenomenology of Higgsless Models at the LHC and the ILC*”, arXiv:hep-ph/0508185,
M. Fabbrichesi, A. Tonerio, L. Vecchi, “*Gauge boson scattering the LHC without a light Higgs boson*” in: *Proceedings on the Workshop on Monte Carlo’s, physics and simulations at the LHC - part I*, arXiv:0902.0293 [hep-ph].
- [98] ATLAS Collaboration, “*Expected Performance of the ATLAS Experiment*”, arXiv:0901.0512v4 (CERN-OPEN-2008-020).
- [99] E. Accomando, A. Ballestrero, S. Bolognesi, E. Maina, C. Mariotti, “*Boson-boson scattering and Higgs production at the LHC from a six fermion point of view: Four jets + $l\nu$ processes at $O(\alpha_{em}^6)$* ”, JHEP 0603 (2006) 093, [arXiv:hep-ph/0512219],
A. Ballestrero, G. Bevilacqua and E. Maina, “*A Complete parton level analysis of boson-boson scattering and ElectroWeak Symmetry Breaking in $l\nu + four jets production at the LHC$* ”, JHEP 0905 (2009) 015, [arXiv:0812.5084 [hep-ph]],
A. Ballestrero, G. Bevilacqua, D. B. Franzosi and E. Maina, “*How well can the LHC distinguish between the SM light Higgs scenario, a composite Higgs and the Higgsless case using VV scattering channels?*”, JHEP 0911 (2009) 126 [arXiv:0909.3838 [hep-ph]],
A. Ballestrero, D. B. Franzosi, E. Maina, “*Vector-Vector scattering at the LHC with two charged leptons and two neutrinos in the final state*”, JHEP 1106 (2011) 013 [arXiv:1011.1514 [hep-ph]],
A. Ballestrero, D. Buarque Franzosi, L. Oggero and E. Maina, “*Vector Boson scattering at the LHC: counting experiments for unitarized models in a full six fermion approach*”, arXiv:1112.1171 [hep-ph],
G. Bevilacqua, “*Vector Boson Scattering as a probe of Electroweak Symmetry Breaking: a six fermion perspective*”, PhD Thesis, Università degli Studi di Torino, 2008,
A. Ballestrero, E. Maina, “*WW Scattering*” in: *Proceedings on the Workshop on Monte Carlo’s, physics and simulations at the LHC - part I*, arXiv:0902.0293v1 [hep-ph],
A. Ballestrero, “*Boson Boson scattering analysis*”, talk given at *LHC2TSP*, September 2011.

- [100] R. Bellan, “*VV-Fusion at CMS*”, talk given at *Frontier Science 2005 - LHC: physics and detectors*, September 2005,
B. Zhu, P. Govoni, Y. Mao, C. Mariotti, W. Wu, “*Same Sign WW Scattering Process as a Probe of Higgs Boson in pp Collision at $\sqrt{s} = 10$ TeV*”, Eur. Phys. J. C71 (2011) 1514 [arXiv:1010.5848 [hep-ex]],
G. Cerminara, “*A Study of the WW-fusion Process at CMS as a Probe of Symmetry Breaking*”, PhD Thesis, Universita degli Studi di Torino, 2003,
N. Amapane *et al.*, “*Study of VV-scattering processes as a probe of electroweak symmetry breaking*”, CMS Analysis Note, CMS AN-2007/005.
- [101] C. Englert, B. Jäger, M. Worek, D. Zeppenfeld, “*Observing Strongly Interacting Vector Boson Systems at the CERN Large Hadron Collider*”, Phys. Rev. D80 (2009) 035027 [arXiv:0810.4861 [hep-ph]].
- [102] K. Doroba, J. Kalinowski, J. Kuczmarski, S. Pokorski, J. Rosiek, M. Szleper, S. Tkaczyk, “ *$W_L W_L$ scattering at the LHC: improving the selection criteria*”, Phys. Rev. D86 No.3 (2012) 036011 [arXiv:1201.2768 [hep-ph]].
- [103] K. Cheung, C.-W. Chiang, T.-Ch. Yuan, “*Partially Strong WW Scattering*”, Phys. Rev. D78 (2008) 051701 [arXiv:0803.2661 [hep-ph]].
- [104] A. Freitas, J. S. Gainer, “*High Energy WW Scattering at the LHC with the Matrix Element Method*”, arXiv:1212.3598 [hep-ph],
I. Volobouev, “*Matrix Element Method in HEP: Transfer Functions, Efficiencies and Likelihood Normalization*”, arXiv:1101.2259 [physics.data-an].
- [105] Y. Cui, Z. Han, “*New light on WW scattering at the LHC with W jet tagging*”, arXiv:1304.4599 [hep-ph],
T. Han, D. Krohn, L.-T. Wang and W. Zhu, “*New Physics Signals in Longitudinal Gauge Boson Scattering at the LHC*”, JHEP 1003 (2010) 082 [arXiv:0911.3656 [hep-ph]].
- [106] S. Godfrey, “*Quartic Gauge Boson Couplings*”, arXiv:hep-ph/9505252.
- [107] A. S. Belyaev, O. J. P. Eboli, M. C. Gonzalez-Garcia, J. K. Mizukoshi, S. F. Novaes, I. Zacharov, “*Strongly Interacting Vector Bosons at the LHC: Quartic Anomalous Couplings*”, arXiv:hep-ph/9805229.
- [108] O. J. P. Eboli, M. C. Gonzalez-Garcia, J. K. Mizukoshi, “ *pp to $jje^\pm\mu^\pm\nu\nu$ and $jje^\pm\mu^\mp\nu\nu$ at $O(\alpha_{em}^6)$ and $O(\alpha_{em}^4\alpha_s^2)$ for the Study of the Quartic Electroweak Gauge Boson Vertex at LHC*”, Phys. Rev. D74 (2006) 073005 [arXiv:hep-ph/0606118].
- [109] ATLAS Collaboration, “*Evidence for electroweak production of $W^\pm W^\pm jj$ in pp collisions at $\sqrt{s} = 8$ TeV with the ATLAS detector*”, Phys. Rev. Lett. 113 (2014) 141803 [arXiv:1405.6241 [hep-ex]].
- [110] CMS Collaboration, “*Measurement of vector boson scattering and search for new physics in events with two jets and two same-sign leptons*”, CMS Public Analysis Summary, CMS PAS SMP-13-015.

- [111] T. Kuśmierczyk, “*Poszukiwanie sygnału rozpraszania bozonów W w eksperymencie CMS przy LHC*”, Bachelor Thesis, University of Warsaw, 2013.
- [112] F. Maltoni, T. McElmurry, R. Putman, S. Willenbrock, “*Choosing the Factorization Scale in Perturbative QCD*”, arXiv:hep-ph/0703156.
- [113] X.-G. Wu, S. J. Brodsky, M. Mojaza, “*The Renormalization Scale-Setting Problem in QCD*”, arXiv:1302.0599v2-1 [hep-ph].
- [114] B. Jäger, C. Oleari and D. Zeppenfeld, “*Next-to-leading order QCD corrections to W^+W^- production via vector-boson fusion*”, JHEP 0607 (2006) 015 [hep-ph/0603177]; “*Next-to-leading order QCD corrections to W^+W^+jj and W^-W^-jj production via weak-boson fusion*”, Phys. Rev. D80 (2009) 034022 [arXiv:0907.0580 [hep-ph]],
B. Jäger and G. Zanderighi, “*NLO corrections to electroweak and QCD production of W^+W^+ plus two jets in the POWHEGBOX*”, JHEP 1111 (2011) 055 [arXiv:1108.0864 [hep-ph]],
T. Melia, P. Nason, R. Rontsch and G. Zanderighi, “ *W^+W^- , WZ and ZZ production in the POWHEG BOX*”, JHEP 1111 (2011) 078 [arXiv:1107.5051 [hep-ph]],
T. Melia, K. Melnikov, R. Rontsch and G. Zanderighi, “*NLO QCD corrections for W^+W^- pair production in association with two jets at hadron colliders*”, Phys. Rev. D83 (2011) 114043 [arXiv:1104.2327 [hep-ph]],
T. Melia, P. Nason, R. Rontsch and G. Zanderighi, “ *W^+W^+ plus dijet production in the POWHEGBOX*”, Eur. Phys. J. C71 (2011) 1670 [arXiv:1102.4846 [hep-ph]],
T. Melia, K. Melnikov, R. Rontsch and G. Zanderighi, “*Next-to-leading order QCD predictions for W^+W^+jj production at the LHC*”, JHEP 1012 (2010) 053 [arXiv:1007.5313 [hep-ph]].
- [115] F. Campanario, M. Kerner, L. D. Ninh, D. Zeppenfeld, “*Next-to-leading order QCD corrections to W^+W^+ and W^-W^- production in association with two jets*”, Phys. Rev. D89 (2014) 054009 [arXiv:1311.6738 [hep-ph]].
- [116] C. Degrande, J.L. Holzbauer, S.-C. Hsu, A.V. Kotwal, S. Li, M. Marx, O. Matelaer, J. Metcalfe, M.-A. Pleier, C. Pollard, M. Rominsky, D. Wackerroth, “*Studies of Vector Boson Scattering And Triboson Production with DELPHES Parametrized FastSimulation for Snowmass 2013*”, arXiv:1309.7452 [physics.comp-ph].
- [117] ATLAS Collaboration, “*Physics at a High-Luminosity LHC with ATLAS*”, ATL-PHYS-PUB-2012-001,
“*Physics at a High-Luminosity LHC with ATLAS (Update)*”, ATL-PHYS-PUB-2012-004,
“*Studies of Vector Boson Scattering with an Upgraded ATLAS Detector at a High-Luminosity LHC*”, ATL-PHYS-PUB-2012-005,
“*Studies of Vector Boson Scattering and Triboson Production with an Upgraded ATLAS Detector at a High-Luminosity LHC*”, ATL-PHYS-PUB-2013-006,
C. Bittrich, “*Study of the Effects of Anomalous Quartic Gauge Couplings on the Scattering of Two Gauge Bosons $VV \rightarrow VV$ at the Large Hadron Collider*”, Bachelor Thesis, Technische Universität Dresden, 2012, CERN-THESIS-2012-259.

- [118] M. Herndon, K. Long, A. Wright, S. Djuric, “*Vector Boson Scattering and Quartic Gauge Coupling Studies*”, CMS Analysis Note, CMS-AN-13-287, CMS Collaboration, “*Vector Boson Scattering and Quartic Gauge Coupling Studies in WZ Production at 14 TeV*”, CMS Public Analysis Summary, CMS PAS FTR-13-006.
- [119] <http://indico.cern.ch/e/fcc-kickoff>.
- [120] S. Tkaczyk, private communication.
- [121] J. Alwall, M. Herquet, F. Maltoni, O. Mattelaer, T. Stelzer, “*MadGraph 5 : Going Beyond*”, JHEP 1106 (2011) 128 [arXiv:1106.0522 [hep-ph]], J. Alwall, P. Demin, S. de Visscher, R. Frederix, M. Herquet, F. Maltoni, T. Plehn, D. L. Rainwater, T. Stelzer, “*MadGraph/MadEvent v4: The New Web Generation*”, JHEP 0709 (2007) 028 [arXiv:0706.2334 [hep-ph]].
- [122] T. Sjöstrand, S. Mrenna, P. Skands, “*PYTHIA 6.4 Physics and Manual*”, JHEP 05 (2006) 026 [arXiv:hep-ph/0603175].
- [123] A. Ballestrero, A. Belhouari, G. Bevilacqua, V. Kashkan and E. Maina, “*PHANTOM: A Monte Carlo event generator for six parton final states at high energy colliders*”, Comput. Phys. Commun. 180 (2009) 401 [arXiv:0801.3359 [hep-ph]], E. Accomando, A. Ballestrero, E. Maina, “*PHASE, a Monte Carlo event generator for six-fermion physics at the LHC*”, JHEP07 (2005) 016.
- [124] The program may be downloaded and some documentation is available from: <http://www.physics.ucdavis.edu/~conway/research/software/pgs/pgs4-general.htm>.